



MISSOURI  
**S&T**

# CENTER FOR TRANSPORTATION INFRASTRUCTURE AND SAFETY



## **Repair of Earthquake-Damaged Bridge Columns with Interlocking Spirals and Fractured Bars**

by

Yang Yang<sup>1</sup>  
Lesley H. Sneed<sup>2</sup>  
Mehdi Saïid Saïidi<sup>3</sup>  
and  
Abdeldjelil Belarbi<sup>4</sup>

<sup>1, 2</sup> Department of Civil, Architectural, and Environmental Engineering  
Missouri University of Science and Technology  
Rolla, MO 65409

<sup>3</sup> Department of Civil and Environmental Engineering  
University of Nevada, Reno  
Reno, NV 89557

<sup>4</sup> Department of Civil and Environmental Engineering  
University of Houston  
Houston, TX 77004

**NUTC  
R298**

**A National University Transportation Center  
at Missouri University of Science and Technology**

## ***Disclaimer***

The contents of this report reflect the views of the author(s), who are responsible for the facts and the accuracy of information presented herein. This document is disseminated under the sponsorship of the Department of Transportation, University Transportation Centers Program and the Center for Transportation Infrastructure and Safety NUTC program at the Missouri University of Science and Technology, in the interest of information exchange. The U.S. Government and Center for Transportation Infrastructure and Safety assumes no liability for the contents or use thereof.

### Technical Report Documentation Page

1. Report No. NUTC R298	2. Government Accession No.	3. Recipient's Catalog No.	
4. Title and Subtitle Repair of Earthquake-Damaged Bridge Columns with Interlocking Spirals and Fractured Bars		5. Report Date July 2014	
		6. Performing Organization Code	
7. Author/s Yang Yang, Lesley H. Sneed, Mehdi Saiid Saiidi, and Abdeldjelil Belarbi		8. Performing Organization Report No. Project #00038671	
9. Performing Organization Name and Address Center for Transportation Infrastructure and Safety/NUTC program Missouri University of Science and Technology 220 Engineering Research Lab Rolla, MO 65409		10. Work Unit No. (TRAIS)	
		11. Contract or Grant No. DTRT06-G-0014	
12. Sponsoring Organization Name and Address U.S. Department of Transportation Research and Innovative Technology Administration 1200 New Jersey Avenue, SE Washington, DC 20590		13. Type of Report and Period Covered Final	
		14. Sponsoring Agency Code	
15. Supplementary Notes			
16. Abstract During earthquakes, reinforced concrete (RC) bridge columns may experience different levels of damage such as cracking, spalling, or crushing of concrete and yielding, buckling, or fracture of reinforcing bars. Although several repair options exist for columns with slight to moderate levels of damage, limited research has been reported in the literature for columns with fractured longitudinal reinforcing bars. A method that has shown success in restoring the strength and ductility to RC columns with fractured and/or buckled bars involves replacement of damaged longitudinal bars, reinstallation of transverse reinforcing bars, and restoring confinement using an external jacket. In some cases however, such as with seismically-designed RC columns with spiral reinforcement, it may not be possible to reinstall the internal transverse reinforcement. Thus alternative methods are needed to restore the performance of damaged RC columns with fractured bars to a desired state. The objective of this study was to develop methods to restore both the load and deformation capacity of earthquake-damaged bridge columns with interlocking spirals and buckled and/or fractured longitudinal reinforcement. The first repair method investigated was considered a permanent repair that involved replacement of the plastic hinge region by removal of spirals, replacement of longitudinal bar segments by mechanically splicing new bar segments attached with mechanical couplers, replacement of concrete, and installation of an externally bonded carbon fiber reinforced polymer (CFRP) jacket. The second method was considered an emergency repair that involved removal of damaged concrete, bonding and embedding CFRP strips for flexural reinforcement, building a jacket from a prefabricated thin CFRP laminate, and repair of the footing with CFRP fabric. The repair methods were evaluated by large-scale component tests on RC column specimens subjected to slow cyclic loading resulting in combined bending, shear, and torsion. Test results showed that the repair methods developed in this study are capable of restoring the seismic performance of the repaired columns to that of the undamaged columns in terms of lateral load and deformation capacity, as well as torsional load and twist capacity. However, both repair methods resulted in lower lateral and torsional stiffness as well as lower energy dissipation capacity; thus, the influence of the repair methods on the seismic response of bridges repaired with these methods is in need of further research.			
17. Key Words bridge, reinforced concrete columns, earthquake, fractured bars, repair, mechanical couplers, CFRP jacke		18. Distribution Statement No restrictions. This document is available to the public through the National Technical Information Service, Springfield, Virginia 22161.	
19. Security Classification (of this report) unclassified	20. Security Classification (of this page) unclassified	21. No. Of Pages 212	22. Price

# **Repair of Earthquake-Damaged Bridge Columns with Interlocking Spirals and Fractured Bars**

by

Yang Yang<sup>1</sup>  
Lesley H. Sneed<sup>2</sup>  
Mehdi Saiid Saiidi<sup>3</sup>  
and  
Abdeldjelil Belarbi<sup>4</sup>

<sup>1,2</sup>Department of Civil, Architectural, and Environmental Engineering  
Missouri University of Science and Technology  
Rolla, MO 65409

<sup>3</sup>Department of Civil and Environmental Engineering  
University of Nevada, Reno  
Reno, NV 89557

<sup>4</sup>Department of Civil and Environmental Engineering  
University of Houston  
Houston, TX 77004

**July 2014**

## Abstract

During earthquakes, reinforced concrete (RC) bridge columns may experience different levels of damage such as cracking, spalling, or crushing of concrete and yielding, buckling, or fracture of reinforcing bars. Although several repair options exist for columns with slight to moderate levels of damage, limited research has been reported in the literature for columns with fractured longitudinal reinforcing bars. A method that has shown success in restoring the strength and ductility to RC columns with fractured and/or buckled bars involves replacement of damaged longitudinal bars, reinstallation of transverse reinforcing bars, and restoring confinement using an external jacket. In some cases however, such as with seismically-designed RC columns with spiral reinforcement, it may not be possible to reinstall the internal transverse reinforcement. Thus alternative methods are needed to restore the performance of damaged RC columns with fractured bars to a desired state. The objective of this study was to develop methods to restore both the load and deformation capacity of earthquake-damaged bridge columns with interlocking spirals and buckled and/or fractured longitudinal reinforcement. The first repair method investigated was considered a permanent repair that involved replacement of the plastic hinge region by removal of spirals, replacement of longitudinal bar segments by mechanically splicing new bar segments attached with mechanical couplers, replacement of concrete, and installation of an externally bonded carbon fiber reinforced polymer (CFRP) jacket. The second method was considered an emergency repair that involved removal of damaged concrete, bonding and embedding CFRP strips for flexural reinforcement, building a jacket from a prefabricated thin CFRP laminate, and repair of the footing with CFRP fabric. The repair methods were evaluated by large-scale component tests on RC column specimens subjected to slow cyclic loading resulting in combined bending, shear, and torsion. Test results showed that the repair methods developed in this study are capable of restoring the seismic performance of the repaired columns to that of the undamaged columns in terms of lateral load and deformation capacity, as well as torsional load and twist capacity. However, both repair methods resulted in lower lateral and torsional stiffness as well as lower energy dissipation capacity; thus, the influence of the repair methods on the seismic response of bridges repaired with these methods is in need of further research.

## **Acknowledgements**

The research reported herein was sponsored by the California Department of Transportation (Caltrans) and the National University Transportation Center (NUTC) at the Missouri University of Science and Technology (Missouri S&T). The principal investigator at the University of Nevada, Reno (UNR) was M. Saiid Saiidi, and the co-principal investigators were Lesley Sneed at Missouri S&T and Abdeldjelil Belarbi at the University of Houston. The experimental research was performed by Missouri S&T. Major contributions to the project were made by Ashkan Vosooghi (post-doctoral researcher at UNR), who contributed to the design of the repair, Ruili He (graduate student at Missouri S&T), who contributed to the experimental work and the information in Chapter 2 of this report, and Adam Morgan (graduate student at Missouri S&T), who contributed to the experimental work. Carbon fiber reinforced polymer composites were donated by Fyfe Co. LLC and QuakeWrap Inc. Mechanical couplers were provided by Erico International Corporation and BarSplice Products Inc. Shoring towers and pumping services were donated by Goedecke. Prospect Steel Company donated materials for the test setup.

## Table of Contents

1	Introduction.....	1
1.1	Problem Statement .....	1
1.2	Project Objective .....	3
1.3	Methodology .....	5
1.4	Organization of Report.....	7
2	Literature Review .....	8
2.1	RC Bridge Columns with Interlocking Spirals .....	8
2.2	Repair Methods for Damaged RC Bridge Columns .....	10
2.3	Concrete Filled FRP Tubes (CFFTs) .....	19
2.4	Rebar Couplers in Seismic Applications.....	24
3	Experimental Work of R-Calt-1 and R-Calt-2.....	28
3.1	Original Column Specimens .....	28
3.1.1	Previous test program .....	29
3.1.2	Damage to Calt-1 and Calt-2 .....	30
3.2	Repair Design.....	32
3.2.1	Repair materials .....	33
3.2.2	Determination of replacement length.....	34
3.2.3	Design of externally bonded CFRP jacket.....	36
3.3	Repair Procedure .....	41
3.3.1	Shoring of column.....	41
3.3.2	Removal of concrete and spirals .....	41
3.3.3	Severing and removal of damaged longitudinal bars.....	42
3.3.4	Straightening of column.....	42
3.3.5	Splicing new replacement bars and installing mechanical bar couplers.....	43
3.3.6	Casting new concrete .....	43
3.3.7	Installing CFRP jacket .....	43
3.4	Test Program .....	43
3.4.1	Test setup .....	43
3.4.2	Instrumentation .....	44
3.4.3	Loading protocol.....	45
3.5	Concluding Remarks .....	45
4	Experimental Results of R-Calt-1 and R-Calt-2.....	73
4.1	General Behavior and Observed Damage to R-Calt-1 and R-Calt-2 .....	73
4.2	Base Shear-Lateral Displacement and Torsional Moment-Twist Relationships .....	76
4.3	Energy Dissipation .....	81
4.4	Measured Strains .....	83
4.5	Concluding Remarks .....	85
5	Experimental Work of R-Calt-3 .....	104
5.1	Original Column Specimen.....	105
5.1.1	Previous test program .....	105
5.1.2	Damage to Calt-3 .....	106
5.2	Repair Design.....	107
5.2.1	Repair scheme.....	107
5.2.2	Repair materials .....	108

5.2.3	Column shear and torsion repair design.....	109
5.2.4	Column flexural repair design .....	109
5.2.5	Embedment length of CFRP jacket and plates .....	111
5.2.6	Footing repair design .....	112
5.2.7	Summary .....	114
5.3	Repair Procedure .....	114
5.3.1	Trenching of footing .....	115
5.3.2	Removal of concrete .....	115
5.3.3	Placement of grout .....	115
5.3.4	Installation of CFRP plates and jacket.....	116
5.3.5	Installation of CFRP straps to footing .....	117
5.4	Test Program .....	117
5.4.1	Test setup .....	117
5.4.2	Instrumentation .....	118
5.4.3	Loading protocol.....	118
5.5	Concluding Remarks.....	119
6	Experimental Results of R-Calt-3.....	144
6.1	General Behavior and Observed Damage to R-Calt-3.....	144
6.2	Base Shear-Lateral Displacement and Torsional Moment-Twist Relationships .....	146
6.3	Energy Dissipation .....	149
6.4	Measured Strains .....	150
6.5	Concluding Remarks .....	152
7	Assessment of Repair Methods.....	171
7.1	Constructability .....	171
7.1.1	Shoring.....	172
7.1.2	Concrete removal .....	172
7.1.3	Reinforcement removal.....	173
7.1.4	Coupler installation and performance.....	174
7.1.5	Concrete placement.....	175
7.1.6	CFRP application to column.....	177
7.1.7	Footing repair.....	177
7.2	Seismic performance .....	178
7.2.1	Strength.....	178
7.2.2	Stiffness.....	179
7.2.3	Ductility .....	180
7.2.4	Energy dissipation.....	181
8	Conclusions and Recommendations .....	189
8.1	Conclusions .....	189
8.2	Recommendations .....	193
8.3	Future work .....	195
9	References.....	198

## List of Tables

Table 2-1 Summary of Studies on Repair of Reinforced Concrete Columns with Fractured Longitudinal Bars.....	27
Table 3-1 Measured Reinforcing Steel Properties for Calt-1, Calt-2, R-Calt-1, and R-Calt-2.....	46
Table 3-2 Measured Concrete Compressive Strength of for Calt-1, Calt-2, R-Calt-1, and R-Calt-2.....	46
Table 3-3 Visible Damage to Columns to Calt-1 and Calt-2 After Original Test .....	46
Table 4-1 Summary of Measured Forces for Calt-1, Calt-2, R-Calt-1, and R-Calt-2 .....	87
Table 4-2 Critical Values of Idealized Load-Displacement Curves for Calt-1, Calt-2, R-Calt-1, and R-Calt-2.....	87
Table 5-1 Measured Compressive Strength of Concrete and Grout for Calt-3 and R-Calt-3.....	120
Table 5-2 Measured Reinforcing Steel Properties for Calt-3 and R-Calt-3.....	120
Table 5-3 Visible Damage to Calt-3 after Original Test.....	120
Table 5-4 Properties of Unidirectional CFRP Plates (GU50C) (provided by manufacturer).....	120
Table 5-5 Properties of QuakeWrap <sup>TM</sup> VU18C Fiber and Laminate (provided by manufacturer).....	120
Table 5-6 Properties of Bidirectional CFRP PLC100.60 (provided by manufacturer) .....	121
Table 5-7 Properties of QuakeBond <sup>TM</sup> 320LV Low Viscosity Resin Epoxy (provided by manufacturer).....	121
Table 5-8 Measured Material Properties of Epoxy-Gravel.....	121
Table 6-1 Summary of Measured Forces of Calt-3 and R-Calt-3.....	153
Table 6-2 Critical Values on Idealized Load-Displacement Curves .....	153
Table 7-1 Constructability Comparison.....	183
Table 7-2 Approximate Time Duration (Per Two Workers) .....	184

## List of Figures

Figure 3-1 Geometry and Reinforcement Details of Calt-1 and Calt-2.....	47
Figure 3-2 Test setups of (a) Calt-1 and Calt-2 (b) R-Calt-1 and R-Calt-2.....	48
Figure 3-3 Loading Protocol of Calt-1, R-Calt-1, Calt-2, and R-Calt-2.....	49
Figure 3-4 Visible Damage After Original Test to (a) Calt-1 and (b) Calt-2 .....	50
Figure 3-5 Definition of Spalled Length and Core Crushing Depth of Concrete.....	51
Figure 3-6 Visible Damage to Longitudinal Reinforcement of Calt-1 After Original Test .....	52
Figure 3-7 Visible Damage to Longitudinal Reinforcement of Calt-2 After Original Test .....	53
Figure 3-8 Strain Gage Layout of Calt-1 and Calt-2 .....	54
Figure 3-9 Strain History of Longitudinal Reinforcement (Calt-1).....	55
Figure 3-10 Strain History of Transverse Reinforcement (Calt-1).....	56
Figure 3-11 Strain History of Longitudinal Reinforcement (Calt-2).....	57
Figure 3-12 Strain History of Transverse Reinforcement (Calt-2).....	58
Figure 3-13 Repair Scheme for Calt-1 and Calt-2 .....	59
Figure 3-14 Cross-Section Model in XTRACT for (a) Calt-1 and Calt-2 and (b) R-Calt-1 and R-Calt-2.....	60
Figure 3-15 CFRP layout for R-Calt-1 and R-Calt-2.....	61
Figure 3-16 Shoring of Calt-1 and Calt-2 During Repair .....	62
Figure 3-17 Removal of Concrete and Spirals of Calt-1 .....	63
Figure 3-18 Removal of Concrete and Spirals of Calt-2 .....	64
Figure 3-19 Severing of Longitudinal Reinforcement in Calt-1 and Calt-2.....	65
Figure 3-20 Reinforcement Details of Repaired Columns R-Calt-1 and R-Calt-2.....	66
Figure 3-21 Splicing of New Replacement Bar Segments and Installation of Couplers of Calt-1.....	67
Figure 3-22 Splicing of New Replacement Bar Segments and Installation of Couplers of Calt-2.....	68
Figure 3-23 CFRP Application Procedure for Calt-1 and Calt-2 .....	69
Figure 3-24 Strain Gage Layout on Replacement Bars and Couplers for R-Calt-1 and R-Calt-2.....	70
Figure 3-25 Strain Gage Layout on CFRP Jacket for R-Calt-1 and R-Calt-2 .....	71
Figure 3-26 String Transducer Layout for R-Calt-1 and R-Calt-2 .....	72
Figure 4-1 Progressive Deformation of R-Calt-1 at Increasing Load Levels.....	88
Figure 4-2 Damage to R-Calt-1 .....	89
Figure 4-3 View of R-Calt-1 after Removal of CFRP Jacket.....	90
Figure 4-4 Plan View of Footing of R-Calt-1 .....	91
Figure 4-5 Isometric View of R-Calt-1 After Removal of First Layer of Footing Reinforcement.....	92
Figure 4-6 Progressive Deformation of R-Calt-2 at Increasing Load Levels.....	93
Figure 4-7 Damage to R-Calt-2 .....	94
Figure 4-8 Load-Displacement Hysteresis Responses of Calt-1, R-Calt-1, Calt-2, and R-Calt-2.....	95
Figure 4-9 Load-Displacement Envelopes of Calt-1, R-Calt-1, Calt-2, and R-Calt-2 .....	96
Figure 4-10 Idealized Load-Displacement Envelopes of Calt-1 and R-Calt-1 .....	97
Figure 4-11 Idealized Load-Displacement Envelopes of Calt-2 and R-Calt-2.....	98
Figure 4-12 Energy Dissipation per Cycle of Calt-1, R-Calt-1, Calt-2, and R-Calt-2 .....	99

Figure 4-13 Cumulative Energy Dissipation of Calt-1, R-Calt-1, Calt-2, and R-Calt-2 .....	100
Figure 4-14 Measured Reinforcing Steel Strain Distribution Along Column Height of (a) and (b) R-Calt-1 and (c) and (d) R-Calt-2 .....	101
Figure 4-15 Measured CFRP Strain Distribution along Column Height of R-Calt-1 .....	102
Figure 4-16 Measured CFRP Strain Distribution along Column Height of R-Calt-2 .....	103
Figure 5-1 Geometry and Reinforcement Details of Calt-3.....	122
Figure 5-2 Loading Protocol of Calt-3 and R-Calt-3.....	123
Figure 5-3 Visible Damage to Calt-3 after Original Test .....	124
Figure 5-4 Visible Damage to Longitudinal Reinforcement of Calt-3 after Original Test .....	125
Figure 5-5 Strain Gage Layout of Calt-3 .....	126
Figure 5-6 Strain History of Longitudinal Reinforcement (Calt-3).....	127
Figure 5-7 Strain History of Transverse Reinforcement (Calt-3).....	128
Figure 5-8 Repair Scheme for Calt-3.....	129
Figure 5-9 Moment-Curvature Analysis Models and Results for Calt-3 and R-Calt-3.....	130
Figure 5-10 Concrete Repair and Trench Details for R-Calt-3.....	131
Figure 5-11 Details of CFRP Plates, CFRP Jacket and Epoxy Fill for R-Calt-3.....	132
Figure 5-12 CFRP Strap Layout on Footing Faces for R-Calt-3 .....	133
Figure 5-13 Footing Trenching Procedure for R-Calt-3 .....	134
Figure 5-14 Column R-Calt-3 Before and After Grout Placement.....	135
Figure 5-15 Installation of CFRP Plates and CFRP Jacket for R-Calt-3.....	136
Figure 5-16 Material Testing Specimens of Epoxy with Gravel for R-Calt-3 .....	137
Figure 5-17 Column R-Calt-3 after Surface Preparation and CFRP Installation .....	138
Figure 5-18 Column R-Calt-3 after Completion of Repair Work.....	139
Figure 5-19 Test Setup of R-Calt-3 .....	140
Figure 5-20 Strain Gage Layout on CFRP Jacket for R-Calt-3.....	141
Figure 5-21 Strain Gage Layout on CFRP Plates for R-Calt-3 .....	142
Figure 5-22 Strain Gage Layout on CFRP Sheet of Footing for R-Calt-3 .....	143
Figure 6-1 Progressive Deformation of R-Calt-1 at Increasing Load Levels.....	154
Figure 6-2 Offset of R-Calt-3 Footing Observed at Drift Ratio of 1%.....	155
Figure 6-3 Damage to R-Calt-3 at Drift Ratio of 2% .....	156
Figure 6-4 Cracking in R-Calt-3 Footing at Drift Ratio of 3%.....	157
Figure 6-5 CFRP Rupture on Column Compression Side at Drift Ratio of 3% (R-Calt-3) .....	158
Figure 6-6 CFRP Rupture on Column Tension Side at Drift Ratio of 3% (R-Calt-3).....	159
Figure 6-7 Damage to Concrete of R-Calt-3.....	160
Figure 6-8 Damage to Reinforcing Bars for Calt-3 and R-Calt-3 .....	161
Figure 6-9 Rupture of CFRP Plates of R-Calt-3.....	162
Figure 6-10 Load-Displacement Hysteresis Responses of Calt-3 and R-Calt-3.....	163
Figure 6-11 Load-Deformation Envelopes of Calt-3 and R-Calt-3 .....	164
Figure 6-12 Idealized Envelopes of Load-Deformation .....	165
Figure 6-13 Energy Dissipation Per Cycle and Cumulative of Calt-3 and R-Calt-3.....	166
Figure 6-14 Measured Longitudinal Strain Profile of CFRP Jacket along Column Height of R-Calt-3 .....	167
Figure 6-15 Measured Transverse Strain Profile of CFRP Jacket along Column Height of R-Calt-3.....	168
Figure 6-16 Measured Longitudinal Strain Profile of CFRP Plates along Column Height of R-Calt-3 .....	169

Figure 6-17 CFRP Strain of Footing vs. Drift Ratio for R-Calt-3 .....170  
Figure 7-1 Installation and Failure of Bar Splice Tensile Tests of Shear-Lock Couplers .....185  
Figure 7-2 Installation and Failure of Bar Splice Tensile Tests of Swaged Couplers .....186  
Figure 7-3 Concrete/Grout Placement of Columns .....187  
Figure 7-4 Restoration Indices of Repair Methods.....188  
Figure 8-1 Repair Design Guide for RC Bridge Columns with Fractured Longitudinal Bars ....197

# 1. INTRODUCTION

## 1.1. PROBLEM STATEMENT

The use of interlocking spirals in reinforced concrete (RC) bridge columns with rectangular or oval cross sections has several advantages. Interlocking spirals confine the concrete more efficiently than rectangular hoops with cross ties, which can reduce the amount of transverse reinforcement required for effective confinement of core concrete. Also, RC columns with interlocking spirals are more easily fabricated than those with overlapping rectangular hoops with cross ties (Tanaka and Park 1993). During earthquakes, RC columns with interlocking spirals may experience damage such as cracking, spalling, or crushing of concrete, yielding of interlocking spirals, and/or yielding, buckling, or fracture of longitudinal reinforcing bars (Buckingham et al. 1993; Tanaka and Park 1993; Correal et al. 2007; Li and Belarbi 2011). For damaged columns that do not contain buckled or fractured longitudinal bars, repair techniques usually include epoxy injection of concrete cracks, replacement of loose concrete, and/or fiber reinforced polymer (FRP) wrapping (Saadatmanesh et al. 1997; Chang et al. 2004; Vosooghi and Saiidi 2012, 2013). For damaged columns with buckled or fractured longitudinal reinforcing bars, repair techniques may also include replacement of the damaged longitudinal bars, reinstallation of the transverse reinforcing bars, replacement of the damaged concrete, and restoration of the concrete confinement using externally bonded FRP or other confining materials (Lehman et al. 2001; Cheng et al. 2003; Saiidi and Cheng 2004; Belarbi et al. 2008; Shin et al. 2011; He et al. 2013; Rutledge et al. 2013).

Replacement of longitudinal bar segments can be achieved by mechanically splicing new bar segments to the existing bars with bar couplers. A reinforcing bar coupler is used to splice two bars together to transfer the axial force from one bar to the other. Bar couplers have shown promise in new construction, and especially in Accelerated Bridge Construction (ABC), to connect precast or cast-in-place (CIP) concrete members to other members (Marsh et al. 2011). In ABC, the couplers are preferably used in column-footing joints or column-cap beam joints for ease of construction. However, these preferred regions usually coincide with the plastic hinge regions that are designated to dissipate energy during earthquakes; thus significant energy dissipating and deformation capacity are required for bar couplers used in these regions. Currently, Caltrans does not permit the use of bar couplers in plastic hinge zones (Caltrans 2006), and limited research has been conducted on the performance of couplers under inelastic cyclic deformation (French et al. 1989; Bai et al. 2003; Rowell and Hager 2010). In column repair applications, replacement of longitudinal bar segments requires considerable effort. This aspect makes this technique less attractive if time to complete the repair is of critical importance. In some cases, such as with seismically detailed RC columns with interlocking spirals, it is not practical to reinstall internal transverse reinforcement; thus alternative solutions are needed to restore the performance of the column.

Restoration of confinement can be achieved using externally bonded FRP composites. Externally bonded FRP can also be used to strengthen RC members in flexure, shear, and/or torsion. Prefabricated FRP strips have been used to increase the flexural capacity of RC beams by externally bonding them to the tension side of the member (ACI 440 2008); they may also be used to compensate for the loss of strength due to the existence of fractured bars, provided they

can be adequately developed. However, little research has been reported on the application of prefabricated FRP strips in the repair of damaged RC columns with fractured bars. The use of externally bonded FRP composites has also shown promise as an emergency repair method due to ease of construction and rapid achievement of material strength (Saiidi and Cheng 2004; Belarbi et al. 2008; He et al. 2013; He et al. 2014; Rutledge et al. 2013). A wet-layup procedure is often used to apply the FRP, which involves concrete surface preparation, dry fiber saturation, wrapping of saturated fibers, and curing. In some cases where more than a few layers of FRP are required, the wet-layup procedure may take more than one day to complete and extend the time required to complete the repair. This aspect makes this procedure less attractive in an emergency repair. The wet-layup process also requires the replacement of any spalled concrete to create a smooth surface before the FRP is applied; this leads to further delay in the repair process.

## 1.2. PROJECT OBJECTIVE

The main objective of this study was to develop methods to repair earthquake-damaged RC bridge columns reinforced with interlocking spirals and containing buckled and/or fractured longitudinal bars with the purpose of restoring both the load and deformation capacity without reinstallation of internal transverse reinforcement. Methods are proposed for the cases of a permanent repair as well as an emergency repair.

As stated in the Emergency Relief Manual by the Federal Highway Administration (FHWA 2013), *“Emergency repairs are repairs made during and immediately following a disaster to restore essential traffic, to minimize the extent of damage, or to protect the remaining facilities. Permanent repairs are repairs undertaken, normally after emergency repairs have been*

*completed, to restore the highway to its pre-disaster condition.*” Considering this statement, a permanent repair to an earthquake-damaged RC column containing buckled and/or fractured longitudinal bars is likely to involve the repair to regions both within and outside the plastic hinge to restore the strength, stiffness, and deformation capacity to its original state. An emergency repair, on the other hand, may involve repair only to the plastic hinge region to limit the time and labor needed to prevent further damage and accommodate essential traffic for disaster mitigation.

The permanent repair method developed in this study included the use of bar couplers to mechanically splice new replacement bar segments to the existing longitudinal bars at each end of the plastic hinge region, and the application of a CFRP jacket. The interlocking spirals were removed from the plastic hinge region and were not replaced. Currently, Caltrans does not permit the use of bar couplers in plastic hinge zones (2006) because limited research has been conducted on the performance of couplers under inelastic cyclic deformation (French et al. 1989; Bai et al. 2003; Rowell and Hager 2010). The repair method developed in this study violates this restriction and helps provide information on the seismic performance of bar couplers in plastic hinge regions.

The emergency repair method developed in this study included the use of externally-bonded prefabricated carbon-FRP (CFRP) strips and a CFRP jacket in the column plastic hinge region that were embedded into the footing. This system was used to compensate for the strength loss. Buckled and/or fractured longitudinal reinforcing bars, as well as the interlocking spirals, were left untreated. This study provides experimental data on the use of prefabricated CFRP strips and

a jacket built from prefabricated thin CFRP laminate to restore the performance of RC columns with fractured longitudinal bars.

### 1.3. METHODOLOGY

The methods proposed in this project to repair earthquake-damaged RC bridge columns containing buckled and/or fractured longitudinal bars were developed and validated by large-scale experiments on RC column specimens subjected to combined loading conditions. Three half-scale prototype bridge columns with an oval-shaped cross section and interlocking spirals had been tested to failure in a previous study under slow reversed cyclic lateral loading resulting in bending, shear, and torsion, as well as a constant axial loading. The major testing variables in the previous study were the torsional moment-to-bending moment (T/M) ratio and whether the column was subjected to uniaxial or biaxial bending. The original columns were designed with the same geometric and reinforcement details. Two columns were subjected to uniaxial bending and T/M of 0.2 and 0.6, which were labeled in the present study as Calt-1 and Calt-2, respectively. The third column, labeled as Calt-3, was tested under biaxial bending with T/M of 0.2. Damage to the columns included concrete crushing, yielding and fracture of longitudinal reinforcement, and yielding of transverse reinforcement in the plastic hinge region, as well as concrete cracking and spalling outside the plastic hinge region.

Calt-1 and Calt-2 were designated to be repaired by a permanent repair scheme. Both Calt-1 and Calt-2 were repaired by removing and replacing segments of the circumferential longitudinal bars and applying an externally bonded CFRP jacket. Within the plastic hinge region, all concrete was removed, and the interlocking spirals were removed to facilitate the installation of

the replacement of bar segments. The replacement bar segments were spliced to the existing bars in the column and the footing with mechanical couplers. A different type of mechanical coupler was used in each column, both of which were approved by California Department of Transportation (Caltrans) for ultimate state. Sleeve lock couplers with shear bolts and sleeve swaged couplers were used in Calt-1 and Calt-2, respectively. No new internal transverse reinforcement was installed around the new replacement bars except within the coupler regions. After new concrete was cast, externally bonded unidirectional carbon fiber reinforced polymer (CFRP) composite was transversely wrapped around the column, with a different number of layers inside and outside the plastic hinge region. The repaired columns corresponding to Calt-1 and Calt-2 were labeled as R-Calt-1 and R-Calt-2, respectively.

The repair of Calt-3 was designated as an emergency repair, and the repair scheme was different from that of Calt-1 and Calt-2. The buckled and fractured longitudinal bars were not treated. Instead, unidirectional CFRP strips and a jacket built from prefabricated thin bidirectional CFRP laminate were installed to compensate for the loss of flexural, shear, and torsional capacity after replacement of damaged concrete with new grout. The CFRP strips and jacket were embedded within the footing to form a member socket column-footing connection (Marsh et al. 2011). The repaired column corresponding to Calt-3 was labeled as R-Calt-3.

The repaired columns were tested under the same loading protocol as the corresponding original columns. The cyclic behavior of the repaired columns under combined loading conditions was compared with that of the corresponding original columns to evaluate the effectiveness of the repair methods in terms of strength, stiffness, and ductility. Constructability and performance of the two types of repair methods utilized in this study were also examined.

#### 1.4. ORGANIZATION OF REPORT

This report is organized into eight chapters. Chapter 2 presents a review of the published literature relevant to this project. Chapter 3 presents the experimental work related to R-Calt-1 and R-Calt-2 including descriptions of the damage to the original columns, repair design, repair procedure, and the test program. Chapter 4 describes the experimental results of R-Calt-1 and R-Calt-2 including observed damage, load-deformation relationships, energy dissipation, and measured strains. Chapter 4 also compares the experiment results with those of the original columns. Chapter 5 presents the experimental work related to R-Calt-3 including descriptions of the damage to the original specimen, repair design, repair procedure, and the test program. Chapter 6 presents the experimental results of R-Calt-3 including the observed damage, load-deformation relationships, energy dissipation, and measured strains. Chapter 7 evaluates the constructability and seismic performance of the proposed repair methods. Chapter 8 summarizes conclusions from the work in this report, and lists recommendations for the repair design and procedure as well as aspects in need of further research.

## 2. LITERATURE REVIEW

This chapter presents a summary of the literature related to different aspects of this project. Section 2.1 presents a background of concrete bridge columns reinforced with interlocking spirals and their damage state after being subjected to earthquake loading. Section 2.2 summarizes and compares repair methods for damaged columns with buckled or fractured longitudinal bars. Section 2.3 describes the use of concrete filled FRP tubes (CFFT) in construction of RC bridge columns. Section 2.4 provides a background on seismic application of reinforcing bar (rebar) mechanical couplers.

### 2.1. RC BRIDGE COLUMNS WITH INTERLOCKING SPIRALS

As discussed in Chapter 1, the use of interlocking spiral reinforcement can provide efficient confinement and simplify fabrication of RC columns. Before the 1990s, the design of RC columns with interlocking spirals was based on experimental and theoretical studies of circular sections with single spirals or circular hoops. As a result, recent research has been conducted to study the behavior of RC columns with interlocking spirals to fill in this gap.

Tanaka and Park (1993) tested four columns, three of which were reinforced with interlocking spirals, under constant axial and reversed cyclic lateral load. One column had a rectangular cross section, while the other three had an oval-shaped cross section. The rectangular column had transverse reinforcement consisting of closed ties and cross-ties. The cross sectional dimensions of the columns were 24 in.  $\times$  16 in. (600 mm  $\times$  400 mm), and the height was 71 in. (1784 mm). The volumetric ratio of the transverse reinforcement was 2.17% for the rectangular column and

1.08%, 0.92%, or 1.15% for the oval columns. For the columns with interlocking spirals, all columns experienced yielding of the spirals during testing. The columns with interlocking spirals were tested until fracture of the spiral occurred. Yielding of the transverse reinforcement in the rectangular column was not observed during testing. Buckling of longitudinal bars occurred eventually in all columns. Each column had a displacement ductility factor of at least 10.

Correal, et al. (2007) studied the experimental behavior of six oval-shaped columns with interlocking spirals with different scale factors, shear indices, and volumetric ratios of transverse reinforcement tested under shake table loading. Two of the columns had scale factor of 0.25, a shear index of 0.3, and a volumetric ratio of transverse reinforcement of 1.1%. The other four had scale factor of 0.2, a shear index of 0.7, and a volumetric ratio of transverse reinforcement of either 0.6% or 0.9%. The cross sections varied from 14.5 in.  $\times$  10 in. (368 mm  $\times$  254 mm) to 20.25 in.  $\times$  12 in. (514  $\times$  305 mm), and the height of columns varied from 58 in. (1473 mm) to 72 in. (1829 mm). Each column was subjected to dynamic load until failure. For columns with low shear, damage included spalling of concrete near bottom of columns, fracture of spirals, and buckling of longitudinal bars. For columns with high shear, damage included extended diagonal cracks, spalling of concrete, fracture of spirals, and fracture or buckling of longitudinal bars.

Li and Belarbi (2011) investigated the behavior of six 1/2-scale oval-shaped columns reinforced with interlocking spirals under constant axial load and reversed cyclic lateral load and twist. The columns were designed with the same geometric dimensions and reinforcement details. The cross section was 36 in.  $\times$  24 in. (915  $\times$  610 mm), and the column height was 132 in. (3350 mm). The longitudinal reinforcement ratio was 2.13%, and the volumetric ratio of the transverse reinforcement was 1.32%. One of the columns was tested under pure torsional loading to failure

at which crushing of core concrete, yielding of spirals and longitudinal reinforcement, and twisting of longitudinal reinforcement were observed. Two of the columns were tested under combined uniaxial bending and torsion with torsional moment-to-bending moment ratios (T/M) of 0.2 and 0.6, respectively. The failure modes and damage of these columns are described in detail in Section 3.1. The remaining three columns were tested under combined biaxial bending and torsional loadings with T/M ratios of 0, 0.2 and 0.4. The failure mode and damage of the column under biaxial bending with T/M ratio of 0.2 is described in Section 5.1. The columns under biaxial bending with T/M ratios of 0 and 0.4 experienced spalling and crushing of concrete, buckling and/or fracture of longitudinal bars, yielding of spirals, and also extensive cracks in footings.

## 2.2. REPAIR METHODS FOR DAMAGED RC BRIDGE COLUMNS

RC bridge columns may experience complex combined axial, shear, bending, and torsional loading during an earthquake. The resulting apparent damage may include cracking or spalling of concrete cover, crushing of the concrete core, and buckling and/or fracture of reinforcement. The existence of fractured longitudinal bars constitutes severe damage to RC columns, and furthermore poses additional challenges associated with treatment of those bars to restore the capacity. Studies on the repair of RC bridge columns with buckled and/or fractured longitudinal bars are discussed in the paragraphs that follow. Studies on that include fractured longitudinal bars are summarized in Table 2.1.

Saadatmanesh, et al. (1997) conducted a study on repairing earthquake-damaged RC columns with prefabricated GFRP composite straps. The specimens included four 1/5-scale RC columns

with seismic deficiencies. Two of the columns had a circular cross section, and two had a rectangular cross section. The columns were tested to failure under reversed cyclic lateral loading and constant axial load. At the end of the initial tests, the columns experienced severe damage including debonding of starter bars, spalling and crushing of concrete, buckling of longitudinal reinforcement, and separation of the longitudinal bars from the core concrete. The repair procedure consisted of casting fresh concrete after removing spalled and damaged concrete in the failure regions, and applying active confinement with FRP. To apply active confinement, spacers were bonded to the finished surface of the columns to create a gap. The column was then wrapped with FRP sheets. Epoxy grout was pressurized in the gap between the column and the sheets to apply active confining pressure on the column. Test results indicated that the repair technique was effective in restoring both the flexural strength and displacement ductility, which were higher than those of the as-built columns. In all repaired specimens, the initial stiffness was lower than that of the as-built column, however, the stiffness deterioration under large loading cycles was lower than that of the corresponding as-built columns.

In a study by Chang, et al. (2004), the seismic performance of two damaged 2/5-scale rectangular bridge columns were effectively restored with a CFRP jacket. The two columns were seismically-detailed, so there was no specific structural deficiency. The two columns were tested to failure under pseudo dynamic loading. Flexural failure occurred in the plastic hinge zone, and none of the longitudinal reinforcing bars fractured. The repair of the plastic hinge zone was based on force-based design. Additionally, a single layer of CFRP was wrapped around the remainder of the column to provide external confinement. Test results showed that the strength and ductility of the columns were successfully restored. However, the initial stiffness of repaired

columns was smaller than that of the as-built columns, which was attributed to the fact that the CFRP did not bridge the cracks near the column-footing joint, and the yielding of longitudinal bars may have penetrated into the footing.

Belarbi et al. (2008) repaired a 1/2-scale circular RC bridge column that was severely damaged under constant axial load (axial load index of 7%) and cyclic lateral and torsional loading using externally bonded CFRP. Damage to the column included spalled cover concrete, crushed core concrete, and buckled longitudinal reinforcing bars. The damaged column was repaired using externally bonded CFRP with fibers oriented both in the column longitudinal and transverse directions. A mechanical anchorage system was used in an attempt to anchor the longitudinal CFRP sheets to the footing. It was concluded from the test results that the repair method could restore and enhance the flexural, torsional, and axial capacity of the column. It was also concluded that the longitudinal CFRP sheets may not have been required in the repair since they pulled out from the footing at low load levels.

Vosooghi and Saiidi (2012) proposed a method using CFRP jackets to rapidly repair circular RC columns with apparent damage corresponding to flexural cracks; minimal spalling and possible shear cracks; extensive cracks and spalling; visible longitudinal and transverse reinforcement; and compressive failure of the concrete core, excluding fracture of reinforcement. The repair procedure included straightening of the column, removal of loose concrete, concrete repair, epoxy injection, surface preparation, CFRP wrapping, and accelerated curing of the CFRP jacket. In their method, yielded spirals were assumed to contribute to the shear strength of the damaged column, while their contribution to confinement was considered to be negligible. They also proposed a softened material model for damaged longitudinal reinforcement to account for the

contribution to the flexural strength of damaged columns. Their method succeeded in restoring both the shear strength and displacement capacity. They also reported the reduced initial stiffness of repaired columns as compared with original columns.

Vosooghi et al. (2008) used CFRP wrap to repair the middle bent of a 1/4-scale two-span bridge model, which was tested to the condition including visible bars, initial buckling in some longitudinal bars, and initial concrete core damage. The columns had a circular cross section. The bridge specimen was tested under near-field motions increasing gradually with simulating the fault rupture, followed by static loading to increase the damage level. The damaged columns were repaired by CFRP wrapping after repair of the damaged concrete with a fast-set grout and epoxy injection of the adjacent cracks. Retesting of the repaired columns showed that the lateral load capacity and the ductility of the bent were fully restored, and the service level stiffness was nearly restored to that of the undamaged bent stiffness.

Vosooghi and Saiidi (2009) reported repairing two high shear, standard RC bridge columns using CFRP jackets. The 1/3-scale seismically detailed circular RC bridge columns with spiral reinforcement were tested to near failure on a shake table. The apparent damage included visible spirals and longitudinal bars, buckled longitudinal bars, and damage of core concrete. For both columns, the damaged concrete was replaced by a fast-set non-shrink mortar, and the cracks were epoxy injected. The two damaged columns were repaired with a different number of CFRP layers and different repair mortar and application methods. Test results indicated that the repair design method fully restored the lateral load and drift capacity of the columns, although the service stiffness was not fully restored. Results also suggested that the spirals were able to contribute to the shear capacity, even though they yielded in the initial tests.

Lehman et al. (2001) reported repair methods for three severely damaged circular RC columns using mechanical couplers, headed bars, or a RC jacket. The columns were 1/3-scale and had different longitudinal reinforcement ratios of 0.75% (407S), 1.5% (415S), and 3% (430S). The as-built columns were tested under a constant axial load (7% of the axial capacity) and cyclic lateral load with increasing levels of displacement until failure. The columns sustained damage to the concrete, the longitudinal reinforcement, and the spiral reinforcement. Three different repair schemes were used considering the nature of damage and details of the as-built columns. Column 407S was repaired by removing and replacing the damaged region, which involved mechanically severing the damaged region, splicing new longitudinal reinforcing bars to the existing bars in both the column and footing with mechanical couplers, placing new spiral reinforcement, and casting new concrete. The repaired column developed comparable stiffness and exhibited higher strength and deformation capacities than the as-built column. Column 415S was repaired by casting a concrete jacket reinforced with headed longitudinal bars along the damage region, so that the flexural plastic hinge was relocated from the base of the column to the region immediately above the jacketed region. The stiffness and strength of the repaired column were comparable to those of the as-built column; however the deformation capacity was reduced, which was attributed to the shorter effective column length. For Column 430S, the repair scheme also included a RC jacket but with the plastic hinge remaining within the jacket at the base of the column. All existing bars were severed at the base of the column, and new reinforcement was provided in the jacket. Tests showed that flexural hinging occurred at the column base, as intended. The deformation capacity of the column, however, was less than that of the as-built column, which may have been due to the reduced longitudinal reinforcement ratio at the base after the jacket was installed.

Cheng et al. (2003) reported a method to repair RC columns with fractured longitudinal bars using dog-bone shaped steel plates and a FRP jacket. Their study included two full-size hollow columns with a circular cross section. The columns were tested to failure under cyclic lateral load with increasing levels of displacement and a constant axial load (10% of the axial capacity). One of the columns failed in flexural with concentrated damage including fractured outer layer longitudinal bars, buckled inner layer bars, and crushed concrete through the thickness of the column wall. The other column was damaged with the outer layer bars fractured at the column hinge and diagonal shear cracks across the mid-height of the column wall, which indicated a flexural-shear failure mode. Dog-bone shaped bars were used to replace the fractured and buckled longitudinal bars in outer layer of cross sections within the plastic hinge, and FRP wrap was used to enhance the deformation capacity of columns. The repair upgraded the failure mode of flexural-shear to flexure-dominant failure mode. The strength of the repaired columns was lower than that of the as-built columns since the inner layer of buckled longitudinal reinforcing bars was not repaired. The ductility of the repaired columns was also lower than that of the as-built columns, although the displacement capacity was increased.

Saiidi and Cheng (2004) proposed a rapid repair method for RC columns containing fractured longitudinal bars using externally bonded FRP with fibers oriented in both the longitudinal and transverse directions of the column. In their study, two 0.4-scale flared columns with different reinforcement ratios were repaired. The cross-sectional dimensions varied along the height of the columns. The columns had been retrofitted with steel jackets and tested to failure under cyclic loading in a previous study. The two columns were tested under cyclic lateral load with increasing levels of displacement and a constant axial load corresponding to 16% of the axial

capacity of the columns. Because of the flared shape of the columns, the longitudinal bars fractured a distance away from the base of the column. To repair the columns, damaged concrete within and near the plastic hinge was removed and replaced with high-strength, low-shrinkage grout. The fractured longitudinal reinforcing bars were left untreated, and unidirectional GFRP and CFRP sheets with fibers orientated along the longitudinal axis of the column were applied to compensate for the flexural strength loss of the fractured bars. The longitudinal FRP was designed to provide the same tensile strength as the yield force of the fractured bars and divided equally between GFRP and CFRP laminates. Because the critical section was located a distance away from the base of the column, adequate length was available to develop the FRP. GFRP sheets were also wrapped around the column to provide shear strength and confinement. Test results showed that the repaired columns developed strength comparable to that of similar undamaged RC columns retrofitted with steel jackets; however, the ductility of the repaired columns was lower than that of similar retrofitted columns.

Shape memory alloy (SMA) was used in a study by Shin and Andrawes (2011) to rapidly repair two 1/3-scale severely damaged circular RC columns. The first column was tested under constant axial load (5% of the axial load capacity) and quasi-static lateral cyclic loading until problems during testing resulted in an accidental increase in one direction from 1.5% to 7% drift ratio. The resulting damage was localized in the plastic hinge region with complete concrete crushing one side of the cross section and cracks at the other side. The longitudinal bars buckled but did not fracture. The repair technique included replacing damaged concrete with quick-setting mortar, straightening, cutting and reconnecting the severely buckled longitudinal bars with mechanical couplers, injecting cracks with epoxy, and wrapping the damaged region with prestrained SMA

wires. Retesting of the repaired column showed that lateral strength, stiffness, and flexural ductility were restored or improved, which was attributed to the ability of the SMA spirals to apply and maintain active confinement on the damaged region of the column and delay the progression of damage. The second column was tested under constant axial load (5% of the axial load capacity) and cyclic lateral load. The damage after the original test included crushed concrete, fractured longitudinal bars, and excessive opening of transverse reinforcement. The repair was accomplished by replacing the damaged concrete with quick-setting mortar, injecting epoxy in the cracks, connecting the fractured bars using rebar couplers, and wrapping the SMA spirals at the repaired region. Retesting the repaired column revealed that the lateral strength was fully restored, and the stiffness was higher than that of the original column. The overall displacement ductility was increased, though the displacement capacity was lower than that of the as-built column.

Three damaged RC bridge columns were repaired by plastic hinge relocation using CFRP with carbon fiber anchors in a study by Rutledge et al. (2013). The columns contained buckled longitudinal bars, and one of the columns also had fractured longitudinal bars. The circular columns were tested under a load history corresponding to specific earthquakes by controlling the lateral displacement applied to the top of the column in a static manner. A constant axial load was also applied (axial load ratio of 6%). Following the initial test, the second column was also subjected to additional cyclic “aftershock” loading in a static manner. To repair the first column, the original plastic hinge was strengthened with transverse and longitudinal CFRP anchored to the footing with carbon fiber anchors. Additionally, transverse fibers were wrapped around the expected new plastic hinge region to achieve higher curvature at the new plastic hinge location

so that the displacement capacity at the top of the column could be restored. Testing of the first repaired column under constant axial load and reversed cyclic lateral displacements indicated an increase in lateral force capacity compared to that of the original column. However, the plastic hinge region did not form in the intended location, which was attributed to underestimation of the confinement provided by the hoop reinforcement. The repair of the second column was similar to that of the first column, except that no hoop fibers were provided for confinement of the expected new plastic hinge region. Testing of the repaired second column indicated a similar increase in strength with respect to the original column, and the plastic hinge was successfully relocated to the location intended. It was concluded that the repair was able to restore the initial stiffness, as well as increase the strength and displacement capacities. Repair of the third column was similar to that of the second column. Test results showed that the repaired column had an increased force and displacement capacity compared to the original column, and the initial stiffness was restored. However, rupture of the carbon fiber anchors was observed during testing. Therefore, the researchers recommended that application of this technique should be limited to columns without fractured bars.

He et al. (2013) rapidly repaired five 1/2-scale square standard bridge columns with different damage conditions using externally bonded CFRP with fibers orientated in the column longitudinal and transverse directions. The columns had been tested to failure under constant axial load (7% of the axial capacity) and combined cyclic lateral and torsional loading with different bending moment-to-torsional moment ratios (T/M). With increasing T/M, the damage region increased along the column height, and the plastic hinge location shifted away from the base. Damage included concrete cracking, cover concrete spalling, and core concrete crushing, as

well as longitudinal reinforcement yielding. Damaged ties failed by yielding and, in some cases, subsequent opening of end hooks. Additionally, longitudinal bars buckled in most of the columns, and longitudinal reinforcing bars fractured in one of the columns tested under lateral loading without torsion. Externally bonded CFRP was used to repair each of the damaged columns, and fractured and buckled bars were left untreated. Retesting of the repaired columns under the same combined loading as the corresponding original columns revealed that the repair method was effective in rapidly restoring the bending and/or torsional strength and ductility if there are no fractured longitudinal bars. The stiffness of the columns was not completely restored, which was attributed to the damage accumulated and the fact that only a portion of the damaged columns was repaired.

### 2.3. CONCRETE FILLED FRP TUBES (CFFTs)

FRP tubes have been used as permanent stay-in-place formwork since the 1990s. The use of FRP tubes can eliminate formwork and the need for its removal, provide high-strength reinforcement to the concrete member, and protect concrete in a corrosive environment. Concrete can be cast in the FRP tubes to make beam-column members. Researchers have extensively investigated the behavior of concrete filled FRP tubes (CFFT) under monotonic and cyclic loading conditions.

Mirmiran, et al. (1999) tested five CFFTs under combined axial and lateral loadings and developed a full moment-thrust interaction diagram for hybrid columns. The CFFTs were square with a cross-sectional dimension of 7 in. (176 mm) and a length of 52 in. (1320 mm). The tubes were comprised of the one interior ply of bidirectional 24-oz E-glass woven roving on the four sides, and 15 E-glass angle plies with a winding angle of  $\pm 75^\circ$ . Longitudinal and transverse ribs

were included along the interior faces of the tubes, which served connectors between the concrete and FRP tube. No internal reinforcing bars were included in the specimens. Test results showed that CFFT columns could provide the same strength as equivalent conventional RC columns with up to 6% reinforcement. The failure of CFFT columns was reportedly ductile; and the ductility was comparable to conventional RC columns.

Shao and Mirmiran (2005) conducted an experimental study on circular CFFTs subjected to constant axial loading and cyclic lateral loading in four-point flexure. A total of six CFFT beam-column specimens were included with two types of tubes. The first type had a wall thickness of 0.5 in. (12.7 mm), an outside diameter of 12 in. (305 mm), and 40 layers in a symmetric layup of  $0^\circ$  and  $\pm 45^\circ$ . The second had a wall thickness of 2 in. (51 mm), and an outside diameter of 21.7 in. (322 mm), and 17 layers in a symmetric layup of  $\pm 55^\circ$ . For each type of tube, one specimen was prepared with no internal reinforcement within its midspan region, the other two incorporated longitudinal reinforcement resulting in steel reinforcement ratios of either 1.7 or 2.5%. All specimens were reinforced in the shear span to ensure a flexural mode of failure. The test results showed that CFFT columns can be designed with ductility comparable to that of RC columns. Additionally, it was concluded that a moderate amount of internal steel reinforcement (1%-2%) may further improve the cyclic behavior of CFFTs.

Zhu, et al. (2006) studied the seismic performance of CFFT column-footing subassemblies with three types of column-footing connections. One type was comprised of a cast-in-place CFFT column with starter bars extending from the footing. The second type included a precast CFFT column with grouted starter bars extending from the footing that were inserted into grouted ducts. The third type included a precast CFFT column post-tensioned to its footing with unbonded high

strength threaded rods. Each column had the same geometry and reinforcement consisting of four No. 5 (15.9 mm dia.) and four No. 6 (19.1 mm dia.) bars in the longitudinal direction as well as No. 4 (12.7 mm dia.) spirals with a diameter of 8.5 in. (216 mm) in the transverse direction. The FRP tubes were made by filament winding with  $\pm 55^\circ$  E-glass fibers and epoxy resin with an inside diameter of 12.3 in. (312 mm) and a wall thickness of 0.2 in. (5 mm). The FRP tube for the precast columns was embedded into the footing to provide sufficient development length, while the concrete surface of the cast-in-place CFFT column inside the tube was left lower than the footing surface to achieve better continuity of the column-footing joint. Each CFFT column was tested under constant axial load and a reverse cyclic displacement history in a number of incremental steps. Results suggested that the CFFT columns performed better in terms of strength and ductility than the companion RC column provided the FRP tubes were securely embedded in the footing.

Fam, et al. (2007) investigated the performance of FRP tubes as an alternative to embedded steel spirals. In their study, six beam column specimens were tested with varied diameter, shear span, and type of FRP. Two types of filament-wound E-glass/epoxy GFRP tubes were investigated, one of which had a diameter of 12.75 in. (324 mm) and a wall thickness of 0.2 in. (5 mm), and the other had a diameter of 8.6 in. (219 mm) and a wall thickness of 0.125 in. (3 mm). The first was composed of nine layers with [88/8/88/8/88/8/88/8/88] stacking sequence, and the second was composed of eight layers with [88/5/88/88/5/88/5/88] stacking sequence. The specimens were divided into three groups, each of which included a control RC specimen and a CFFT specimen. The control specimens were reinforced with spirals having the same circumferential stiffness as the FRP tubes. Columns in the first group were also reinforced with eight

pretensioned 0.5 in. (13 mm) 7-wire strands as longitudinal reinforcement, and the CFFT in the first group had the thicker tube. Columns in both the second and third groups were reinforced with six 0.63 in. (16 mm) diameter bars as longitudinal reinforcement, and the CFFT columns had the thinner FRP tubes. Columns in the second group had a diameter of 8 in. (203 mm) and a length of 86.6 in. (2200 mm). Columns in the third group had a length of 17.3 in. (440 mm) with the same diameter as those in the second group. Columns in the first and second groups were tested to failure in failure using four-point flexure test, while columns in the third group were tested to failure in shear using three-point flexure test. Test results showed that concrete filled FRP tubes with internal reinforcement and loaded in bending could fail in a progressive and sequential manner, leading to pseudo-ductile behavior. The researchers also concluded that FRP tubes were effective in shear.

Ozbakkaloglu and Saatcioglu (2007) studied the use of stay-in-place FRP formwork as concrete confinement reinforcement for high-strength concrete columns with a square section. In their study, six large-scale specimens were tested. Each specimen consisted of a 10.6 in. (270 mm) square section. The shear span for each column was 78.7 in. (2000 mm). The columns were reinforced with varied number of longitudinal bars without transverse reinforcement. Formwork with or without crossties for all columns was made from CFRP with all fibers aligned in the circumferential/transverse direction. Each column was tested under constant axial load and incrementally increasing cyclic lateral load. The test results showed that high-strength concrete columns confined by carbon CFRP stay-in-place formwork can develop ductile behavior, and the use of FRP crossties improved the efficiency of CFRP stay-in-place formwork.

Sadeghian, et al. (2011) proposed a new CFFT column- footing moment connection by fitting the tube and adhesively bonding it to a short reinforced concrete stub protruding from the footing. After testing several specimens with varied height of the stub, they found that the minimum height of stub required to achieve flexural failure in the CFFT was 1.05 times the diameter of the tube. Their specimens consisted of a CFFT column with outer diameter of 6.65 in. (169 mm) and inner diameter of 6.37 in (162 mm) and a stub with diameter of 6.25 in. (159 mm). The shear span for all specimens was 51.18 in. (1300 mm). The tubes consisted of nine layers of GFRP with wall thickness of 0.138 in. (3.5 mm) in alternate angles of  $9^\circ$  and  $-86^\circ$  with respect to the column longitudinal axis. They also tested two specimens with a stub higher than required length under cyclic lateral loading or combined constant axial compression and cyclic lateral loading. Based on the cyclic test results, they concluded that the CFFT column without axial compression could reach a ductility ratio of 5 with no strength degradation, while the CFFT column with a small amount of axial compression could have a higher lateral strength and more stable cyclic behavior.

Sadeghian and Fam (2011) proposed an analytical method to determine the required embedment length for a moment connection between the CFFT column and footing, which involves direct embedment of the CFFT into footing or column cap without using dowel-bar reinforcement. They also conducted a parametric study on factors that influence the required embedment length, which showed that increasing bond strength between the FRP tube and concrete footing or the compressive strength of the footing reduces the required embedment length. They also concluded that higher compressive strength of concrete encased in FRP tubes or higher longitudinal

strength of the tubes required longer embedment length due to the increased force transfer, and that increasing axial compression reduces the embedment length.

#### 2.4. REBAR COUPLERS IN SEISMIC APPLICATIONS

A rebar coupler is used to splice two bars together to transfer the axial force from one bar to the other. Rebar couplers have been widely used in practice; however, their performance under cyclic loadings has not yet been well documented. Caltrans (2013) listed the types of rebar couplers for ASTM A706 reinforcing bars that are prequalified for service and ultimate limit states. The most common types include swaged sleeve, forged sleeve, sleeve with lock shear bolts, sleeve with tapered thread, sleeve with metal filler, and sleeve with grout filler couplers. Since the 1980s, researchers have been studying the performance of these types of couplers in seismic applications.

French, et al. (1989) used sleeve with thread and sleeve with tapered thread couplers to splice threaded bars within the plastic hinge region in their proposed beam-column connections. The specimens included a precast column and a precast, partially prestressed beam and were tested under cyclic loading. Based on test results, they concluded that the threaded rebar connection with sleeve-tapered thread couplers had a behavior similar to ordinary reinforced concrete.

Bai, et al. (2003) summarized the standard criteria for rebar couplers in seismic applications. They mentioned that the rebar couplers should satisfy requirements in both static and seismic conditions. In static conditions, the strength of couplers should exceed that of the rebar, and slippage between coupler and rebar should be less than the permissible crack width in the service limit state. To evaluate the seismic performance of rebar couplers, slippage within the couplers

should be determined by testing the samplers under both elastic and plastic cyclic tests conditions.

Rowell and Hager (2010) reported the experimental tests of five types of rebar couplers under high strain rates. The five types of couplers included sleeve with straight thread and upset-head, sleeve with grout filler, sleeve with shear bolts, sleeve with tapered thread, and thread-like deformed reinforcing bar coupler system. The specimens were tested under strain rates from 0.001/sec to 3.5/sec. The failure of the sleeves with grout filler occurred within the sleeves, while the failure of other types of couplers occurred where the process to make the connection was required. Their test results also showed that the threaded rebar coupler performed the best in terms of the dynamic ultimate strength, maximum strain, and ductility ratio.

Marsh (2011) summarized the advantages and disadvantages of types of rebar couplers in the precast concrete industry. He mentioned that couplers could be used as connections for column to footing, splices between column segments or cap beam segments, and connections for column to cap beam. He also pointed out several areas in need of further research such as inelastic cyclic performance-drift capacity of members spliced with couplers, influence of coupler on bar strain distribution, and influence of coupler location and orientation on inelastic performance.

Billah and Alam (2012) analyzed four columns containing rebar couplers under selected earthquakes. The columns were 126 in. (3200 mm) high with a 17.7 in. (450 mm) square cross section. The columns were reinforced with either stainless steel or FRP bars in the non-plastic hinge region and either stainless steel or shape memory alloy (SMA) bars within the plastic hinge region. The bars in the non-plastic hinge region and bars inside the plastic hinge region were spliced with mechanical couplers or mechanical-adhesive couplers. They also obtained the

stress-slip relationships for the three types of couplers used in their specimens using pull-out tests and developed a bond-slip model to implement the behavior of the couplers. The analytical results showed that the SMA - FRP and SMA - SS combinations had better energy dissipation than the SS - SS combination because of significant slippage of the FRP and SMA bars inside the coupler. Furthermore, the hysteretic loops of the SS - FRP combination were larger than those of the SMA combinations.

Table 2-1 Summary of Studies on Repair of Reinforced Concrete Columns with Fractured Longitudinal Bars

Reference	Scale	Cross-Section Shape	Axial Load Index	Lateral Load Type	Brief Description of Apparent Damage/Failure	Repair Method	Strength	Displacement Ductility	Stiffness
Lehman et al. (2001)	1/3	Circular	7%	Cyclic lateral loading	Buckled longitudinal bars; fractured longitudinal and spiral bars	Severed damaged region; spliced new longitudinal bars connected to the footing and column with mechanical couplers; placed new spirals; cast new concrete	Enhanced	Enhanced	Restored
						Installed RC jacket reinforced with headed longitudinal bars (relocation of the plastic hinge)	Restored	Lower	Restored
						Severed all existing bars in the plastic hinge to maintain plastic hinge location; provided RC jacket with replacement bars	Lower	Lower	Not reported
Cheng et al. (2003)	Full	Hollow circular	10%	Cyclic lateral loading	Buckled and fractured longitudinal bars; crushed concrete	Repaired concrete; repaired fractured longitudinal bars with dog-bone welded steel plate; replaced transverse bar; installed EB transverse FRP	Lower	Lower	Not reported
Saïdi & Cheng (2004)	2/5	Flared	16%	Cyclic lateral loading	Fractured longitudinal bars; crushed concrete	Repaired concrete; installed EB longitudinal CFRP and GFRP; installed EB transverse GFRP	Restored or enhanced	Lower	Restored
Shin and Andrawes (2011)	1/3	circular	5%	Cyclic lateral loading	Buckled and fractured longitudinal bars; crushed concrete	Repaired concrete; reconnected longitudinal bars with mechanical couplers; installed SMA wrap	Restored or enhanced	Enhanced	Enhanced
He et al. (2013)	1/2	Square	7%	Cyclic lateral loading	Buckled and fractured longitudinal bars; crushed concrete	Repaired concrete; installed EB longitudinal CFRP with anchorage system; installed EB transverse CFRP	Lower	Lower	Lower
Rutledge et al. (2013)	-	Circular	6%	*Cyclic lateral loading	Buckled and fractured longitudinal bars; crushed concrete	Repaired concrete; relocated the plastic hinge using EB longitudinal CFRP with CFRP anchors, installed EB transverse CFRP	Enhanced	Restored	Restored

Note: \* The loading history used in the original study corresponded to specific earthquake load history, applied by controlling the lateral displacement applied to the top of the column in a static manner.

### 3. EXPERIMENTAL WORK OF R-CALT-1 AND R-CALT-2

The purpose of the experimental work of R-Calt-1 and R-Calt-2 was to develop a permanent repair method for earthquake-damaged concrete bridge columns reinforced with interlocking spirals containing buckled and/or fractured longitudinal bars using replacement bar segments and an externally bonded CFRP jacket. The experimental program included two 1/2-scale oval bridge columns that had been tested to failure in a previous study (Li and Belarbi 2011). After the previous test, the columns were damaged with buckled and/or fractured longitudinal bars, and cracked and crushed concrete. These columns were tested to failure under combined axial, shear, bending, and torsion with varied torsional moment-to-bending moment ratios (T/M). The background of the columns is described in Section 3.1. Repair design and procedure are described in Sections 3.2 and 3.3, respectively. The damage to the longitudinal bars was repaired with the application of new replacement bars attached with mechanical couplers. The loss of shear and torsion capacity due to damage or removal of interlocking spirals was compensated by adding externally bonded CFRP. The test program is discussed in Section 3.4 including test setup, instrumentation, and loading protocol.

#### 3.1. ORIGINAL COLUMN SPECIMENS

The experimental work discussed in Chapters 3 and 4 was conducted with two 1/2-scale oval-shaped RC bridge columns that were tested to failure under constant axial loading and cyclic lateral loading resulting in bending moment, shear, and torsional moment in a previous study (Li

and Belarbi 2011). This section describes the objective of the previous study, the original column specimens, and the damage to these specimens prior the repair conducted in the current study.

### 3.1.1. Previous test program

The previous study was focused on the seismic performance of RC bridge columns under combined loading of bending moment, shear, and torsional moment. Both columns were designed with the same geometric and material properties, and the primary test variable was the torsional moment-to-bending moment (T/M) ratio. The test specimens were designed to represent typical existing bridge columns as shown in Figure 3-1.

The columns had an oval-shaped cross section of 24 in. x 36 in. (610 mm x 915 mm), and the clear concrete cover to the spiral reinforcement was 1 in. (25 mm). The total height of the specimen was 166 in. (4.2 m) with an effective height of 132 in. (3.35 m) measured from the top of footing to the centerline of applied loads. Thus, the aspect ratio was 5.5. Twenty No. 8 bars (25.4 mm dia.) provided longitudinal reinforcement with a reinforcement ratio of 2.13%. Interlocking spiral reinforcement was provided by No. 4 bars (12.5 mm dia.) with a pitch of 2.75 in. (70 mm) resulting in a transverse reinforcement volumetric ratio of 1.32%. The measured yield strength of the longitudinal and tie reinforcing bars was 76 ksi (524 MPa) and 61 ksi (424 MPa), respectively. Reinforcing bars were ASTM A706 Gr. 60. Table 3-1 summarizes the mechanical properties of the reinforcing steel bars in the test specimens. Table 3-2 shows the concrete compressive strengths measured at 28 days and the test day in accordance with ASTM C39-04 using 6 in. x 12 in. (150 mm x 300 mm) cylinders.

The two columns are referred to in this chapter as Calt-1 and Calt-2 and were tested under combined loading with T/M ratios of 0.2 and 0.6, respectively. The combination of bending

moment, shear, and torsional moment loadings was applied using two hydraulic MTS actuators connected to the loading cap of the columns with steel loading frames as shown in Figure 3-2a. The lateral load was applied perpendicular to the weak axis of the cross-section. A constant axial load of 220 kips (979 kN), equivalent to 7% of the axial capacity of the column, was applied with 7 prestressing strands through a PVC pipe located at the axial centerline of the column that were post-tensioned by a hydraulic jack at the top of the column and an anchorage system at the bottom of the footing.

During testing, ten levels of force-control loading were applied to specimens up to the estimated first yielding point of either the longitudinal or transverse reinforcement with the increment corresponding to 10% of the predicted first yielding force (either bending moment or torsional moment). Each force-control level was applied for one reversed cycle. After the first yielding point, several levels of displacement-control loading were applied to the specimens up to the failure of the specimen with each level corresponding to multiples of the displacement (either top displacement or twist) at the first yielding point. Each displacement-control level was applied for three reversed cycles. The loading protocols for Calt-1 and Calt-2 are shown in Figure 3-3. It should be noted that values of the lateral force or torsional moment are not illustrated in this figure; instead, the top displacement or twist corresponding to the applied forces during the force-control phase is shown in this figure.

### 3.1.2. Damage to Calt-1 and Calt-2

After the original tests, the damage to Calt-1 and Calt-2 was determined by visual inspection and analysis of measured data. This section describes damage to the columns including the measured length of concrete spalling and depth of concrete crushing, fracture location and buckled region

of longitudinal reinforcement, and yielding region of both the longitudinal and transverse reinforcement.

As shown in Figure 3-4a, for Calt-1 with T/M of 0.2, the cover concrete spalled from the column base to a height of 37 in. (940 mm). Concrete near the column base crushed into the core with a depth of 6 in. to 10 in. (150 mm to 250 mm). The definitions of the spalled length and core crushing depth of concrete are shown in Figure 3-5. Spirals swelled at three different locations (refer to Figure 3-4a). Six of the longitudinal bars buckled, and eight fractured (refer to Figure 3-6). The fracture locations and buckled regions of longitudinal reinforcement are shown in Figure 3-6.

Strain gages were applied at various locations along the length of the longitudinal reinforcing bars during the original testing, see Figure 3-8. Typical longitudinal reinforcement strain history is shown in Figure 3-9, and typical transverse reinforcement strain history is shown in Figure 3-10. Based on analysis of the measured strain data, all of the longitudinal bars yielded during the original test. Yielding of the longitudinal bars was indicated by strain gages located in the region 4.0 in. to 45.25 in. (100 mm to 1150 mm) above the top of footing. It should be noted that the yielding may also have occurred within the footing but could not be verified since no strain gages were installed on the portion of the bars inside the footing. Yielding of the spirals was indicated by strain gages located in the region 20.5 in. to 37.0 in. (520 mm to 940 mm) above the top of footing.

As shown in Figure 3-4b, for Calt-2 with T/M of 0.6, the cover concrete spalled from the column base to a height of 90 in. (2290 mm). Concrete near the column base crushed into the core with a depth of 12 in. (305 mm) (refer to Figure 3-5). No spirals swelled, and 14 of the 16

circumferential longitudinal bars buckled (none fractured) (refer to Figure 3-7). It should be noted that the four longitudinal bars within the core were also discovered to have buckled after removing the sound core concrete during repair. The buckled regions of longitudinal reinforcement are shown in Figure 3-7. Based on analysis of the measured strain data (refer to Figure 3-11), all of the longitudinal bars yielded. Yielding was indicated by strain gages located in the region 4.0 in. to 45.25 in. (100 mm to 1150 mm) above the top of footing. The yielding may also have penetrated into the footing but could not be verified because no strain gages were installed on the portion of the bars inside the footing. Yielding of the spirals was measured by strain gages located in the region 4.0 in. to 37.0 in. (100 mm to 940 mm) above the top of footing (refer to Figure 3-12).

### 3.2. REPAIR DESIGN

As shown in Figure 3-13, the repair scheme for Calt-1 and Calt-2 involved removal and replacement of the longitudinal bar segments within the plastic hinge with new bar segments spliced to the existing longitudinal bars with mechanical couplers. The repair goal for these two columns was to restore both the load and deformation capacities. Repair materials used in this project are described in Section 3.2.1. The mechanical couplers used in this project were approved by California Department of Transportation (Caltrans) for ultimate limit state. The repair design for the longitudinal reinforcement involved the determination of the region in need of replacement. As presented in Section 3.1.2, longitudinal reinforcement within the plastic hinge experienced yielding, fracture, and/or buckling, which reduces the load and deformation capacities; thus, the damaged portion of longitudinal reinforcement was designated to be replaced. The methodology to determine the replacement length is presented in Section 3.2.2. To

facilitate the replacement of longitudinal reinforcement within the plastic hinge region, the transverse reinforcement was removed and not reinstalled; thus, a CFRP jacket was designated to provide similar confinement, shear capacity, and torsional capacity as that of the removed spirals. Outside the plastic hinge region, extensive flexure-shear and torsional cracks were observed in the damaged columns (refer to Figure 3-4); thus, a CFRP jacket was also applied in this region to preclude further spalling of the concrete cover as well as premature shear or torsional failure in this region. The design to determine the required number of layers of CFRP for the regions within the plastic hinge and outside the plastic hinge is described in Section 3.2.3. The repaired columns were labeled R-Calt-1 and R-Calt-2 corresponding to original columns Calt-1 and Calt-2, respectively.

#### 3.2.1. Repair materials

Repair materials included uni-directional CFRP sheets (*Tyfo*<sup>®</sup> *SCH-41*), No. 8 (25.4 mm dia.) replacement longitudinal reinforcing bars, mechanical couplers, and new concrete with a design compressive strength of 5000 psi (34.5 MPa).

The design properties of CFRP provided by the manufacturer are: Young's modulus:  $E_j=11.9 \times 10^6$  psi (82.0 GPa); ultimate tensile strength:  $f_u=12.1 \times 10^4$  psi (834 MPa); ultimate tensile strain:  $\epsilon_{ult}=0.0085$ ; thickness of single layer: 0.04 in. (1 mm). The replacement longitudinal bar segments were ASTM A706 Gr 60. Measured properties of the replacement bar segments and the replacement concrete are summarized in in Table 3-1 and Table 3-2.

Different types of mechanical couplers were used in the repair of Calt-1 and Calt-2. To repair Calt-1, a shear bolt coupler was used, which was Lenton Lock B series for No. 8 (25.4 mm dia.) bars provided by Erico. To repair Calt-2, a swaged type coupler was used, which was BarSplice

XL for No. 8 (25.4 mm dia.) bars provided by BarSplice, Inc. Both couplers met the requirements for Type 2 mechanical splices in ACI 318 (2011) and are included in the Caltrans list of approved couplers for ultimate limit state (Caltrans, 2013).

### 3.2.2. Determination of replacement length

The length of plastic hinge region controlled the portion of the longitudinal bars that needed replacement. This section compares two empirical methods from the literature to determine the plastic hinge length with the results from strain data analysis.

The plastic hinge can be associated with the length of the yielded portion of longitudinal bars. As discussed in Section 3.1.2, yielding of longitudinal reinforcement of Calt-1 and Calt-2 was measured to a column height of 45.25 in. (1149 mm) in both columns. The depth of yielding penetration into the footing could not be determined with the strain data because strain data were not available inside the footing.

As proposed by Caltrans (2006), the plastic hinge region can also be estimated to be the largest of: 1.5 times the cross-sectional dimension in the direction of bending, the region of column where the moment exceeds 75% of the maximum plastic moment, and 0.25 of the length of column from the point of maximum moment to be point of contra-flexure. Using this method, the plastic region for these two columns can be estimated as the region up to a column height of 36 in. (914 mm).

Lehman et al. (2001) also proposed a method to estimate the length of the plastic hinge region given as follows:

$$L_{pl} = L_{flexure} + L_{tension} \quad (\text{Equation 3-1})$$

where  $L_{flexure}$  is the length due to flexure and  $L_{tension}$  is the length based on tension shift effect.

$L_{flexure}$  and  $L_{tension}$  can be computed from Equations 3-2 and 3-3:

$$L_{flexure} = L_{column} \left( 1 - \frac{M_y}{M_u} \right) \quad (\text{Equation 3-2})$$

where  $L_{column}$  is the length of the column;  $M_y$  is the yield moment; and  $M_u$  is the ultimate moment capacity of the column as determined from a moment curvature analysis.

$$L_{tension} = \frac{D_{column}}{\sqrt{3}} \quad (\text{Equation 3-3})$$

where  $D_{column}$  is the diameter of the column. Based on this method, the plastic hinge region can be estimated as the region from the top of footing to a column height of 42.9 in. (1090 mm).

Lehman's method provides a value close to the estimation by strain data; however, it should be noted that both the Caltrans method and Lehman's method are based on bending and do not include the effects of torsion. The use of strain data is the most accurate way to determine the plastic hinge length; however, in practical applications, strain data are usually unavailable, and an empirical method is usually more attractive especially in cases in which a quick repair is needed. Because the Caltrans method is the most convenient to use and would likely be used in field applications, it was used to determine the plastic hinge length in both Calt-1 and Calt-2. For this reason, as well as for constructability, the longitudinal bars were severed and replaced from the base of the column to a height of 36 in. (914 mm) above the base.

### 3.2.3. Design of externally bonded CFRP jacket

The externally bonded CFRP jacket was designed for confinement, shear, and torsion independently.

Design for confinement was conducted for the plastic hinge region. The required number of layers of CFRP was designed to provide confinement that was equivalent to that of the removed interlocking spirals. Sectional analysis was conducted for the original and repaired sections to compare moment-curvature behavior for the selection of CFRP layers. Design for shear was conducted using the method proposed by Vosooghi and Saiidi (2012) for the regions inside and outside the plastic hinge with the goal of restoring the plastic shear strength of the original column. Inside the plastic hinge region, the shear strength was designed to be provided by the full shear strength of the replaced concrete and the CFRP wrap. Outside the plastic hinge region, the shear strength was designed to be provided by a reduced shear strength of the concrete (because of existing cracking) (Vosooghi and Saiidi 2012), the spiral reinforcement, and the CFRP wrap. Design for torsion was conducted using NCHRP (2010) provisions for the regions inside and outside the plastic hinge with the goal of restoring the torsional strength of the original column. Inside the plastic hinge region, the thickness of CFRP was designed to provide the same torsional strength as that provided by the spirals in the original columns. Outside the plastic hinge region, the torsional strength was designed to be provided by the spirals and the CFRP. Finally, the thickness (number of layers) of CFRP inside and outside the plastic hinge region was designed based on the larger of that required for the confinement and shear. The CFRP thickness was then increased by adding the thickness required for torsion. The number of layers of CFRP were the same for both columns. Design for confinement, shear, and torsion are discussed in the sections that follow.

### 3.2.3.1. Design for confinement

The flexural strength and ductility of RC columns can be enhanced by confinement. Confinement was to be provided by an externally bonded CFRP jacket. Two methods can be used to determine the required number of FRP layers for confinement. One is based on the retrofit design (this was not used in the final repair design inside the plastic hinge but rather for the purpose of comparison). The other is based on comparison of moment-curvature relationships of the original and repaired members with externally bonded FRP by conducting the sectional analysis.

The retrofit method was first proposed by Seible et al. (1997). This method involves the determination of the required FRP layers for confinement in both the plastic hinge region and the region outside the plastic hinge region using Equation 3-4:

$$t_j = \frac{f_c D}{2E_j \varepsilon_j} \quad (\text{Equation 3-4})$$

where  $t_j$  is the required FRP thickness;  $E_j$  is the Young's modulus of FRP;  $\varepsilon_j$  is effective strain of FRP which is usually taken as 0.004 in retrofit design;  $f_c$  is the confining stress which is taken as 300 psi for the plastic hinge region and 150 psi for the region outside plastic hinge; and  $D$  is the dimension of the cross-section in the bending direction. Based on this method, 2 layers of CFRP were required in the plastic hinge region, and 1 layer was required for the region outside the plastic hinge for columns Calt-1 and Calt-2.

The number of layers of CFRP required for confinement was also computed using moment-curvature relationships. Due to the lack of experimental results for the column under pure bending (no torsion), the moment-curvature relationship of the original cross-section was used as

the control data. The flexural repair included replacing the circumferential longitudinal bars, casting new replacement concrete, and wrapping CFRP as confinement. Thus, within the plastic hinge region, the cross-section of the repaired columns included the new CFRP-confined concrete and new longitudinal bars while outside the plastic hinge, the cross-section of the repaired columns was the same as that of the original columns. The moment-curvature analysis for both the original and repaired sections was conducted using the program XTRACT (see Figure 3-14). The FRP-confined concrete model used in the analysis was determined based the study by Samaan et al. (1998). Based on the analytical results, 1 layer of CFRP was required for the plastic hinge region, and no CFRP was required for confinement outside the plastic hinge region for both columns. However, in order to prevent further spalling of the cracked concrete outside the plastic hinge region and with consideration of the retrofit requirement described previously, one layer of CFRP was to be used outside the plastic hinge region.

#### 3.2.3.2. Design for shear

Shear repair involved casting new replacement concrete in the plastic hinge region and wrapping CFRP in regions inside and outside the plastic hinge. The objective of the shear repair was to restore the shear strength to the original shear capacity of the columns.

Vosooghi and Saiidi (2012) proposed a method to determine the required number of FRP layers to restore the shear capacity. In this method, the Equation 3-5 was used to determine the required contribution of the CFRP to the column's shear capacity:

$$V_j = \frac{V_0}{\phi} - (R_c V_c + R_s V_s) \quad (\phi = 0.85) \quad \text{(Equation 3-5)}$$

where  $V_j$  is the required shear resistance from the FRP;  $V_0$  is the shear capacity of the original column;  $V_c$  and  $V_s$  are the shear resistance from existing concrete and transverse reinforcement respectively, both of which can be calculated from Caltrans (2006);  $R_c$  and  $R_s$  are the reduction factors for cracked concrete and yielded transverse reinforcement, respectively. Vosooghi and Saiidi (2012) also suggested values for  $R_c$  and  $R_s$  based on the damage level of the column. The required thickness of CFRP for shear resistance can be obtained with Equation 3-6:

$$t_j = \frac{V_j}{\frac{\pi}{2} \varepsilon_j E_j D} \quad (\text{Equation 3-6})$$

where  $t_j$  is the required thickness;  $\varepsilon_j$  is effective strain of FRP, which is usually taken as 0.004 in shear design;  $E_j$  is Young's modulus of FRP;  $D$  is the dimension of the cross-section in the bending direction; and  $V_j$  is the required shear resistance given by Equation 3-5.

Based on the method mentioned above, 1.575 layers of CFRP were required for the plastic hinge region, while no CFRP was needed for the region outside the plastic hinge region for both columns.

#### 3.2.3.3. Design for torsion

Similar to shear repair, torsion repair also involved casting new replacement concrete in the plastic hinge and wrapping CFRP in the regions inside and outside the plastic hinge. Very limited literature is available on determination of the required number of layers of FRP for torsional repair of RC columns (He et al. 2014). Zureick (2010) proposed a method to calculate the required number of layers of FRP for retrofit extrapolated from AASHTO (1998). The number of layers of CFRP required for torsion is based on Equation 3-7:

$$T_r = \phi T_n + \phi_{frp} T_{frp} \quad (\text{Equation 3-7})$$

where  $T_r$  is the torsional capacity of original column;  $T_n$  is the nominal torsional strength of the existing cross-section based on AASHTO (1998);  $T_{frp}$  is the torsional resistance provided by FRP; and  $\phi$  and  $\phi_{frp}$  are the strength reduction factors for the existing section and FRP layers respectively, which are usually taken as 0.9 and 0.65, respectively. The torsional resistance provided by the FRP can be calculated with following equations:

$$T_{frp} = N_{frp}^e \alpha_t x_1 y_1 \quad [\alpha_t = 0.66 + 0.33(y_1/x_1)] \quad (\text{Equation 3-8})$$

where  $x_1$  is the lesser dimension of the member;  $y_1$  is the larger dimension of the member; and  $N_{frp}^e$  is the effective tensile force per unit length provided by FRP straps given by Equation 3-9:

$$N_{frp}^e = N_s + \frac{1}{2}(N_{frp,w} - N_s), \quad N_{frp,w} = 0.5N_{ult} \geq N_s \quad (\text{Equation 3-9})$$

where  $N_s$  is the tensile force per unit length given by Equation 3-10; and  $N_{ult}$  is the ultimate tensile force per unit length of FRP given by the manufacturer.

$$N_s = t_j E_j \varepsilon_j \quad (\text{Equation 3-10})$$

Based on the procedure above, 4.512 layers of CFRP were needed in plastic hinge for torsion repair, while no CFRP was needed for the region outside the plastic hinge for both columns.

#### 3.2.3.4. Summary

The number of layers of CFRP was designed for the larger of the amounts required for combined confinement + torsion and for combined shear + torsion. Both columns were designed with the same layout of CFRP.

Inside plastic hinge:  $1(\text{confinement})+4.512(\text{torsion}) = 5.512 = 6 \text{ layers}$

-or-

$1.575(\text{shear})+4.512(\text{torsion}) = 6.087 = 7 \text{ layers}$  <- *Governs*

Outside plastic hinge:  $1(\text{confinement}) = 1 \text{ layer}$  <- (*based on retrofit design*)

The CFRP layout is shown in Figure 3-15.

### 3.3. REPAIR PROCEDURE

Based on the repair design described in Section 3.2, the repair procedure included a total of eight steps: (1) shoring the column; (2) demolishing the concrete and removing the spirals inside the plastic hinge region; (3) severing and removing the damaged longitudinal bars; (4) straightening the columns; (5) splicing new longitudinal bar segments to the existing bars with mechanical bar couplers; (6) casting new concrete; (7) preparing the concrete surface for CFRP; and (8) installing the CFRP jacket. This section describes these steps in detail. Constructability aspects of all the repairs are discussed in Chapter 7.

#### 3.3.1. Shoring of column

For both Calt-1 and Calt-2, two scaffolding towers shown in Figure 3-16 were assembled for the shoring and straightening work. Screw jacks on both the top and bottom ends of the towers were used to adjust the height of the column.

#### 3.3.2. Removal of concrete and spirals

An electric jack hammer was used to demolish the concrete within the plastic hinge of Calt-1 (as shown in Figure 3-17a). Both an electric jack hammer and a hydraulic breaker mounted on a

skid-steer loader were used to demolish concrete within the plastic hinge of Calt-2 (as shown in Figure 3-18a). For Calt-1, cover concrete was removed by the jack hammer to expose the interlocking spirals, which were cut with an angle grinder to facilitate the demolition of the core concrete by the jack hammer as shown in Figure 3-17b. Column Calt-1 after removal of concrete and spirals is shown in Figure 3-17c, which also illustrates the removal of concrete from the footing to the first layer of horizontal reinforcement in the footing. For Calt-2, spirals were cut after concrete was demolished with the hydraulic jack hammer above the footing. The concrete near the footing was then removed by the electric jack hammer. Column Calt-2 after removal of concrete and spirals is shown in Figure 3-18b.

### 3.3.3. Severing and removal of damaged longitudinal bars

Severing of damaged longitudinal bars was accomplished with a torch. The sever location of each bar was determined by the designated location of the center of each coupler that is shown in Figure 3-20. All circumferential longitudinal bars of Calt-1 were severed and removed, while the four core bars were not treated since they were not buckled or fractured. Column Calt-1 after bar severing is shown in Figure 3-19a. All bars of Calt-2 were severed and removed since the four core were also buckled (see Figure 3-18b). Column Calt-2 after bar severing is shown in Figure 3-19b.

### 3.3.4. Straightening of column

Straightening of the columns was conducted after bar severing by adjusting the bottom screw jacks of the shoring towers.

### 3.3.5. Splicing new replacement bars and installing mechanical bar couplers

Mechanical bar couplers with shear lock bolts were used to splice the new replacement bars to the existing bars in Calt-1. The shear bolts were installed with an impact wrench, and the heads of the bolts were sheared off when the specified torque was reached (see Figure 3-21b). For Calt-2, swaged bar couplers were used. The sleeves were swaged with a hydraulic swaging machine provided by the manufacturer. Figure 3-22 shows the couplers used to repair Calt-2.

After the couplers were installed, No. 4 (12.7 mm. dia.) reinforcing steel hoops were installed around the couplers to enhance the strength of the transition region (see Figure 3-21c).

### 3.3.6. Casting new concrete

Highly-flowable concrete was used to replace the removed concrete in both columns to avoid voids inside the columns. The details of concrete placement are discussed in Section 7.1.5.

### 3.3.7. Installing CFRP jacket

Finally, the CFRP was installed using a wet-layup procedure including surface preparation, dry fiber saturation, and fiber wrapping. The application procedure is illustrated in Figure 3-23. The surface of column was prepared by roughly grinding using a concrete grinder (see Figure 3-23a), following which epoxy mixed with silica fume (provided by the manufacturer) was filled into any cavities on the column surface (see Figure 3-23b).

## 3.4. TEST PROGRAM

### 3.4.1. Test setup

The repaired columns were subjected to cyclic lateral loading and constant axial loading (refer to Figure 3-3). The test setup for R-Calt-1 and R-Calt-2 is shown in Figure 3-2b. Cyclic torsional and bending moments were applied to the columns with two hydraulic actuators mounted onto a

reaction wall. The actuators were connected to the steel frames that were attached to the top of the columns. A constant axial compression force was applied to the top of the columns to simulate the service load from the bridge superstructure, which corresponded to 7% of the axial capacity of the original columns. Axial compression was applied to the column by a prestressing system, which was composed of a hydraulic jack placed on top of the column, seven prestressing strands placed through a PVC pipe at the center of column, and an anchorage system at the bottom of the footing. The columns were positioned on two RC blocks that were anchored to the reaction floor by DYWIDAG bars. Two steel wide flange beams were placed on the top surface of the footing and tied down by two steel double channels, which were anchored by four DYWIDAG bars.

#### 3.4.2. Instrumentation

Load cells and LVDTs integrated within the two actuators were used to measure and control force and displacement during testing. Two load cells with capacity of 200 kips were also installed under the hydraulic jack on the top of column to record the variation of axial load. Four levels of string extensometers were also installed between a reference frame and the columns (see Figure 3-26). Two string extensometers were installed at each level to measure the global behavior of the columns in terms of both the lateral deformation and twist. Uniaxial electrical resistance strain gages were mounted on the longitudinal reinforcing bar segments and couplers as well as on the surface of the CFRP. Six levels of eight strain gages were installed on the replacement bars segments within the plastic hinge region to measure the axial strain in the bars (see Figure 3-24). Nine levels of six gages were installed on the surface of the CFRP to measure the strain in the wrap direction (see Figure 3-25).

### 3.4.3. Loading protocol

Similar to the loading protocol applied to the original columns, the repaired columns were loaded in force control to the estimated first yielding point of the longitudinal reinforcing steel in ten steps. Displacement control was then used to apply lateral displacement and twist to the free end of the columns after first yielding point was reached. At each displacement control level, three cycles were applied to observe the degradation to the columns at the same displacement level. For R-Calt-1, due to the limitation of the stroke capacity of the actuators, only positive cycles at levels 7 and 8 were applied until the displacement of the column exceeded the stroke capacity of the actuators in the positive direction as well (as shown in Figure 3-3a). For R-Calt-2, only positive cycles at levels 4 and 5 were applied due to the torsional limitation of the actuators (as shown in Figure 3-3d).

## 3.5. CONCLUDING REMARKS

This chapter describes damage to two oval-shaped columns reinforced with interlocking spirals tested to failure under T/M ratio of 0.2 and 0.6 respectively, the method used to repair these columns, and the testing program of the repaired columns including test setup, instrumentation, and loading protocol. The experimental work presented in this chapter illustrates that the repair method was practical and may be implemented in field applications.

Table 3-1 Measured Reinforcing Steel Properties for Calt-1, Calt-2, R-Calt-1, and R-Calt-2

Reinforcing Bar	Yield Strength ksi (MPa)	Ultimate Strength ksi (MPa)
Original No. 8 Bars (25.4 mm dia.)	76.7 (529)	104.1 (717)
Original No. 4 Spirals (12.7 mm dia.)	65.8 (454)	98.0 (676)
Replacement No. 8 Bars (25.4 mm dia.)	65.5 (452)	97.9 (675)

Table 3-2 Measured Concrete Compressive Strength of for Calt-1, Calt-2, R-Calt-1, and R-Calt-2

Column ID	Calt-1	Calt-2	R-Calt-1	R-Calt-2
28 days	4360 psi (30.0 MPa)	5670 psi (39.1 MPa)	4280 psi (29.5 MPa)	4050 psi (27.9 MPa)
Test date	5430 psi (37.4 MPa)	5260 psi (36.3 MPa)	4920 psi (33.9 MPa)	5010 psi (34.5 MPa)

Table 3-3 Visible Damage to Columns to Calt-1 and Calt-2 After Original Test<sup>1</sup>

Column ID	Concrete Damage		Reinforcing Steel Damage				Fracture/Buckling Location <sup>2</sup>
	Spalled Length <sup>3</sup>	Core Crush Depth	No. of Yielded Long. Bars <sup>4</sup>	No. of Buckled Long. Bars	No. of Fractured Long. Bars	No. of Swelled Spirals	
Calt-1	37 in. (940 mm)	6- 10 in. (152-254 mm)	Unavailable	6/20	8/20	3	3-13 in. (76-330 mm)
Calt-2	90 in. (2290 mm)	>12 in. (305 mm)	Unavailable	14/20	0/20	0	12-28 in. (305-711 mm)

<sup>1</sup> These descriptions are based on visible observation; the actual damage may be more extensive;

<sup>2</sup> The height range of the fracture/buckling points of longitudinal bars measured from the column footing;

<sup>3</sup> The definition of spalled length and core crush depth are shown in Figure 3-5;

<sup>4</sup> Number of yielded longitudinal bars determined from the measured strain data, 15 to 16 of the 20 bars yielded for both columns;

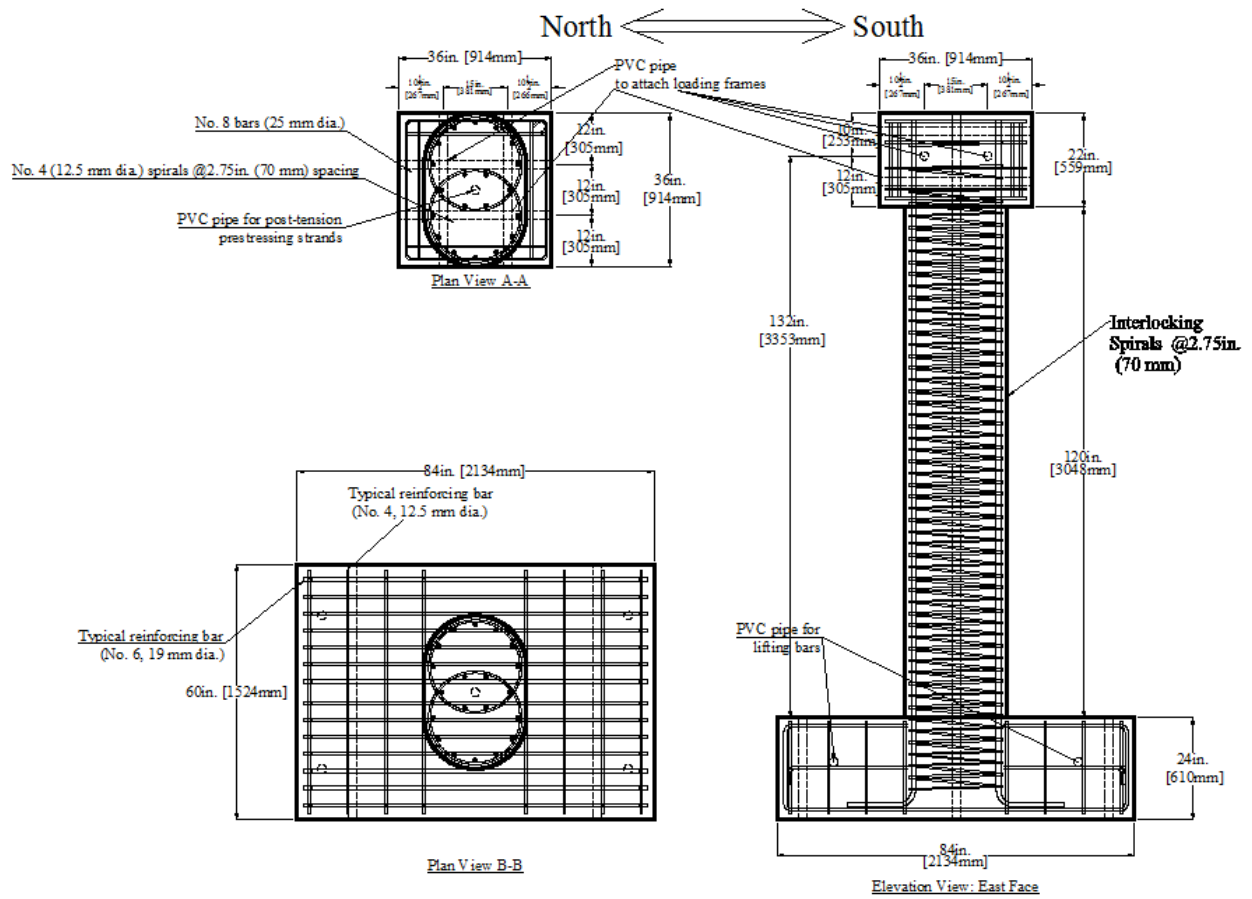


Figure 3-1 Geometry and Reinforcement Details of Calt-1 and Calt-2

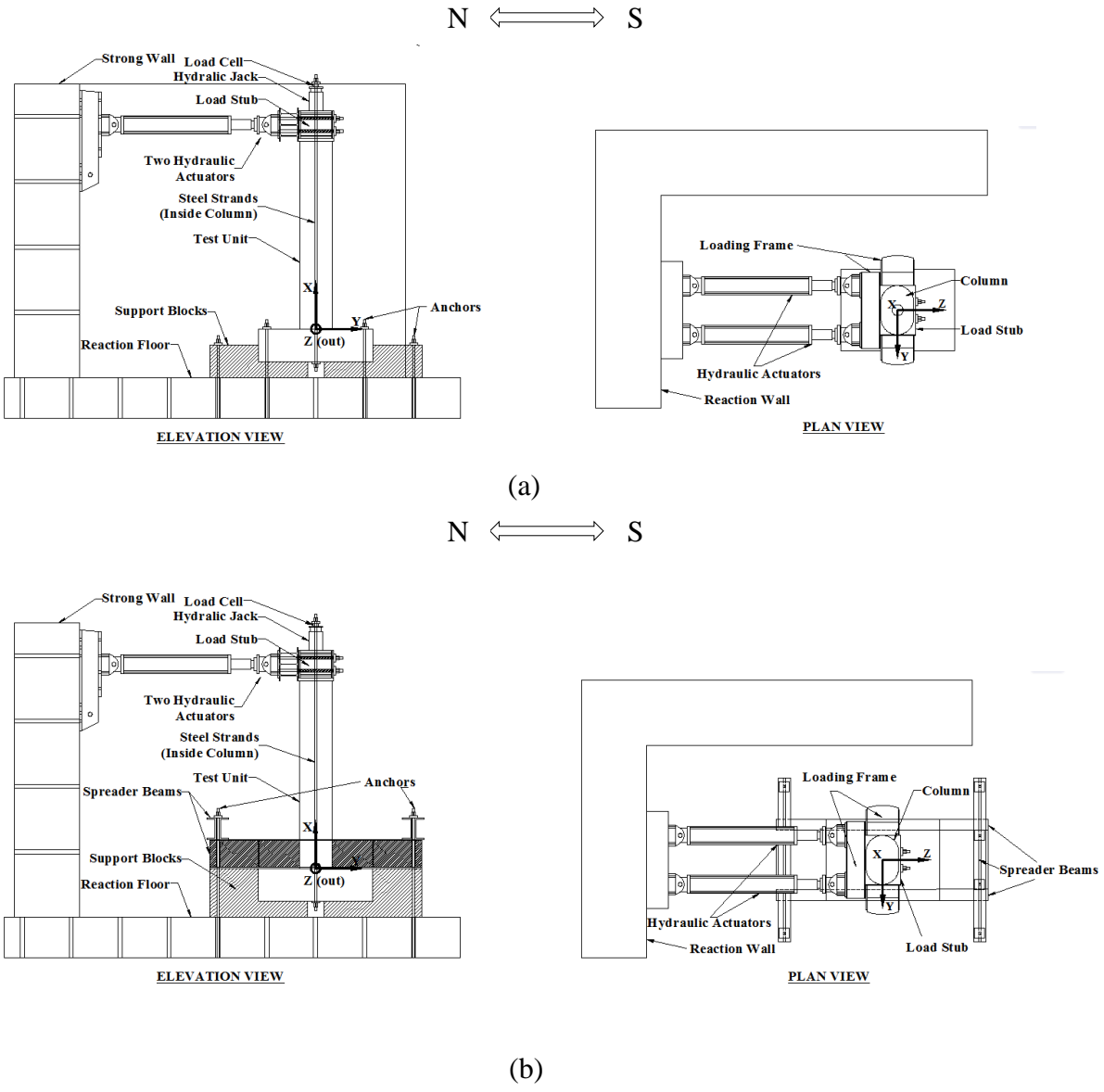


Figure 3-2 Test setups of (a) Calt-1 and Calt-2 (b) R-Calt-1 and R-Calt-2

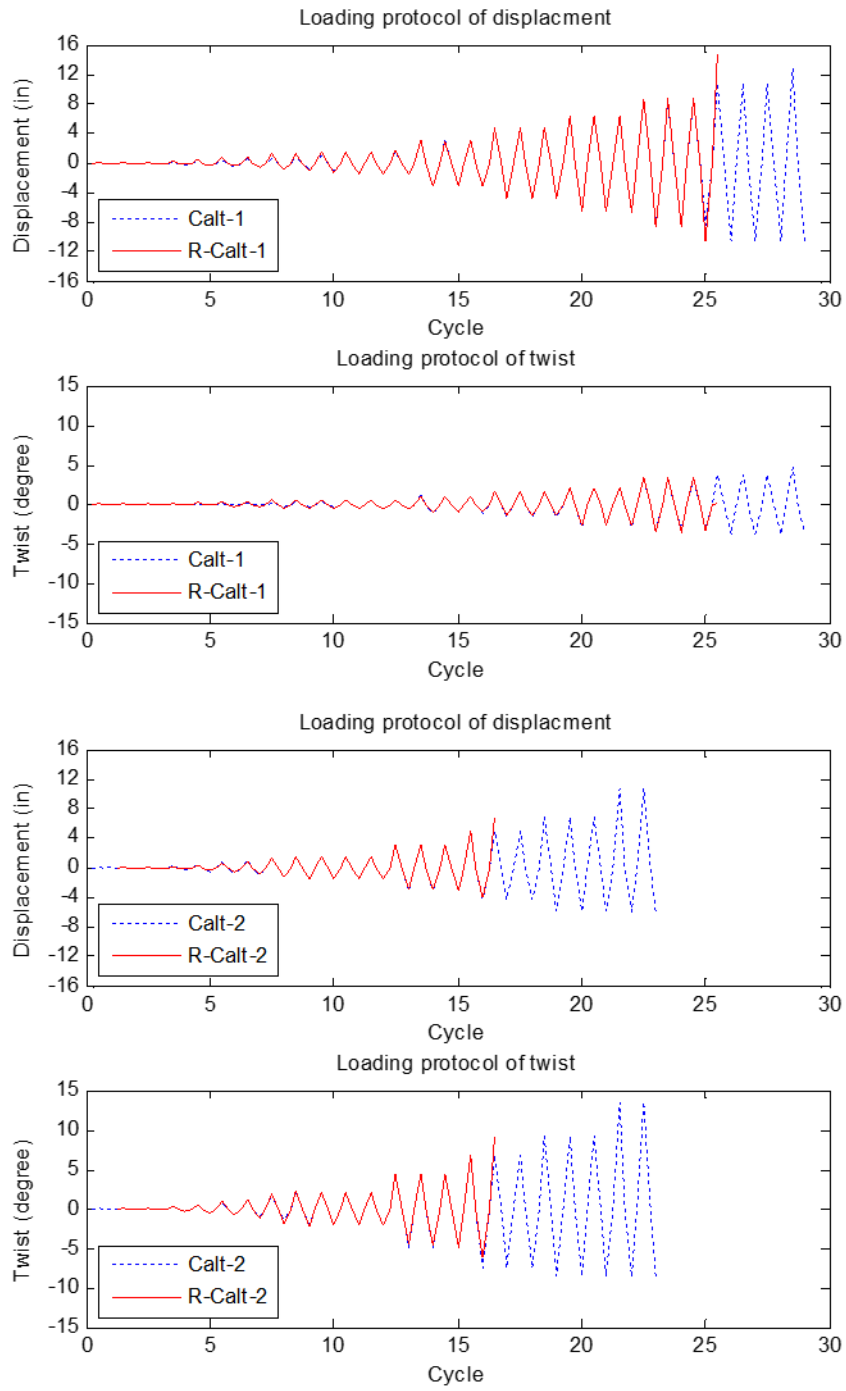


Figure 3-3 Loading Protocol of Calt-1, R-Calt-1, Calt-2, and R-Calt-2

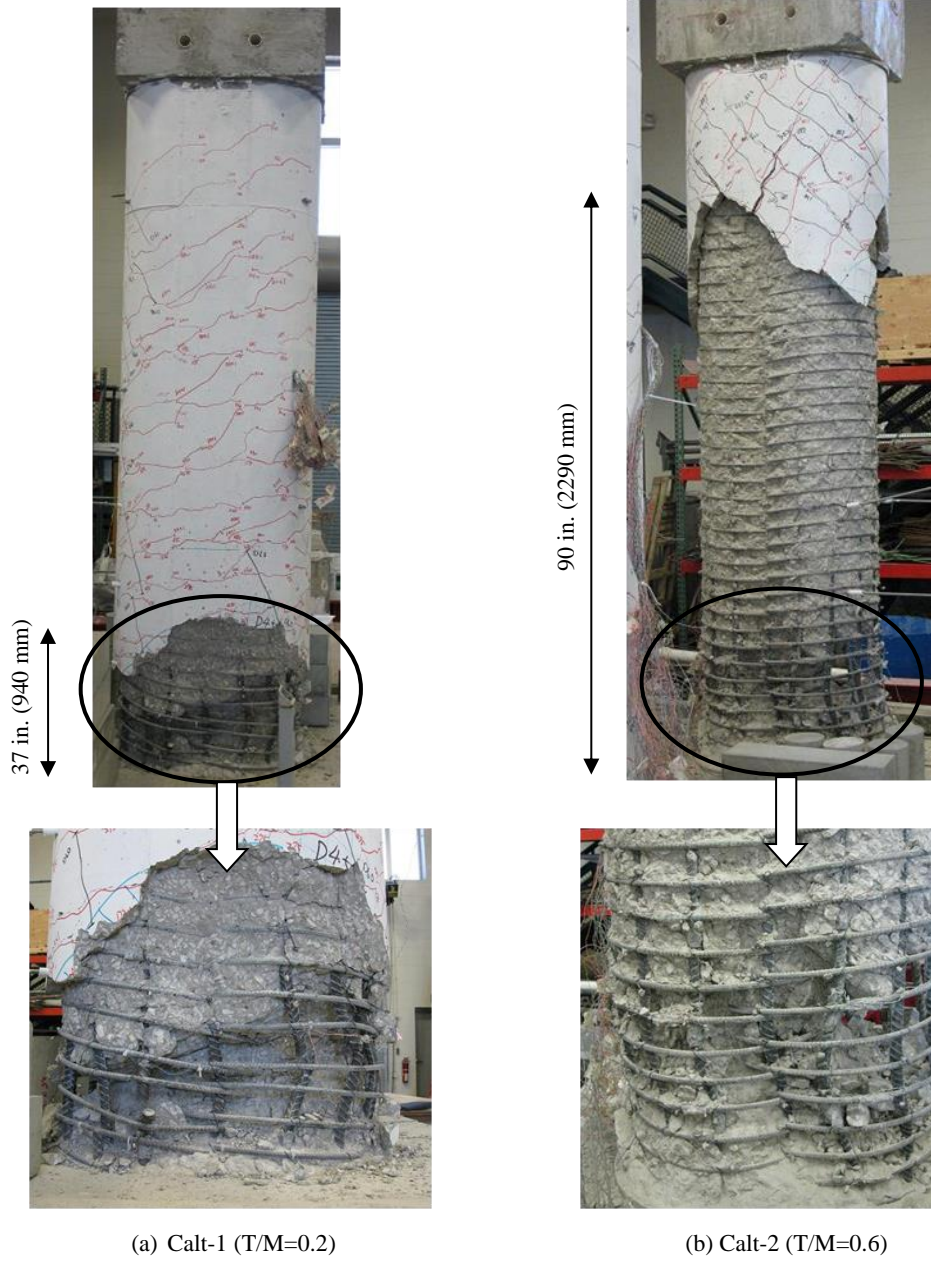


Figure 3-4 Visible Damage After Original Test to (a) Calt-1 and (b) Calt-2

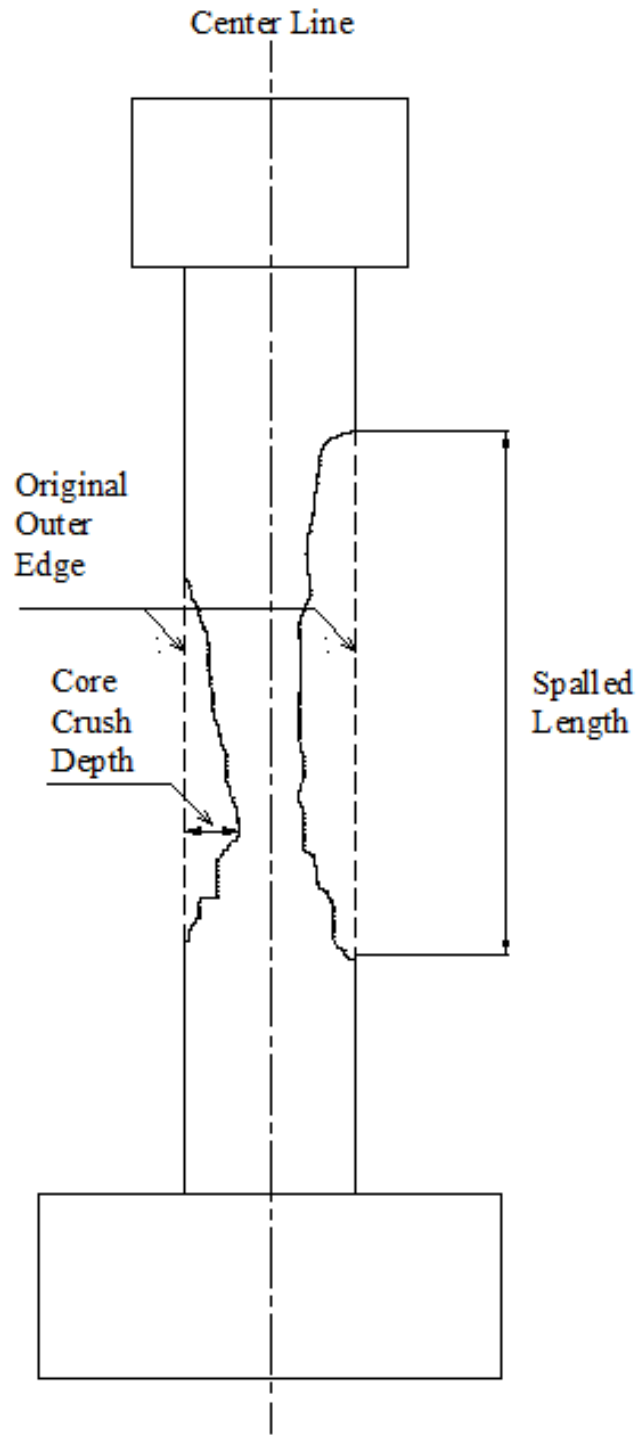
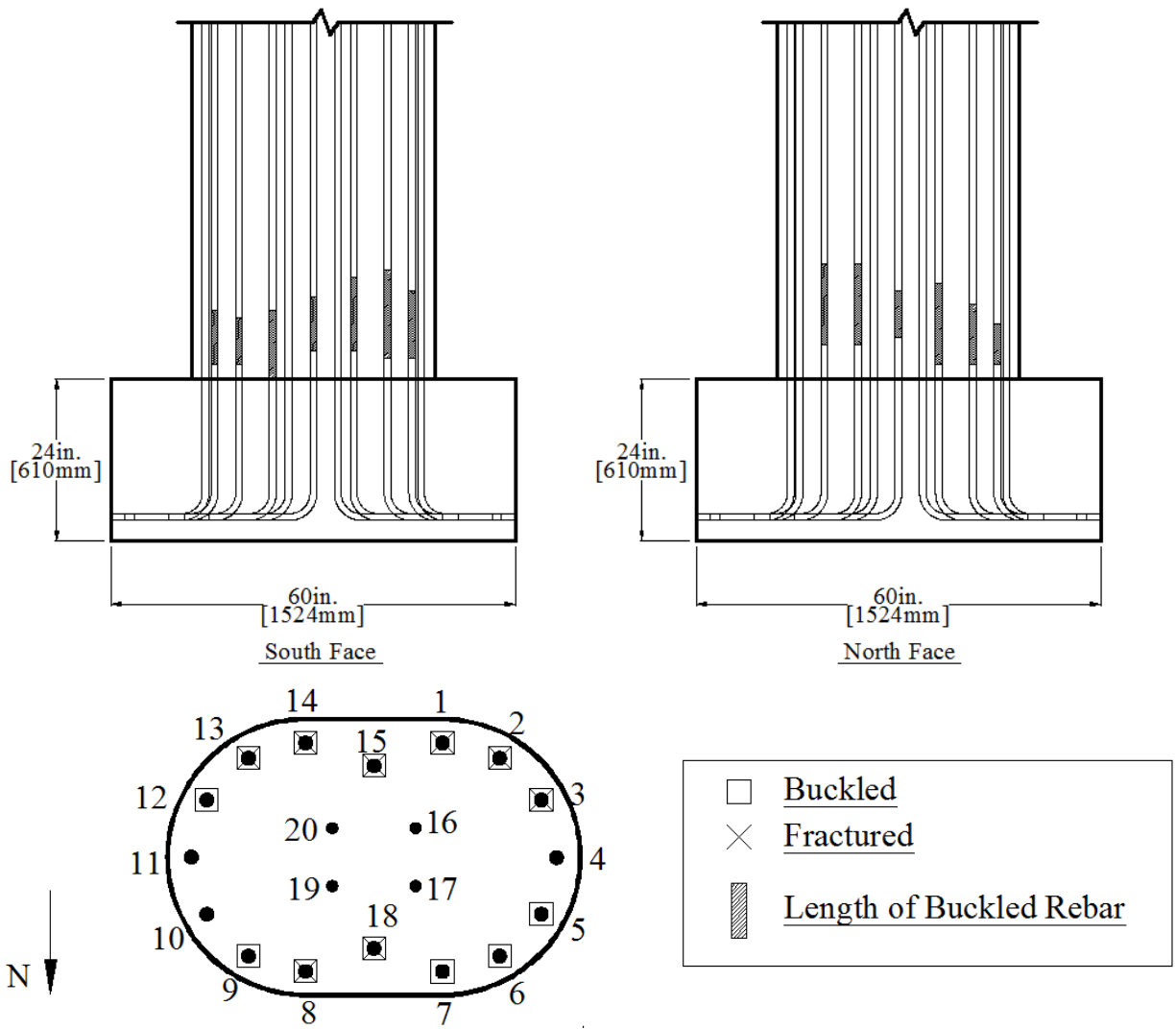


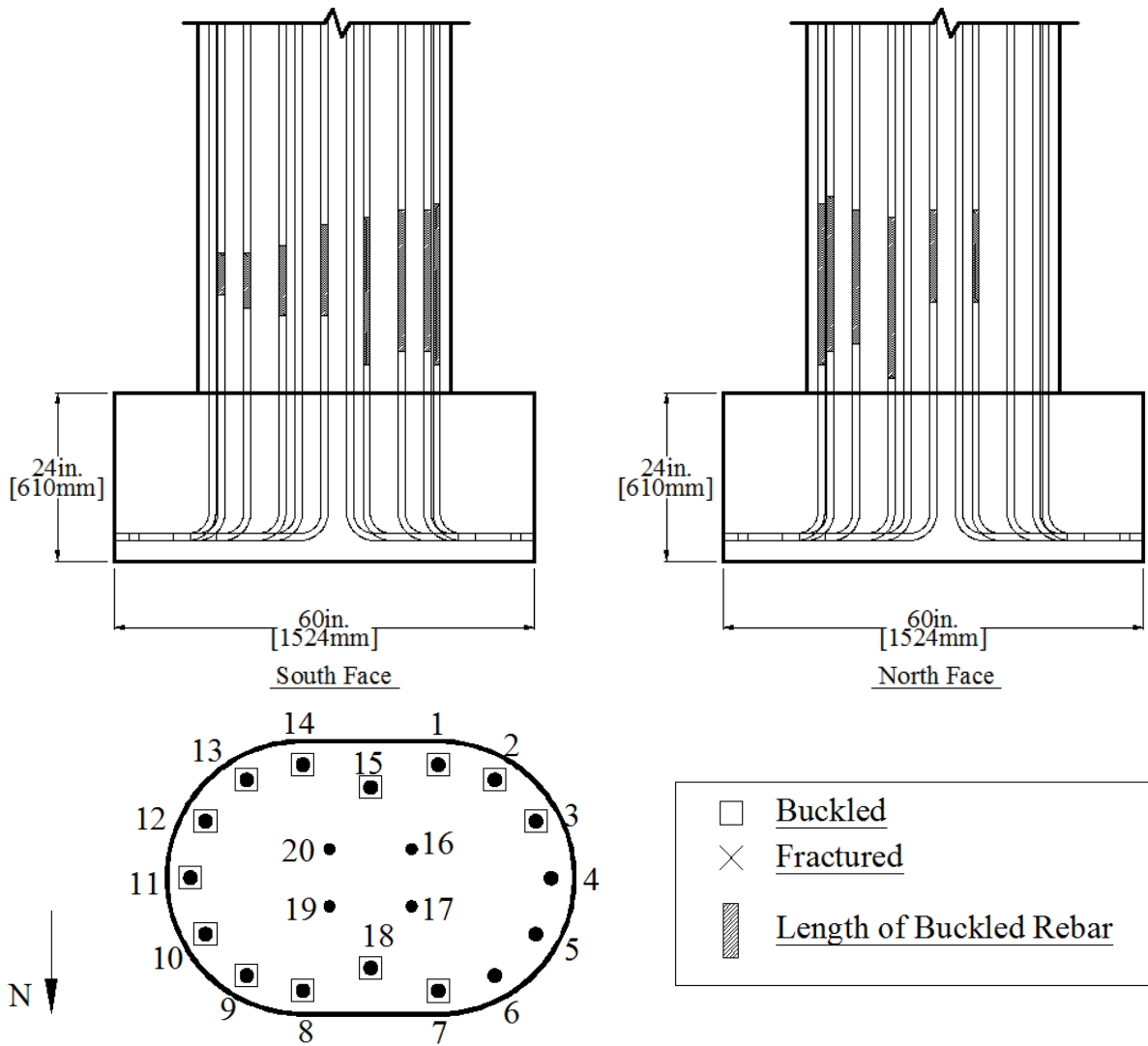
Figure 3-5 Definition of Spalled Length and Core Crushing Depth of Concrete



Note: all damage locations were measured from the top of footing

Bar Number	1	2	3	5	6	7	8	9	12	13	14	15	18
Fracture Location (in.)	5	2.5	4	-	-	-	11	-	-	10.5	9	6	7
Buckled Region (in.)	11~21	12~20	14~20	13~26	2~25	7~26	6~28	4~27	6~26	6~26	4~25	11~24	13~26

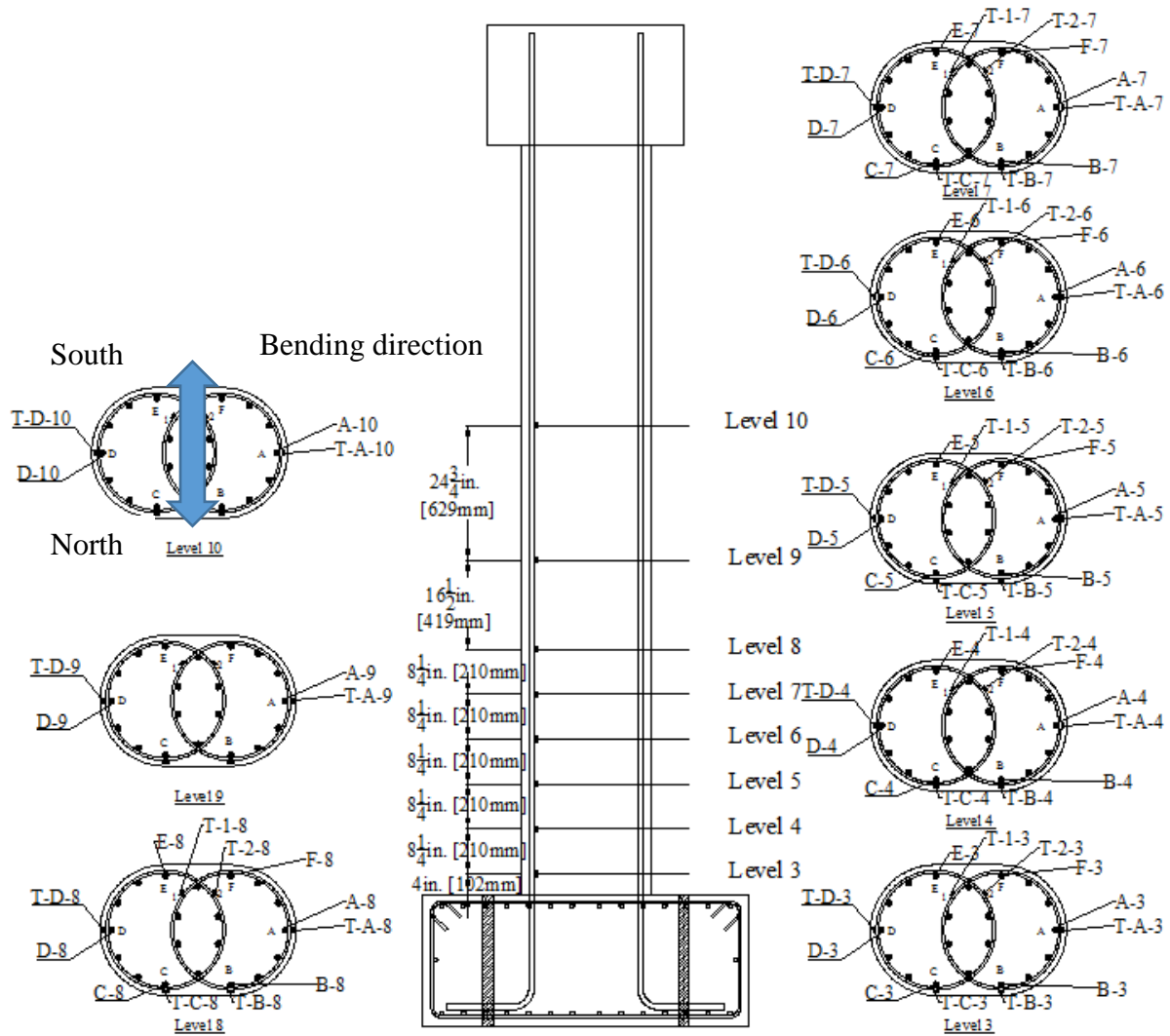
Figure 3-6 Visible Damage to Longitudinal Reinforcement of Calt-1 After Original Test



Note: all damage locations were measured from the top of footing

Bar Number	1	2	3	7	8	9	10	11	12	13	14	15	18
Fracture Location (in.)	-	-	-	-	-	-	-	-	-	-	-	-	-
Buckled Region (in.)	11~21	12~20	14~20	13~26	2~25	7~26	6~28	4~27	6~26	6~26	4~25	11~24	13~26

Figure 3-7 Visible Damage to Longitudinal Reinforcement of Calt-2 After Original Test



- Notes: (1) “T” denotes “gage on transverse reinforcement”;  
 (2) 40 gages were installed on longitudinal reinforcement;  
 (3) 40 gages were installed on transverse reinforcement.

Figure 3-8 Strain Gage Layout of Calt-1 and Calt-2

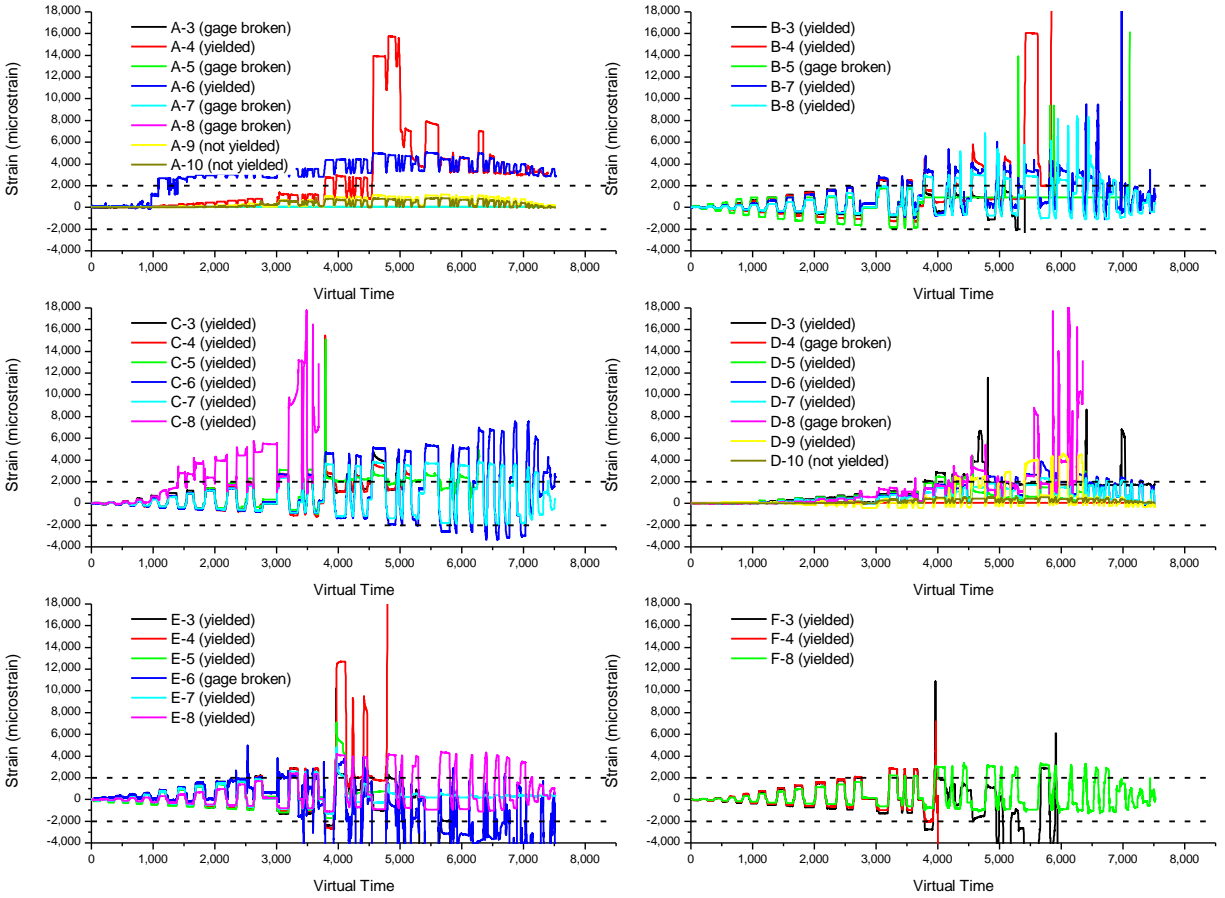


Figure 3-9 Strain History of Longitudinal Reinforcement (Calt-1)

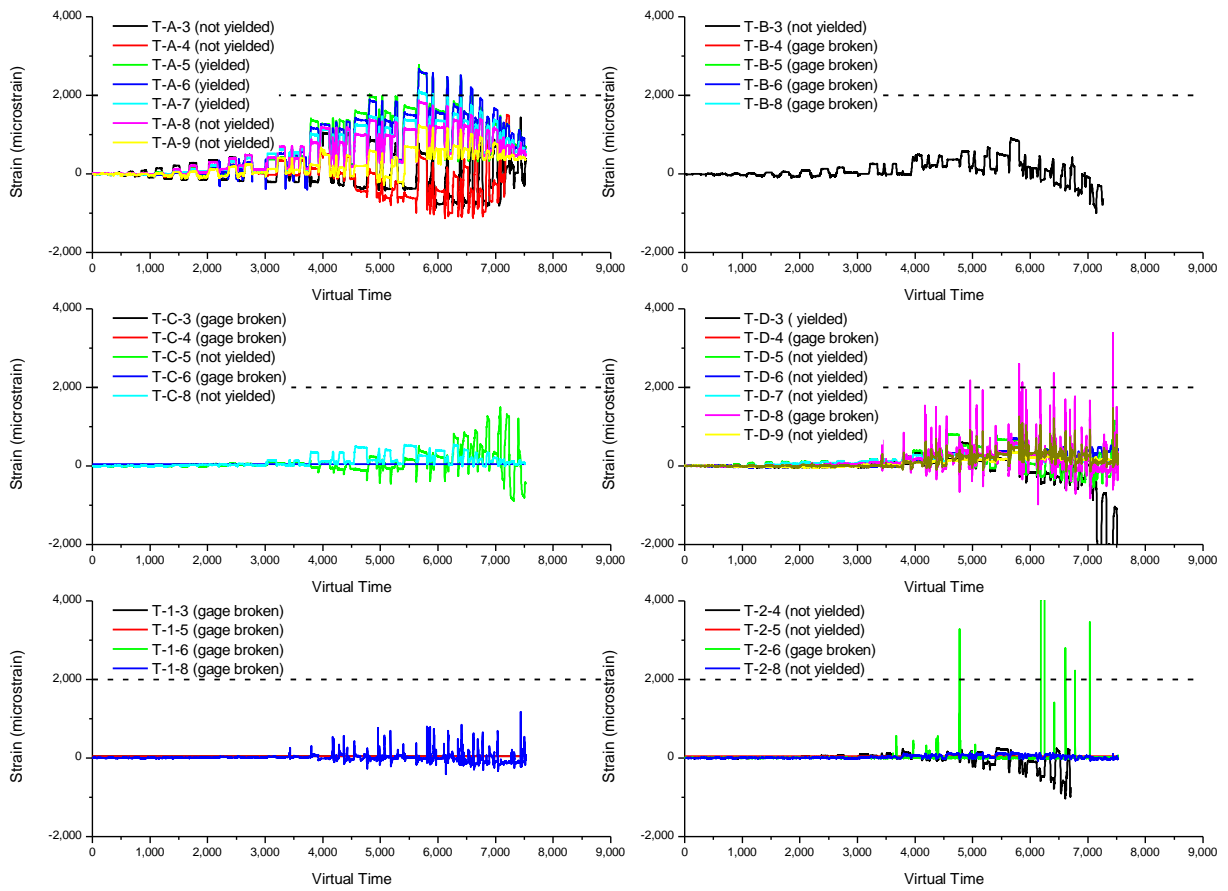


Figure 3-10 Strain History of Transverse Reinforcement (Calt-1)

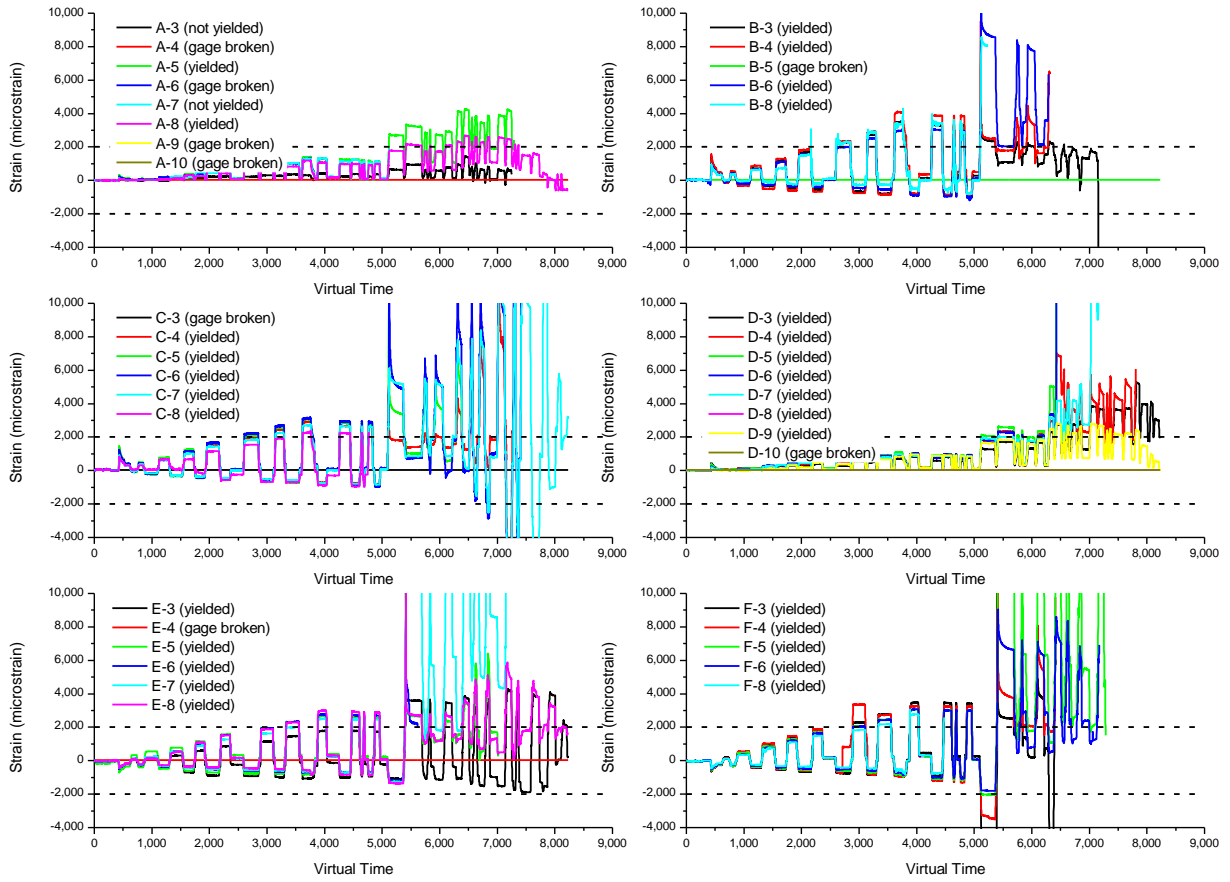


Figure 3-11 Strain History of Longitudinal Reinforcement (Calt-2)

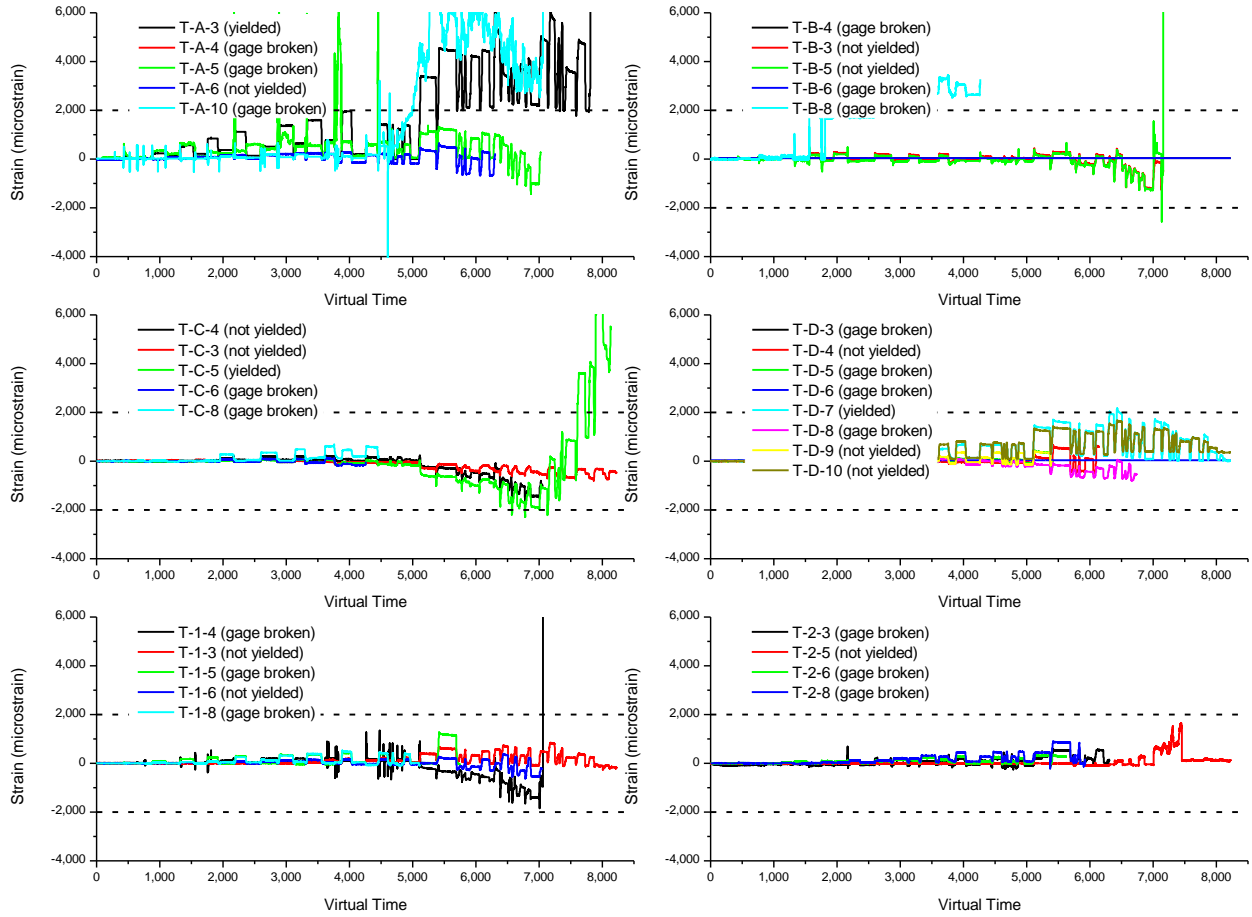


Figure 3-12 Strain History of Transverse Reinforcement (Calt-2)

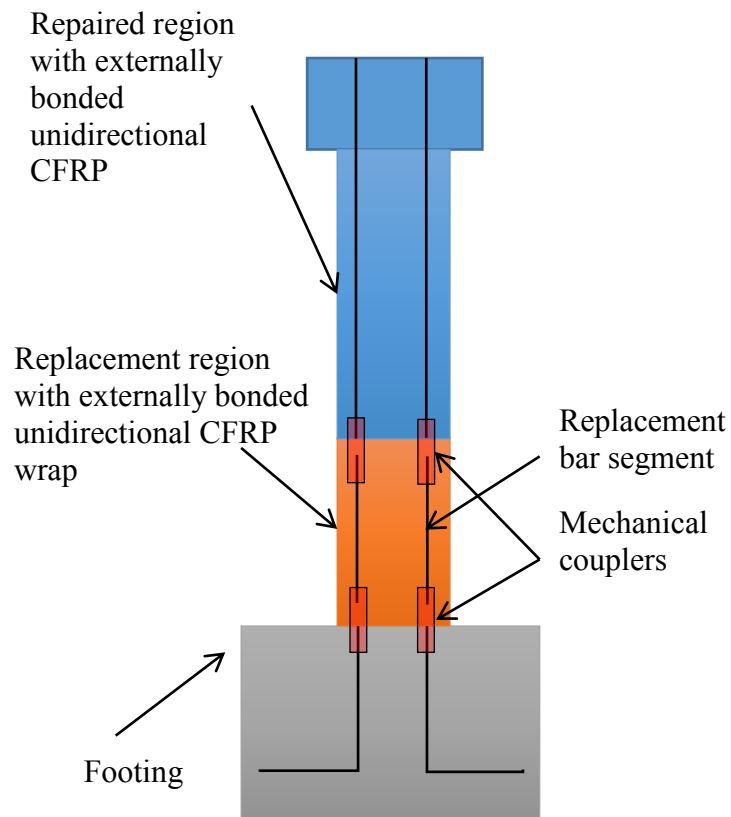
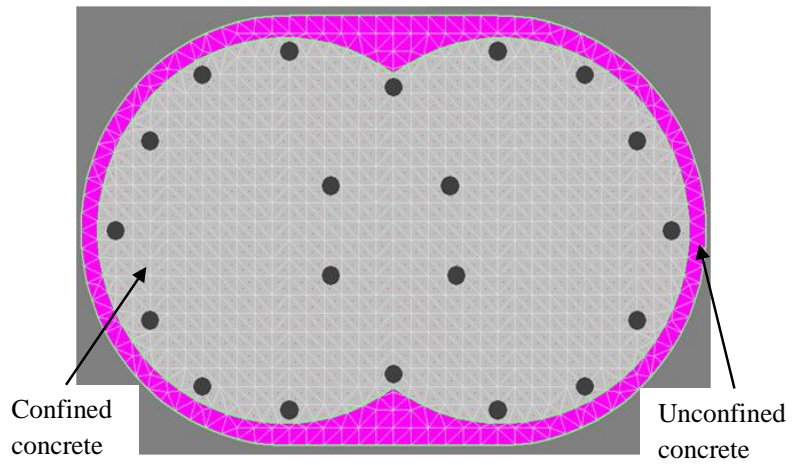
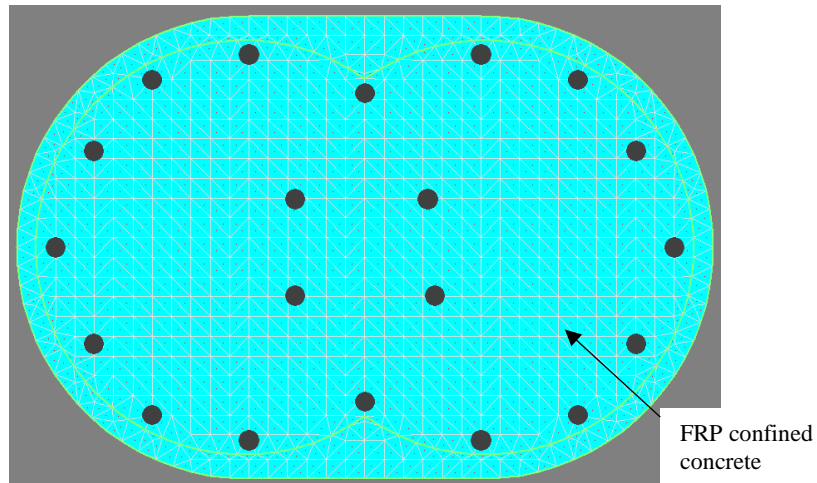


Figure 3-13 Repair Scheme for Calt-1 and Calt-2

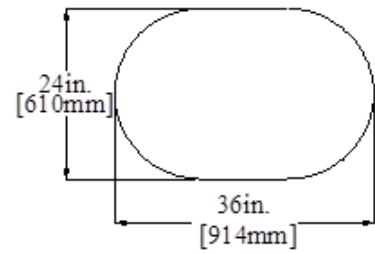
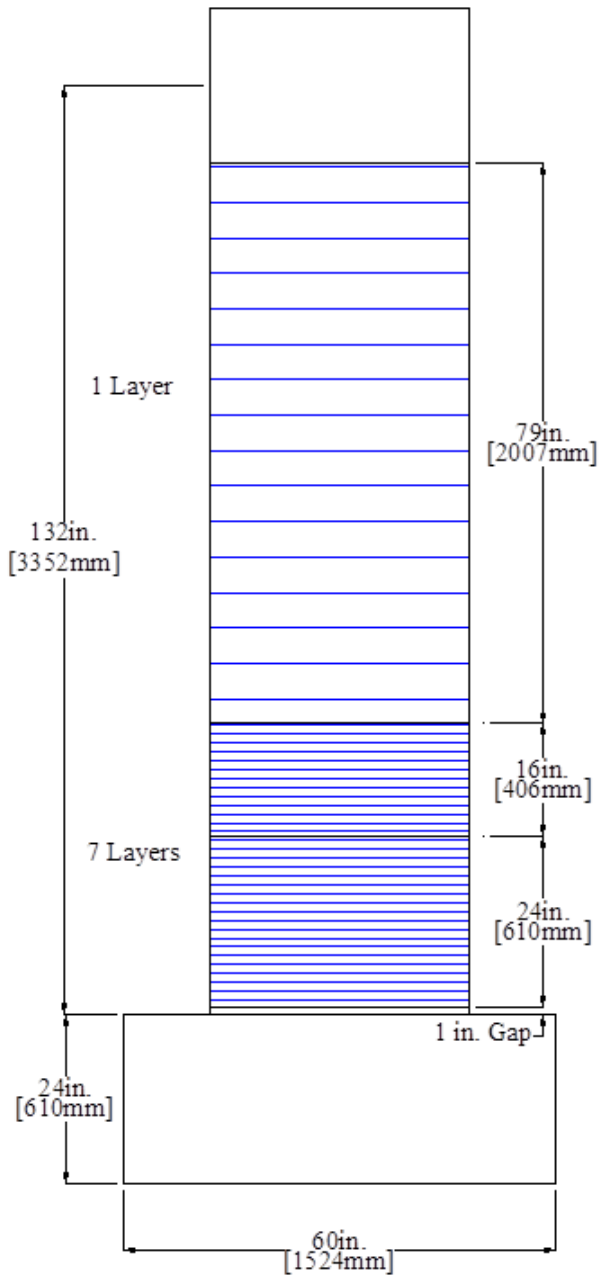


(a) Cross section of original columns



(b) Cross section of repaired columns

Figure 3-14 Cross-Section Model in XTRACT for (a) Calt-1 and Calt-2 and (b) R-Calt-1 and R-Calt-2



- Notes:
1. CFRP is Tyfo SCH-41 with unidirectional fibers by Fyfe;
  2. Fibers are oriented perpendicular to longitudinal axis of the column.

Figure 3-15 CFRP layout for R-Calt-1 and R-Calt-2



(a) Calt-1



(b) Calt-2



Spreader  
beams

Adjustable  
feet with  
screw  
threads

(c) Shoring towers

Figure 3-16 Shoring of Calt-1 and Calt-2 During Repair



(a) Electric jack hammer



(b) Concrete demolition in progress



(c) Column after removal of concrete and spirals

Figure 3-17 Removal of Concrete and Spirals of Calt-1



(a) Concrete demolition in progress



(b) Column after removal of concrete and spirals

Figure 3-18 Removal of Concrete and Spirals of Calt-2



(a) Bar severing with torch

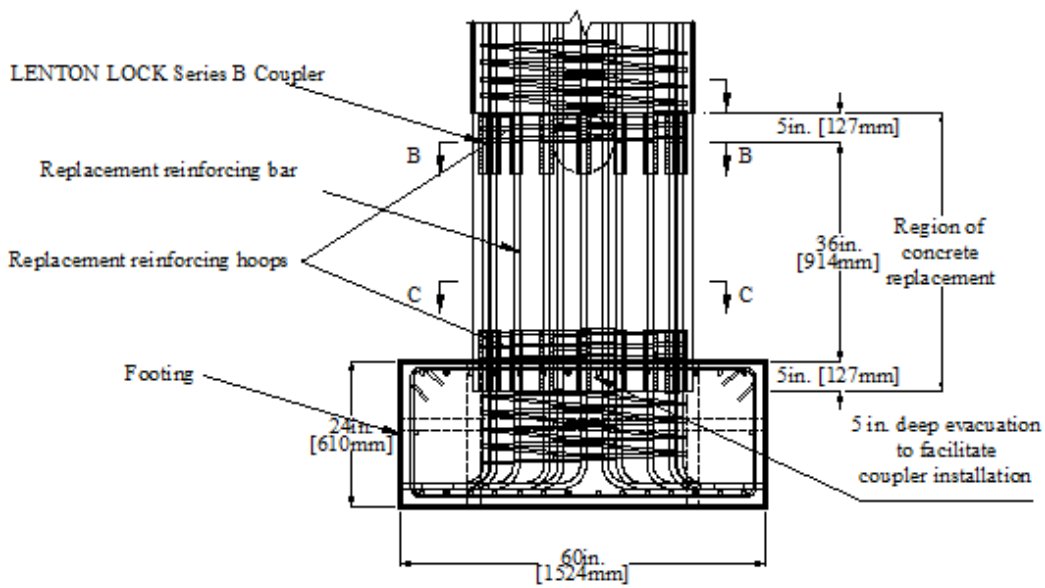


(b) Calt-1 after removal of longitudinal bars

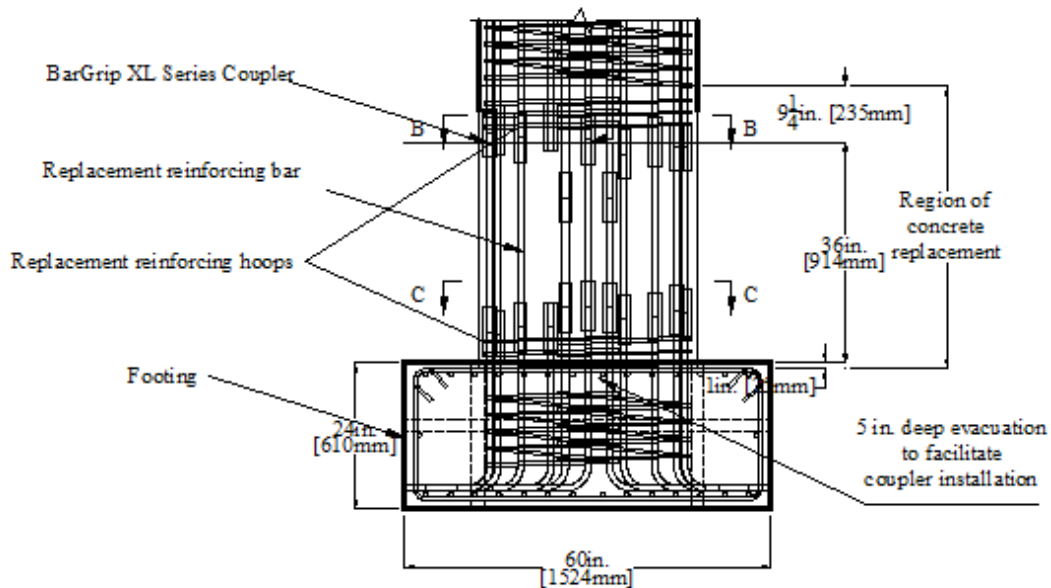


(c) Calt-2 after removal of longitudinal bars

Figure 3-19 Severing of Longitudinal Reinforcement in Calt-1 and Calt-2



(a) R-Calt-1 (T/M=0.2)



(b) R-Calt-2 (T/M=0.6)

Figure 3-20 Reinforcement Details of Repaired Columns R-Calt-1 and R-Calt-2



(a) Bottom couplers



(c) Column after reinforcement replacement



(b) Top couplers

Figure 3-21 Splicing of New Replacement Bar Segments and Installation of Couplers of Calt-1



(a) Coupler swaging in progress



(b) Couplers

Figure 3-22 Splicing of New Replacement Bar Segments and Installation of Couplers of Calt-2



(a) Surface grinding



(b) Surface filling



(c) CFRP wrapping



(d) Column after wrapping

Figure 3-23 CFRP Application Procedure for Calt-1 and Calt-2

S  $\longleftrightarrow$  N

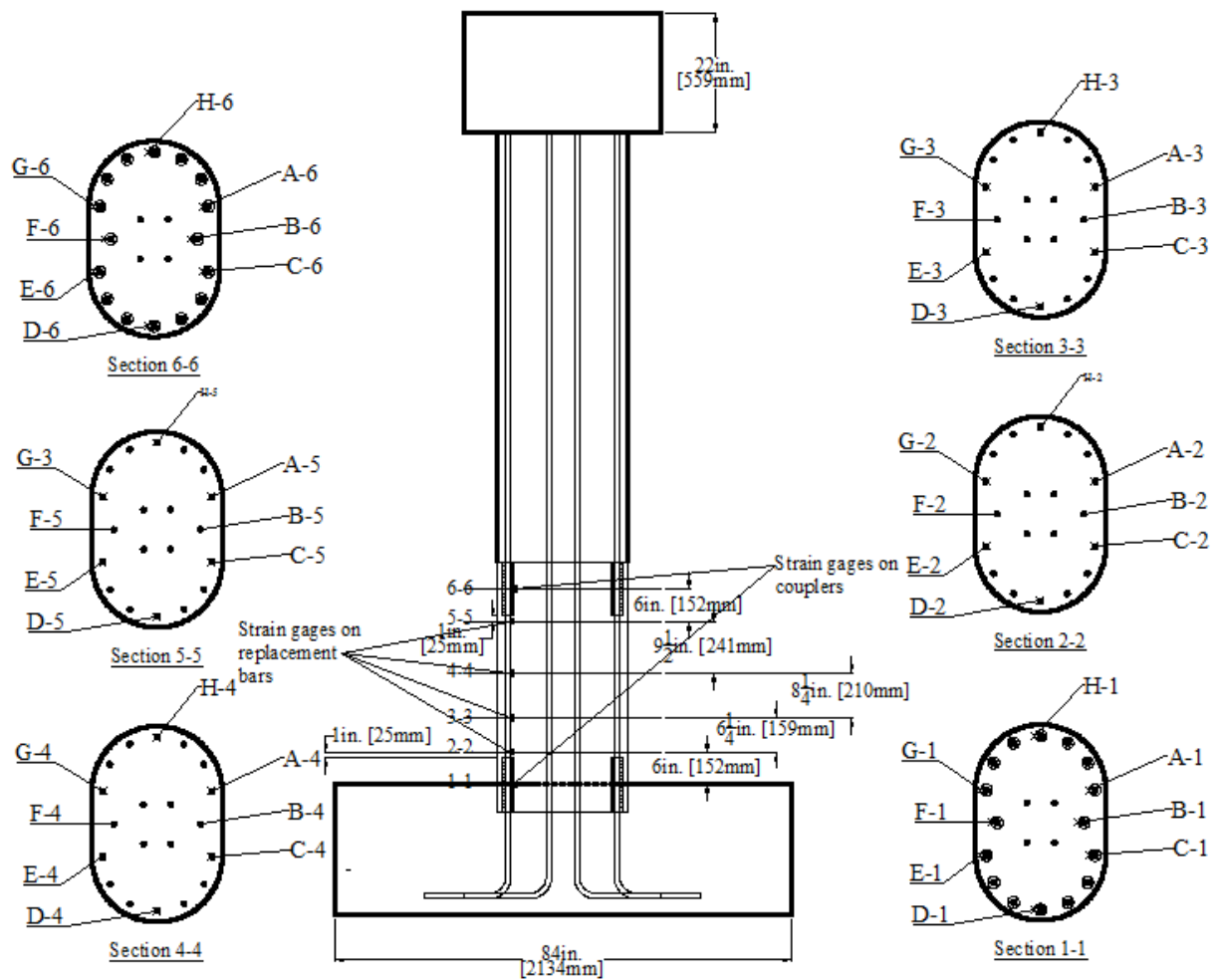


Figure 3-24 Strain Gage Layout on Replacement Bars and Couplers for R-Calt-1 and R-Calt-2

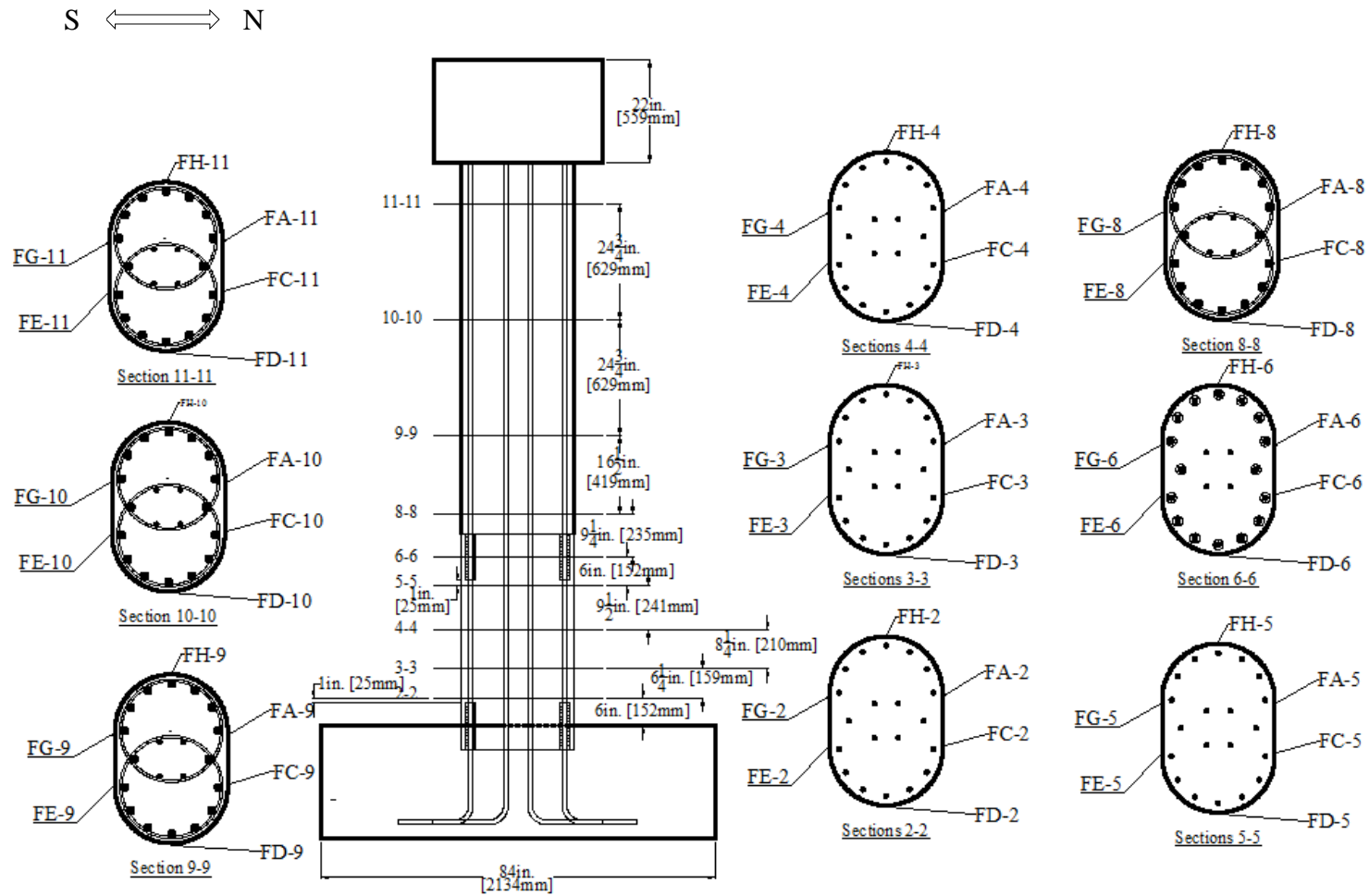


Figure 3-25 Strain Gage Layout on CFRP Jacket for R-Calt-1 and R-Calt-2

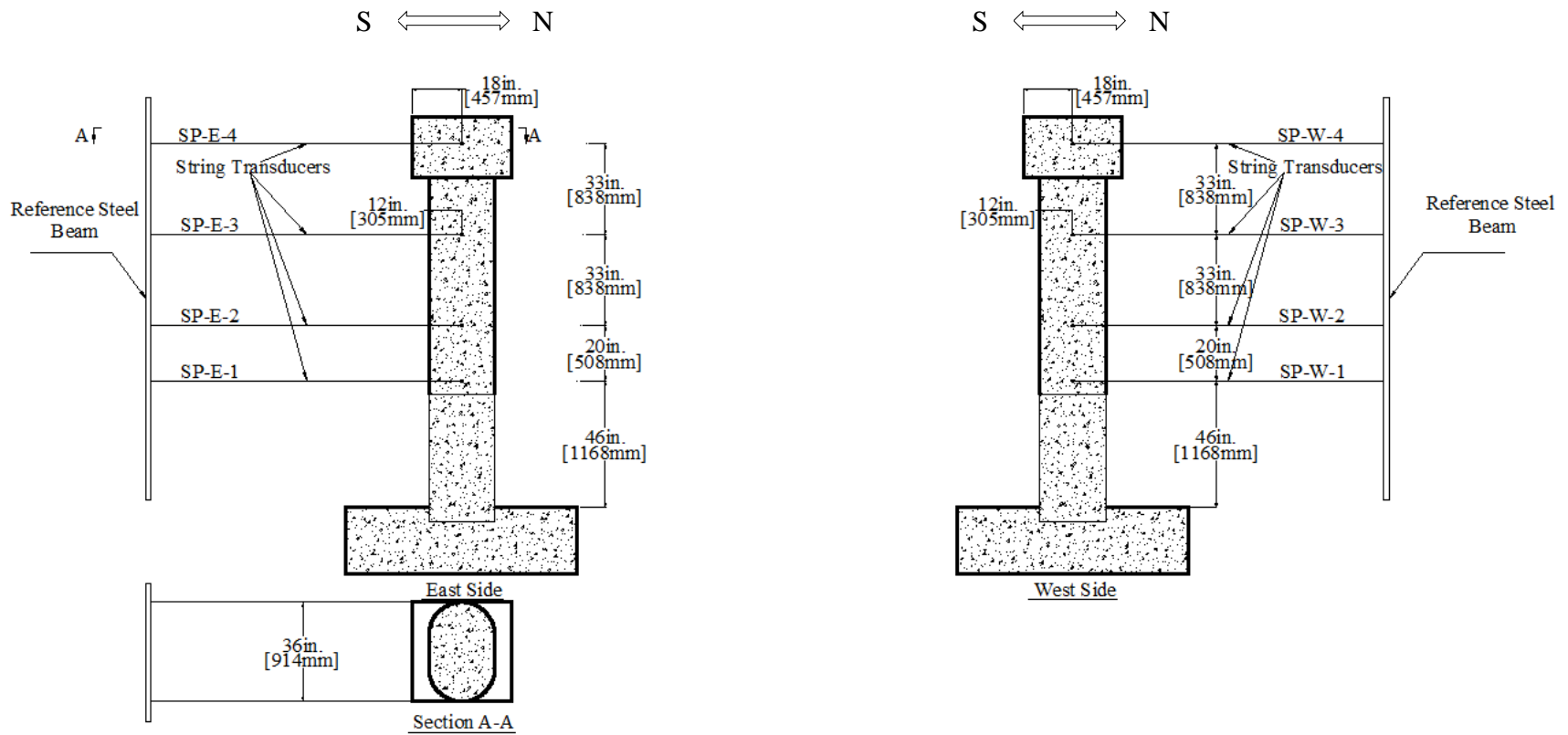


Figure 3-26 String Transducer Layout for R-Calt-1 and R-Calt-2

## 4. EXPERIMENTAL RESULTS OF R-CALT-1 AND R-CALT-2

This chapter presents the experimental results of R-Calt-1 and R-Calt-2 including observed damage to the repaired columns during testing, load-deformation relationships, energy dissipation, and strain history. Section 4.1 describes the damage to both columns observed during testing and the results of a forensic investigation of the damage to longitudinal reinforcement after testing of R-Calt-1. Section 4.2 presents the measured hysteresis response of the load-deformation relationships, and the calculated envelopes as well as idealized bilinear relationships based on the hysteresis responses. Section 4.3 presents the energy dissipation per each loading cycle. Section 4.4 presents the measured strain results of both the longitudinal reinforcing steel bars and the CFRP jacket. Section 4.5 summarizes the experimental results and makes concluding remarks.

### 4.1. GENERAL BEHAVIOR AND OBSERVED DAMAGE TO R-CALT-1 AND R-CALT-2

Testing of R-Calt-1 was terminated when the free end displacement of the column reached the stroke capacity of the two actuators. As shown in Figure 4-1, after the force control phase, the column was subjected to seven displacement-control (DC) levels in the positive direction (Push/South) and six DC levels in negative direction (Pull/North). In this figure, “DC” denotes the displacement control phase; the number after “DC” denotes the corresponding level; and “+/-” denotes the loading direction as positive or negative, respectively. The deformed shape of the column at the peak displacement of each DC level is also shown in Figure 4-1. No rupture of the

CFRP was observed during testing, while extensive flexural cracks occurred on the top surface of the footing on both sides of the column in the loading direction as shown in Figure 4-2a and Figure 4-2b. The first cracks formed parallel to the loading direction on the top of the footing on the north side at the eighth force-control cycle (FC-8(+)). With increasing loading, the cracks extended from the column to the edge of the footing. The cracks in the footing surface at the north side of the column at DC-7(+) are shown in Figure 4-2c. The CFRP jacket experienced horizontal splitting (shown in Figure 4-2d) at varied heights along the column at large DC levels due to the tension force induced by the applied bending moment.

Damage to the longitudinal reinforcement could not be verified during testing without removal of the CFRP jacket and concrete, although a loud noise that sounded like bar fracture was heard when the maximum lateral load was passed during the displacement control phase. In order to confirm the origin of the suspicious sound and to determine whether a bar had fractured, forensic inspection was conducted after testing. First, the CFRP jacket and loose concrete were removed from the bottom end of the column (Figure 4-3). As shown in this figure, no fracture was observed above the couplers in any of the longitudinal bars. No openings or fracture were found in the spirals. Thus, it was suspected that the fracture point may have occurred within the footing, i.e., the damage to the longitudinal reinforcement may have extended downwards into the footing. In order to confirm this, reinforcement within the footing needed to be exposed after removal of concrete. To do so, the column was disconnected from the footing by removing the loose concrete and cutting the longitudinal bars to facilitate the work on the footing. Concrete within the footing was loosened with a jackhammer and then removed. Figure 4-4a shows the footing after the removal of top cover concrete. As shown in this figure, one No. 4 (12.7 mm dia.) bar

was observed to have fractured due to the jackhammer impact force during concrete loosening work. No visible damage was observed in the other No. 4 (12.7 mm dia.) bars or the No. 6 (19.1 mm dia.) bars within the footing. No damage was observed within the couplers. In order to determine whether there was longitudinal bar fracture below the couplers, additional core concrete was to be removed to expose the lower portions of the longitudinal bars. The first layer of footing reinforcement including the No. 4 (12.7 mm dia.) and No. 6 (19.1 mm dia.) bars were cut and removed from the footing to facilitate the removal of concrete. Figure 4-4b shows the footing after the removal of the first layer of footing reinforcement. As shown in Figure 4-5, the exposed length of longitudinal bar below the couplers was approximately 6 in. (150 mm). No fracture was found in any of the longitudinal bars. The core concrete below this level shown in Figure 4-5 was well-confined by the spirals and footing reinforcement, and it was extremely difficult to induce further damage with the jackhammer, suggesting no fracture beneath that location. In summary, no fractured longitudinal footing bars were found during the forensic investigation. This can also be verified by the fact that the core concrete was still sound during testing due to the good confinement provided by the CFRP that experienced no rupture, which also helped prevent the longitudinal bars from fracture due to repeated buckling.

In summary, R-Calt-1 performed well up to a drift ratio of 11% with only minor cracks in the footing. No bar buckling, bar fracture, CFRP rupture, or concrete crushing was observed during testing.

The progressive deformation of R-Calt-2 during testing is shown in Figure 4-6. Testing was terminated when the CFRP started to rupture near the mid-height of the column above the plastic hinge region (see Figure 4-7); and only positive cycles at displacement-control levels 4 and 5

were applied due to the limitation of the actuators to apply additional torsional loading. The CFRP in the other regions of the column appeared to be sound without any failure. The cover concrete spalled in the region of CFRP rupture due to loss of confinement. No fractured bars were observed during testing.

#### 4.2. BASE SHEAR-LATERAL DISPLACEMENT AND TORSIONAL MOMENT-TWIST RELATIONSHIPS

The base shear and torsional moment applied to the columns were calculated from the forces recorded by the two actuators. The free-end lateral displacement and twist angle were calculated based on the geometry of the test setup and the displacement of the two actuators. Base shear-lateral displacement and torsional moment-twist hysteresis responses of the original columns and corresponding repaired columns are compared in Figure 4-8. Maximum values from Figure 4-8 are summarized in Table 4-1.

The base shear and lateral displacement relations for R-Calt-1 and Calt-1 are compared in Figure 4-8a, where “push” was defined as positive and “pull” as negative. The hysteretic behavior of R-Calt-1 was asymmetric with a higher maximum base shear in the pull direction than in the push direction, while that of Calt-1 was more symmetric. The asymmetric behavior of R-Calt-1 can be attributed to the asymmetric damage unrepaired within the column. The higher lateral displacement applied in the push direction was due to the fact that the actuators had a larger stroke capacity in the push direction (positive displacement) than in the pull direction (negative displacement). The maximum base shear of R-Calt-1 was also larger than that of Calt-1, which indicates that the repair method was successful in restoring and even enhancing the lateral

strength. R-Calt-1 experienced no lateral strength degradation until testing was stopped in both directions, while the lateral strength of Calt-1 started to degrade at a drift ratio of 5% in both directions. This indicates that the repair method was also successful in restoring and enhancing the lateral displacement capacity of the column. The cyclic loops of R-Calt-1 had a similar shape to those of Calt-1 with similar unloading stiffness before strength degradation of Calt-1. The pinching effect was negligible in both R-Calt-1 and Calt-1. It is worth noting that the lateral strength could be restored with the use of bar couplers for the 16 circumferential bars (80% of the total longitudinal bars) within the plastic hinge region.

The base shear and lateral displacement envelopes for R-Calt-1 and Calt-1 are compared in Figure 4-9a. As shown in this figure, the initial lateral stiffness of R-Calt-1 was very similar to that of Calt-1 in both directions; however, the lateral stiffness of R-Calt-1 started to decrease more rapidly than that of Calt-1 after relatively small lateral loads in both directions. This may have been due to the damage to the footing that occurred during coupler installation, which involved demolition of footing concrete and could have compromised the integrity of the footing. Other possible reasons may be the unrepaired damage in the column, shear deformation between the replacement plastic hinge region and the non-plastic hinge region, and/or slip within the couplers.

Idealized envelopes representing an elasto-plastic curve for Calt-1 and R-Calt-1 are shown in Figure 4-10a and Figure 4-10b, respectively. The bilinear envelopes were idealized by setting the initial slope to pass through the first yield point recorded during testing and adjusting the plastic portion to equate the areas under the measured and idealized curves at the highest displacement level tested. Table 4-1 summarizes the maximum values obtained from Figure 4-10. In this table,

for Calt-1, the equivalent yield base shear or torsional moment is the average value of base shears or torsional moments in both directions. The equivalent lateral or torsional stiffness is the average value of the stiffness calculated in both directions. The equivalent lateral or torsional ductility ratios are the larger values of lateral or torsional ductility ratio in one direction are listed due to the asymmetric loading history. As shown in Table 4-2, the equivalent elastic lateral stiffness of R-Calt-1 was approximately 64% of that of Calt-1. It should be noted that the lateral ductility of R-Calt-1 should be higher than the value shown in Table 4-2 (4.9) since testing was stopped before the column experienced any strength degradation. Since the lateral ductility of Calt-1 was approximately 4.7, this indicates that the repair method was able to restore the lateral ductility as well.

Figure 4-8b shows the hysteresis of torsional moment and twist relations where clockwise torsion was defined as positive and counterclockwise torsion as negative. No degradation in torsional strength of R-Calt-1 in either direction was observed during testing, while the torsional strength of Calt-1 started to degrade at small twist angles. Lack of degradation in torsional strength of R-Calt-1 was attributed to the influence of the CFRP jacket, which helped delay the crushing of concrete within the plastic hinge region. The maximum torsional moment of R-Calt-1 was also larger than that of Calt-1. The torsional moment and twist envelopes are compared in Figure 4-10b. As shown in this figure, the initial torsional stiffness of R-Calt-1 was lower than that of Calt-1. This may be due to the relative torsional movement between the replacement plastic hinge region and the non-plastic hinge region and the loss of integrity of the footing during repair. Elasto-plastically idealized torsional moment and twist curves are shown in Figure 4-10c and Figure 4-10d. As shown in these two figures, the equivalent elastic torsional stiffness

of R-Calt-1 was 48% of that of Calt-1. Since no torsional strength degradation was observed for R-Calt-1 during testing, the actual torsional ductility of R-Calt-1 should be larger than the value (3.8) listed in Table 4-2. On the other hand, the torsional strength of Calt-1 started to degrade at the twist angle of 3 degrees; thus, the torsional ductility of R-Calt-1 may be larger than that of Calt-1 (4.0). This indicates that the repair method restored the torsional behavior of the column.

Figure 4-8c compares the base shear and lateral displacement hysteresis responses of R-Calt-2 and Calt-2. As shown in this figure, the maximum base shear of R-Calt-2 was larger than that of Calt-2. As the testing was stopped when the CFRP ruptured, the recorded lateral displacement of R-Calt-2 was smaller than that of Calt-2; however, this does not imply that the lateral displacement capacity of R-Calt-2 was lower than that of Calt-2, since R-Calt-2 may still have additional deformation capability even with ruptured CFRP if there are no fractured bars since FRP rupture due to torsional loading is a progressive process (He et al. 2014). The shape of the hysteresis response of R-Calt-2 was also similar to that of Calt-2 with similar unloading stiffness and negligible pinching effect. The base shear and lateral displacement envelopes are compared in Figure 4-9c. As shown in this figure, the initial lateral stiffness of R-Calt-2 was smaller than, but similar to, that of Calt-2. This may be due to the fact that none of the reinforcing bars in the footing were cut during installation of couplers. Maximum values from Figure 4-9 are summarized in Table 4.1. Elasto-plastically idealized curves are shown in Figure 4-11a and Figure 4-11b. Values from Figure 4-11 are summarized in Table 4.2. The equivalent lateral stiffness of R-Calt-2 was about 71% of that of Calt-2. Since the base shear capacity did not experience any degradation during testing of R-Calt-2, the ductility of R-Calt-2 may be larger

than that of Calt-2, which was approximately 5.9. This may imply that the repair method was able to restore or enhance the lateral ductility of the column.

Figure 4-8d compares the hysteresis of torsional moment and twist of R-Calt-2 and Calt-2. As shown in this figure, the maximum torsional moments of R-Calt-2 in both directions were similar, while the positive maximum torsional moment of Calt-2 was larger than the absolute value of the negative maximum torsion moment. The maximum torsional moment of R-Calt-2 was also larger than that of Calt-2. The torsional moment capacity of R-Calt-2 did not experience any degradation up to a twist angle of 8 degrees, while that of Calt-2 started to degrade at an angle of 7.5 degrees. The hysteretic shape of R-Calt-2 was also similar to that of Calt-2 before the degradation mentioned previously with similar unloading torsional stiffness and negligible pinching effect. The torsional moment and twist envelopes of R-Calt-2 and Calt-2 are compared in Figure 4-9d. As shown in this figure, the initial torsional stiffness of R-Calt-2 was similar to that of Calt-2; however, after a very small value of twist, the torsional stiffness of R-Calt-2 started to decrease and become smaller than that of Calt-2. This may be due to the relative torsional movement between the replacement plastic hinge region and the non-plastic hinge region. The elasto-plastically idealized curves of torsional moment and twist of R-Calt-2 and Calt-2 are compared in Figure 4-11d. As shown in Table 4.2, the equivalent torsional stiffness of R-Calt-2 was about 59% of that of R-Calt-2. Since no degradation in torsional moment capacity of R-Calt-2 was observed during testing, R-Calt-2 may still deform more torsionally (He et al. 2014) and experience higher torsional ductility than that of Calt-2, which was approximately 8.1. The repair method improved the torsional behavior and was also able to enhance the torsional strength.

Based on the comparison of the base shear-lateral displacement and torsional moment-twist relations for both repaired and original columns, it can be concluded that the repair method used to repair R-Calt-1 and R-Calt-2 was able to enhance the strength and ductility of the repaired columns but resulted in a lower flexural and torsional stiffness. For R-Calt-2, the reduction in flexural stiffness was not as significant as for R-Calt-1. This may be due to the fact that coupler installation did not disturb the footing as much as for R-Calt-1. Other reasons for the reduction in lateral stiffness may be due to the relative lateral displacement at the interface between the replacement region and non-plastic hinge region or footing and/or slip within couplers. The reduction in torsional stiffness may be due to the torsional movement at the interface between the replacement regions and non-plastic hinge region or footing. Application of CFRP across the interface with fibers oriented along the longitudinal axis of the column may help bridge the interface and increase the torsional stiffness of repaired columns.

### 4.3. ENERGY DISSIPATION

Energy dissipated in each loading cycle can be calculated as the summation of the enclosed area for each cycle of the base shear-displacement and torsional moment-twist relations (Priestley et al 1996). The energy dissipation per cycle for both the repaired and corresponding original columns is shown in Figure 4-12.

As shown in Figure 4-12a, the dissipated energy for each cycle prior to the 13<sup>th</sup> cycle was negligible for both R-Calt-1 and Calt-1 due to the fact that yielding of reinforcement and spalling or crushing of concrete was very limited prior to that cycle. After the 13<sup>th</sup> cycle and prior to the 26<sup>th</sup> cycle, the dissipated energy per cycle was more obvious and increased with increasing

applied displacement. In this phase, the energy was mainly dissipated by extensive yielding of reinforcement, and/or cracking, spalling, and/or crushing of concrete. For most of this phase, the energy dissipation of R-Calt-1 was less than that of Calt-1 since R-Calt-1 experienced very limited spalling or crushing of concrete due to the confinement provided by the CFRP. At the same displacement level, the energy dissipation for the second and third cycles was less than that of the previous cycle since the energy dissipation in the first cycle was irreversible, and the specific displacement level could not induce additional concrete spalling or crushing in the subsequent cycles. The energy dissipation per cycle of Calt-1 decreased after the 26<sup>th</sup> cycle due to the sequential fracture of longitudinal reinforcement and the progression of concrete crushing into the core.

As shown in Figure 4-12b, the dissipated energy per cycle prior to the 5<sup>th</sup> cycle was negligible for Calt-2. After the 5<sup>th</sup> cycle, the energy dissipation per cycle increased with increasing displacement level. At the same displacement level, the energy dissipation in the 2<sup>nd</sup> and 3<sup>rd</sup> cycles was less than that of the previous cycle for the same reason mentioned above for R-Calt-1. Generally, energy dissipation per cycle of R-Calt-2 was smaller than that of Calt-2. This may be due to the fact that yielding of the spirals within the plastic hinge region of Calt-2 contributed to the energy dissipation, while R-Calt-2 did not have spirals within plastic hinge region and thus lacked that contribution to the energy dissipation.

Cumulative energy dissipation was also compared between original and repaired columns. As shown in Figure 4-13, both repaired columns showed smaller cumulative energy dissipation at the end of each load cycle than the corresponding original columns.

#### 4.4. MEASURED STRAINS

Strain gages were installed on the replacement bar segments, couplers, and CFRP to record the strain history during testing. The strain distribution along the column height at different stages of displacement control loading is shown in Figure 4-14, Figure 4-15, and Figure 4-16. Figure 4-14 compares the measured steel strain distribution within the plastic hinge region for both the repaired and corresponding original columns. Figure 4-15 and Figure 4-16 show the measured CFRP strain distribution along the column height for the repaired columns. In these figures, the letters “R” and “O” in the legend refer to the “repaired” and “original” columns, respectively; “DC” and the number following it denotes “displacement control” and corresponding stage; “+” and “-” indicates that the displacement was applied in the “push” and “pull” directions, respectively.

In Figure 4-14, the lowest and upper-most data points for the repaired columns in each figure were the strains measured in the couplers, while the other data points were measured in replacement bars. All the data for the original columns were measured in the longitudinal bars. As shown in these figures, the strain distribution along the longitudinal reinforcement including bars and couplers in the repaired columns (solid lines in the figures) was different from that in the original columns (dashed lines in the figure). The maximum strain at a given displacement control stage of Calt-1 was usually located at the column base at the location of maximum moment, while that of R-Calt-1 was located a short distance from the top end of the couplers. Additionally, the maximum strain at a given displacement control stage of Calt-2 was located within the region between 20 in. to 36 in. (510 mm to 915 mm) with accumulating damage to the concrete, while that of R-Calt-2 was located a short distance from the top end of the couplers.

This indicated that repair changed the strain distribution along the longitudinal reinforcement. The figures also show that at the displacement control stages, most of the replacement bars yielded, and that the plastic hinge length of the repaired columns was similar to that of the original columns. It should also be noted that for larger displacement control states, positive strains were recorded in the longitudinal reinforcing bars at specific locations in both the push and pull cycles for R-Calt-1, which are attributed to residual positive strain (induced by tension) from the previous cycle(s).

Figure 4-15 summarizes the CFRP hoop strain distribution along the column height for R-Calt-1. As shown in this figure, the maximum CFRP strain measured during testing was 0.008, which was close to the design rupture strain of the CFRP system provided by the manufacturer; however no CFRP rupture was observed during testing, which implies that the design strain was conservative. The maximum hoop strain in the direction perpendicular to the loading direction at each displacement control stage was measured 10 to 30 in. (250 to 750 mm) from the base of the column (Figure 4-15a, b, d, and e), while the maximum hoop strain parallel to the loading direction at each displacement control stage was measured 20 to 40 in. (500 to 1016 mm) from the base of the column (Figure 4-15c and f). This suggests that the CFRP would likely rupture in these locations with additional loading. As shown in Figure 4-15a, b, d, and e, the hoop strain perpendicular to the loading direction at a specific displacement control level was greater on the tension side than that on the compression side.

Figure 4-16 summarizes the CFRP strain distribution along the column height for R-Calt-2. As shown in this figure, at lower displacement control stages, the hoop strain increased with the increasing elevation, and the maximum hoop strain was measured at the elevation nearest to the

free end of the column. At higher displacement control stages, the measured hoop strain at locations from a height of 55 in. to 80 in. (1400 mm to 2030 mm) increased drastically due to the rupture of CFRP at these locations. The maximum hoop strain within the plastic hinge was approximately 0.0065 at an elevation of approximately 10 in. (250 mm) from the base of the column. Generally, the hoop strain measured within the plastic hinge region was relatively small compared to that outside the plastic hinge region, which may imply that more layers of CFRP were required outside the plastic hinge region while the number of layers within the plastic hinge region may be reduced.

In summary, the use of the mechanical bar couplers in the repaired columns changed the strain distribution along the longitudinal reinforcement; however, the plastic hinge location did not change. Although R-Calt-1 was not able to be tested to failure, it appears that additional displacement would have resulted in CFRP rupture at the height of 10 to 20 in. (250 to 500 mm) above the top of footing, since the measured strain values were close to the rupture strain. For R-Calt-2, the design of the CFRP within the plastic hinge region may have been slightly conservative using the procedure mentioned above.

#### 4.5. CONCLUDING REMARKS

This chapter presents the evaluation of the repair method proposed in Chapter 3 by comparing the experimental results obtained from testing the repaired and corresponding original columns. Based on the discussions and investigations in this chapter, the following conclusions may be made: (1) the repair method was able to enhance both the flexural and torsional strength and ductility; (2) the repair method improved the torsional behavior; (3) the repair method resulted in

reduced lateral and torsional stiffness; (4) energy dissipation per cycle as well as cumulative energy dissipation of the repaired columns was lower than that of the original columns; (5) based on the longitudinal reinforcing steel strain distribution, the plastic hinge zone of the repaired columns was similar to that of the original columns; (6) the design method to determine required number of layers of CFRP was conservative enough to avoid damage to the CFRP jacket within the plastic hinge region; (7) since stiffness and energy dissipation of the repaired columns were lower than those of the original columns, the influence of the repair method on the response of the entire bridge structure needs to be investigated before the proposed repair method is adopted.

Table 4-1 Summary of Measured Forces for Calt-1, Calt-2, R-Calt-1, and R-Calt-2

Column ID	Maximum Positive Base Shear kip (kN)	Maximum Negative Base Shear kip (kN)	Maximum Positive Torsional Moment kip-ft (kN-m)	Maximum Negative Torsional Moment kip-ft (kN-m)
Calt-1	90.3 (402.7)	87.7 (390.1)	207.3 (281.1)	238.4 (323.2)
R-Calt-1	96.7 (430.1)	115.2 (512.4)	320.5 (434.5)	345.0 (467.8)
Calt-2	63.9 (284.2)	70.0 (311.4)	541.1 (733.6)	419.0 (568.1)
R-Calt-2	87.4 (388.8)	87.3 (388.3)	564.9 (765.9)	568.6 (770.9)

Table 4-2 Critical Values of Idealized Load-Displacement Curves for Calt-1, Calt-2, R-Calt-1, and R-Calt-2

Column ID	Equivalent Average Yielding Base Shear kip (kN)	Equivalent Average Yielding Torsional Moment kip-ft (kN-m)	Equivalent Average Lateral Stiffness kip/in (kN/mm)	Equivalent Average Torsional Stiffness kip-ft/rad (kN-m/rad)	Equivalent Lateral Ductility Ratio	Equivalent Torsional Ductility Ratio
Calt-1	85.0 (378.0)	216.0 (292.9)	49.9 (8.73)	21,922 (16,166)	4.7	4.0
R-Calt-1	99.2 (441.3)	271.6 (368.2)	31.7 (5.55)	10,573 (7,797)	4.9*	3.8*
Calt-2	61.2 (272.2)	419.1 (568.2)	40.5 (7.09)	16,946 (12,497)	5.9	8.1
R-Calt-2	78.4 (348.7)	560.0 (759.3)	28.6 (5.01)	9,940 (7330)	2.4*	2.9*

\*Note: actual values may be larger than the tabulated due to early termination of the testing.



DC-1(-)



DC-2(-)



DC-3(-)



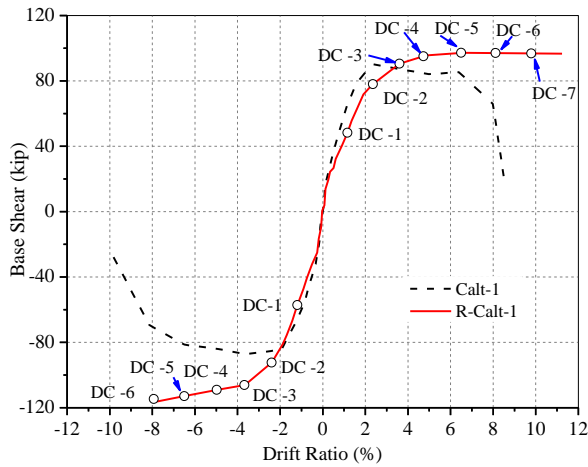
DC-4(-)



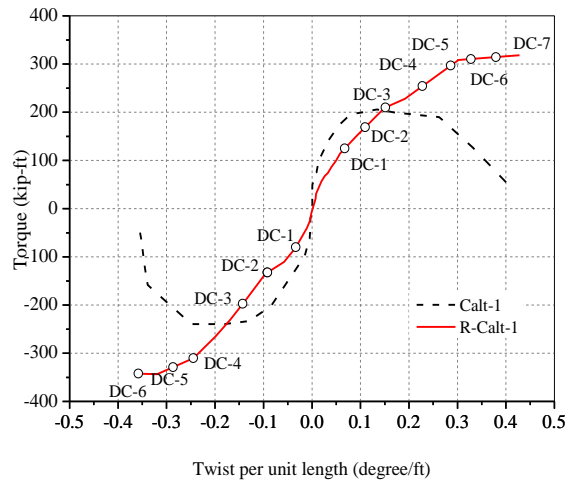
DC-5(-)



DC-6(-)



Envelope of Base Shear vs. Drift Ratio



Envelope of Torque vs. Twist Per Unit Length



DC-1(+)



DC-2(+)



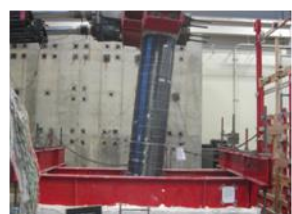
DC-3(+)



DC-4(+)



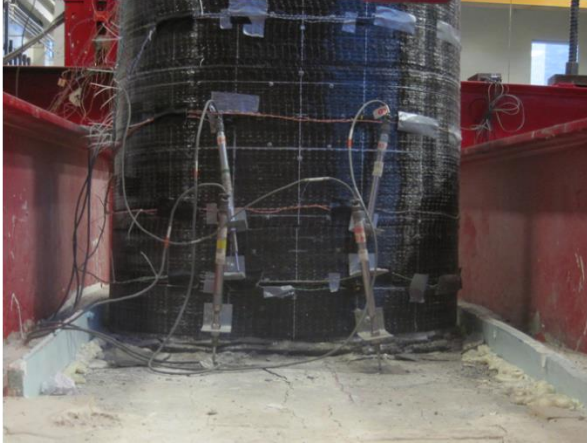
DC-5(+)



DC-6(+)



Figure 4-1 Progressive Deformation of R-Calt-1 at Increasing Load Levels



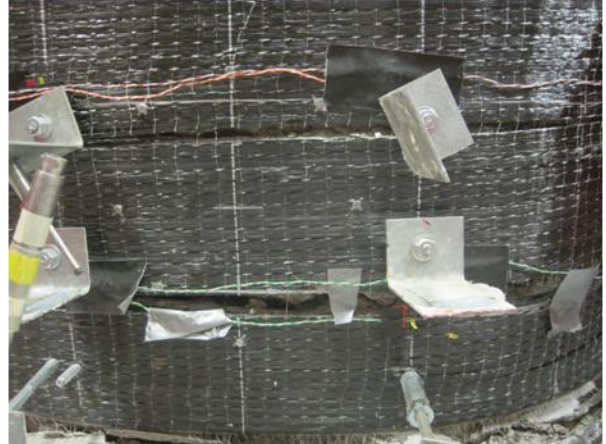
(a) Cracking of Footing on North Side at DC-6 (+)



(b) Cracking of Base on North Side at DC-6 (-)



(c) Cracking of Footing on North Side at DC-7 (+)



(d) Splitting of CFRP on North Side at DC-7 (+)

Figure 4-2 Damage to R-Calt-1



(a) South Face



(b) North Face

Figure 4-3 View of R-Calt-1 after Removal of CFRP Jacket



(a) After Removal of Top Cover



(b) After Removal of First Layer of Footing Reinforcement and Core Concrete

Figure 4-4 Plan View of Footing of R-Calt-1



(a) North Face



(b) South Face



(c) West Face



(d) East Face

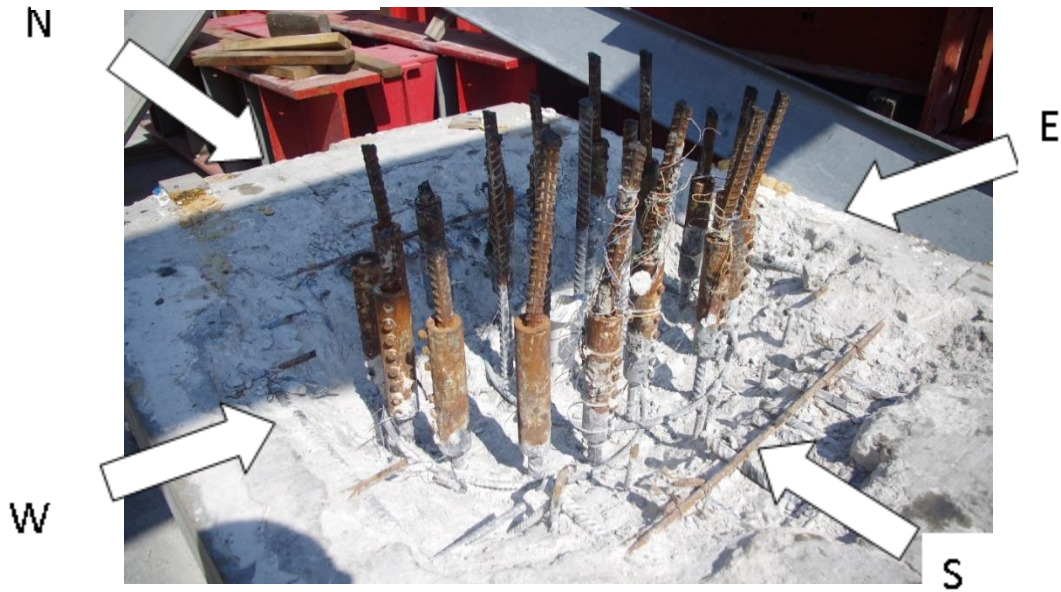


Figure 4-5 Isometric View of R-Calt-1 After Removal of First Layer of Footing Reinforcement

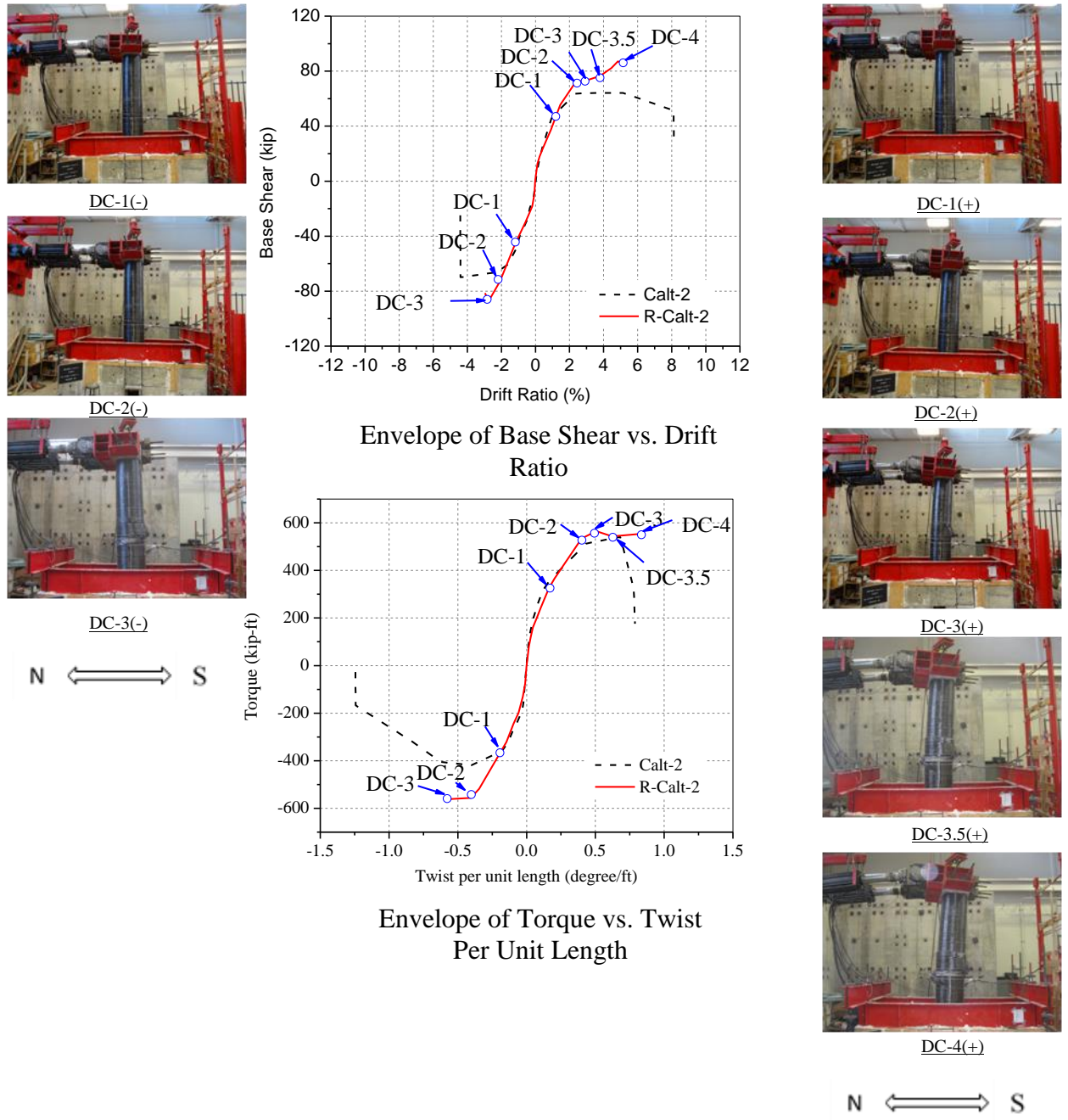
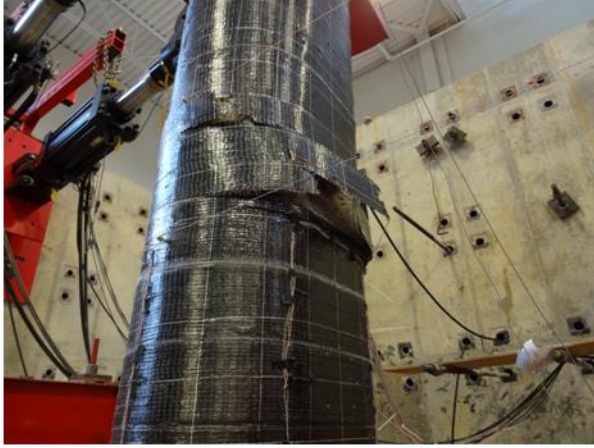


Figure 4-6 Progressive Deformation of R-Calt-2 at Increasing Load Levels



(a) Fracture of CFRP South Side at DC-3 (+)



(b) Fracture of CFRP on West Side at DC-3 (-)



(c) Fracture of CFRP on South Side at DC-3.5 (+)



(d) Fracture of CFRP on South Side at DC-4 (+)

Figure 4-7 Damage to R-Calt-2

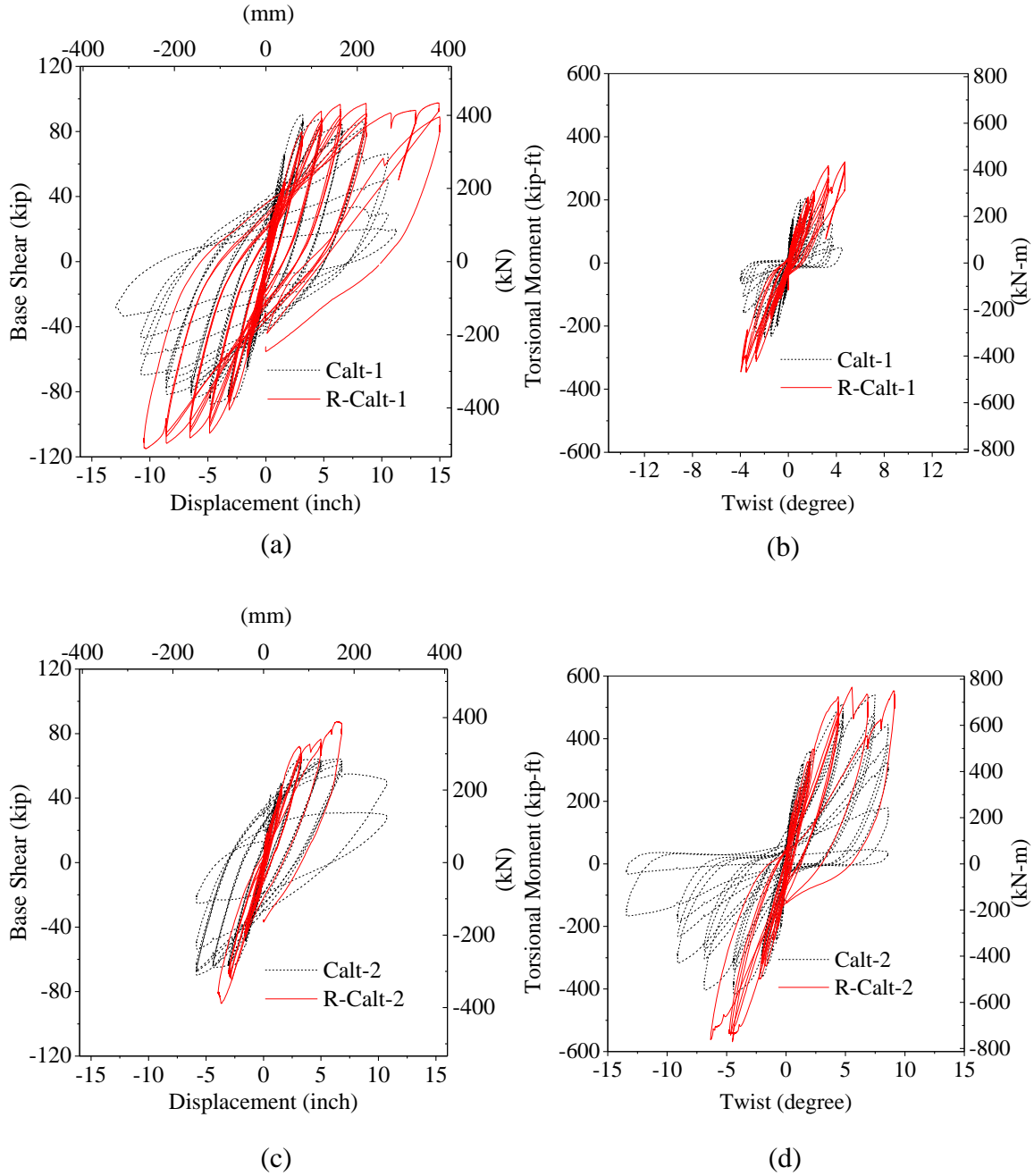


Figure 4-8 Load-Displacement Hysteresis Responses of Calt-1, R-Calt-1, Calt-2, and R-Calt-2

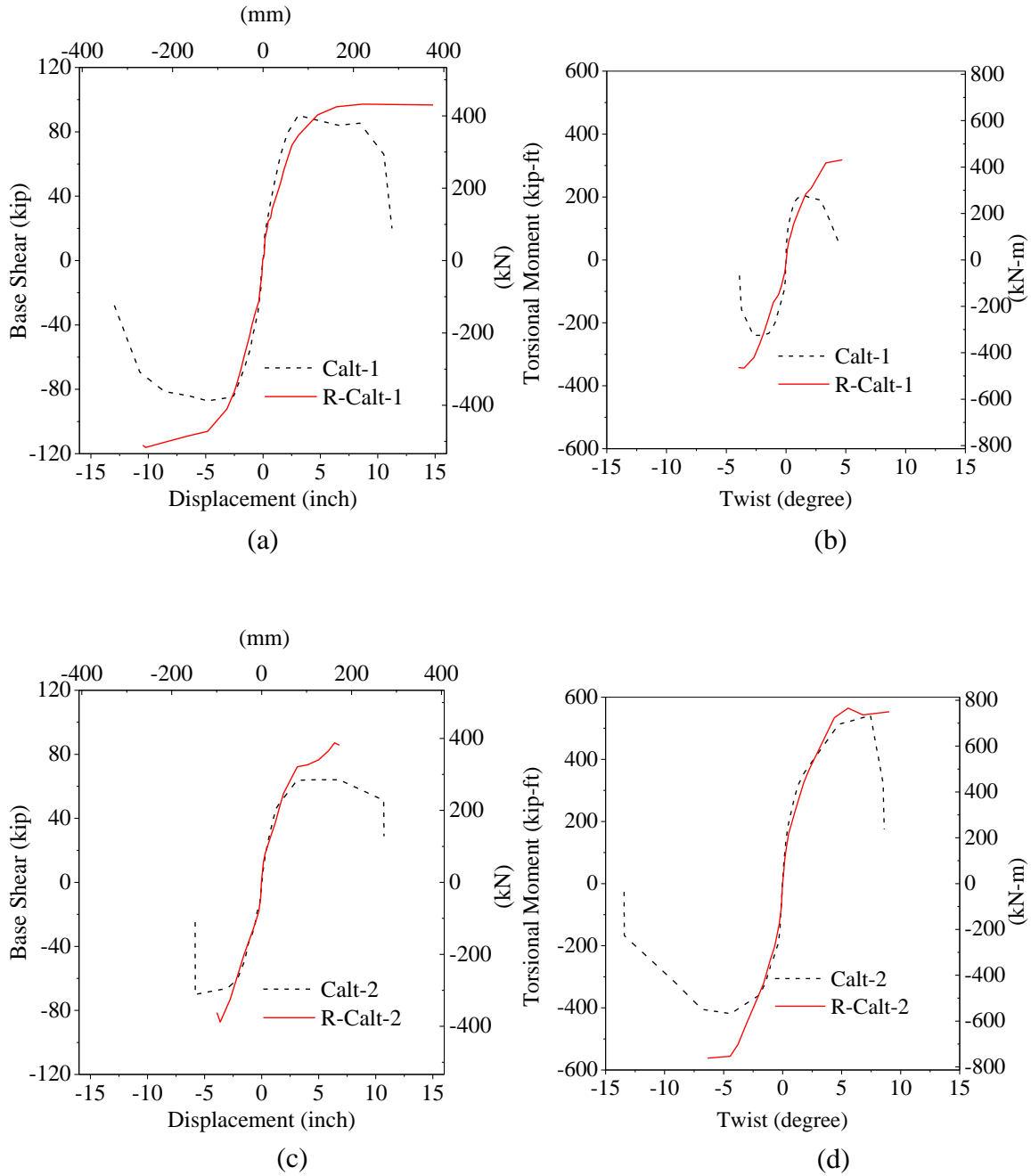
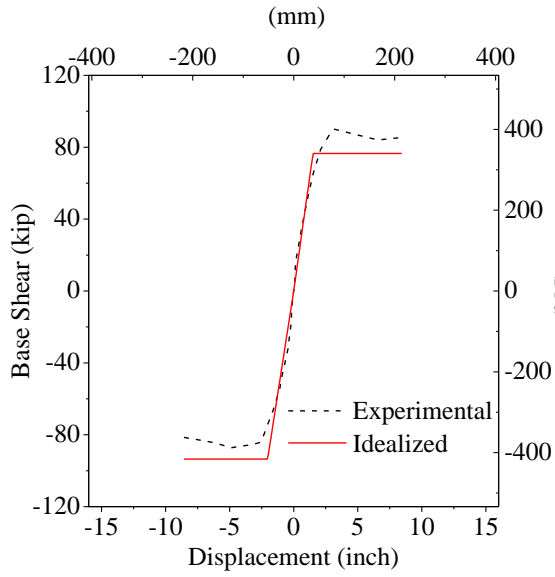
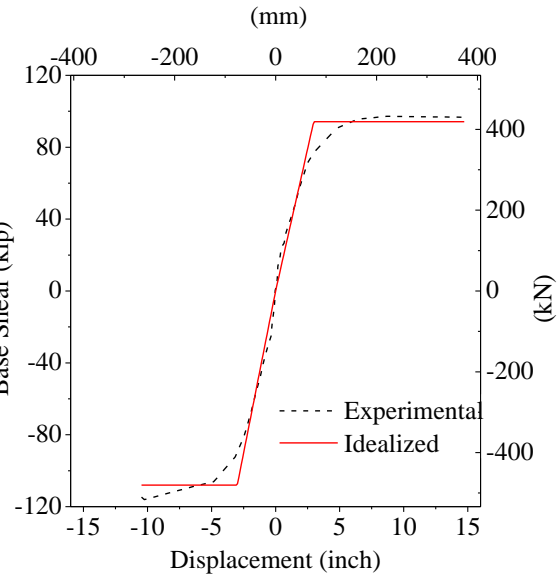


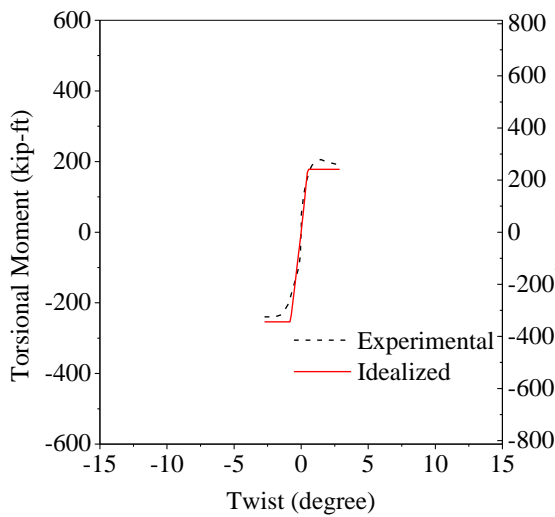
Figure 4-9 Load-Displacement Envelopes of Calt-1, R-Calt-1, Calt-2, and R-Calt-2



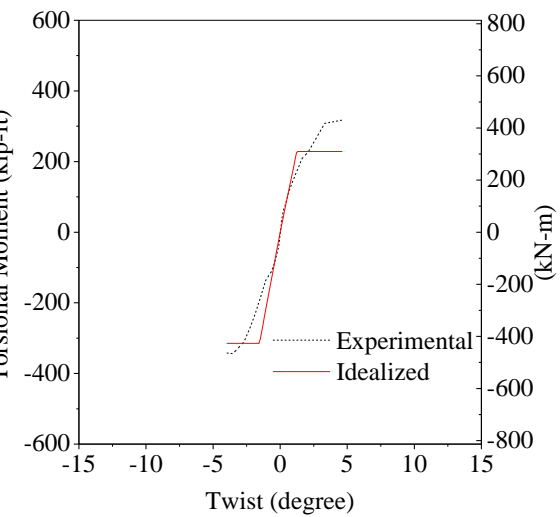
(a) Calt-1



(b) R-Calt-1

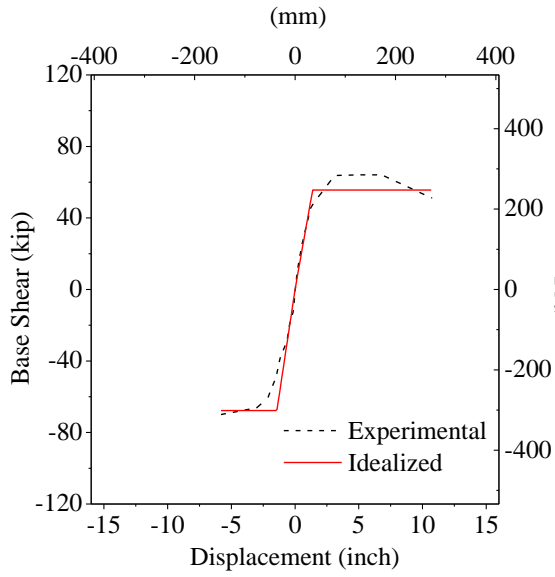


(c) Calt-1

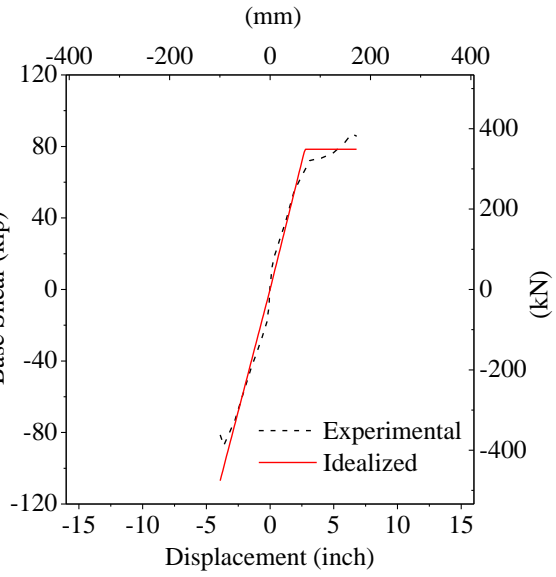


(d) R-Calt-1

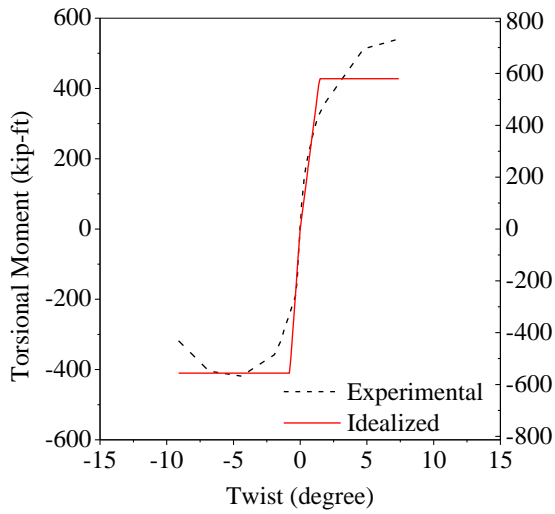
Figure 4-10 Idealized Load-Displacement Envelopes of Calt-1 and R-Calt-1



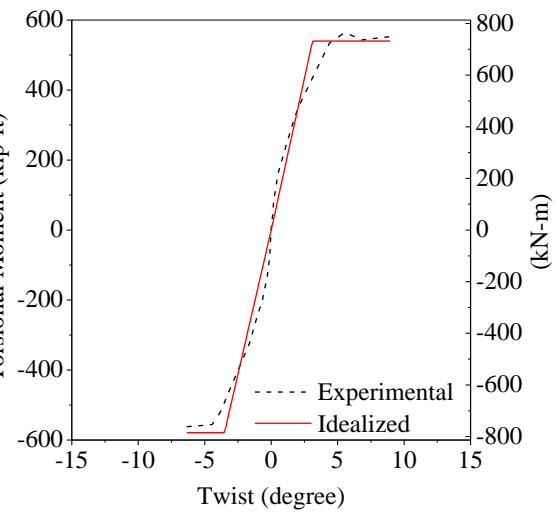
(a) Calt-2



(b) R-Calt-2

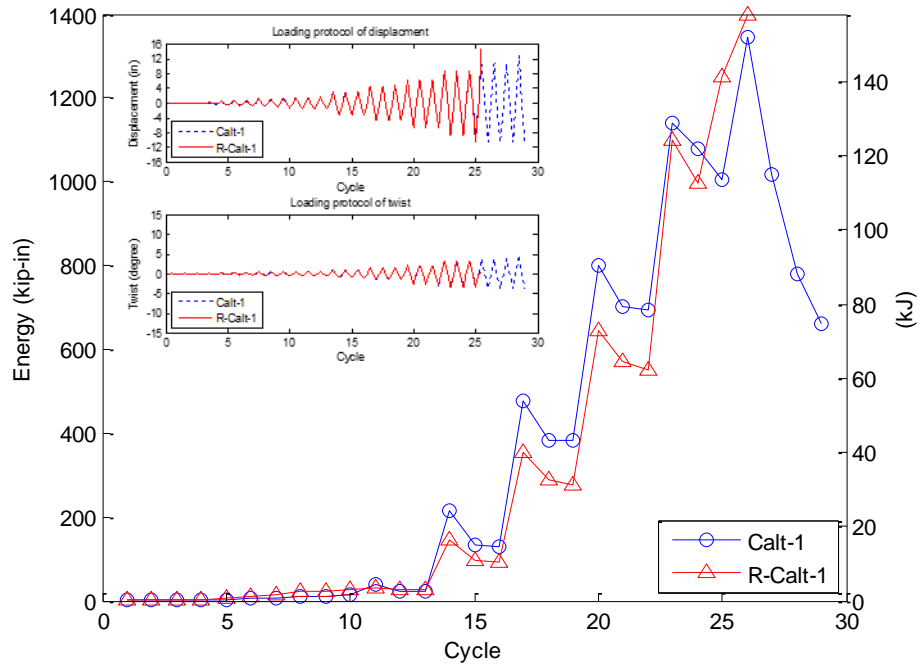


(c) Calt-2

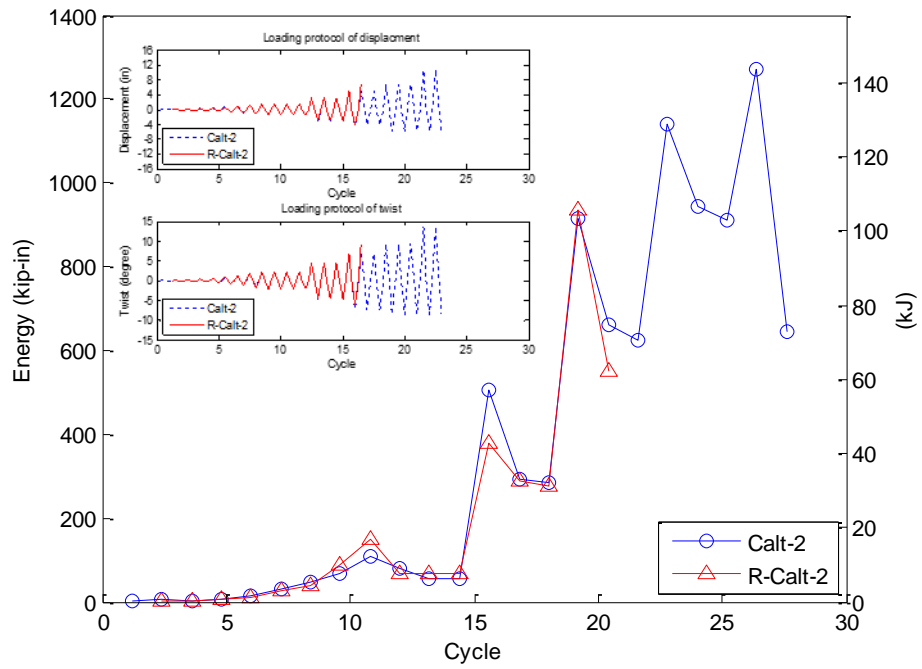


(d) R-Calt-2

Figure 4-11 Idealized Load-Displacement Envelopes of Calt-2 and R-Calt -2

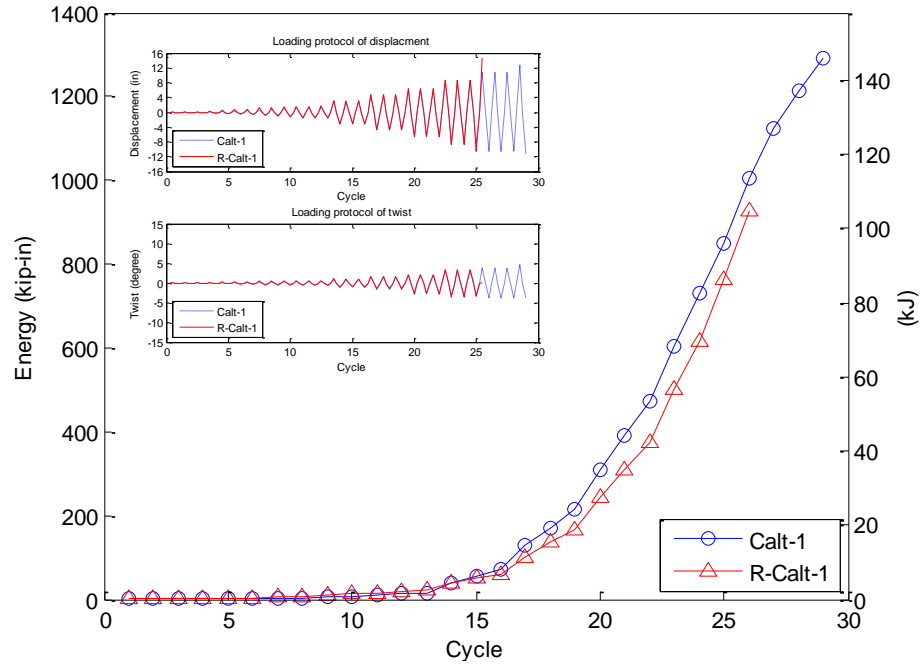


(a)

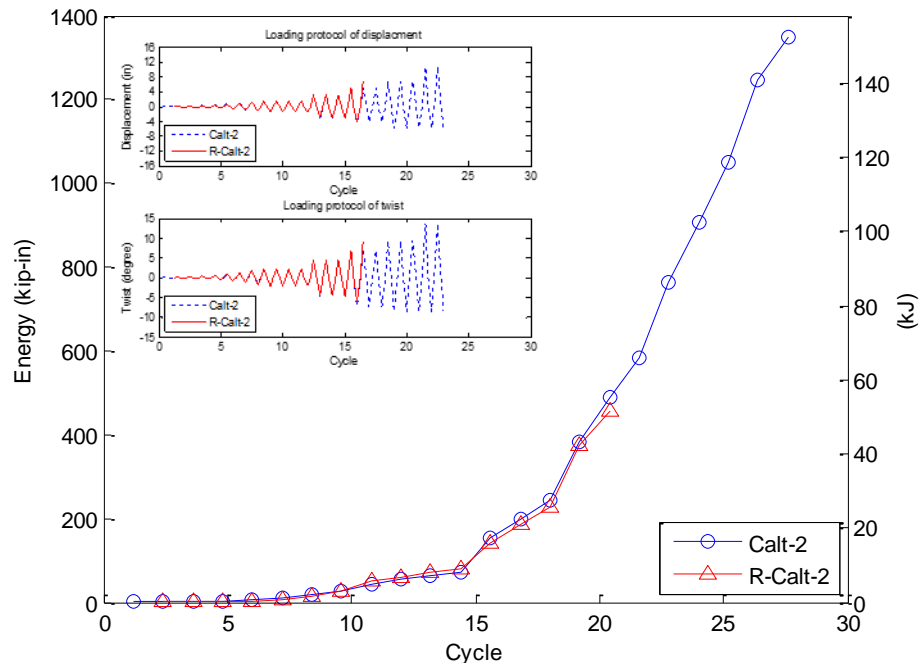


(b)

Figure 4-12 Energy Dissipation per Cycle of Calt-1, R-Calt-1, Calt-2, and R-Calt-2



(a)



(b)

Figure 4-13 Cumulative Energy Dissipation of Calt-1, R-Calt-1, Calt-2, and R-Calt-2

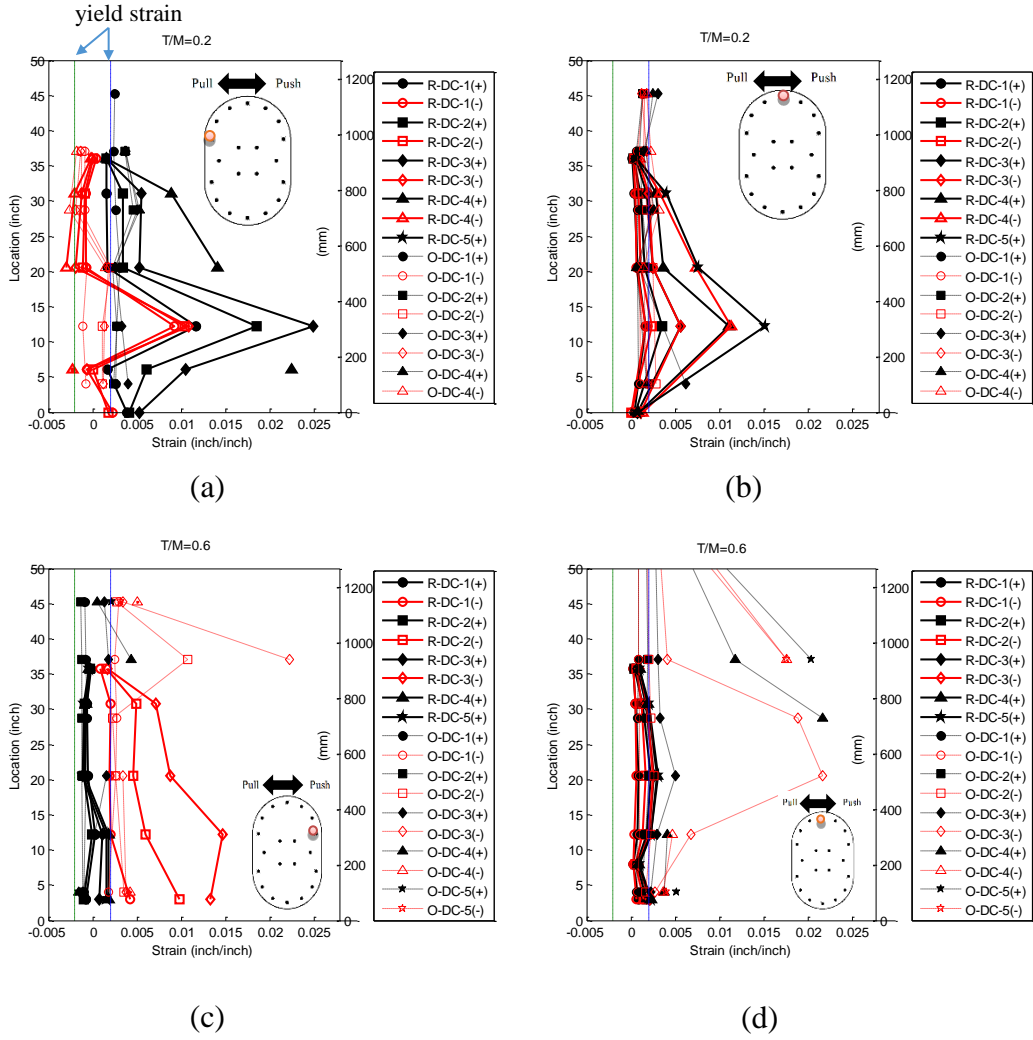


Figure 4-14 Measured Reinforcing Steel Strain Distribution Along Column Height of (a) and (b) R-Calt-1 and (c) and (d) R-Calt-2

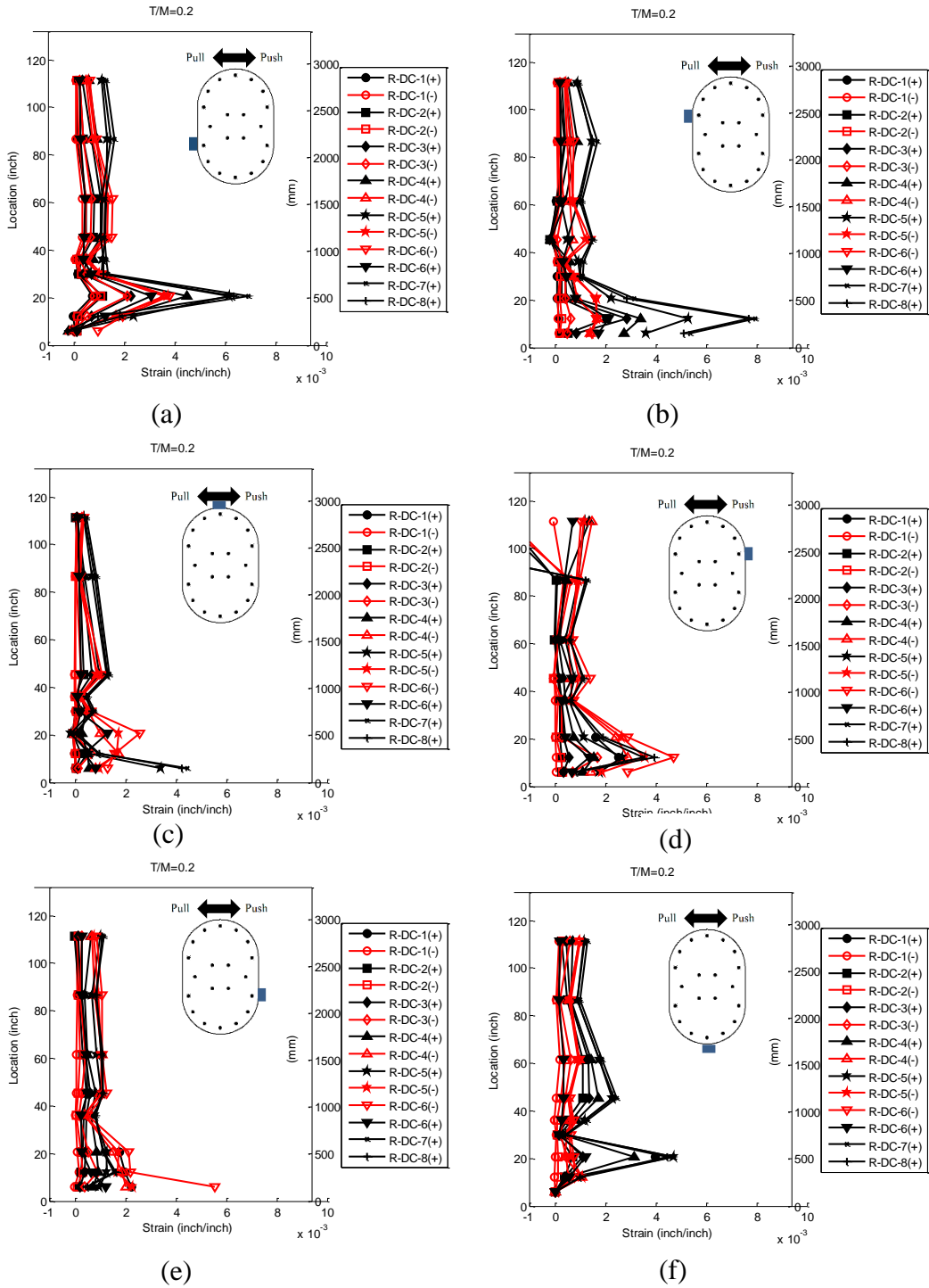


Figure 4-15 Measured CFRP Strain Distribution along Column Height of R-Calt-1

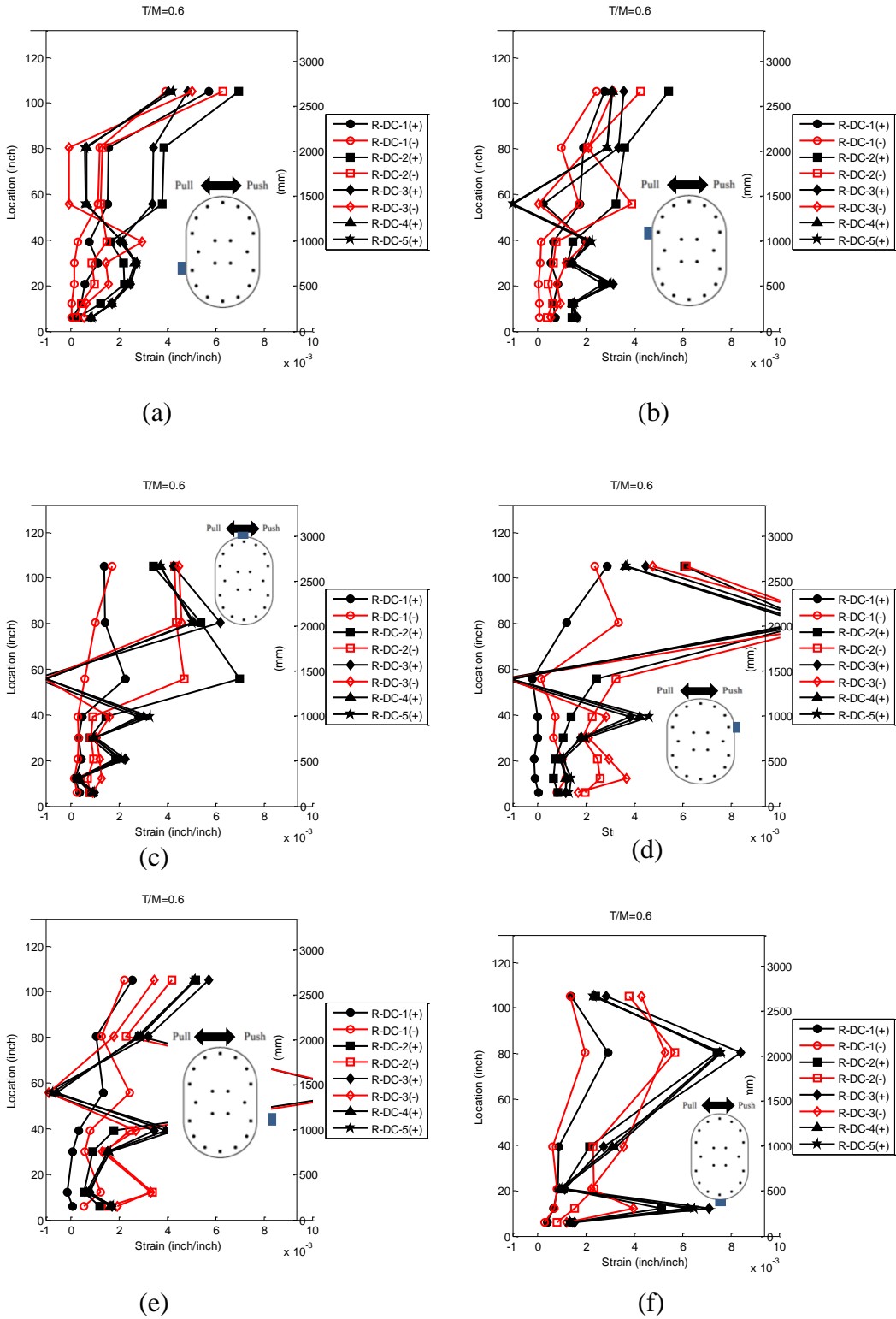


Figure 4-16 Measured CFRP Strain Distribution along Column Height of R-Calt-2

## 5. EXPERIMENTAL WORK OF R-CALT-3

The purpose of the experimental work of R-Calt-3 was to validate a proposed emergency repair method for earthquake-damaged bridge column reinforced with interlocking spirals and containing fractured longitudinal bars. One column had been tested to failure under a constant axial loading corresponding to 7% of the axial capacity of the column and reversed cyclic lateral loading resulting in combined bending moment, shear, and torsional moment. . The lateral loading was applied to the column with an angle of 35 degrees to the weak axis of the cross-section of the column, resulting in biaxial bending. The damage to the plastic hinge region of the column during the previous test included spalling and crushing of concrete, yielding, buckling, and/or fracture of longitudinal reinforcement, and yielding of transverse reinforcement. Extensive concrete cracking was observed in the region outside the plastic hinge. The repair procedure was based on an emergency repair philosophy and involved cutting a trench in the footing around the column perimeter, removing loose concrete, placing new grout, installing externally bonded unidirectional CFRP plates, installing a jacket built from prefabricated thin bidirectional CFRP laminate, filling the trench with mixed gravel and epoxy, placing epoxy into the gap between CFRP jacket and concrete/grout substrate, and repairing of footing with externally bonded CFRP sheets. The repaired column was tested under the same loading protocol as the original column. Section 5.1 describes the background of column tested in the previous study, including the test program and damage to the original column. Section 5.2 presents the design of the proposed repair method. Section 5.3 describes the repair procedure. Section 5.4 presents the test program for the repaired column including test setup, instrumentation, and loading protocol.

## 5.1. ORIGINAL COLUMN SPECIMEN

The experimental work discussed in Chapters 5 and 6 included one 1/2-scale oval-shaped RC bridge column that was tested to failure under constant axial loading and cyclic lateral loading resulting in combined bending moment, shear, and torsional moment in a previous study (Li and Belarbi 2011). This section describes the objective of the previous study and the damage to the column specimen prior to the repair conducted in the current study.

### 5.1.1. Previous test program

The original column is referred to in this chapter as Calt-3 (the repaired counterpart is referred as R-Calt-3) and was tested under constant axial loading and cyclic loading including torsion with T/M ratio of 0.2. The geometry and reinforcement details of Calt-3 are shown in **Error! Reference source not found.** Bending was applied about an axis with an angle of 35 degree to the weak axis. A constant axial load of 220 kips (979 kN), equivalent to 7% of the axial capacity of the column, was applied with 7 prestressing strands through a PVC pipe located at the axial centerline of the column post-tensioned by a hydraulic jack at the top of the column and an anchorage system at the bottom of the footing. The combination of bending moment, shear, and torsional moment loadings was applied using two hydraulic MTS actuators connected to the loading cap of the column with a steel loading frame as shown in Figure 3-2a. During testing, ten levels of force-control loading were applied to specimen up to the estimated first yielding point of either the longitudinal or transverse reinforcement with the increment corresponding to 10% of the predicted first yielding force (either bending moment or torsional moment). Each force-control level was applied for one reversed cycle. After the first yielding point, several levels of displacement-control loading were applied to specimen up to the failure of the specimen with the

increment corresponding to the displacement (either top displacement or twist) at the first yielding point. Each displacement-control level was applied for three reversed cycles. The loading protocol for Calt-3 is shown in Figure 5-2. It should be noted that the values of the lateral force or torsional moment are not illustrated in this figure. Instead, the top displacement or twist corresponding to the applied forces during the force-control phase is shown in this figure.

#### 5.1.2. Damage to Calt-3

After the original test, the damage to the column was inspected visually and determined by analysis of measured data. This section describes damage to the column including measured length of concrete spalling and depth of concrete crushing, fracture location and buckled region of longitudinal reinforcement, and yielding region of both the longitudinal and transverse reinforcement.

As shown in Table 5-3 and Figure 5-3, for Calt-3 with T/M of 0.2, cover concrete spalled from the column base to a height of 39 in. (990 mm). Concrete near the column base crushed into the core with a depth of 5 in. (127 mm). The definition of the spalled length and core crushing depth of concrete is shown in Figure 3-5. No spirals swelled, four of the longitudinal bars buckled, and six of the longitudinal bars fractured (refer to Table 5-3). The fracture locations and buckled regions of longitudinal reinforcement are shown in Figure 5-4. Strain gages were applied at various locations along the length of the longitudinal reinforcing bars during the original testing, as shown in Figure 5-5. Typical longitudinal reinforcement strain history is shown in Figure 5-6, and typical transverse reinforcement strain history is shown in Figure 5-7. Based on analysis of the measured strain data, all of the longitudinal bars yielded. Yielding of the longitudinal bars was indicated by strain gages located in the region 4.0 in. to 61.75 in. (100 to 1568 mm) above

the top of footing. The yielding may also have occurred within the footing but could not be verified since no strain gages were installed on the portion of the longitudinal bars inside the footing. Strain data were also investigated to determine the strain history of the spirals. Most gages mounted on the spirals within the plastic hinge region stopped functioning prior to termination of testing. The strain values collected from those gages before they malfunctioned and from other sound strain gages did not exceed the yield strain of the spirals. However, yielding of spirals may have still occurred near the base of the column for the reason that crushing of core concrete was observed and is usually considered to be a result of loss of confinement, which suggests that the spirals yielded.

## 5.2. REPAIR DESIGN

### 5.2.1. Repair scheme

The objective of repairing Calt-3 was to restore the flexural, shear, and torsion strength of the column; thus the method was considered an emergency repair rather than a permanent repair that aims to restore the deformation capacity as well. As shown in Figure 5-8, crushed and loose concrete near the column-footing joint were replaced with repair grout while the concrete in remaining portion of the column was not to be treated. Buckled and/or fractured longitudinal bars were not treated. Unidirectional CFRP strips were bonded to the external surface of the column to compensate for the loss of flexural strength due to the fractured longitudinal bars. A bidirectional CFRP jacket was installed in the plastic hinge region to compensate for the loss of confinement, shear, and torsional strength. Both the CFRP strips and the CFRP jacket were to be embedded into the footing to provide a connection to transfer the bending moment, shear force, and torsional moment into the footing. As a result, several reinforcing bars in the footing needed

to be cut to facilitate the embedment of the CFRP plates and jackets. Thus, CFRP sheets were externally bonded to the top surface of the footing to compensate for the loss of strength due to cutting the bars in the footing. Since the repaired column would be subjected to loading resulting in a torsional moment-to-bending moment (T/M) ratio of 0.2, a flexure-dominant failure was anticipated.

Section 5.2.2 describes the repair materials. Section 5.2.3 presents design of shear and torsion repair. Section 5.2.4 presents the flexural design including moment curvature analysis and determination of CFRP embedment length. Section 5.2.6 describes the footing repair design. Section 5.2.7 summarizes the details of the repair scheme.

#### 5.2.2. Repair materials

Repair grout with a similar compressive strength as the existing concrete was used to repair the plastic hinge region of the column. The material properties of concrete of the original column and the new replacement grout are provided in Table 5-1. Three types of CFRP were used. CFRP strips bonded to the surface of the column were unidirectional prefabricated CFRP (*QuakeWrap<sup>TM</sup> GU50C*). Material properties of the strips are listed in Table 5-4. Unidirectional CFRP (*QuakeWrap<sup>TM</sup> VU18C*) fabric with a density of 18.5 oz/sq yd (627 g/sq m) was used to repair the footing, and the properties are listed in Table 5-5. The properties of the prefabricated CFRP (*PileMedic<sup>TM</sup> PLC100.60*) laminate that was used to construct the jacket are listed in Table 5-6. An epoxy paste (*QuakeBond<sup>TM</sup> J201TC*) was used as the adhesive for the inter-layer bond of the CFRP jacket. Low-viscosity epoxy resin (*QuakeBond<sup>TM</sup> 320LV*) was used as the adhesive to bond the CFRP jacket to the repaired concrete surface and the footing. The properties of the epoxy resin are listed Table 5-7.

### 5.2.3. Column shear and torsion repair design

Within the plastic hinge region, the thickness of the CFRP jacket (i.e., number of layers) required for shear and torsion was determined by equalizing the contribution of the CFRP jacket to the shear and torsion resistance with the contribution of the existing spirals, which was considered to be 50% of that of original spirals at the damage state described previously (Vosooghi and Saiidi 2012). The contribution of CFRP jacket to the shear resistance was calculated according to the method by Vosooghi and Saiidi (2012), while the contribution of CFRP jacket to torsion resistance was calculated based on the method by Zureick et al. (2010). It should be noted that the material properties in the  $0^\circ$  direction of the jacket (transverse to the longitudinal axis of the column) were used for the shear and torsion design. Based on this design procedure, five layers of CFRP were required within the plastic hinge region.

### 5.2.4. Column repair – flexure and confinement

Unidirectional CFRP strips and a bidirectional CFRP jacket were used to restore the flexural performance.

The required number of CFRP strips on each side of the column was designed to provide the equivalent breaking tensile force corresponding to the measured yield strength of the fractured longitudinal bars on that side. Based on the properties of the CFRP strip listed in Table 5-4 and the properties of steel reinforcement given in Table 5-2, four CFRP strips were required on each tension side.

As suggested by the manufacturer of the CFRP jacket, at least two layers were required for the confinement. With consideration of the design for shear and torsion as presented in Section 5.2.3, at least seven layers of transverse CFRP were required in total, which implied that there were

also seven layers of CFRP in the longitudinal direction (because the jacket had bidirectional fibers). The design with the seven-layer CFRP jacket and four CFRP strips on the tension side was analyzed using moment-curvature analysis. Both the original and repaired sections were analyzed using XTRACT under biaxial bending. Fractured longitudinal bars were removed from the repaired column cross-section in the analysis. The material properties in the  $0^\circ$  direction of the bi-directional CFRP jacket were used to calculate the stress-strain relationship of the FRP-confined concrete using the model proposed by Samaan et al. (1998), while the material properties in the  $90^\circ$  direction were used for contribution along the longitudinal axis of the column.. The moment-curvature analysis models and results are shown in Figure 5-9. In Figure 5-9c, the moment-curvature relationships about both the x-axis and y-axis were calculated based on the corresponding models. In this figure, “nL=7” denotes that seven layers of longitudinal CFRP in the jacket were considered in the model; “nT=2” denotes two layers of transverse CFRP in the jacket were considered in the model; and “s=4” denotes four CFRP strips on the tension side of the cross-section were considered in the model. It can be observed that with this design, the moment capacities in both directions of the repaired section exceed those of the original section, while the curvature capacities are lower than those of the original section.

Although moment curvature analysis of the repaired section indicated a much more brittle than the original section due to the low rupture strain of CFRP, it was noted that the behavior of the repaired column may be more ductile than predicted in this manner and have a behavior more similar to the original column as mentioned by Zhu et al (2006) due to different plastic hinge lengths of CFRP-wrapped columns and RC columns; however, this aspect needed to be investigated by the experimental work. In summary, seven layers of longitudinal CFRP in the

jacket and four unidirectional CFRP strips on each tension side were required for flexural repair in the plastic hinge region, while no CFRP was needed in the region outside plastic hinge.

#### 5.2.5. Embedment length of CFRP jacket and strips

The success of the proposed repair depended on the development of the full strength of the CFRP jacket and strips; thus they were to be embedded into the footing to provide a connection to achieve rupture failure of the CFRP. Recent studies proposed a minimum embedment length required to achieve this failure mode. Zhu et al. (2006) proposed a embedment length of 1.1D, where D is the diameter of a circular CFRP jacket. Zakaib and Fam (2012) suggested an embedment length of at least 0.7D for a circular jacket. It is worth noting that in their studies normal strength concrete was used in the footing, thus a relatively long length is needed. Sadeghian and Fam (2010) proposed a simplified equation to calculate the required embedment length as shown in Equation 5-1 below:

$$\frac{X}{D} = 5.5 \frac{\tau_{max}}{f_c'} \left( \sqrt{1 + 0.31 \frac{f_c'}{\tau_{max}^2} \frac{M}{D^3}} - 1 \right) \quad (\text{Equation 5-1})$$

where X is the minimum required embedment length; D is the diameter of a circular jacket;  $\tau_{max}$  is the bond strength between the CFRP jacket and footing concrete; M is the bending moment transferred to the footing; and  $f_c'$  is the compressive strength of concrete. Sadeghian and Fam (2010) also mentioned that Equation 5-1 would result in an embedment of length of 0.7D in cases of Zhu et al. (2006) and Zakaib and Fam (2012) and is conservative when axial compressive load exists.

In the present study, the moment required to be transferred to the footing is 26,000 kip-in. (2938 kN-m), which corresponds to the moment capacity based on the results shown in Figure 5-9; the

concrete compressive strength of concrete was assumed to be 5,000 psi (34.5 MPa); the bond strength between the CFRP jacket and footing concrete was taken as 800 psi (5.5 MPa) (see Table 5-7); and  $D$  can be taken as a value ranging from 24 in. (610 mm) to 36 in. (914 mm), depending on the direction of bending. Using the method by Zakaib and Fam (2012), the required embedment length is 16.56 in. (427 mm) to 28.56 in. (725 mm), depending on the direction of bending. If  $0.7D$  is used, the required embedment length is 16.8 in. (427 mm) to 25.2 in. (640 mm), which is close to the length estimated with Equation 5-1. Considering practical limitations, however, demolition of concrete down into the footing with this depth may have compromised the strength of the footing, especially since additional layers of footing reinforcement might be damaged unexpectedly. Furthermore, only a portion of the moment capacity of the cross-section was required to be transferred by the CFRP into the footing, since the existing longitudinal bars could still contribute to the moment transfer. Thus, the CFRP embedment length was taken as 12 in. (305 mm) in this study, which was less than that estimated by either of the methods described above.

#### 5.2.6. Footing repair

Several reinforcing bars in the footing needed to be cut to facilitate the embedment of the CFRP jacket and strips (as shown in Figure 5-10). Thus, CFRP fabric was externally bonded to the top surface of the footing to compensate for the loss of strength. Unidirectional CFRP fabric was cut into 12 in. (305 mm) straps to provide the required materials. The layout and orientation of the CFRP straps are shown in Figure 5-12. The number of CFRP layers was determined as follows.

Saini and Saiidi (2013) proposed an equation to calculate the effective strain of FRP sheets as shown in Equation 5-2.

$$\varepsilon_{fe} = 0.015 \times (t_f)^{-0.5} E_f^{-0.36} \left(\frac{f_c'}{5}\right)^{0.67} \quad (\text{Equation 5-2})$$

where  $\varepsilon_{fe}$  equation is effective strain of FRP;  $t_f$  is the thickness of FRP;  $E_f$  is the Young's modulus of FRP; and  $f_c'$  is the compressive strength of the substrate concrete. The required layers of FRP can be determined using Equation 5-3.

$$nt_f = \frac{4 \times A_s \times f_{ys}}{E_f \varepsilon_{fe} w \cos \alpha} \quad (\text{Equation 5-3})$$

where  $n$  is the layers of FRP;  $w$  is the width of FRP strap;  $\alpha$  is the angle of FRP strap relative to the footing's longer axis;  $A_s$  is the area of the reinforcing bars; and  $f_{ys}$  is the yield stress of the reinforcing bars. The development length of FRP can be determined using Equation 5-4 (ACI 440.2R-08):

$$l_{df} = 0.057 \sqrt{\frac{n E_f t_f}{\sqrt{f_c'}}} \quad (\text{Equation 5-4})$$

Using Equations 5-2 and 5-3 would result in 30 layers of CFRP to be required, which is impractical and ineffective. Instead, U-shaped straps were considered where the straps could be extended and bonded onto the sides of the footing, and an effective strain of 0.004 was used for the CFRP rather than the value computed with Equation 5-2. Thus, as shown in Figure 5-12, 10 layers of 12 in. wide CFRP straps were required on four sides of the column to compensate for the loss of strength due to cutting of the footing bars. The CFRP straps were also to be extended to the side faces of the footing to secure the full development of the straps (see Figure 5-12).

### 5.2.7. Summary

Repair design for Calt-3 involved determination of number of CFRP strips, number of layers of CFRP jacket, and number of layers of CFRP straps for footing repair. Because the fractured longitudinal bars were untreated, both transverse and longitudinal CFRP were required for restoring the flexural, shear, and torsional strength of the column. The number of layers of transverse CFRP were designed with the goal of restoring the shear and torsional strength to that of the original column, which required five layers in transverse direction. The number of CFRP strips in longitudinal direction was calculated with the methodology of having them provide the equivalent breaking tensile force to compensate for the fractured No. 8 (25.4 mm dia.) bars on the extreme tension sides of the column. Two layers of transverse CFRP were used for restoring confinement. The final design result included four unidirectional CFRP strips in the longitudinal direction on both extreme tension sides of the column and a seven-layer bidirectional CFRP jacket. The flexural strength of the repaired section was verified through moment-curvature analysis. Detailing at the column-footing joint to full develop the strength of the CFRP jacket and strips was designed with information provided in literature. The number of layers of CFRP straps required for footing repair was determined using a procedure similar to that provided by ACI 440.2R-08.

## 5.3. REPAIR PROCEDURE

The damaged column was relatively straight vertically and could support its own weight; thus, shoring and straightening was not conducted during the repair procedure. This section describes the repair procedure that involved five steps: (1) cutting the trench around the base of the column in the footing; (2) removing the loose concrete from the column; (3) placement of grout; (4)

installing the CFRP strips on the column surface; (5) wrapping the epoxy coated prefabricated laminate around the column to create a 7-ply jacket ; (6) lowering the jacket into the cut trench; (7) filling the trench with an epoxy grout and gravel; (8) injecting a low viscosity resin between the jacket and the column; (9) and installing the CFRP fabric on the footing surface. Constructability aspects of all the repairs are discussed in Chapter 7.

#### 5.3.1. Trenching of footing

As shown in Figure 5-10, a 4 in. (100 mm) wide and 12 in. (300 mm) deep trench was made in the footing around the perimeter of the column. The top cover concrete of the footing was removed with an electric jackhammer to expose the first layer of horizontal reinforcement in the footing (see Figure 5-13a). As shown in Figure 5-13b, a torch was used to cut the portion of all the footing reinforcement in the way of deepening the trench. After the footing reinforcement was cut, the jackhammer was used to deepen the trench as shown in Figure 5-13d.

#### 5.3.2. Removal of concrete

All loose concrete was removed from the column.

#### 5.3.3. Placement of grout

The formwork used for casting the original column was used to place the new grout to ensure the column would have the same cross-sectional dimension as that of the original column. The formwork was 60 in. (1525 mm) high and included two plastic semi-circle shells with a diameter of 24 in. (606 mm) and two wooden plate forms with a width of 12 in. (303 mm). The formwork was inserted down into the trench and touched the base of the trench. As described earlier, the prefabricated laminates could also be used to build formwork around the column, although this was not the case in this study. Before casting the grout, the trench was filled with an expansive

foam to prevent leakage from the bottom of the formwork. Gaps between each part of the formwork were sealed with foam to prevent leakage. A high-fluidity grout was cast in the formwork. Its compressive strength (see Table 5-1) was measured by testing 2 in. x 2 in. x 2 in. (50 mm x 50 x 50 mm) cubes according to ASTM C109. As shown in Table 5-1, the compressive strength of the grout measured on the test day was very close to that of the concrete of the original column. The column before and after grout placement is shown in Figure 5-14.

#### 5.3.4. Installation of CFRP strips and jacket

The CFRP strips were placed next to the column. Figure 5-15 shows the procedure involved in the installation of CFRP strips and jacket. Strain gages were mounted on the CFRP strips before they were installed onto the concrete surface. Each of the strips was secured in position to the concrete surface with a tacky adhesive applied to the top of the strip. A piece of CFRP prefabricated laminate 4-ft wide x 60-ft long (1.2 m x 18.3 m) was then wrapped tightly around the column, layer by layer, to make the jacket. The epoxy paste was applied to the laminate (the green material shown in Figure 5-15b) as it was wrapped around the column. After the seven layers were in place, the jacket was wrapped tightly with plastic sheet and fastened with ratchet straps to prevent loosening of the jacket. The jacket was then pushed into the trench and touched the base of it. The gap within the trench between the outer surface of the jacket and the footing was then filled with a mixture of gravel and a low viscosity epoxy (QuakeBond™ 320LV as shown in Figure 5-15c as the black material). The epoxy was cured in approximately 30 minutes, and a noticeable amount of heat was generated during curing process. After material in the footing hardened adequately, QuakeBond™ 320LV was then filled into the gap (approximately 1 in. [25 mm]) between the CFRP jacket and the concrete surface to provide a bond between the column and the jacket and to bond the CFRP strips to the concrete column. The column after

filling the epoxy is shown in Figure 5-15d. 4 in. (100 mm) x 8 in. (200 mm) cylinders were also cast from the epoxy-filled gravel material (as shown in Figure 5-16a). Splitting tensile tests and compression tests were conducted to determine the mechanical properties of this material (as shown in Figure 5-16c and d) according to ASTM C496 and ASTM C39. The mechanical properties are listed in Table 5-8.

#### 5.3.5. Installation of CFRP straps to footing

Footing repair was conducted using CFRP fabric (QuakeWrap<sup>TM</sup> VU18C) that were externally bonded to the surface to compensate for the loss of strength due to severing of the bars. A wet-layup procedure was used to bond the CFRP straps to the footing. The application procedure included surface preparation with a concrete grinder, application of thickened epoxy as putty and primer, saturation of fabric, and application of fabric to the footing surface. The column after surface preparation and application of fibers is shown in Figure 5-17. An overview of the column after completion of the repair work is shown in Figure 5-18.

### 5.4. TEST PROGRAM

#### 5.4.1. Test setup

The test setup used to test R-Calt-3 was modified from the setup used to test R-Calt-1 and R-Calt-2 (described in Section 3.4.1) because a higher bending moment was expected to fail this column. In this version, two more double channels were placed on the top of the two wide flange beams and anchored to the reaction floor by two DYWIDAG bars in each. Based on analysis with a finite element model, this test setup would be able to transfer the applied load to the reaction floor without exceeding the capacity of the anchors. The test setup is shown in Figure 5-19.

#### 5.4.2. Instrumentation

Two load cells were integrated within the two actuators that measured force during testing. Two load cells were also installed under the hydraulic jack on the top of column to record the variation of axial load. Cables were used to connect all the load cells to a data acquisition system (DAS).

Two integrated DCVTs within the two actuators recorded the displacement during testing. Four levels of string extensometers were also installed between a reference frame and the column. Each level was composed of two string extensometers in order to measure the lateral deformation and twist of the column at each level. All displacement transducers were connected to the DAS with cables.

Strain gages were installed on the surface of the CFRP jacket to measure both the longitudinal and transverse strains (refer to Figure 5-20). Five levels of strain gages were also installed onto four of the CFRP strips before they were installed onto the column (refer to Figure 5-21). Four strain gages were installed on the CFRP straps on each side of the footing to measure the surface strains of the CFRP (refer to Figure 5-22).

#### 5.4.3. Loading protocol

Before lateral loading was applied to the repaired column, axial loading was applied and kept constant during the entire test by a hydraulic jack mounted on the top of the column and anchored prestressing strands placed through the center of the column with a value of 220 kips equal to 7% of the axial loading capacity of the repaired column.

The repaired column was subjected to reversed cyclic lateral loading by controlling the displacement of the actuators. The first cycles included ten levels with one cycle per level up to

the displacement corresponding to the last force-control level of the original column. After that, three cycles per each displacement level were applied to the repaired column with the same loading protocol as that of the original column. The loading protocol for both the repaired column and the original column is shown in Figure 5-2.

## 5.5. CONCLUDING REMARKS

This chapter describes damage to one oval-shaped column reinforced with interlocking spirals tested to failure under biaxial bending and T/M ratio of 0.2, the emergency repair method aimed at restoring the strength of the column and footing, and the testing program of the repaired column including test setup, instrumentation, and loading protocol. The repair was conducted based on the philosophy to limit the time and labor needed for construction; thus, only the plastic hinge zone was repaired, and the non-plastic hinge zone was left unrepaired. The experimental work presented in this chapter illustrates that the repair method was practical and may be implemented in field applications for this purpose.

Table 5-1 Measured Compressive Strength of Concrete and Grout for Calt-3 and R-Calt-3

	Test Day ksi (MPa)
Calt-3 (concrete)	5.86 (40.4)
R-Calt-3 (grout)	6.01 (41.4)

Table 5-2 Measured Reinforcing Steel Properties for Calt-3 and R-Calt-3

	Yield Strength ksi (MPa)	Ultimate Strength ksi (MPa)
No. 8 (25.4 mm dia.) Longitudinal Bars (Calt-3 and R-Calt-3)	76.7 (529)	104.1 (717)
No. 4 (12.7 mm dia.) Spirals (Calt-3 and R-Calt-3)	65.8 (454)	98.0 (676)

Table 5-3 Visible Damage to Calt-3 after Original Test

Unit ID	Concrete Damage		Reinforcing Steel Damage				Damage Location <sup>5</sup>
	Spalled Length <sup>6</sup>	Core Crush Depth	No. of Yielded Long. Bars <sup>7</sup>	No. of Buckled Long. Bars	No. of Fractured Long. Bars	No. of Swelled Spirals	
Calt-3	39 in. (991 mm)	6 in. (127 mm)	Unavailable	4/20	6/20	0	5-16 in. (125-405 mm)

Table 5-4 Properties of Unidirectional CFRP Strips (GU50C) (provided by manufacturer)

Tensile Strength	Elongation at Break	Tensile Modulus	Nominal Laminate Thickness in. (mm)	Width
ksi (MPa)	%	ksi (GPa)		in. (mm)
400 (2758)	1.7%	24,000 (165)	0.0472 (1.2)	4 (101.6)

Table 5-5 Properties of QuakeWrap<sup>TM</sup> VU18C Fabric (provided by manufacturer)

	US Units	SI Units
Fiber Properties		
Tensile Strength	550 ksi	3,800 MPa
Tensile Modulus	33,500 ksi	231,000 MPa
Ultimate Elongation	1.64%	1.64%
Fabric Laminated with J300SR		
Tensile Strength	102.7 ksi	708 MPa
Tensile Modulus	9,950 ksi	68,600 MPa
Ultimate Elongation	1.1%	1.1%
Ply thickness	0.0399 in.	1.01 mm

<sup>5</sup> The definition of spalled length and core crush depth are shown in Figure 4;

<sup>6</sup> Number of yielded longitudinal bars can be determined from the strain data; 15~16 out of the 20 bars yielded in most cases;

<sup>7</sup> The height range of the buckled points of longitudinal bars from the column-footing joint

Table 5-6 Properties of Bidirectional Prefabricated CFRP Laminate PLC100.60 (provided by manufacturer)

	US Units	SI Units
<b>Longitudinal (0°) Direction</b>		
Tensile Strength (ASTM D3039)	101 ksi	698 MPa
Modulus of Elasticity (ASTM D3039)	7,150 ksi	49,280 MPa
Ultimate Elongation (ASTM D3039)	0.85%	0.85%
<b>Transverse (90°) Direction</b>		
Tensile Strength (ASTM D3039)	64.2 ksi	443 MPa
Modulus of Elasticity (ASTM D3039)	2,940 ksi	20,260 MPa
Ultimate Elongation (ASTM D3039)	1.42%	1.42%
<b>Laminate Properties</b>		
Ply Thickness	0.026 in.	0.66 mm

Table 5-7 Properties of QuakeBond™ 320LV Low Viscosity Resin Epoxy (provided by manufacturer)

Tensile Strength psi (MPa)	Compressive Strength psi (GPa)	Elongation at Break %	Adhesive to Concrete psi (MPa)
7,900 (54.5)	11,200 (77.2)	4.8%	>800 (5.5); 100% failure in concrete

Table 5-8 Measured Material Properties of Epoxy-Gravel

	Test Day ksi (MPa)
Compressive Strength	6930 (47.8)
Splitting Tensile Strength	700 (4.8)

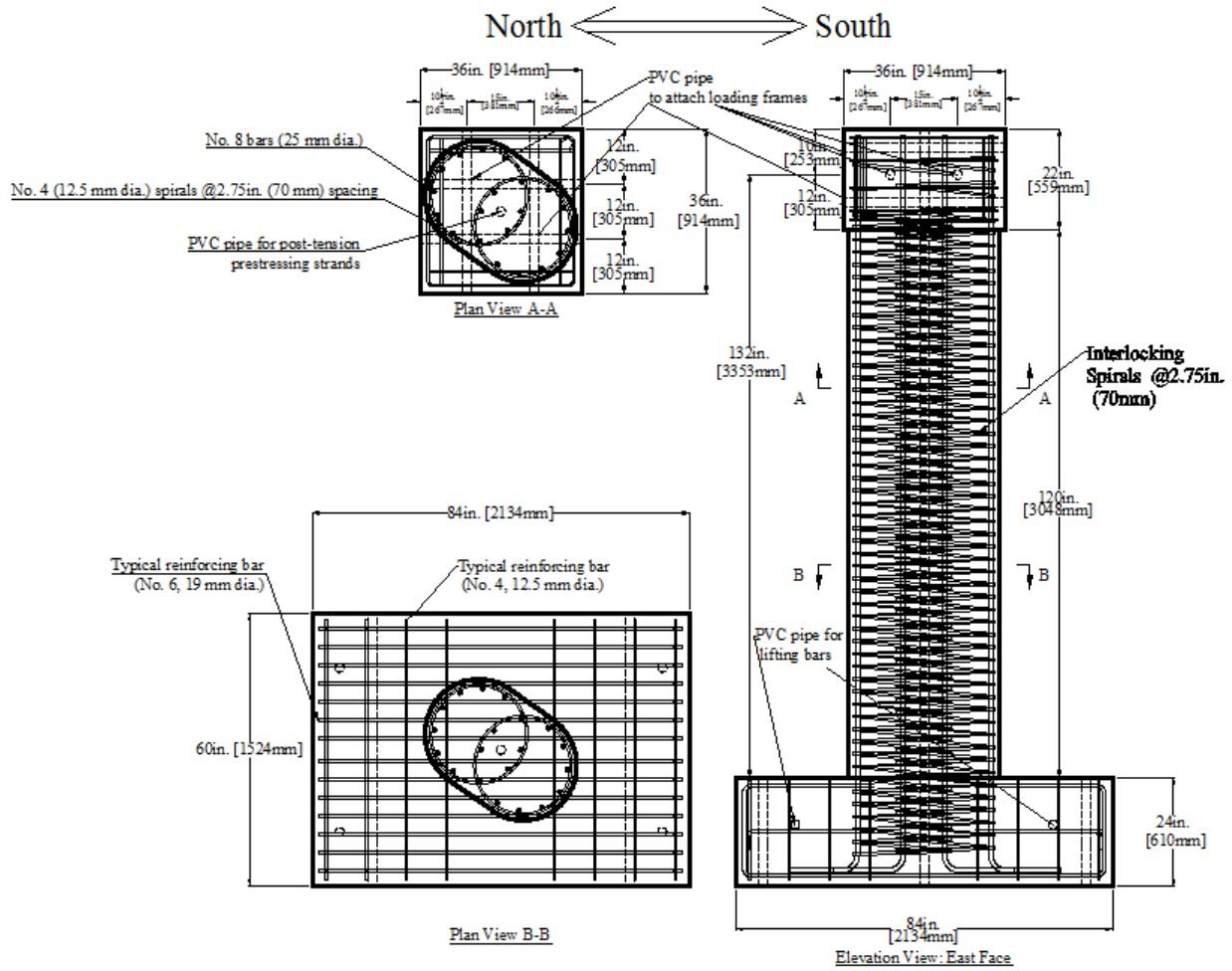


Figure 5-1 Geometry and Reinforcement Details of Calt-3

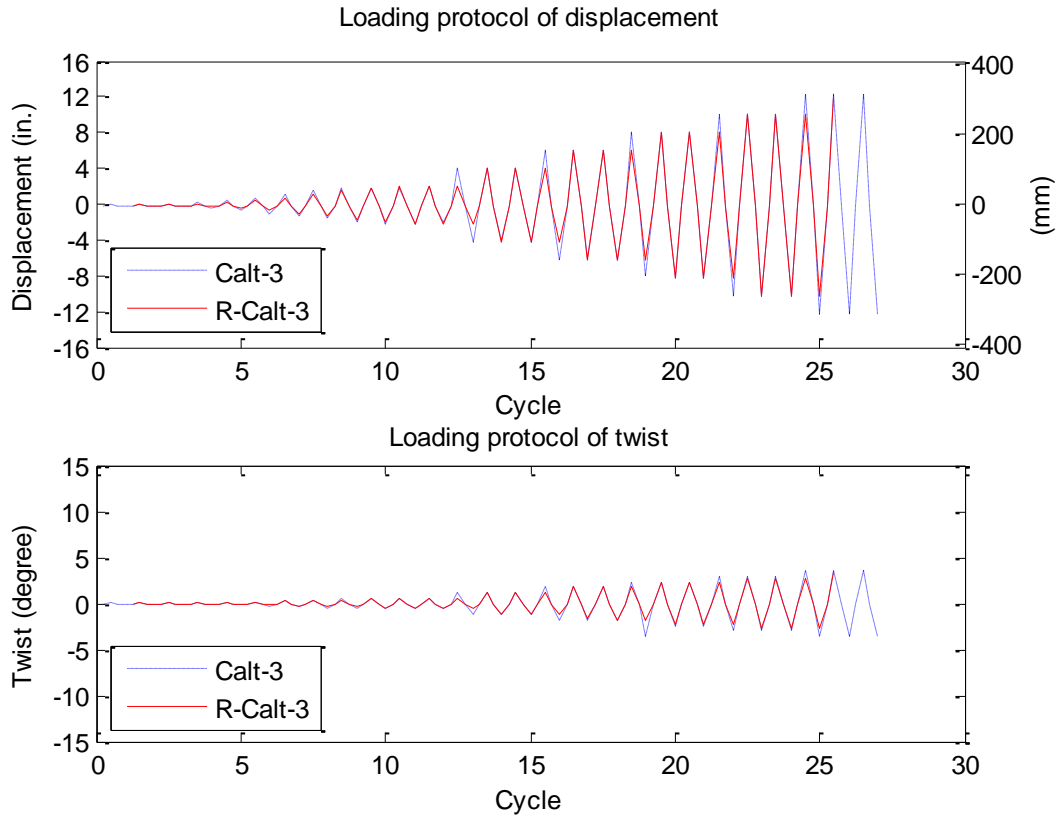
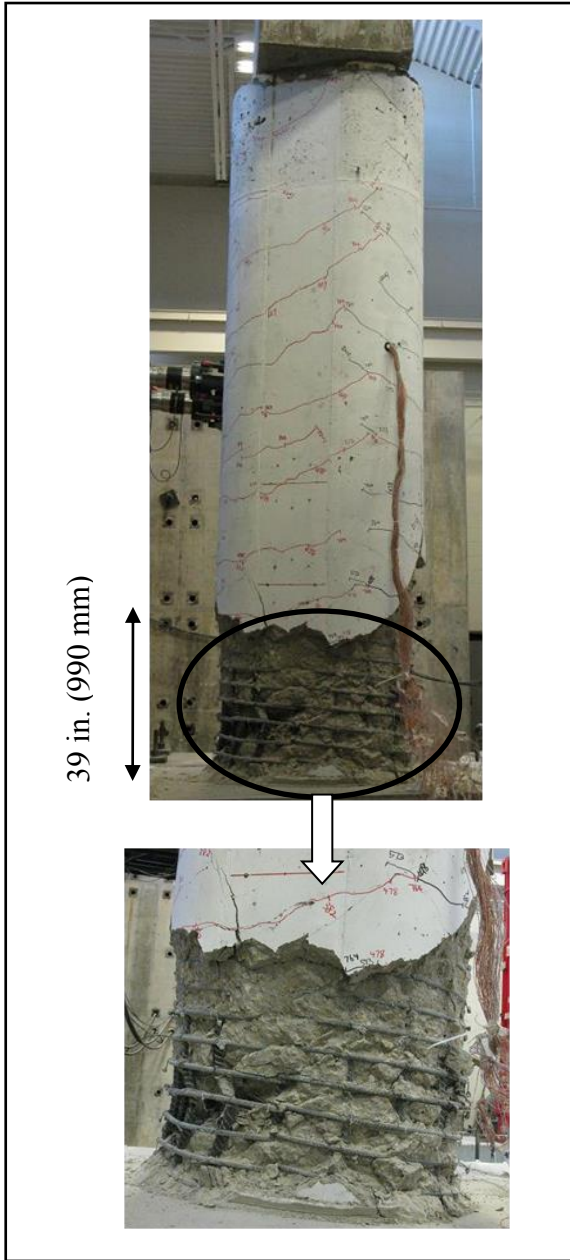
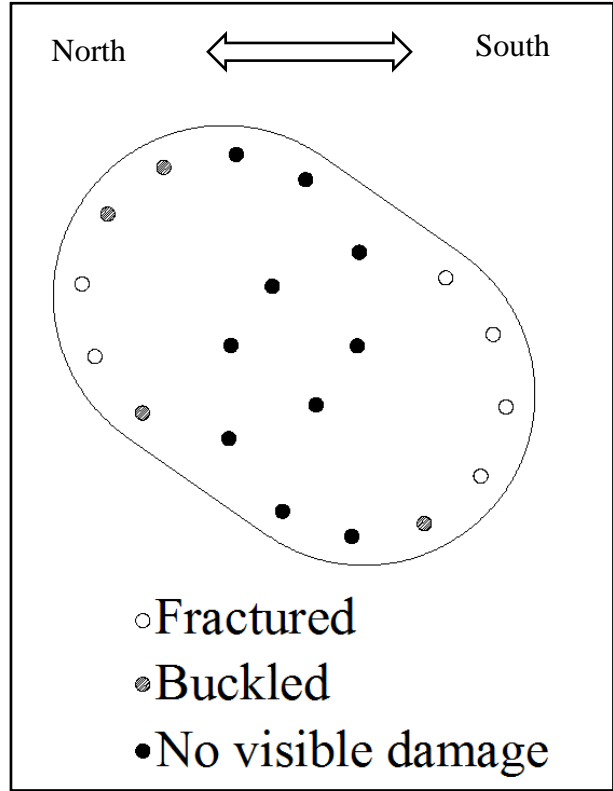


Figure 5-2 Loading Protocol of Calt-3 and R-Calt-3

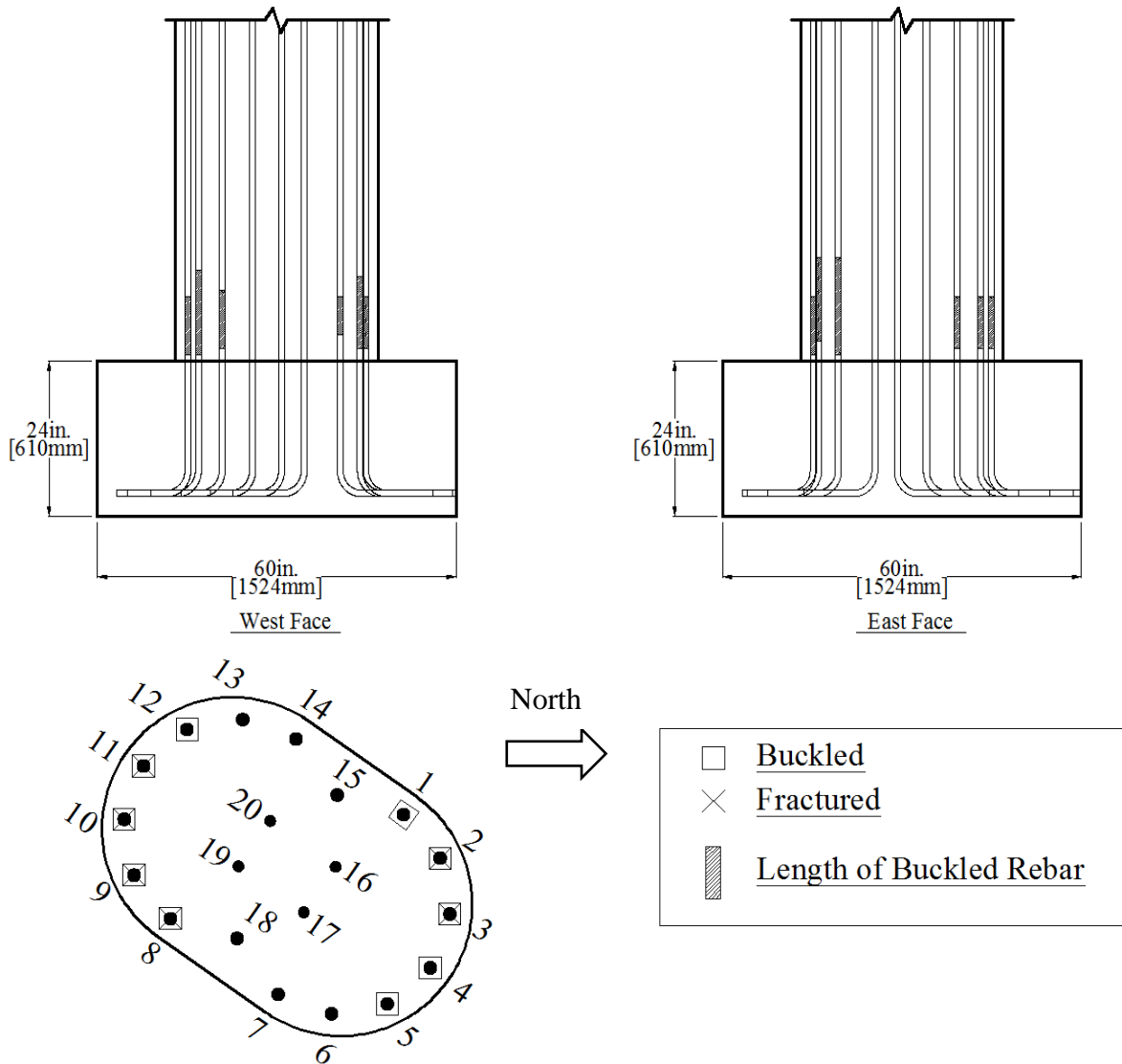


(a)



(b)

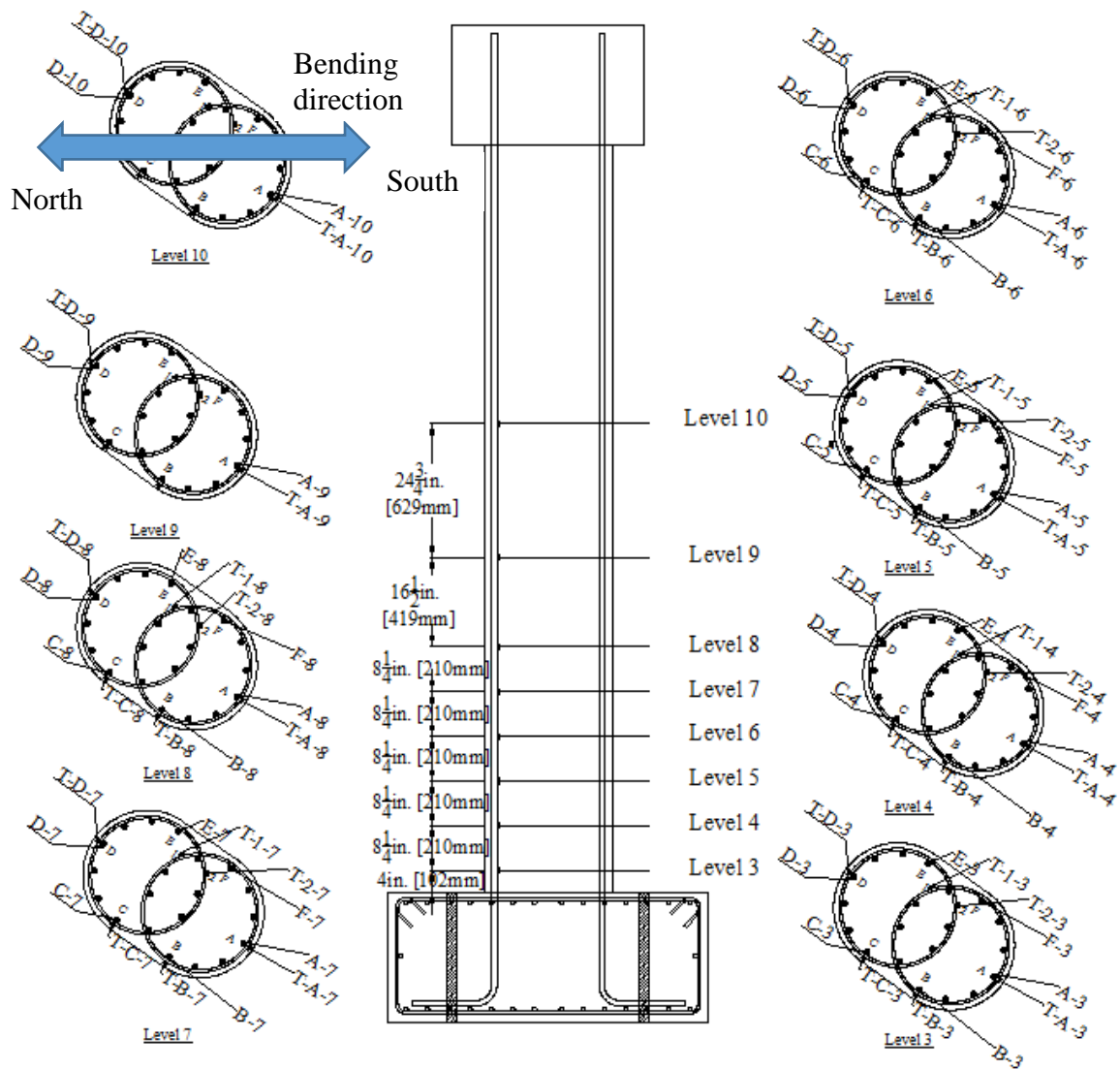
Figure 5-3 Visible Damage to Calt-3 after Original Test



Bar Number	1	2	3	4	5	8	9	10	11	12
Fracture Location (in.)	-	4	3	-	-	3	2	5	2	-
Buckled Region (in.)	4~10	2~13	2~10	2~10	2~10	1~16	3~16	1~10	1~14	2~11

Note: all distances in this table were measured from the top of the footing.

Figure 5-4 Visible Damage to Longitudinal Reinforcement of Calt-3 after Original Test



- Notes: (1) "T" denotes gage on transverse reinforcement;  
 (2) 40 gages were installed on longitudinal reinforcement;  
 (3) 40 gages were installed on transverse reinforcement.

Figure 5-5 Strain Gage Layout of Calt-3

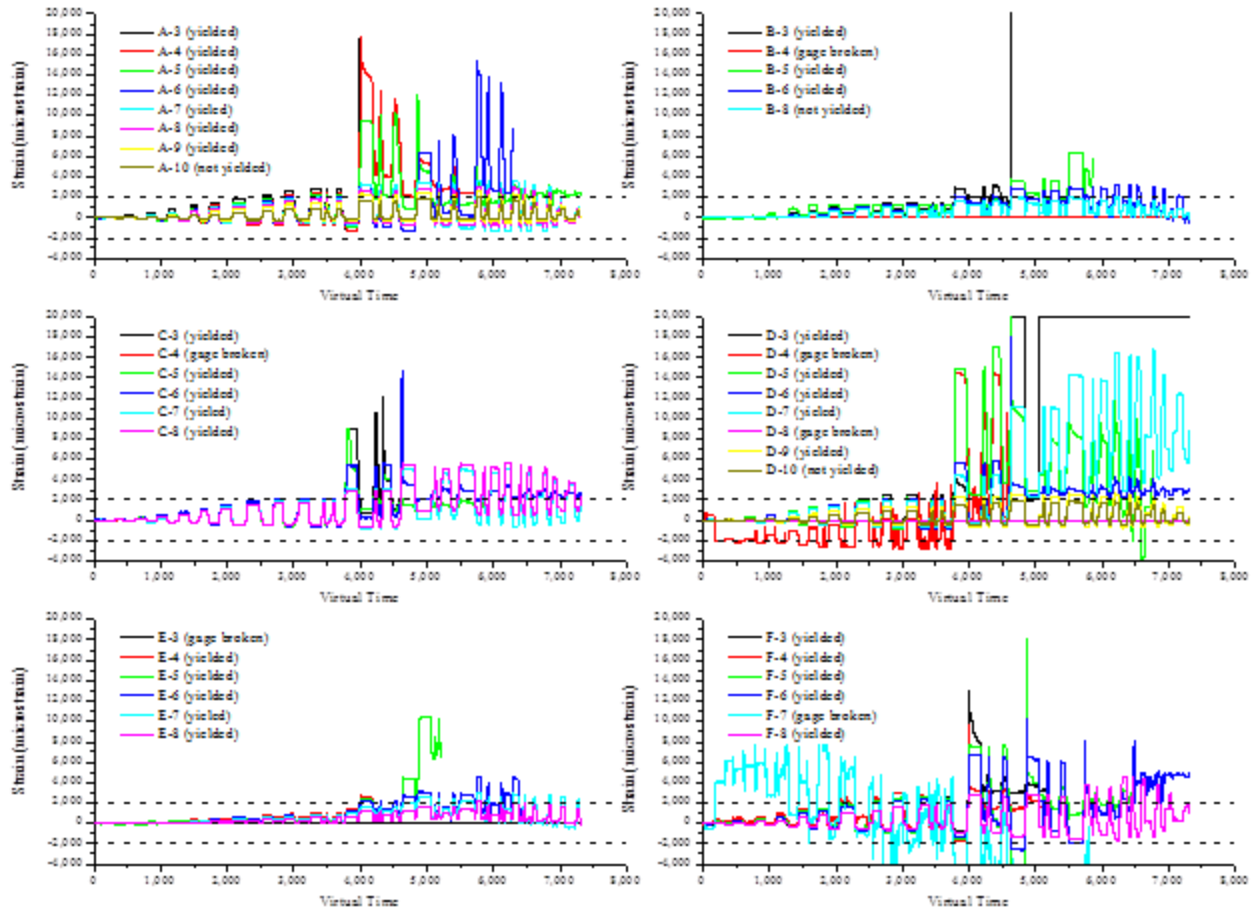


Figure 5-6 Strain History of Longitudinal Reinforcement (Calt-3)

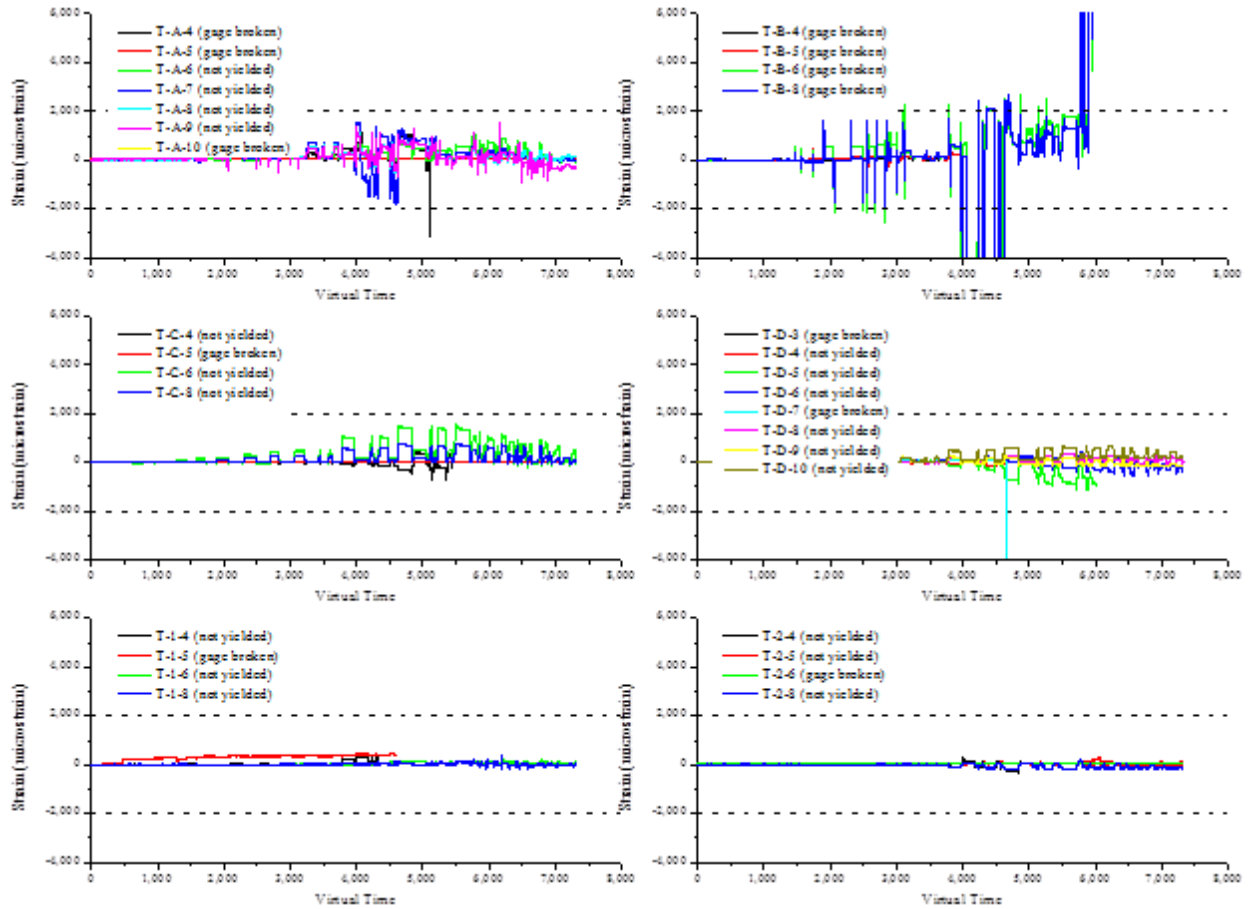


Figure 5-7 Strain History of Transverse Reinforcement (Calt-3)

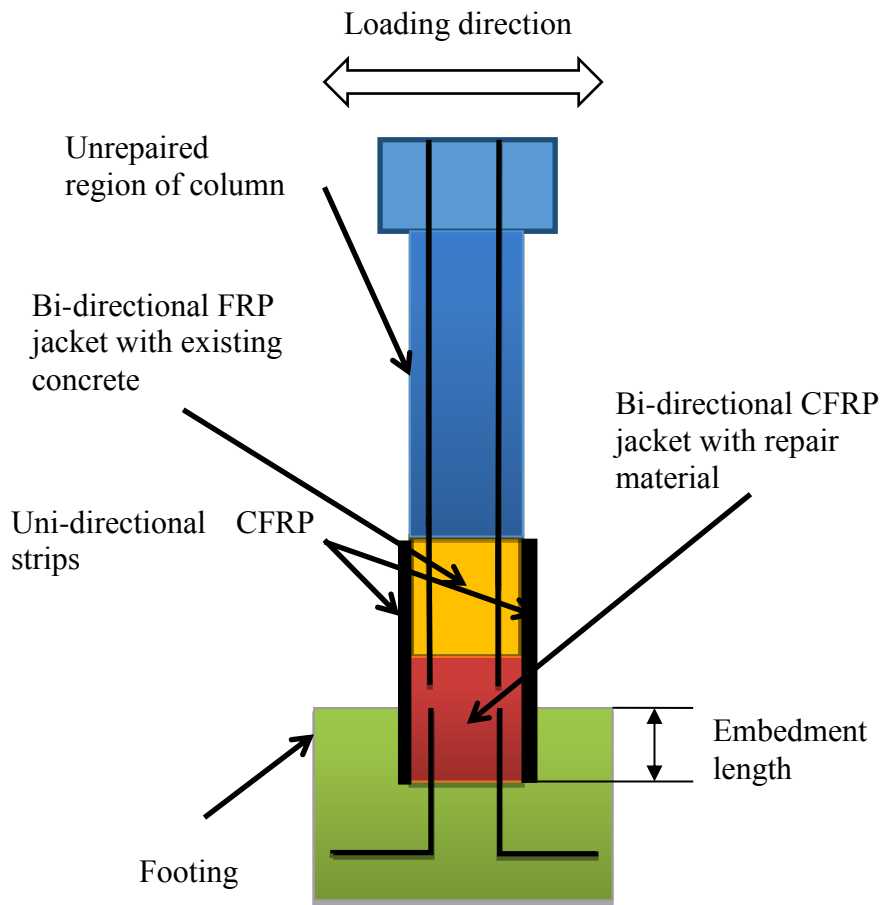
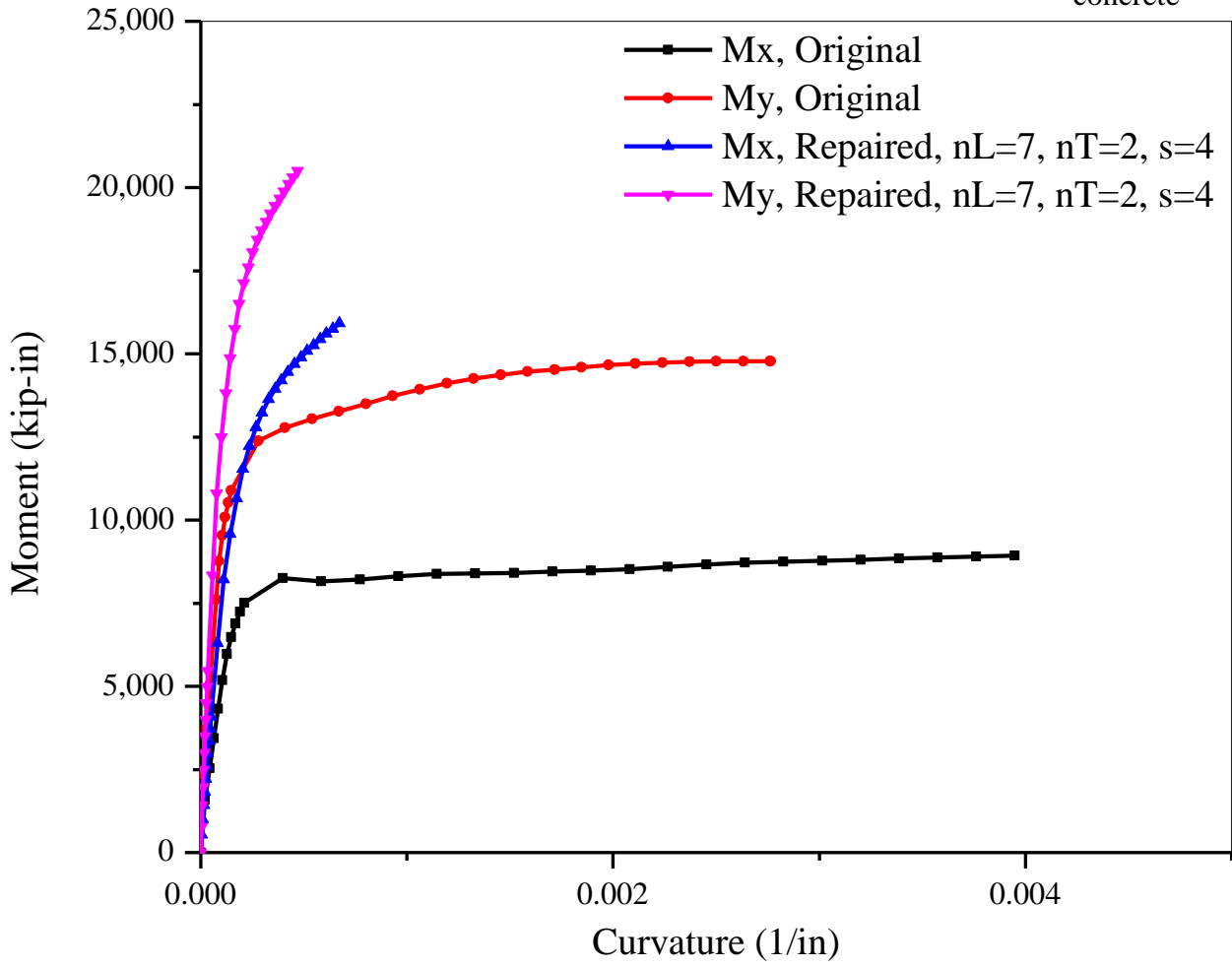
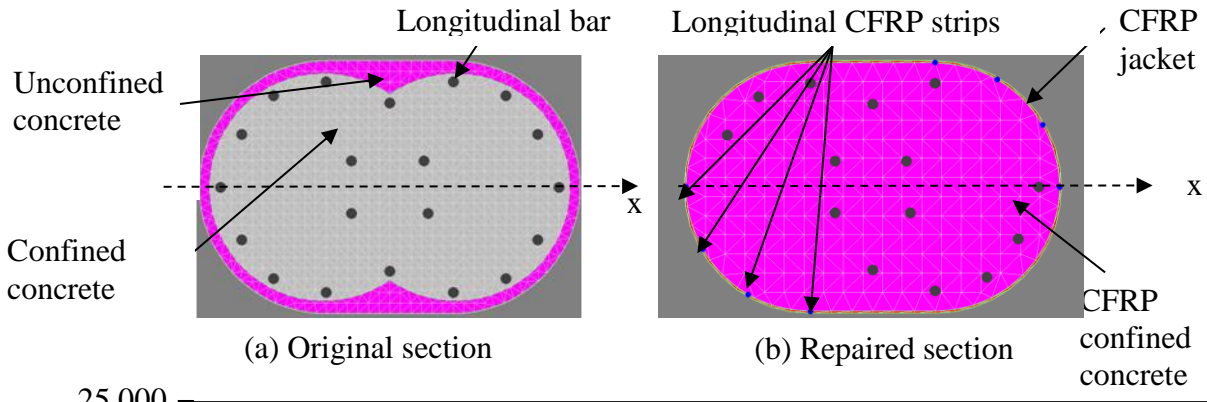


Figure 5-8 Repair Scheme for Calt-3



(c) Moment-curvature comparison

Figure 5-9 Moment-Curvature Analysis Models and Results for Calt-3 and R-Calt-3

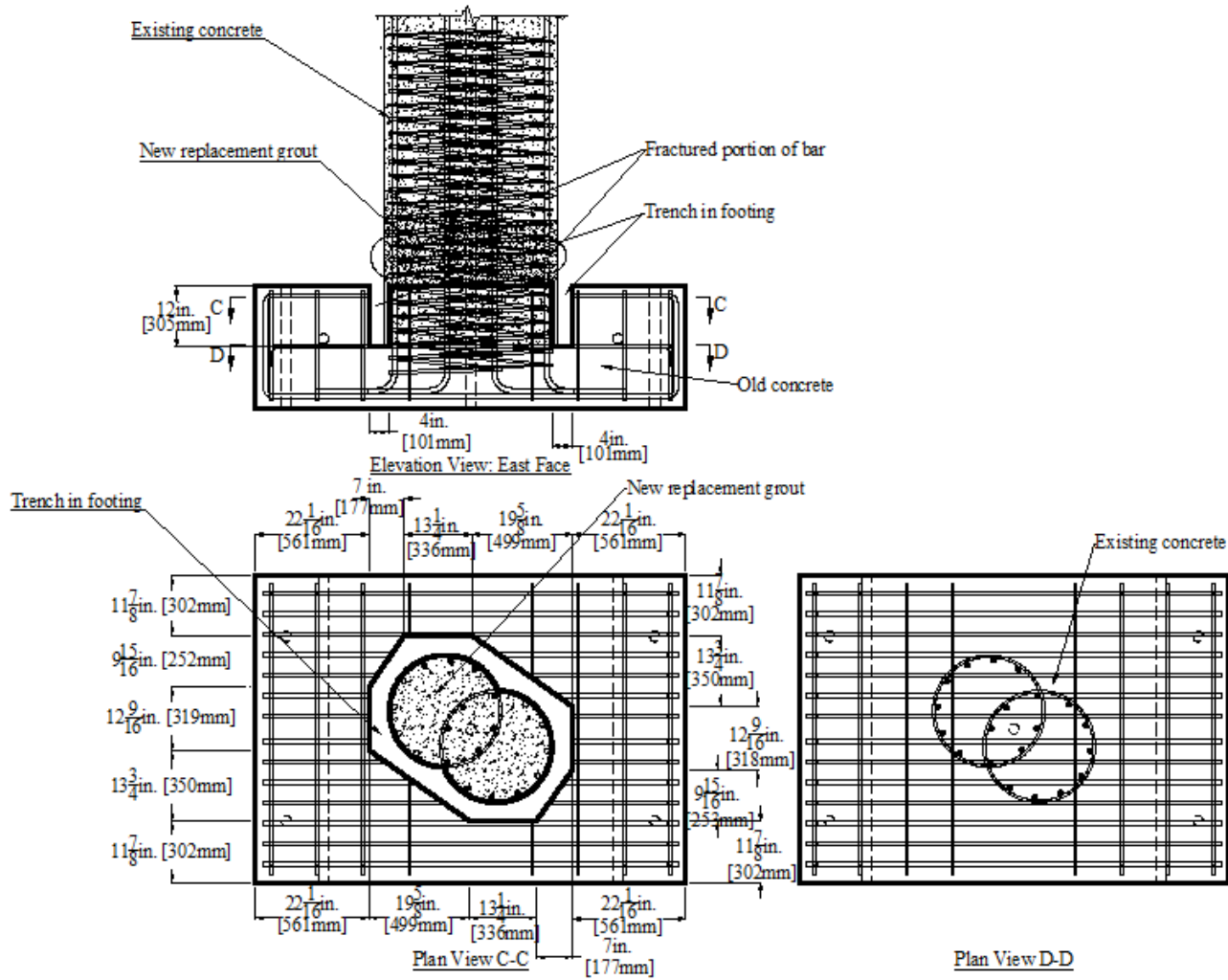
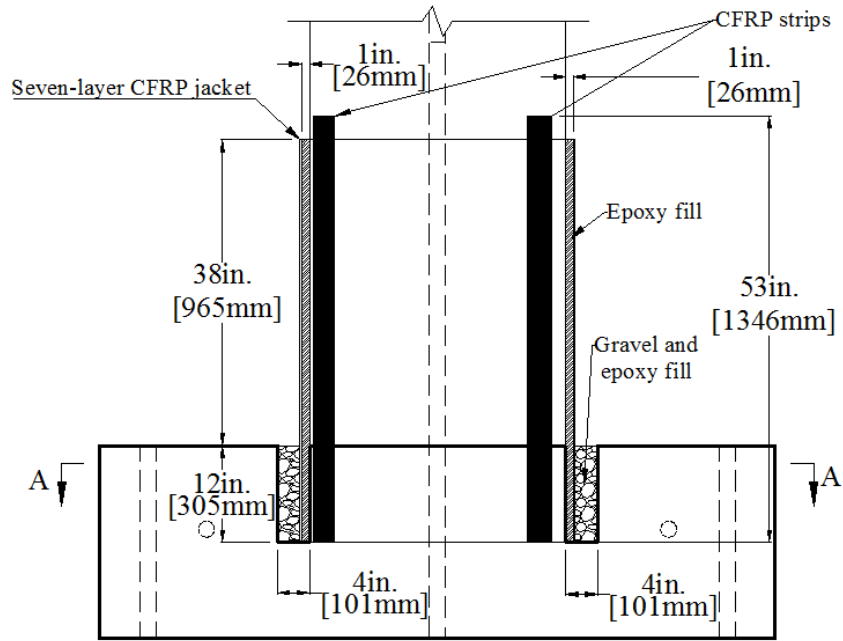
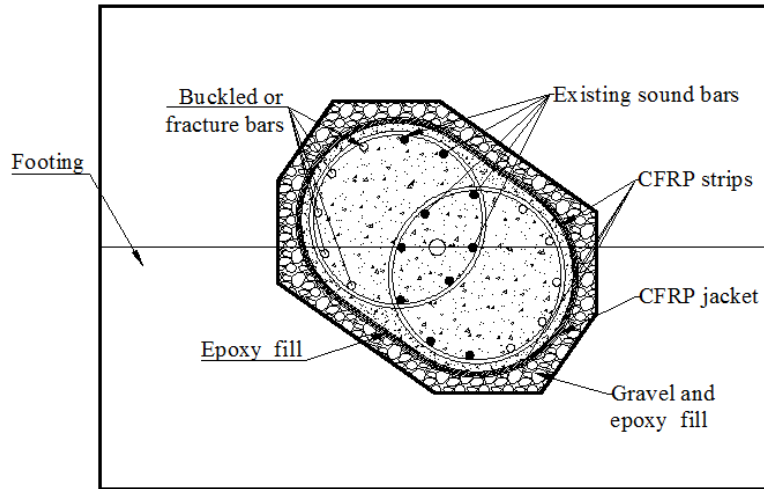


Figure 5-10 Concrete Repair and Trench Details for R-Calt-3



Elevation View: East Face



Plan View A-A

Figure 5-11 Details of CFRP Strips, CFRP Jacket and Epoxy Fill for R-Calt-3

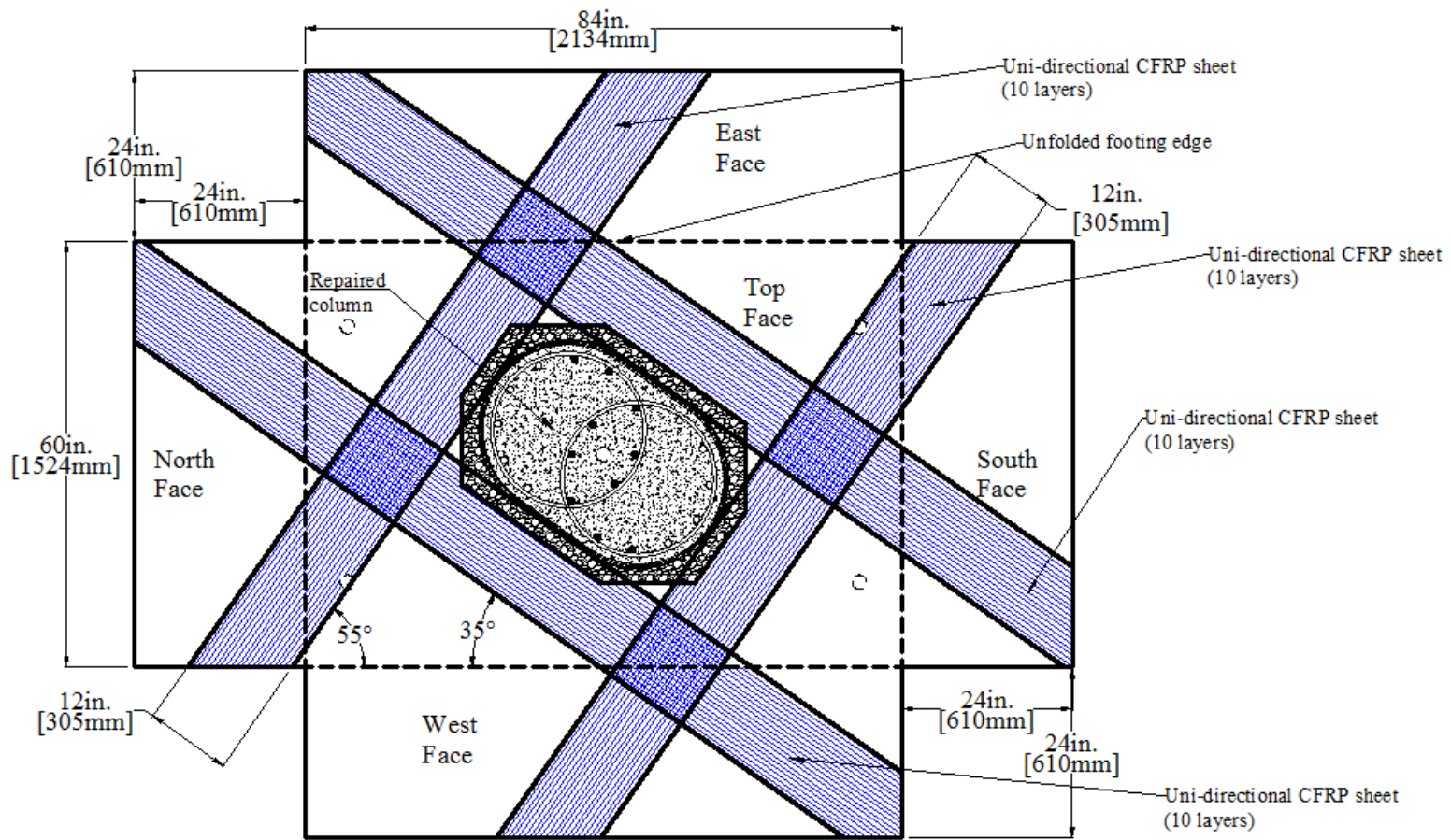


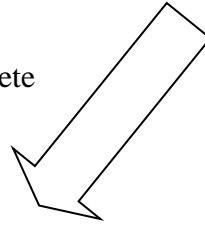
Figure 5-12 CFRP Strap Layout on Footing Faces for R-Calt-3



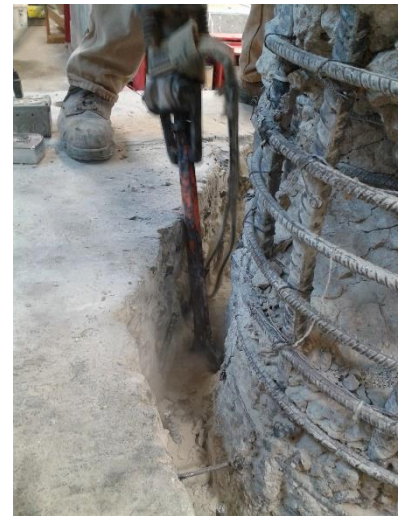
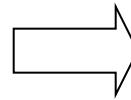
(a) Footing after removal of top cover concrete



(b) Cutting rebar with torch



(c) Trench after cutting rebar



(d) Deepening trench with jackhammer

Figure 5-13 Footing Trenching Procedure for R-Calt-3



(a) Concrete damage after trenching

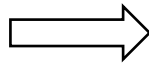


(b) After grout placement

Figure 5-14 Column R-Calt-3 Before and After Grout Placement

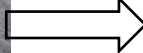


Strain gages



(a) CFRP plate installation

(b) CFRP Jacket wrapping



Epoxy filled into gap between jacket and concrete

(c) Filling trench with epoxy and gravel

(d) Column after gap filling with epoxy

Figure 5-15 Installation of CFRP Strips and CFRP Jacket for R-Calt-3



(a) 4 in. x 6 in. cylinders



(b) Splitting tensile failure



(c) Compression failure

Figure 5-16 Material Testing Specimens of Epoxy with Gravel for R-Calt-3



(a) Column and footing after surface preparation

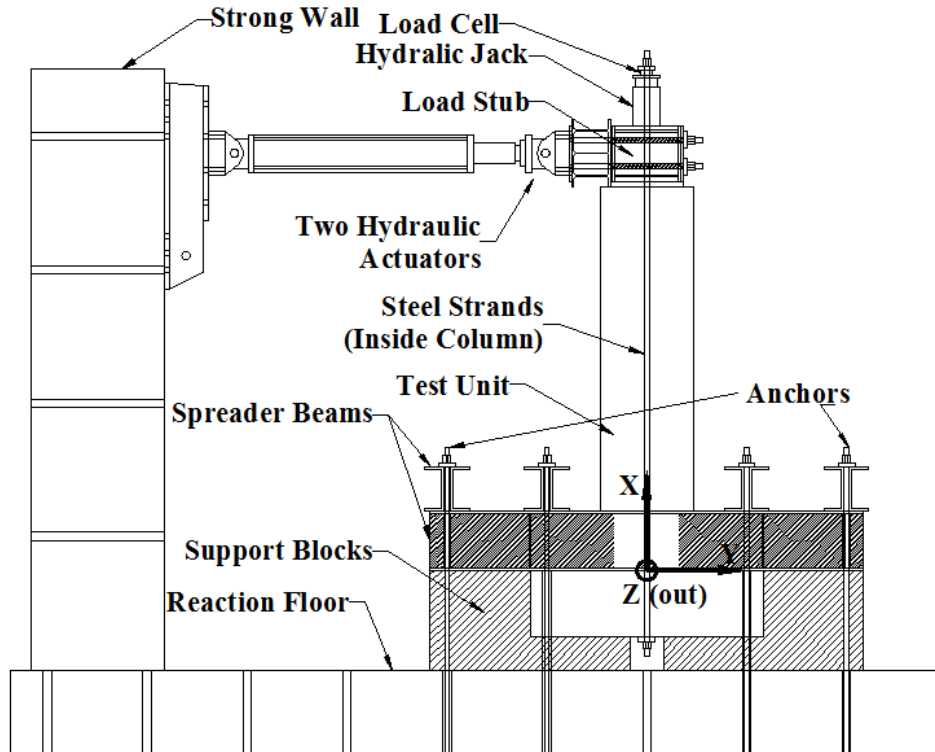


(b) Column and footing after CFRP installation

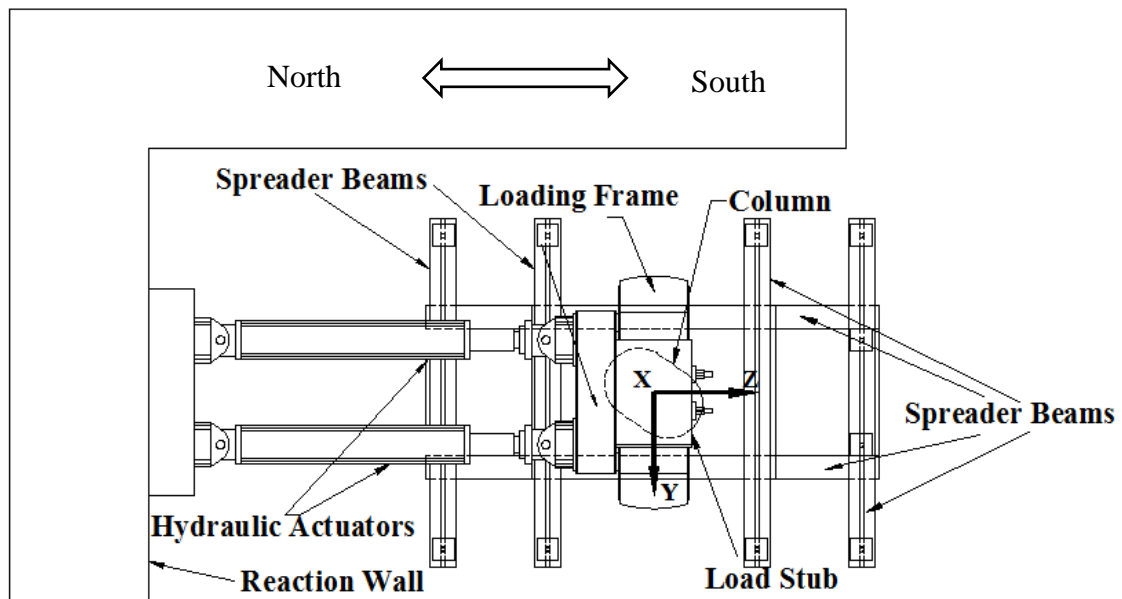
Figure 5-17 Column R-Calt-3 after Surface Preparation and CFRP Installation



Figure 5-18 Column R-Calt-3 after Completion of Repair Work

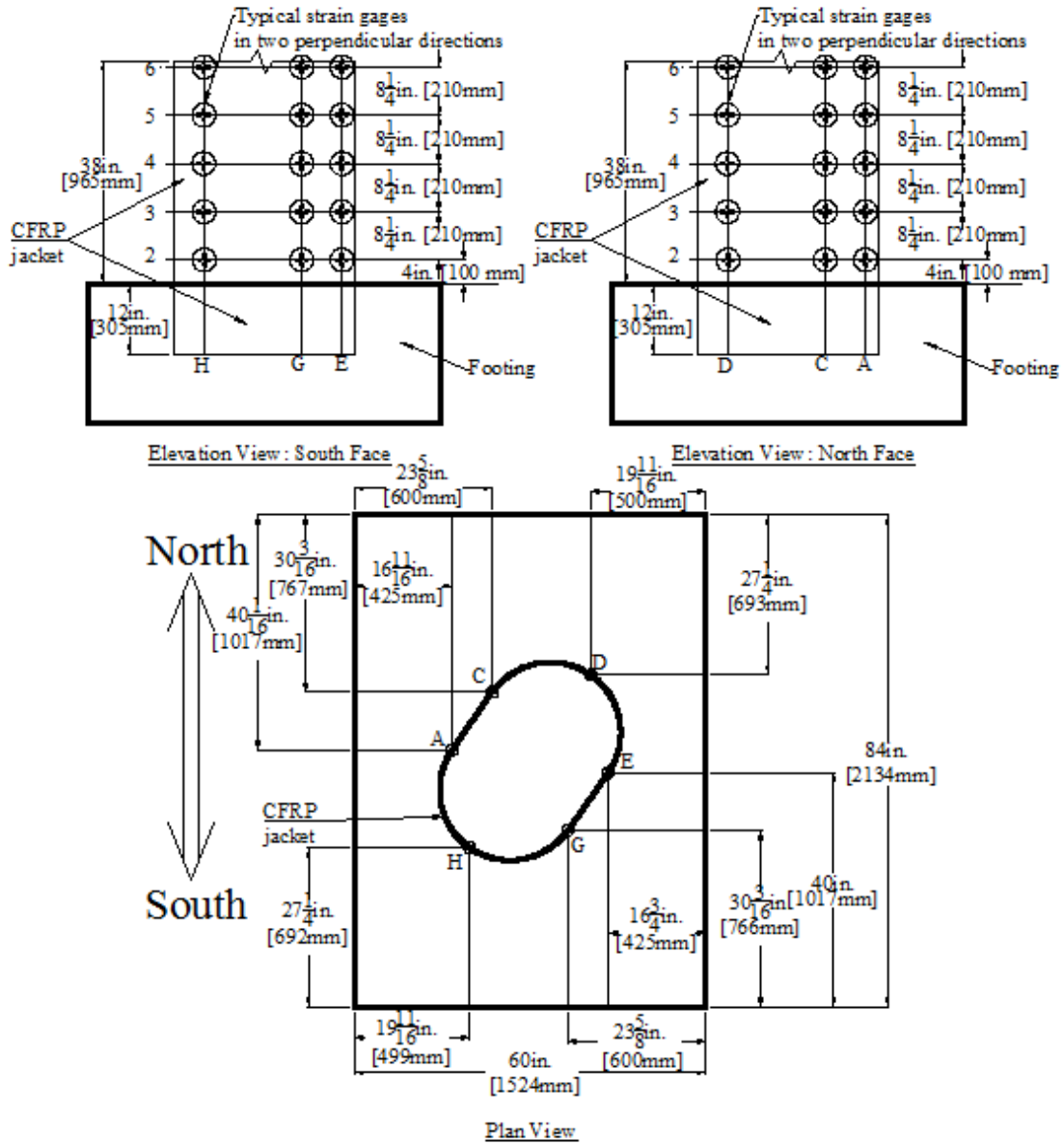


(a) Elevation view



(b) Plan view

Figure 5-19 Test Setup of R-Calt-3



- Notes: (1) Internal reinforcement not shown  
 (2) Strain gages in transverse direction: 30  
 (3) Strain gages in longitudinal direction: 30

Figure 5-20 Strain Gage Layout on CFRP Jacket for R-Calt-3



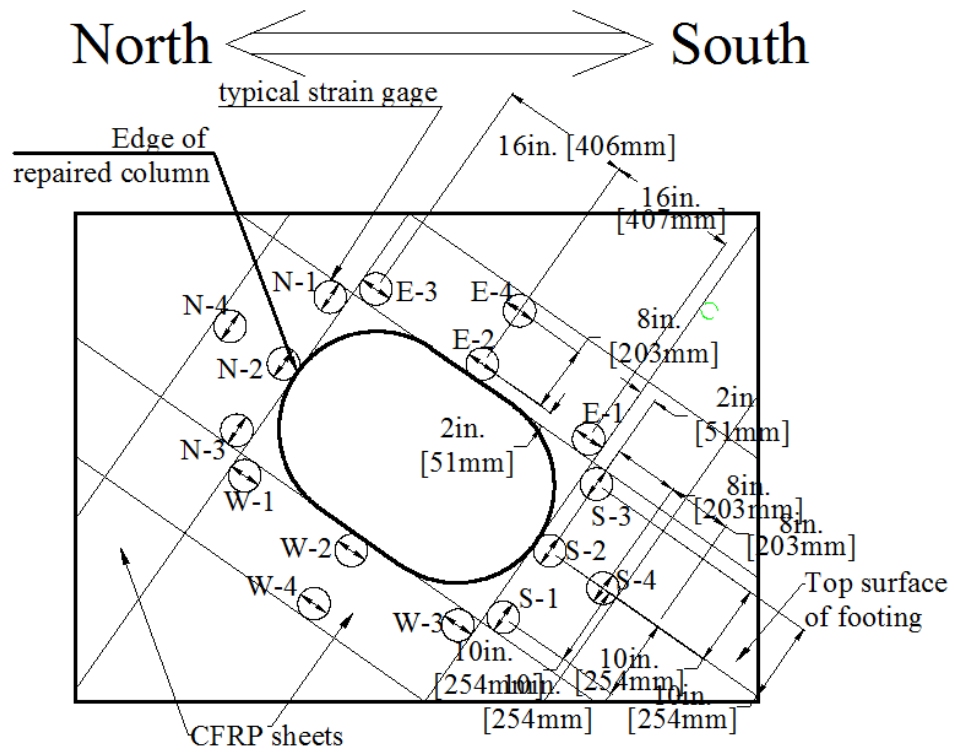


Figure 5-22 Strain Gage Layout on CFRP Sheet of Footing for R-Calt-3

## 6. EXPERIMENTAL RESULTS OF R-CALT-3

This chapter presents the experimental results of R-Calt-3 including observed damage to the repaired column during testing, load-deformation relationships, energy dissipation, and strain history. Section 6.1 describes the damage to R-Calt-3 observed during testing and the results of a forensic investigation of the damage after testing. Section 6.2 describes the measured hysteresis response of the load -deformation relationships, and the calculated envelope as well as idealized bilinear relationships based on the hysteresis response. Section 6.3 presents the energy dissipation for each loading cycle. Section 6.4 presents the measured strain results of the CFRP jacket, CFRP strips, and CFRP straps on the footing. Section 6.5 summarizes the experimental results and makes concluding remarks.

### 6.1. GENERAL BEHAVIOR AND OBSERVED DAMAGE TO R-CALT-3

Testing of R-Calt-3 was terminated when the free end displacement of the column reached the maximum displacement applied to the original column. As shown in Figure 6-1, after the low-amplitude displacement-control phase (drift ratio less than 1%) that corresponded to the force-control phase for the original column, the repaired column was subjected to six displacement-control (DC) levels in positive direction (Push/South) and five DC levels in negative direction (Pull/North). In Figure 6-1, “Drift” denotes the displacement levels expressed as drift ratios; the number after “Drift” denotes the corresponding drift ratios; and “+/-” denotes the loading direction as positive or negative, respectively. The deformed shape of the column at the peak displacement of each DC level is also shown in Figure 6-1.

Damage to the longitudinal reinforcement (either the reinforcing bars or the CFRP strips) could not be verified during testing without removal of CFRP jacket and concrete, although a noise that sounded like bar fracture was heard when the maximum lateral load was passed. In order to confirm the origin of the suspicious sound and to determine whether a bar had fractured, forensic inspection was conducted after the testing.

At low-amplitude levels of displacement (drift ratio  $< 1\%$ ), no damage was observed to R-Calt-3 except for a clicking noise that was heard, possibly due to the slip between the CFRP and the concrete substrate. The footing was also observed to be offset from its original position at drift ratio of 1%, which was attributed to the soft torsional resistance provided by the test setup (see Figure 6-2). At a drift ratio of 2%, wrinkles in the CFRP jacket on the compression side of the column started to be noticeable (see Figure 6-3a). Existing inclined cracks in the concrete above the CFRP jacket were also widened at a drift ratio of 2% (see Figure 6-3b). At a drift ratio of 3%, vertical and inclined cracking were observed on both the east and west sides of the footing due to the shear and bending moment applied transferred to the footing (see Figure 6-4). During loading to drift ratio of 3%, a loud noise was heard that was later proved to be fracture of one of the existing longitudinal bars. The CFRP jacket started to rupture on the compression side at a drift ratio of 3% (see Figure 6-5), which may explain why the lateral load capacity dropped at this level. Slip of the CFRP jacket from the footing was also noticed at the level. At higher levels (drift ratio  $>3\%$ ) of loading, rupture of the CFRP jacket progressed and was observed on both sides of the column (see Figure 6-6).

A forensic inspection was conducted after termination of testing to observe the damage to the concrete, existing steel reinforcement, and the CFRP strips by removing the CFRP jacket. The

CFRP jacket was cut into pieces with an angle grinder and peeled off of the column piece by piece. Figure 6-7 shows the damage to concrete after removal of the CFRP jacket. As shown in this figure, concrete damage was localized to a region from the top of the footing to a height of 8 in. (200 mm) above the footing. The concrete above this region was still sound for the reason that there was no damage to the CFRP jacket above this region. No additional damage was observed to the existing spirals. Figure 6-8 shows the additional damage to the longitudinal bars. As shown in Figure 6-8a, on the north side of the damaged original column, Bars 1 and 4 were only buckled while Bars 2 and 3 were fractured after the original test. After testing of the repaired column, Bars 1 and 4 were observed as fractured as shown in Figure 6-8b. The CFRP strips also ruptured during testing as shown in Figure 6-9.

## 6.2. BASE SHEAR-LATERAL DISPLACEMENT AND TORSIONAL MOMENT-TWIST RELATIONSHIPS

The base shear and torsional moment applied to the columns were calculated from the forces recorded by the two actuators. The free-end lateral displacement and twist angle were calculated based on the geometry of the test setup and the displacement of the two actuators. Load-displacement and torsional moment-twist hysteresis responses of the original column and repaired column are compared in Figure 6-10.

The base shear-lateral displacement hysteresis for R-Calt-3 and Calt-3 are compared in Figure 6-10a. The hysteretic behavior of R-Calt-3 was asymmetric with higher maximum base shear in the push direction than in the pull direction, while that of Calt-3 was more symmetric. This may be due to the fact that the rupture of CFRP jacket of R-Calt-3 in the positive cycle reduced the

load capacity in the subsequent negative cycle. The higher maximum lateral displacement in the push direction was due to the fact that the actuators had a larger stroke capacity in the push direction (positive displacement) than in the pull direction (negative displacement). The maximum positive base shear of R-Calt-3 was also larger than that of Calt-3, which implies that the repair method was successful in restoring or even enhancing the lateral strength. The lateral strength of R-Calt-3 started to degrade at 4 in. (100 mm) in both directions due to rupture of the CFRP jacket, which was similar to the response of Calt-3, which started to degrade at a displacement of 4 in. (100 mm) in both directions. This implies that the repair method was also successful in restoring the lateral displacement capacity of the column. However, the strength degradation rate of R-Calt-3 was much higher than that of Calt-3. This may be due to the lower rupture strain of the longitudinal CFRP strips than that of steel reinforcement. The cyclic loops of R-Calt-3 had a similar shape as those of Calt-3 with similar unloading stiffness before strength degradation of both columns. The pinching effect was more noticeable in R-Calt-3 than in Calt-3, which implies that the repair method reduced the energy dissipation capacity.

The base shear and lateral displacement envelopes for R-Calt-1 and Calt-1 are compared in Figure 6-10a. As shown in this figure, the initial lateral stiffness of R-Calt-1 was lower than that of Calt-1 in both directions. This may have been due to slip of the CFRP jacket relative to the substrate since the adhesive layer was as thick as 1 in. (22 mm) in places and had a much lower stiffness than both the CFRP and concrete. Table 6-1 summarizes the maximum base shear and torsional moment in both directions. As shown in this figure, this method was successful in restoring both the lateral strength and torsional strength.

Idealized envelopes representing an elasto-plastic curve for Calt-3 and R-Calt-3 are shown in Figure 6-12a and Figure 6-12b, respectively. The bilinear envelopes were idealized by setting the initial slope to pass through the first yield point recorded during testing of Calt-3 and adjusting the plastic portion to equate the areas under the measured and idealized curves. Table 6-2 summarizes the maximum values obtained from Figure 6-12. In this table, the equivalent yield base shear or torsional moment is the average value of base shears or torsional moments in both directions. The equivalent lateral or torsional stiffness is the average value of the stiffness calculated in both directions. The equivalent lateral or torsional ductility ratios are the average value in the both directions. As shown in Table 4-1, the equivalent yielding lateral force, the equivalent elastic lateral stiffness, and the equivalent lateral ductility ratio of R-Calt-3 was approximately 92%, 95%, and 98% of that of Calt-3, respectively. This implies that the repair method was successful to restore the lateral behavior of the column.

Figure 6-10b shows the hysteresis of torsional moment and twist relations where clockwise torsion is defined as positive and counterclockwise torsion as negative. Degradation of the torsional strength of R-Calt-3 was observed at an angle of 2.5 degrees in the positive direction, while no degradation of the torsional strength of R-Calt-3 was observed in the negative direction. The torsional moment and twist envelopes are compared in Figure 6-b. As shown in this figure, the initial torsional stiffness of R-Calt-3 was much lower than that of Calt-3. This may be due to relative movement (slip) between the CFRP jacket and the column due to the low modulus of the epoxy filled in between them. The elasto-plastically idealized torsional moment and twist curves are shown in Figure 6-12c and Figure 6-12d, from which critical values were calculated and summarized in Table 6-2. As shown in this table, the equivalent yielding torsional moment of R-

Calt-3 was 97% of that of Calt-3, while the equivalent elastic torsional stiffness and torsional ductility ratio of R-Calt-3 was only 36% and 28% of that of Calt-3, respectively. This implies that the repair method was successful in restoring the torsional strength; however, it did not restore the torsional stiffness and ductility.

### 6.3. ENERGY DISSIPATION

Energy dissipated in each loading cycle can be calculated as the summation of the enclosed area for each cycle on the base shear-displacement and torsional moment-twist relations (Priestley et al 1996). The energy dissipation per cycle for both the repaired and original columns is shown in Figure 6-13a.

As shown in Figure 6-13a, the dissipated energy for each cycle prior to the 12<sup>th</sup> cycle was negligible for both R-Calt-3 and Calt-3 due to the fact that the yielding of reinforcement and spalling or crushing of concrete was very limited prior to that cycle. At the same displacement level, the energy dissipation for the second and third cycles was smaller than that of the previous cycle since the energy dissipation in the first cycle was irreversible, and the specific displacement level could not induce additional yielding, concrete spalling or crushing in the subsequent cycles.

Cumulative energy dissipation was also compared between original and repaired columns. As shown in Figure 6-13b, the repaired column showed smaller cumulative energy dissipation at end of each load cycle than the corresponding original column. This is attributed to the nonductility of the CFRP reinforcement and the significant amount of plastic deformation that had already occurred in the internal steel reinforcement during the original test.

#### 6.4. MEASURED STRAINS

Strain gages were installed on the CFRP jacket, CFRP strips, and the CFRP straps on the footing to record the strain history during testing. The strain distribution along the column height at different stages of displacement control loading is shown in Figure 6-14, Figure 6-15, and Figure 6-. Figure 6-14 and Figure 6-15 show the measured longitudinal and transverse strains of the CFRP jacket along the column height, respectively. Figure 6- shows the measured longitudinal strains of the CFRP strips along the column height. In these figures, “DR” and the number following it denotes “drift ratio” and corresponding stage; “+” and “-” indicates that the displacement was applied in the “push” and “pull” directions, respectively. The strain-drift ratio hysteresis relationship of the CFRP straps on the footing is shown in Figure 6-17.

As shown in Figure 6-14, the longitudinal fibers in the CFRP jacket experienced obvious deformation in both tension and compression, which implies the CFRP jacket contributed to the flexural strength of R-Calt-3. The maximum measured tensile strain was at location “H” of the cross-section at a height of 4 in. (100 mm) from the top of the footing. The maximum value was measured at a drift ratio of -2% and was close to 0.008, which is 56% of the rupture strain in that direction (0.0142 provided by provided by the manufacturer, refer to Table 5-6). The maximum measured compressive strain was also at a location of “H” at a height of 12.25 in. (310 mm) from the top of the footing. The maximum value was measured at a drift ratio of +5% and was equal to 0.008. The measured strain values also imply no rupture of CFRP in longitudinal direction, which was consistent with the observation during testing that rupture of CFRP occurred within a region no higher than 2 in. (50 mm) from the top of the footing.

As shown in Figure 6-15, strains measured in the transverse fibers in the CFRP jacket were mainly tensile strains. The maximum tensile strain was measured at location “E” at a drift ratio of +5% at a height of 4 in. (100 mm) from the top of the footing. The measured value was between 0.008 and 0.01, which was close to the rupture strain of the CFRP jacket in that direction (0.0085 provided by the manufacturer, refer to Table 5-6).

As shown in Figure 6-16, the CFRP strips experienced obvious deformation in both tension and compression. The maximum tensile strain was measured at location “B” at a drift ratio of +3% at a height of 4 in. (100 mm) for the reason that the strain gages at this location malfunctioned at higher drift ratios. The measured value was 0.006, which was 60% of the rupture strain provided by the manufacturer (refer to Table 5-4). The maximum compressive was measured at location “C” at a drift ratio of +3%. The measured value was also 0.006. Figure 6-16 also shows that the strain penetrated into the footing to a depth of 4 in. (100 mm) with a maximum tensile strain of 0.003 and maximum compressive strain of 0.005 measured at location “B”. It should be noted that the strains in the CFRP strips at the column-footing joint might be higher than that at the 4 in. (100 mm) high location because the strips ruptured at the base of the column as discussed in Section 6.1.

Figure 6-17 shows the strain-drift ratio hysteresis relationship measured from the CFRP straps bonded to the top surface of the footing. As shown in this figure, the CFRP straps resisted tensile force in both the positive and negative cycles. However, the straps on the north side took larger forces in the positive cycles than in the negative cycles, while the straps on the south side took larger forces in the negative cycles than in the positive cycles. The straps on both the east and west sides took similar forces regardless of the loading direction. The maximum measured

tensile strain was between 0.0015 and 0.002, which was only 38% to 50% of the design effective strain as described in Section 5.2.4. This figure also shows that the strain values along the length or the width of straps were similar; thus, the length and width of the straps specified in this study was effective in restoring the footing strength.

## 6.5. CONCLUDING REMARKS

This chapter presents the evaluation of the emergency repair method proposed in Chapter 5 by comparison of the experimental results obtained from testing the repaired and original columns. Based on the discussions and observations in this chapter, the following conclusions may be made: (1) the repair method was able to enhance the lateral strength, stiffness, and ductility, which suggests that it might also be applicable for the case of a permanent repair. However, the performance of this repair method depends on the bond provided by the epoxy that was filled in between the column and the CFRP jacket as well as the column-footing joint integrity provided by the gravel-filled epoxy within the trench. Therefore, long-term durability and bond performance of the epoxy and epoxy-gravel should be investigated for the case of a permanent repair; (2) the repair method restored the torsional strength but resulted in a lower torsional stiffness and ductility compared to that of the original column; (3) energy dissipation per cycle as well as cumulative energy dissipation of the repaired column was lower than that of the original column; (4) the design method for the transverse CFRP in this study was conservative enough to preclude damage to the transverse CFRP; (5) the footing repair was successful and effective with no observed debonding of CFRP from the footing; (6) since stiffness and energy dissipation of the repaired column was different from that of the original column, more work may needed to investigate the influence of the repair method on the response of the entire bridge structure.

Table 6-1 Summary of Measured Forces of Calt-3 and R-Calt-3

Column ID	Maximum Positive Base Shear kip (kN)	Maximum Negative Base Shear kip (kN)	Maximum Positive Torsional Moment kip-ft (kN-m)	Maximum Negative Torsional Moment kip-ft (kN-m)
Calt-3	121.4 (540.0)	118.7 (528.0)	247.6 (342.3)	358.4 (485.9)
R-Calt-3	130.5 (580.5)	103.5 (460.4)	257.1 (348.6)	238.0 (322.7)

Table 6-2 Critical Values on Idealized Load-Displacement Curves

Column ID	Equivalent Average Yielding Base Shear kip (kN)	Equivalent Average Yielding Torsional Moment kip-ft (kN-m)	Equivalent Average Lateral Stiffness kip/in (kN/mm)	Equivalent Average Torsional Stiffness kip-ft/rad (kN-m/rad)	Equivalent Lateral Ductility Ratio	Equivalent Torsional Ductility Ratio
Calt-3	112.7 (501.3)	243.0 (329.5)	56.0 (9.79)	16979 (23020)	4.1	5.8
R-Calt-3	103.6 (460.8)	236.8 (321.1)	53.4 (9.33)	6175 (8372)	4.0	1.6



Drift 1% (-)



Drift 2% (-)



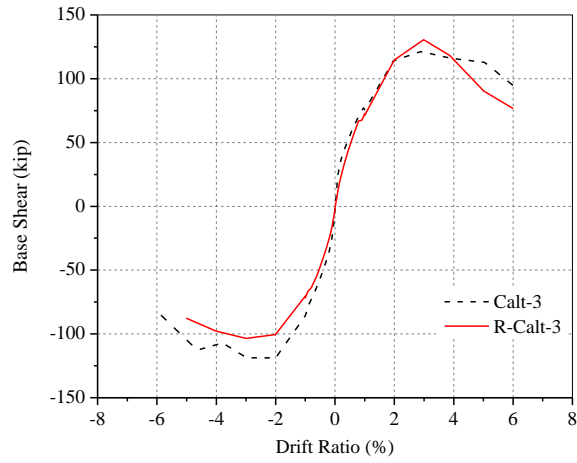
Drift 3% (-)



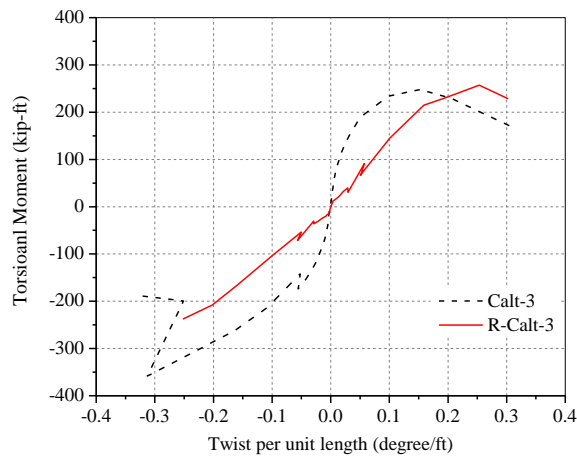
Drift 4% (-)



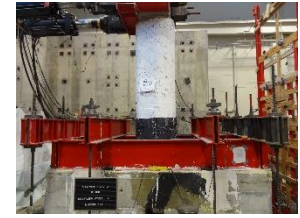
Drift-5%(-)



Envelope of Base Shear vs. Drift Ratio



Envelope of Torque vs. Twist Per Unit Length



Drift 1% (+)



Drift 2% (+)



Drift 3% (+)



Drift 4% (+)



Drift 5%(+)



Figure 6-1 Progressive Deformation of R-Calt-1 at Increasing Load Levels

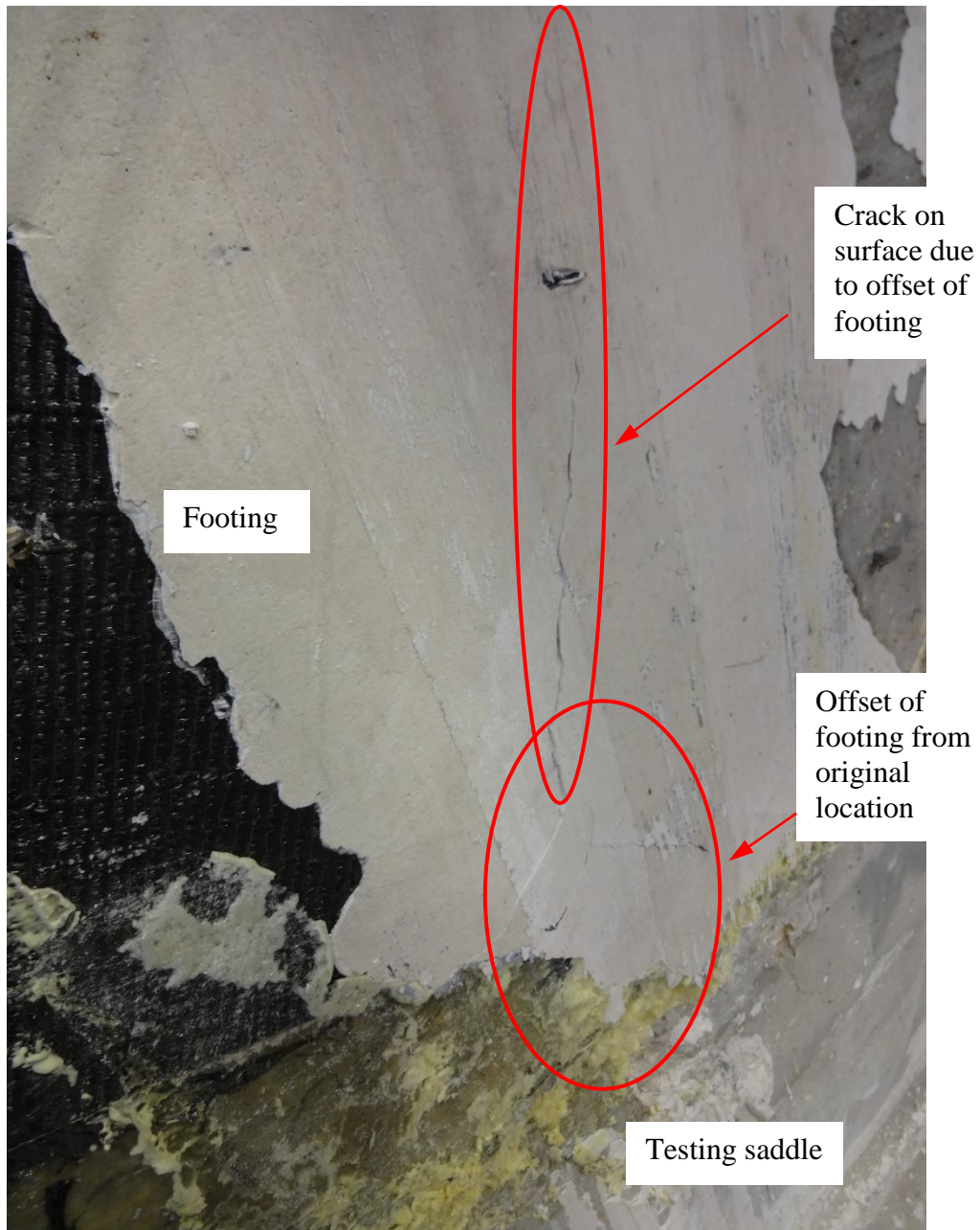
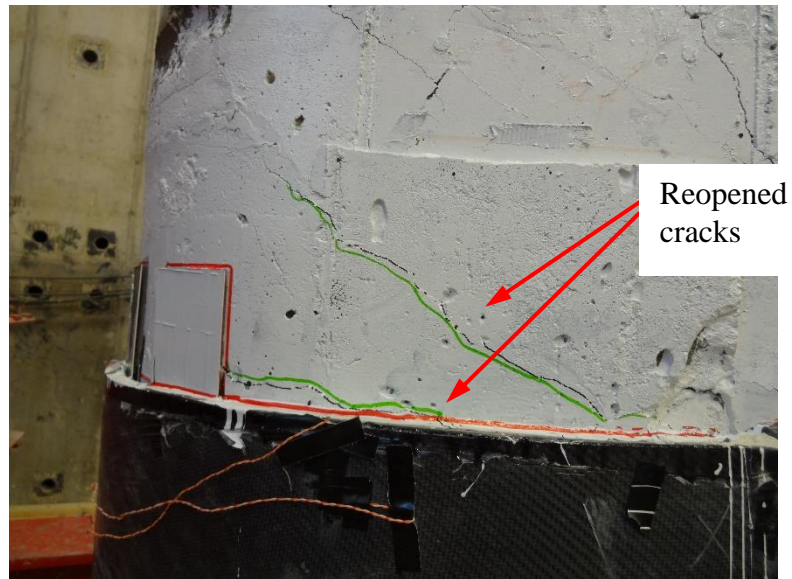


Figure 6-2 Offset of R-Calt-3 Footing Observed at Drift Ratio of 1%



(a) Wrinkles in CFRP jacket on column compression side



(b) Reopening of cracks on west side

Figure 6-3 Damage to R-Calt-3 at Drift Ratio of 2%



(a) East side



(b) West side

Figure 6-4 Cracking in R-Calt-3 Footing at Drift Ratio of 3%

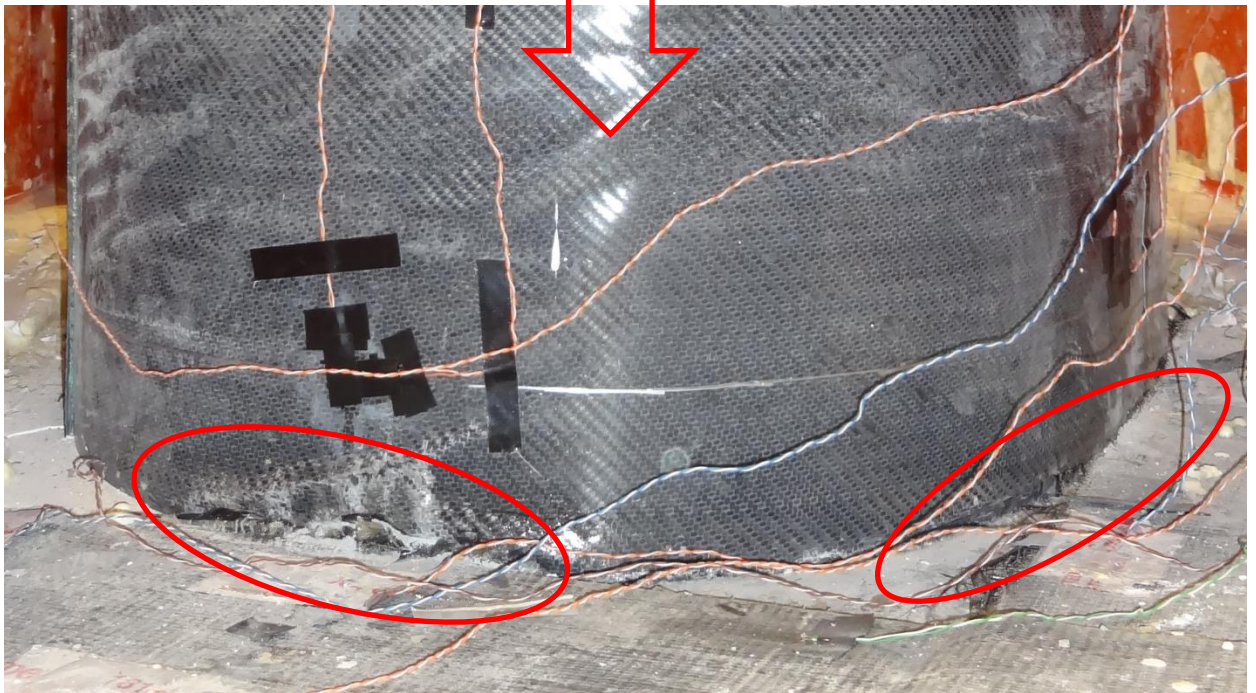


Figure 6-5 CFRP Rupture on Column Compression Side at Drift Ratio of 3% (R-Calt-3)

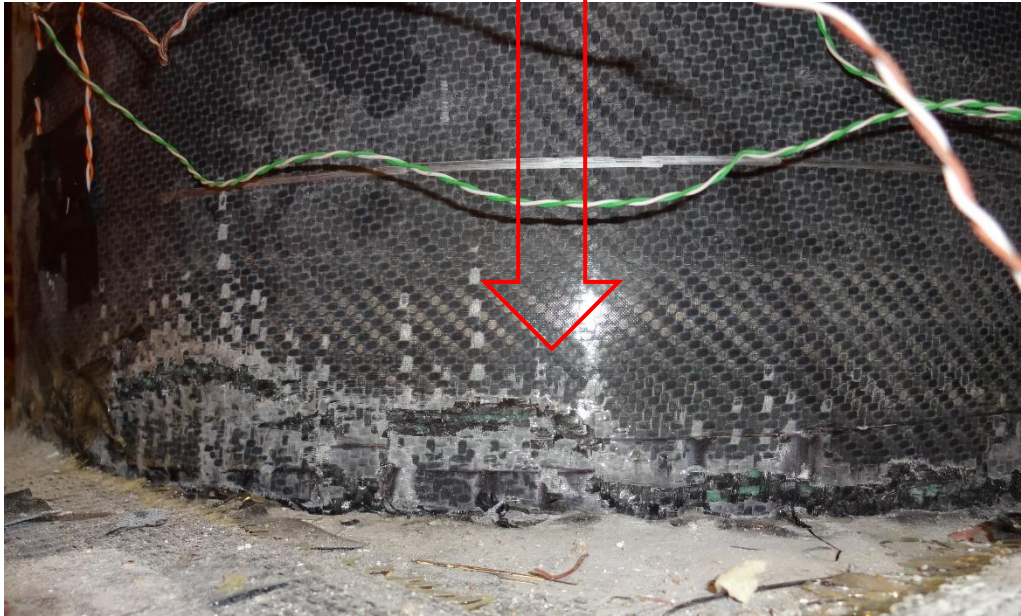
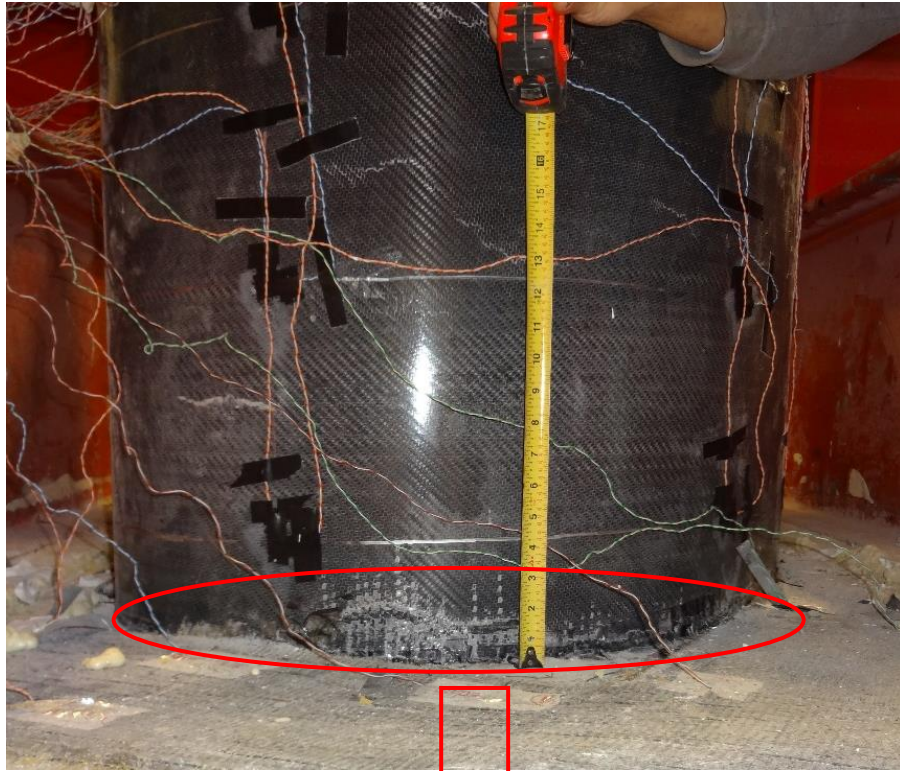


Figure 6-6 CFRP Rupture on Column Tension Side at Drift Ratio of 3% (R-Calt-3)

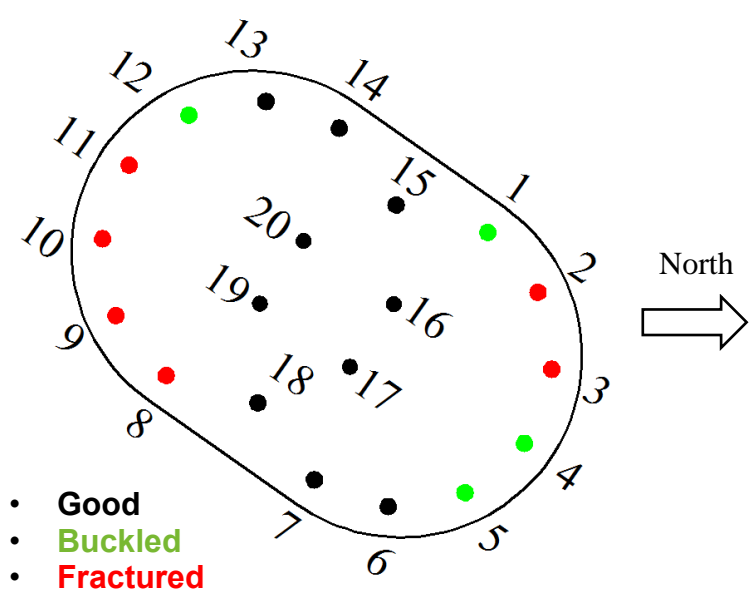


(a) North side

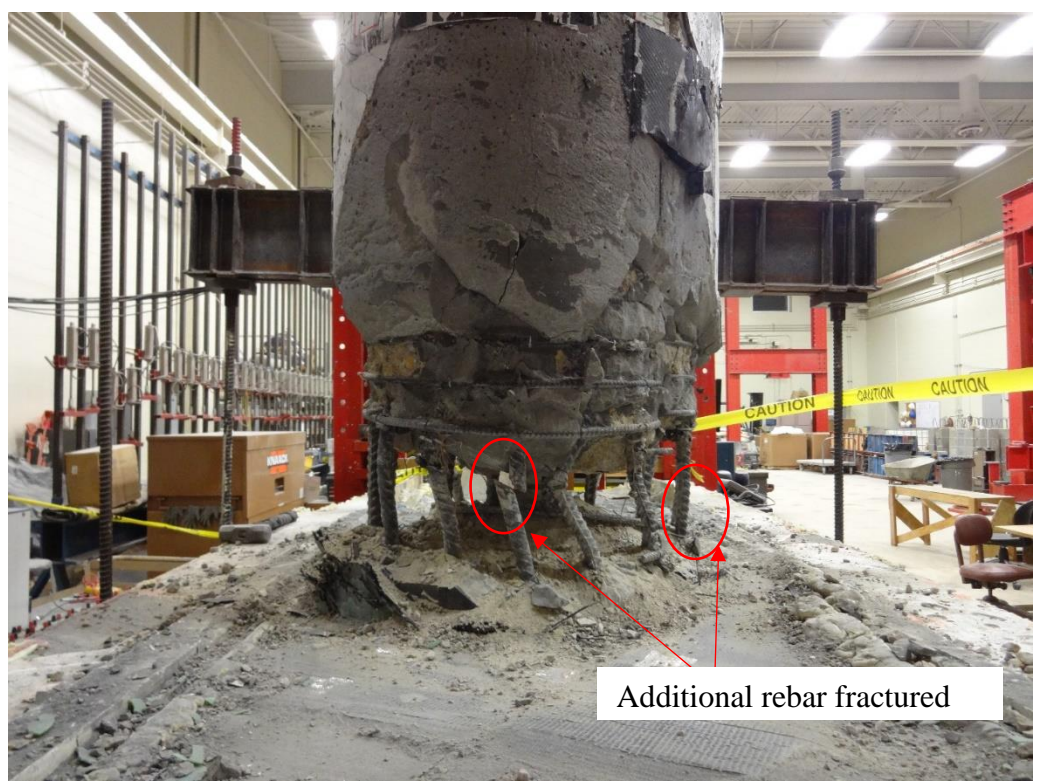


(b) South side

Figure 6-7 Damage to Concrete of R-Calt-3



(a) Rebar damage to Calt-3

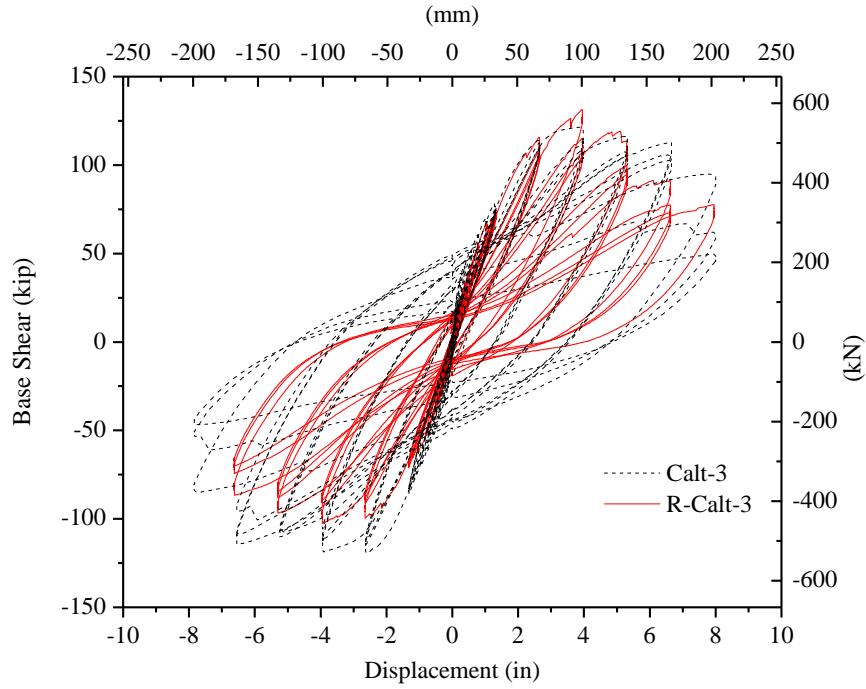


(b) Rebar damage to R-Calt-3 (North Side)

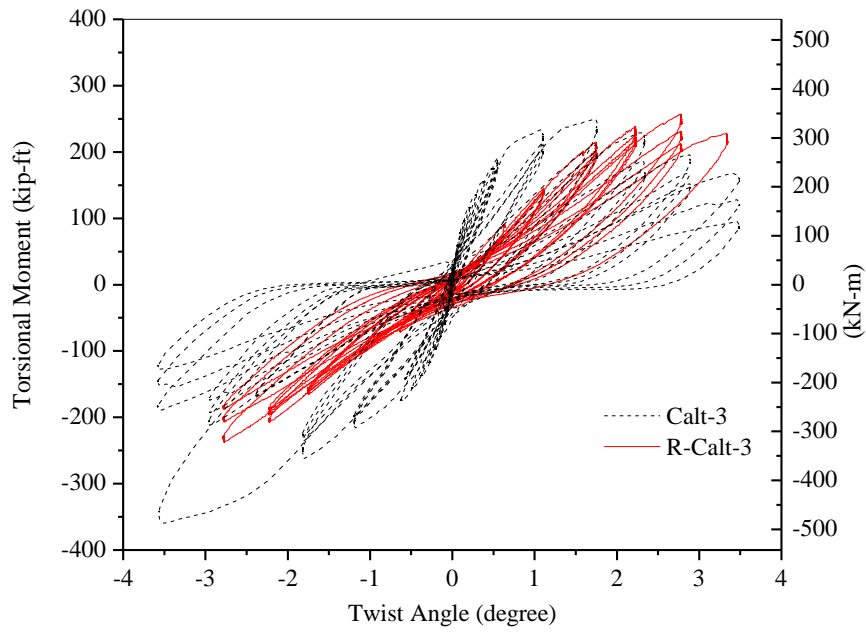
Figure 6-8 Damage to Reinforcing Bars for Calt-3 and R-Calt-3



Figure 6-9 Rupture of CFRP Strips of R-Calt-3

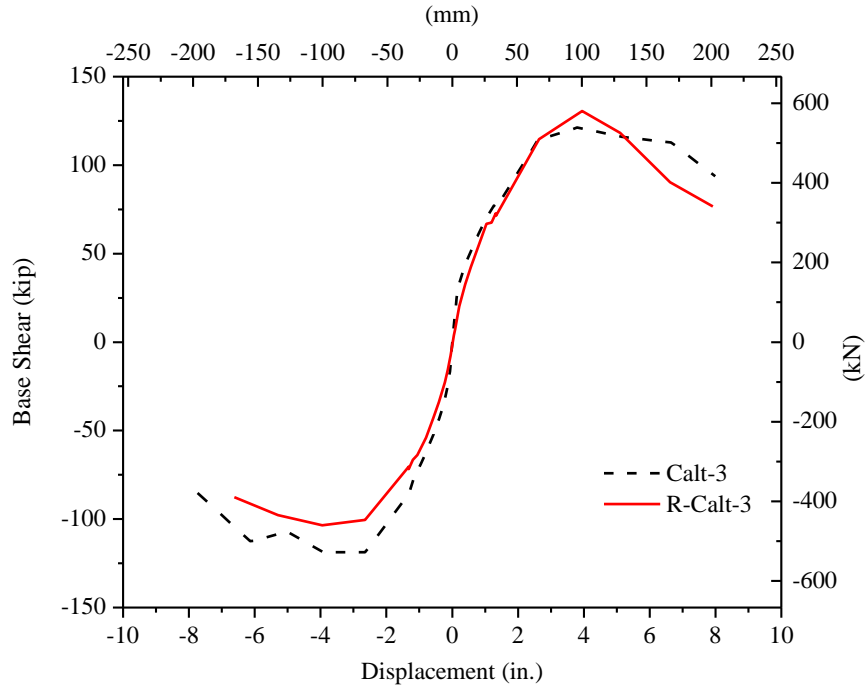


(a) Base shear vs. displacement

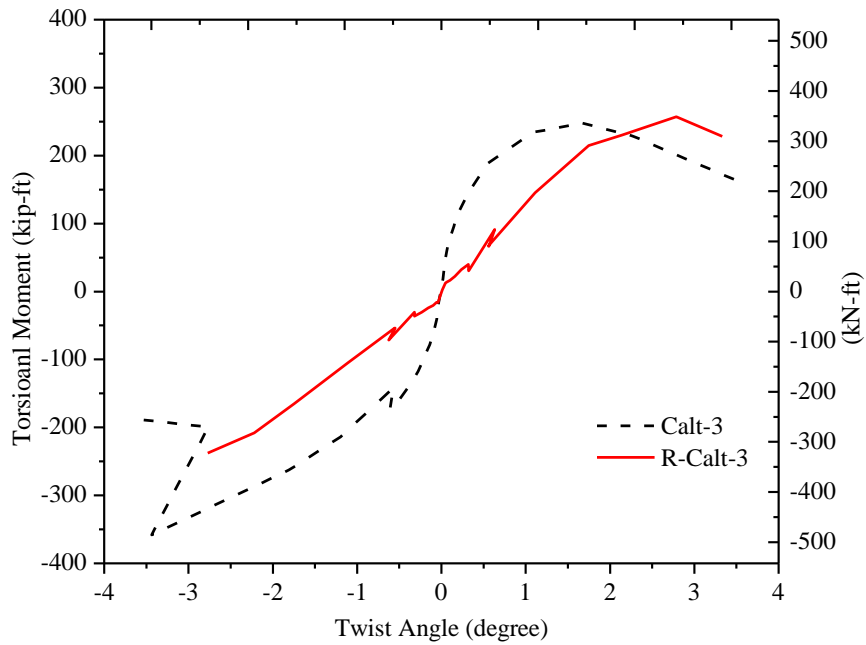


(b) Torsional moment vs. twist angle

Figure 6-10 Load-Displacement Hysteresis Responses of Calt-3 and R-Calt-3

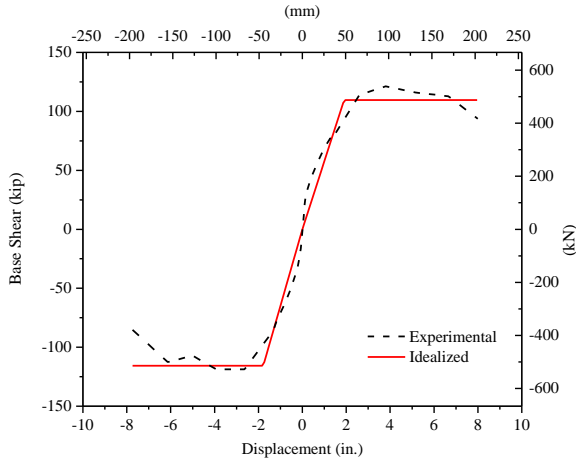


(a) Base shear vs. displacement

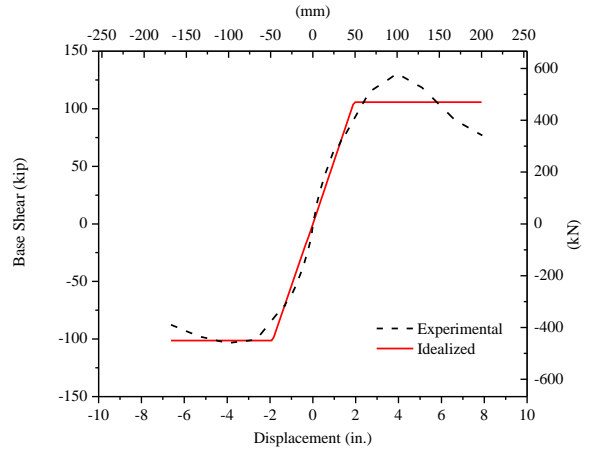


(b) Torsional moment vs. twist angle

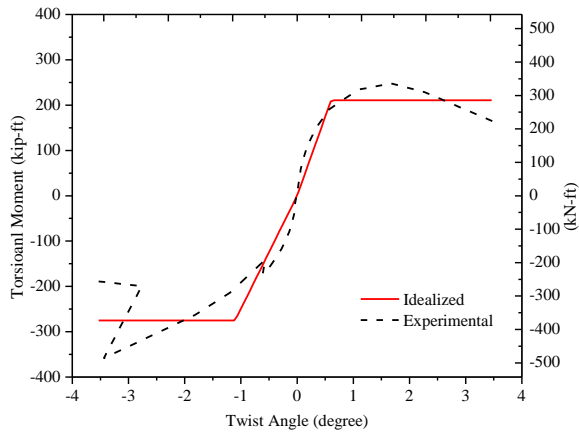
Figure 6-11 Load-Deformation Envelopes of Calt-3 and R-Calt-3



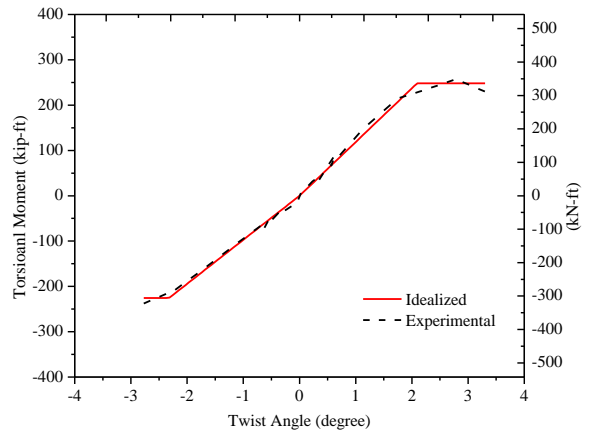
(a) Base shear v.s. displacement (Calt-3)



(b) Base shear v.s. displacement (R-Calt-3)

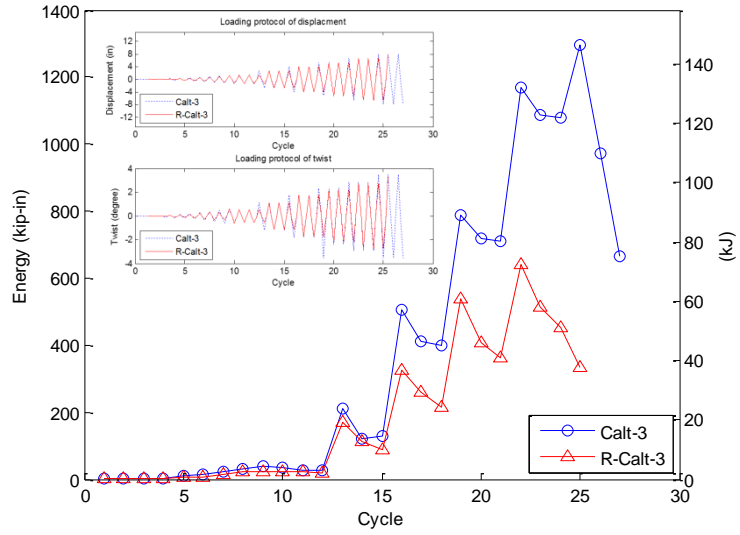


(c) Torsional moment v.s. twist (Calt-3)

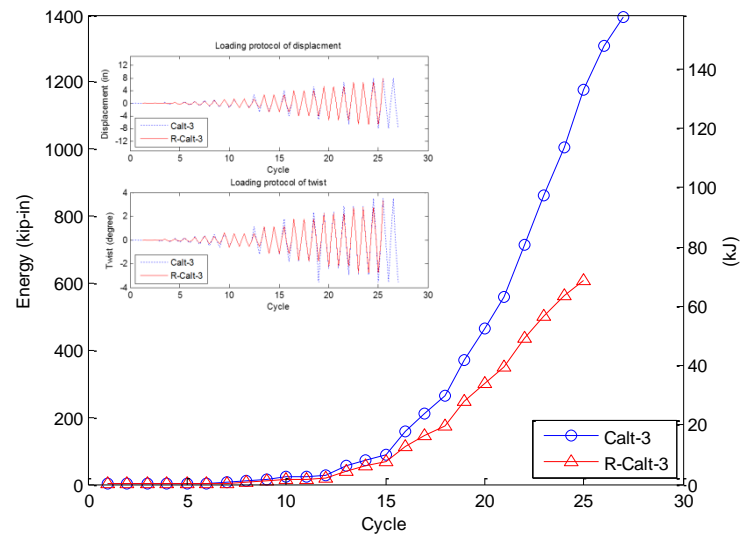


(d) Torsional moment v.s. twist (R-Calt-3)

Figure 6-12 Idealized Envelopes of Load-Deformation

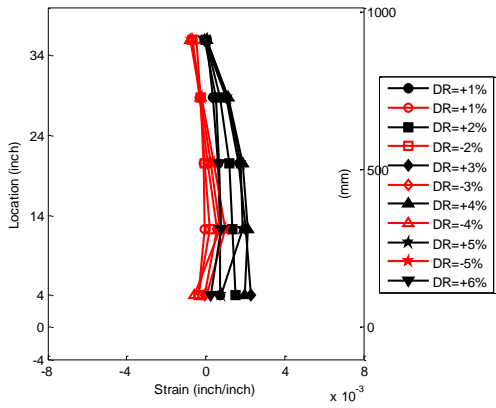


(a) Energy dissipation per cycle

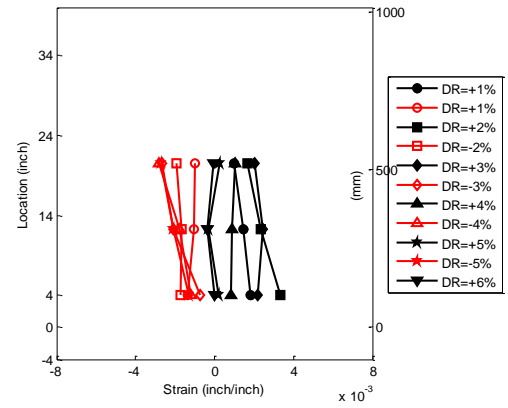


(b) Cumulative energy dissipation

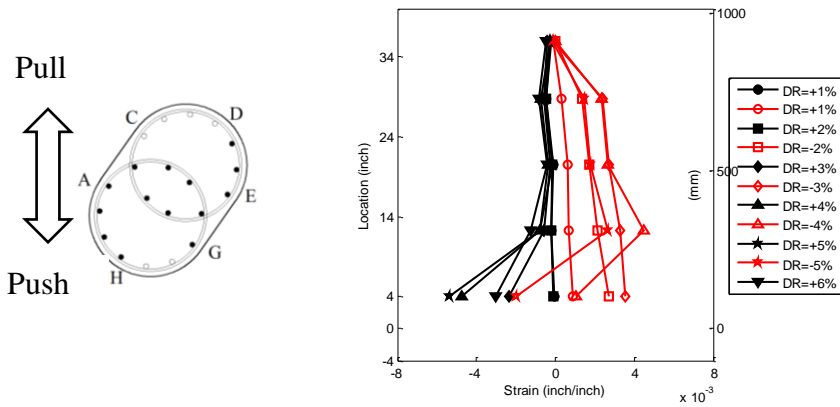
Figure 6-13 Energy Dissipation Per Cycle and Cumulative of Calt-3 and R-Calt-3



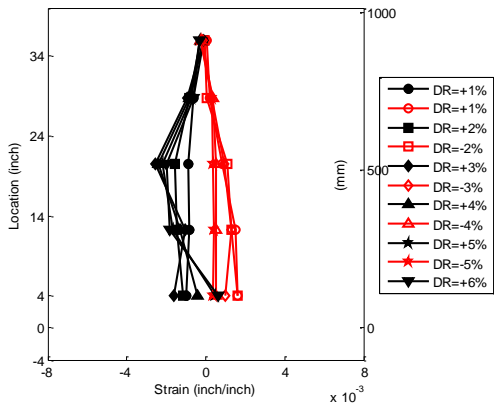
(a) Along line A



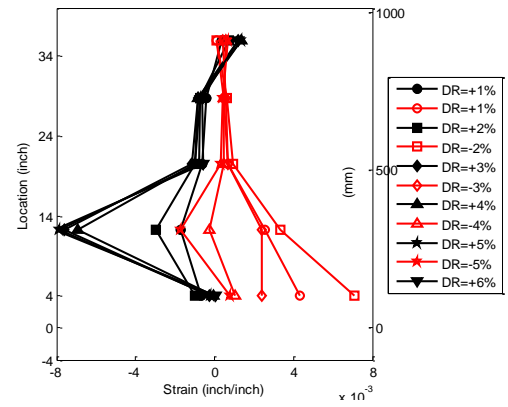
(b) Along line C



(c) Along line E



(d) Along line G



(e) Along line H

Figure 6-14 Measured Longitudinal Strain Profile of CFRP Jacket along Column Height of R-Calt-3

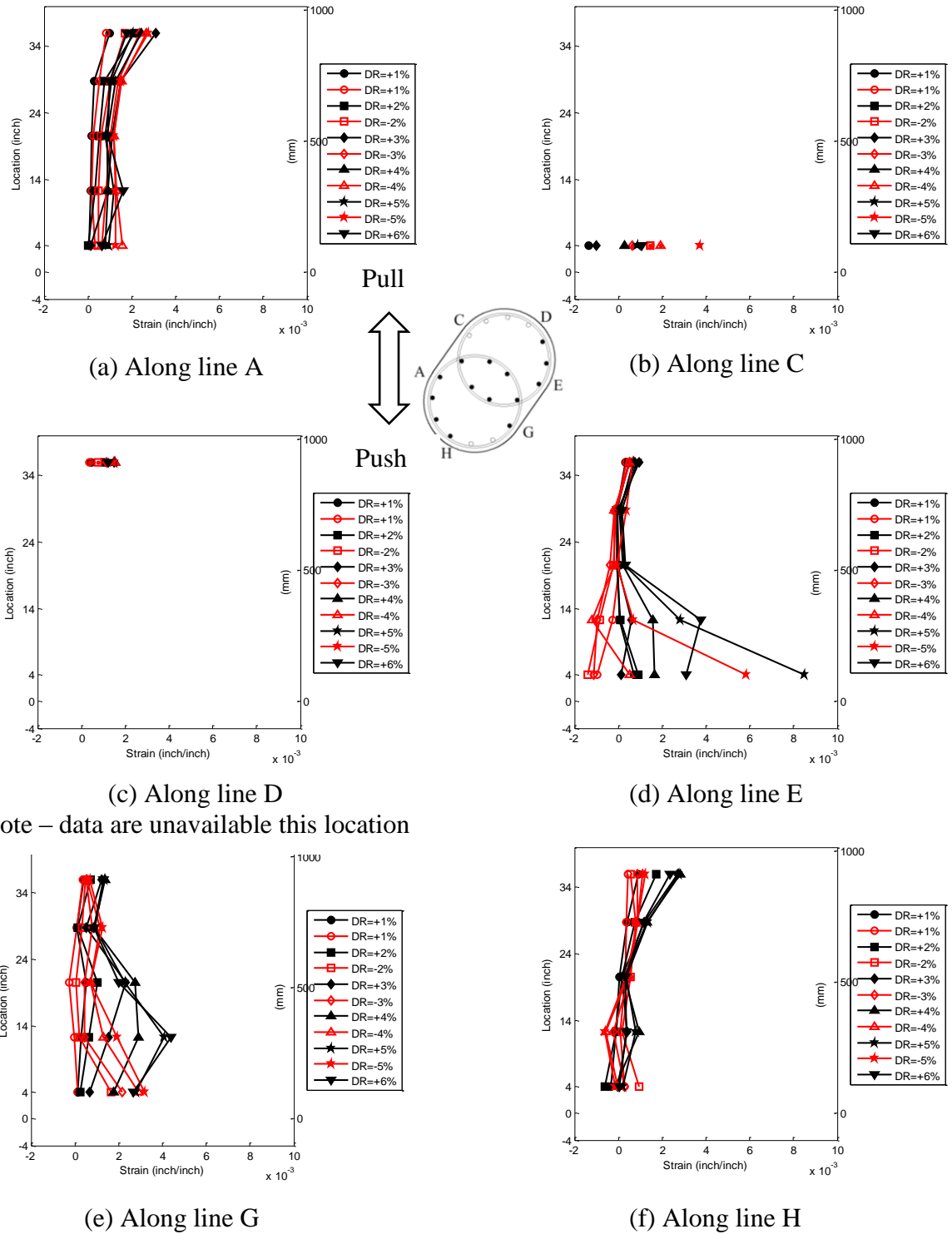


Figure 6-15 Measured Transverse Strain Profile of CFRP Jacket along Column Height of R-Calt-3

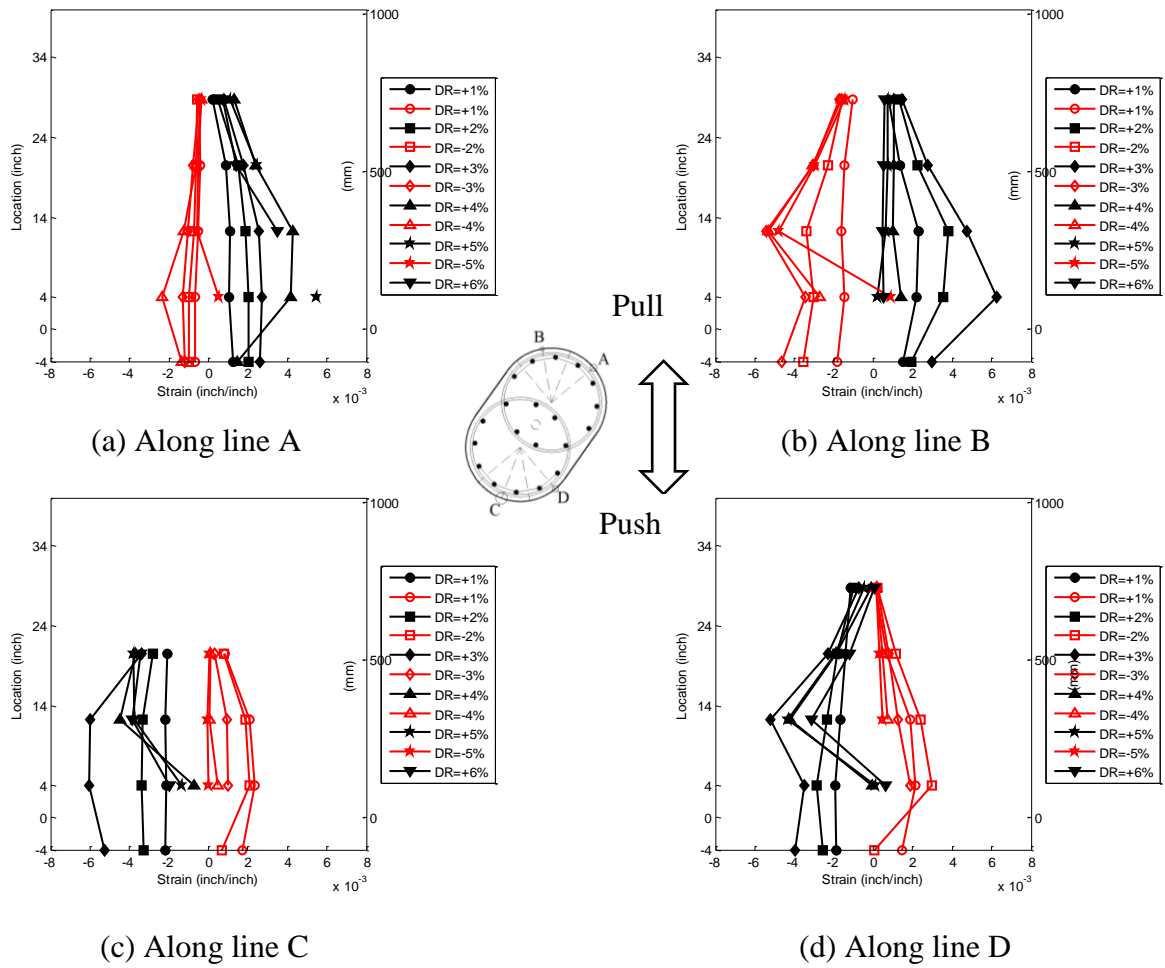
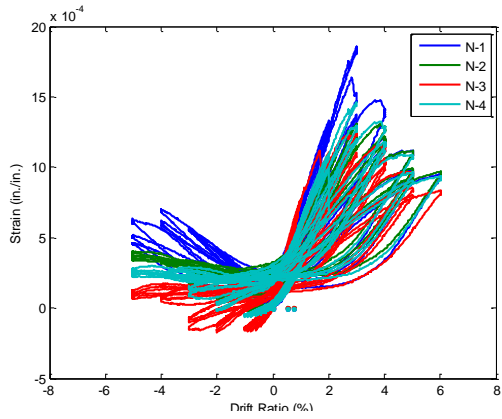
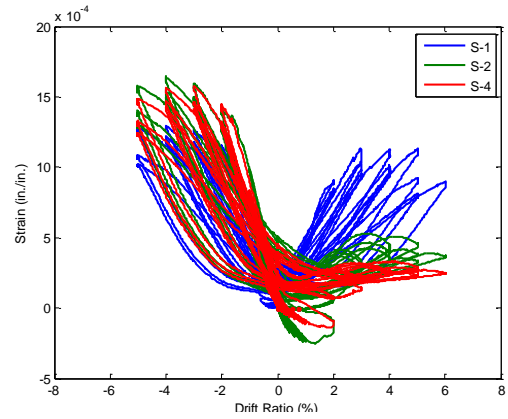


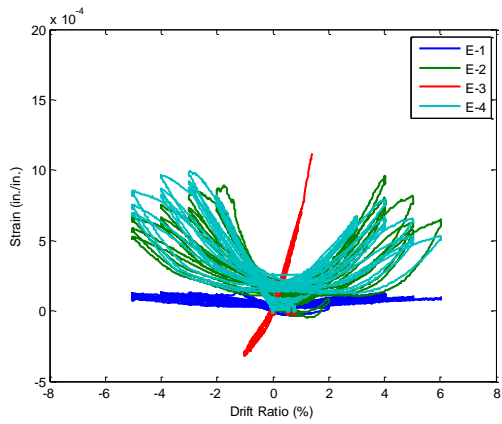
Figure 6-16 Measured Longitudinal Strain Profile of CFRP Strips along Column Height of R-Calt-3



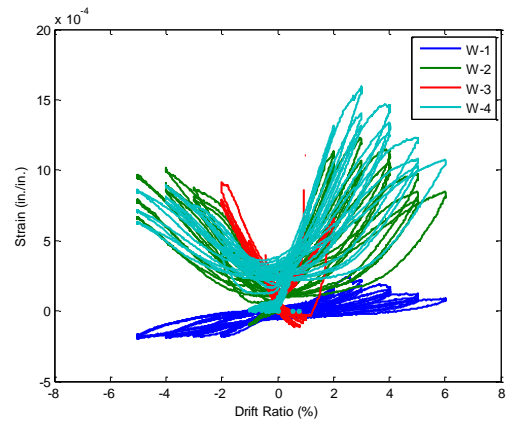
(a) North side



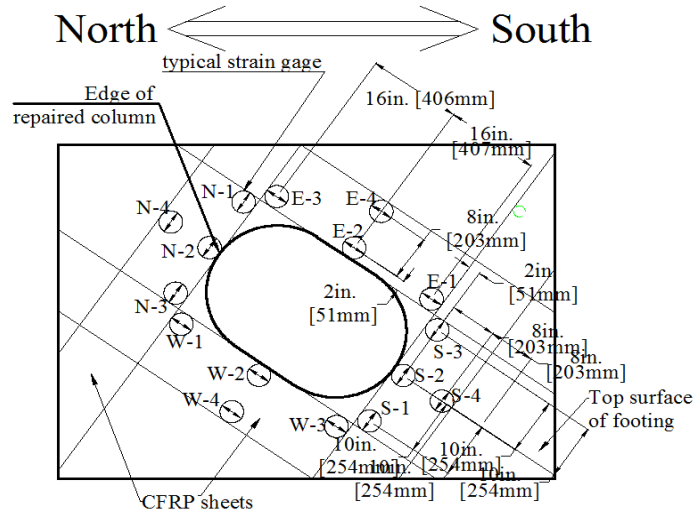
(b) South side



(c) East side



(d) West side



(e) Strain gage layout

Figure 6-17 CFRP Strain of Footing vs. Drift Ratio for R-Calt-3

## 7. ASSESSMENT OF REPAIR METHODS

This chapter compares the constructability of the methods used to repair the three columns included in this study and the seismic performance of the repaired columns in order to assess the pros and cons of the repair methods. In general, two methods were proposed and examined in this study to repair earthquake-damaged RC bridge columns with interlocking spirals and fractured bars. The first method (used for R-Calt-1 and R-Calt-2) involved replacement of the plastic hinge region by removal of spirals, replacement of longitudinal bar segments with new bars attached with mechanical couplers, replacement of concrete, and installation of externally bonded CFRP. The second method (used for R-Calt-3) involved removal of damaged concrete, bonding and embedment of pre-impregnated CFRP strips and jacket, and repairing of the footing with externally bonded CFRP straps. Section 7.1 discusses the constructability of the two repair methods proposed in this study. Section 7.2 describes the seismic performance of the columns repaired using the two methods. Section 7.3 summarizes the assessment and makes several concluding remarks.

### 7.1. CONSTRUCTABILITY

Constructability of each repair method was assessed from aspects including shoring, straightening, concrete removal, reinforcement replacement, coupler installation, concrete replacement, CFRP application, and footing repair where applicable. This section describes the assessment in detail and compares the construction of each repair. Section 7.1.1 discusses the column shoring; Section 7.1.2 describes the concrete removal; Section 7.1.3 discusses the reinforcement removal; Section 7.1.4 describes the coupler installation; Section 7.1.5 presents

some details of concrete or grout placement; Section 7.1.6 describes the CFRP application procedure; and Section 7.1.7 discusses the requirement for footing repair. The comparison of constructability is summarized in Table 7-1.

#### 7.1.1. Shoring

As discussed in Chapter 3, most or all of the longitudinal reinforcement within the plastic hinge region was removed for R-Calt-1 and R-Calt-2; thus, a shoring system was required for the repair work of these two columns. Two commercially available shoring towers were used to shore each of these two columns during the repair procedure. Additional steel spreader beams were also used for the shoring to attach the column cap and transfer the load to the towers. During the initial repair work on these two columns, the columns were not able to support their own self weight, and certainly would not have been able to support additional weight from the superstructure above. Thus, a more complex shoring system may be needed in field application to support both the weight of the superstructure as well as the column itself. The shoring work presented in this report took two workers a total of 8 hours as shown in Table 7-2.

As discussed in Chapter 5, no shoring was used for R-Calt-3 since no longitudinal bars were cut during the repair process, and minimal residual drift resulted from the previous test. The column was able to support its own self weight during the repair, however, it should be noted that the axial load on the column was not present during the repair. Therefore, the field application of the repair method for R-Calt-3 may require shoring to support the superstructure.

#### 7.1.2. Concrete removal

For R-Calt-1 and R-Calt-2, all the concrete within the plastic hinge region of the column was removed to facilitate the replacement of the longitudinal bars. The top cover concrete of the

footing at the base of the column was also removed to facilitate the installation of the bottom couplers. Either an electric jack hammer or a hydraulic jack hammer was used to demolish the sound concrete within the designated regions, where concrete was demolished using the jack hammers both vertically (downward) and horizontally. Demolishing sound concrete took time and effort, especially when the electric jack hammer had to be oriented in the horizontal direction. As shown in Table 7-2, it took two workers approximately 40 hours to demolish the concrete of R-Calt-1 using an electric jack hammer, and approximately 8 hours to demolish the concrete of R-Calt-2 using an electric and hydraulic jack hammer.

For R-Calt-3, only loose concrete was removed from the plastic hinge region of the column. An electric jack hammer was also used to make the trench in the footing around the column perimeter by demolishing the concrete vertically. The concrete demolition in the footing was easier to accomplish than the demolition in both the column and footing of R-Calt-1; however, it still took approximately 20 hours to complete. .

#### 7.1.3. Reinforcement removal

As discussed in Section 3.3.3, segments of the longitudinal bars were severed using a torch and removed in the repair of R-Calt-1 and R-Calt-2. The length of the segments removed was approximately equal to the length of the plastic hinge. To facilitate the removal of concrete and damaged longitudinal bars within the plastic hinge region, all the spirals were cut with an angle grinder and removed from this region in R-Calt-1 and R-Calt-2. The reinforcement severing took two workers approximately four hours to complete. As presented in this study, the method used to sever the reinforcement using torch and angle grinders is achievable in the field. For the repair

of R-Calt-3, the longitudinal bars of were untreated, and no treatment to the spirals was conducted.

#### 7.1.4. Coupler installation and performance

For R-Calt-1, several No. 6 (19.1 mm dia.) bars in the footing were bent to make space for the bottom couplers as shown in Figure 7-1a. The heads of the coupler bolts were sheared off during installation using an impact torque wrench in most locations. The entire installation process took two workers approximately 40 hours due to the dense reinforcement in the footing, which required the use of a hand wrench. Three bar splices composed of the type of couplers used in R-Calt-1 and No. 8 (25.4 mm dia.) bar were tested to failure under pure tension as shown in Figure 7-1b. As shown in this figure, two of the splices failed with bar fracture within the couplers due to the stress concentration at the exterior bolt. Only one of the couplers failed with bar fracture away from the coupler after necking. However, these couplers performed well in restoring the ductility capacity of the repaired column, as discussed in Chapter 4.

For R-Calt-2, due to the higher T/M ratio than that of R-Calt-1 (0.6 and 0.2, respectively), the bent (i.e. buckled) portions of the damaged longitudinal bars were further from the footing than for the longitudinal bars of R-Calt-1; thus, after cutting the bars, the portion of the existing bars protruding from the footing was longer than that of the bars of R-Calt-1, and there was enough length available for the swaging machine to swage most of the couplers. Thus, the time required for the installation was approximately 16 hours with two workers, which was less than that of R-Calt-1. However, two of the protruding bars from the footing were too short to swage the couplers along the entire length (see Figure 7-2a). In this case, approximately a 1 in. (25 mm) length of the two couplers was not swaged as shown in Figure 7-2b. To investigate whether the

unswaged region would reduce the capacity of the splice, one splice sample with a coupler that was not fully swaged was tested to failure under pure tension and compared to the results of three couplers that were fully swaged. The failure modes of the splices that were fully or not fully swaged are shown in Figure 7-2c. As shown in this figure, the splice with the coupler with a 1 in. (25 mm) long unswaged region developed a fracture in the bar at a location away from the coupler. The bar experienced necking before fracture, which was similar to the failure of splices with fully swaged couplers. The results indicated that couplers used in R-Calt-2 that were not fully swaged would also develop the desired failure mode. These couplers performed well in restoring the ductility capacity of the repaired column, as discussed in Chapter 4.

Reinforcing bars of R-Calt-3 were not replaced, therefore no couplers were installed.

#### 7.1.5. Concrete placement

Conventional concrete with similar design strength to that of the original columns was cast to replace the removed concrete within the plastic hinge region for R-Calt-1 and R-Calt-2. High-fluidly grout was cast to replace the damaged concrete for R-Calt-3.

As shown in Figure 7-3a, the formwork for R-Calt-1 was composed of two semi-circular plastic shells and two stiffened wooden forms. The plastic shells were commercially available and were the same as those used to construct the original columns. Concrete was placed through a hole preserved at the top of the formwork (see Figure 7-3b). Concrete was consolidated by limited vibration. The column after concrete placement was shown in Figure 7-3c. As shown in this figure, the top level of the newly cast concrete did not reach the existing concrete and resulted in a 4 in. (100 mm) wide cavity. Honeycombing was also found near the bottom of the column due to limited vibration. The removed top cover of the footing was also not fully filled due to the low

flowability of the concrete. This indicated that the concrete placement method for R-Calt-1 was not successful, and grout filling as well as patching was needed before application of the CFRP jacket.

With the lesson learned from the concrete placement of R-Calt-1, a different method was used to place the concrete for R-Calt-2, which involved more flowable concrete and a pump to ensure better placement of the concrete. Formwork similar to that of R-Calt-1 was used as shown in Figure 7-3d. Highly-flowable concrete with design strength similar to that of the original column was pumped into the formwork (see Figure 7-3e). The column after placement of concrete was shown in Figure 7-3f, which shows that the placement method used for R-Calt-2 was improved compared to that used for R-Calt-1.

For R-Calt-3, high-fluidly grout with design strength similar to that of the original column was cast to replace the damaged concrete. A pump was not used to place the grout. The formwork used for R-Calt-3 was similar to that described for R-Calt-1 and R-Calt-2. The column after grout placement is shown in Figure 7-3g, which also shows the success of the grout placement method used.

It is noted that the same prefabricated CFRP laminates used to build the jacket for R-Calt-3 could be used to create a temporary formwork around the column for placement of grout or concrete, as suggested by the manufacturer. The laminate without the application of any epoxy could be wrapped a few times around the column and held in position with ratchet straps to create a form. Once the concrete or grout is placed in this form and hardens, the ratchet straps and the jacket could be removed to expose smooth finished concrete surface. The same laminate could be wiped clean and coated with epoxy to be used in strengthening the column. While not used in

this laboratory study, this feature of the prefabricated laminates is advantageous as it eliminates the need for securing the services of a mason to repair the column.

For each column, the concrete or grout placement, including the formwork erection, was completed in 8 hours by 2-4 workers.

#### 7.1.6. CFRP application to column

The CFRP jacket of R-Calt-1 and R-Calt-2 was applied using a wet-layup procedure involving matrix impregnation of the fibers. As shown in Table 7-2, a two-week time period was required before installing the CFRP jacket to reduce the influence of moisture after concrete placement. With the wet lay-up procedure, only four layers of fiber sheets could be installed in one day for the reason that additional layers of saturated fibers would cause the jacket to slide down the column due to self-weight, which made installation difficult. Thus, additional layers were installed on the following day after the first four layers were cured overnight. The pre-impregnated CFRP strips and jacket of R-Calt-3 were applied with a dry-layup procedure. The dry layup procedure required less time (eight hours) and effort than the wet layup procedure; however, the quality of the adhesive layer between the jacket and the substrate during dry layup was more difficult to verify. Both methods are commonly used in field applications and can be achievable in a repair.

#### 7.1.7. Footing repair

Minor damage was induced to the footing during the repair of R-Calt-1 and R-Calt-2. No. 6 (19.1 mm dia.) bars in the top of the footing that were oriented in the loading direction were bent in plane where necessary to facilitate coupler installation. Similarly, No. 4 (12.7 mm dia.) bars in the top of the footing that were oriented perpendicular to the loading direction were cut. No

repair was attempted on these bars, and no obvious influence on the response of the repaired columns was observed.

For R-Calt-3, CFRP was externally bonded to the surface of the footing to compensate for the loss of strength due to cutting of footing bars to create the trench around the perimeter of the column. A wet-layup procedure was used to apply the CFRP. Because the surface to which the CFRP was applied was horizontal, application was much easier compared to the vertical application of the wet-layup procedure used to install the CFRP jackets for columns R-Calt-1 and R-Calt-2. Ten layers of CFRP straps were able to be installed in one day (16 hours) by two workers.

## 7.2. SEISMIC PERFORMANCE

In this section, the seismic performance of the repaired columns is evaluated in terms of strength, stiffness, ductility, and energy dissipation.

### 7.2.1. Strength

The equivalent yielding base shear and torsional moment calculated from the measured values during testing of repaired columns were compared to those of the original columns to evaluate whether each repair method was able to restore the strength. In this section, a strength index is used for this purpose. The strength index is defined by Equation 7-1:

$$\text{Strength Index (STRI)} = \frac{F_r}{F_o} = \frac{T_r}{T_o} \quad \text{Equation 7-1}$$

where  $F_r$  and  $F_o$  (or  $T_r$  and  $T_o$ ) denote the equivalent yielding base shear (or torsional moment) of the repaired and original columns that was reported in Sections 4.2 and 6.2.

Figure 7-4 shows the strength index for each column. As shown in this figure, the repair methods used for R-Calt-1 and R-Calt-2 enhanced both the lateral and torsional strength with strength indices over 110%. The repair method used for R-Calt-3 was successful in restoring both the lateral and torsional strength to over 90% of the original column. Thus, it can be concluded that both repair methods proposed were able to restore both the lateral and torsional strength.

### 7.2.2. Stiffness

The equivalent elastic lateral and torsional stiffnesses calculated based on the measured values during testing of the repaired columns were compared to that of the corresponding original columns to evaluate whether each repair method was able to restore the stiffness. In this section, a stiffness index is used for this purpose. The stiffness index is defined by Equation 7-2:

$$\text{Stiffness Index (STFI)} = \frac{S_r}{S_o} \quad \text{Equation 7-2}$$

where  $S_r$  and  $S_o$  denote the equivalent lateral or torsional stiffness of the repaired and original columns reported in Sections 4.2 and 6.2.

Figure 7-4 shows the stiffness index for each repaired column. As shown in this figure, each of the repair methods resulted in lower lateral and torsional stiffness compared to that of the corresponding original columns. Both repair methods were more successful in restoring the lateral stiffness than the torsional stiffness. The repairs of R-Calt-1, R-Calt-2, and R-Calt-3 restored the lateral stiffness to 64%, 71%, and 95% of that of the original columns, respectively. However, the torsional stiffness was only restored to 48%, 59%, and 36% of that of the original columns, respectively. The restoration of stiffness for R-Calt-1 and R-Calt-2 was similar due to the similar repair procedure. The repair method for R-Calt-3 was successful in restoring the

lateral stiffness in part due to the enlarged cross-section as a result of the 1 in. (25 mm) wide annual space between the concrete substrate and the jacket within the plastic hinge region. However, the repair method used for R-Calt-3 resulted in the lowest torsional stiffness index due to cutting the reinforcing bars within the footing around the column, which reduced the torsional stiffness at the joint.

### 7.2.3. Ductility

The equivalent lateral and torsional ductility ratios calculated based on the measured values during testing of the repaired columns were compared to that of the corresponding original columns to evaluate whether each repair method was able to restore the column ductility. In this section, a ductility index is used for this purpose. The ductility index is defined by Equation 7-3:

$$\text{Ductility Index (DCTI)} = \frac{D_r}{D_o} \quad \text{Equation 7-3}$$

where  $D_r$  and  $D_o$  denote the equivalent lateral or torsional ductility ratio of the repaired and original columns reported in Sections 4.2 and 6.2.

Figure 7-4 shows the ductility index for each column. As shown in this figure, the repair method for R-Calt-1 increased the lateral ductility to 104% of that of the original column, while the repair method for R-Calt-2 restored the lateral ductility to 98% of that of the original column. It should be noted that the ductility index calculated for R-Calt-2 may not be the actual value due to the early termination of testing of R-Calt-2. The actual lateral ductility ratio may be larger than what is shown in this figure due to the fact that the CFRP jacket in the plastic hinge region was still sound after testing, and no longitudinal reinforcement fractured during testing. The lateral ductility ratio of R-Calt-3 was about 95% of that of Calt-3, indicating that the repair

method for this column was successful in restoring lateral ductility. The repair methods proposed in this study were not able to restore the torsional ductility. The most successful restoration of torsional ductility was for R-Calt-1, or 78% of that of the original column. Although the repair methods for R-Calt-1 and R-Calt-2 were similar, R-Calt-1 had a lower T/M ratio, and therefore less torsional demand. Therefore, it can be concluded the repair methods proposed in this study were able to restore or enhance the lateral ductility but were unable to restore the torsional ductility.

#### 7.2.4. Energy dissipation

The cumulative energy dissipation of repaired columns was compared to that of the original columns to evaluate whether each repair method was able to restore energy dissipation capacity. In this section, an energy dissipation index is used for this purpose. The energy dissipation index is defined by Equation 7-4:

$$\text{Energy Dissipation Index (ENDI)} = \frac{E_r}{E_o} \quad \text{Equation 7-4}$$

where  $E_r$  and  $E_o$  denote the cumulative energy dissipation of the repaired and original columns at the cycle where testing of the repaired columns was terminated (Sections 4.4 and 6.3).

Figure 7-4 shows the energy dissipation index for each column. It should be noted that more loading cycles (total) were applied to the original columns than the repaired columns; thus, the cumulative energy dissipation at the last cycle of the repaired column was compared to that of the original column at the same cycle level. As shown in this figure, repair methods for R-Calt-1 and R-Calt-2 were successful in restoring the energy dissipation capacity with energy dissipation

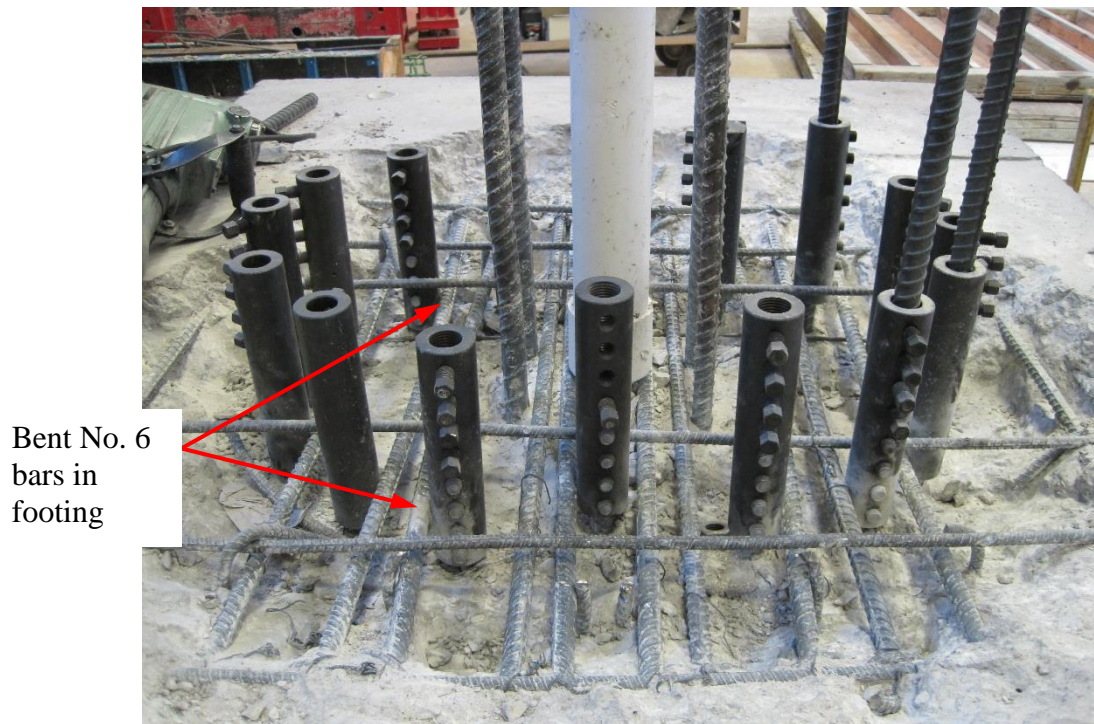
indices of 95% and 98%, respectively; however, the repair method for R-Calt-3 was only able to restore the energy dissipation to 54% of that of the original column.

Table 7-1 Constructability Comparison

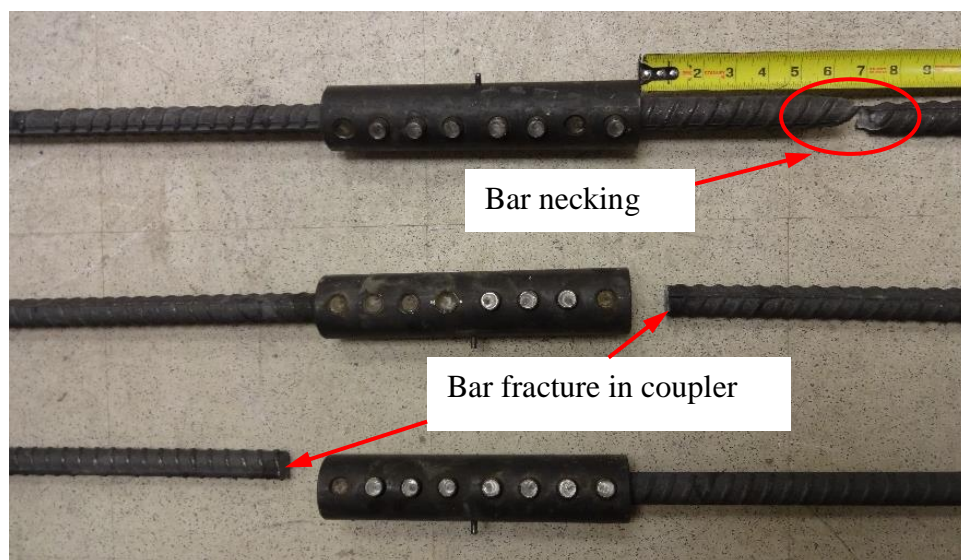
Column ID	R-Calt-1	R-Calt-2	R-Calt-3
Shoring	Necessary for the test specimen	Necessary for the test specimen	Unnecessary for the test specimen
Concrete removal	Entire plastic hinge region and top cover of footing at the column base	Entire plastic hinge region and top cover of footing at the column base	Loose concrete and trench in footing around column perimeter
Reinforcement severing	Removal of all spirals in plastic hinge region; severing of longitudinal bars	Removal of all spirals in plastic hinge region; severing of longitudinal bars	Severing of footing reinforcement
Coupler installation	Impact wrench required; bending and cutting of footing bars as needed	Swaging machine required; cutting of footing bars as needed	N.A.
Concrete/grout placement	Column formwork; and vibration needed	Column formwork and pump needed	Column formwork needed; little vibration
FRP application	Wet-layup of CFRP fabric	Wet-layup of CFRP fabric	Wrapping of prefabricated thin CFRP laminate around column, and applying epoxy paste to the laminate as it was wrapped around the column.
Footing Repair	N.A.	N.A.	Wet-layup of CFRP fabric

Table 7-2 Approximate Time Duration (Per Two Workers)

Column ID	R-Calt-1	R-Calt-2	R-Calt-3
Shoring (hrs)	8	8	N.A.
Concrete removal (hrs)	40	8	20
Reinforcement severing (hrs)	4	4	4
Coupler installation (hrs)	40	16	N.A.
Concrete/grout placement (hrs)	8	8	8
Concrete/grout curing (hrs)	336	336	24
FRP application (hrs)	24	24	8
Footing repair (hrs)	N.A.	N.A.	16
Total (hrs)	460	404	80



(a) Footing after coupler installation

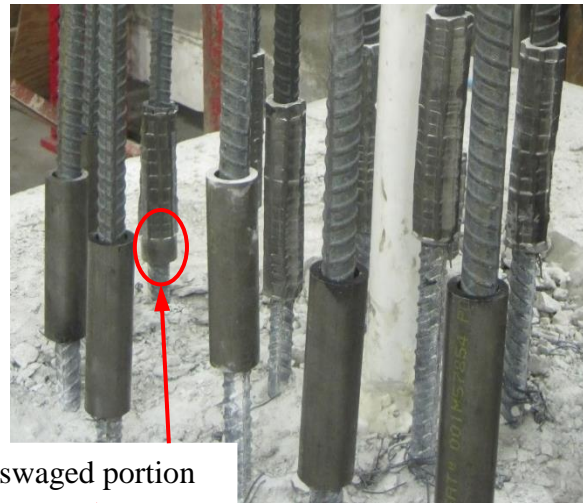


(b) Failure of splices under tensile test

Figure 7-1 Installation and Failure of Bar Splice Tensile Tests of Shear-Lock Couplers



(a) Existing longitudinal bars after severing



(b) Bar splices during swaging



(c) Failure of splices under tensile test

Figure 7-2 Installation and Failure of Bar Splice Tensile Tests of Swaged Couplers



(a) Formwork of R-Calt-1



(b) R-Calt-1 during concrete casting



(c) R-Calt-1 after concrete casting



(d) Formwork of R-Calt-2



(e) R-Calt-2 during concrete pumping

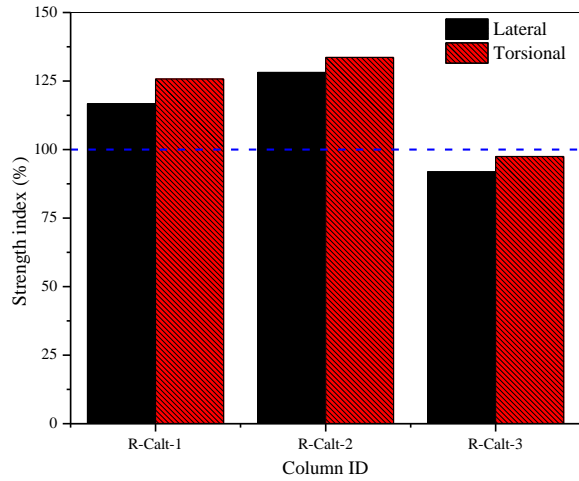


(f) R-Calt-2 after concrete

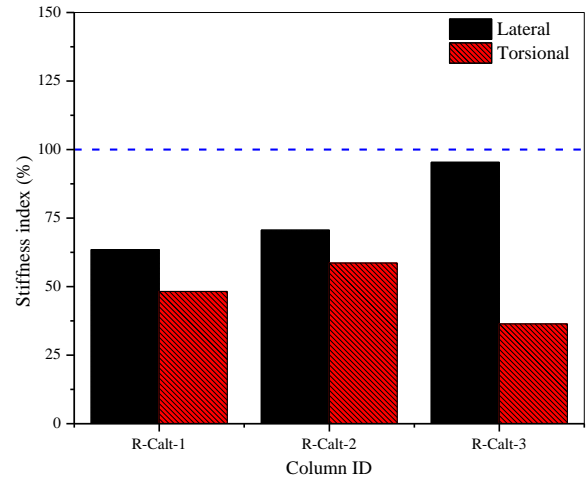


(g) R-Calt-3 after grout casting

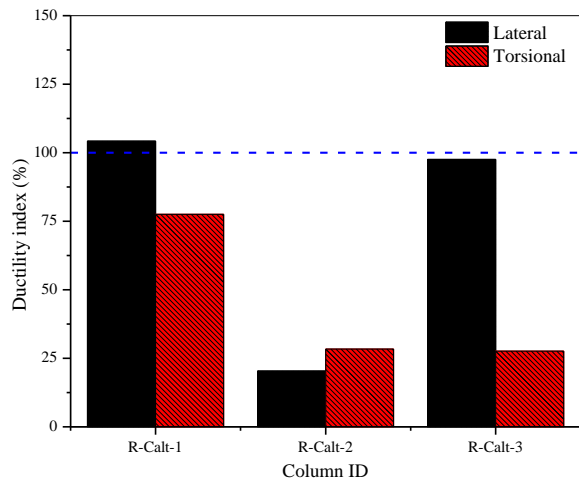
Figure 7-3 Concrete/Grout Placement of Columns



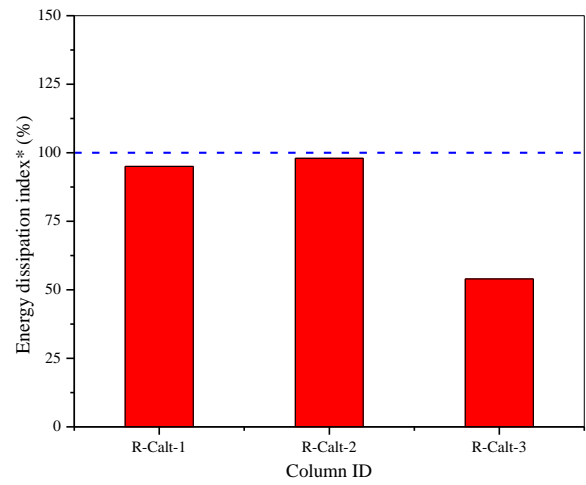
(a)



(b)



(c)



(d)

Figure 7-4 Restoration Indices of Repair Methods

## 8. CONCLUSIONS AND RECOMMENDATIONS

This chapter summarizes conclusions related to the experimental work of the three columns repaired with the proposed methods in this study, following which recommendations to repair design and construction are also presented. Future work in need of further research is also discussed in this chapter.

### 8.1. CONCLUSIONS

Two methods are proposed in this study to repair earthquake-damaged RC bridge columns with interlocking spirals and fractured longitudinal bars. The first method was considered a permanent repair that involved replacement of the plastic hinge region by removal of spirals, replacement of longitudinal bar segments with new bars attached with mechanical couplers, replacement of concrete, and installation of a CFRP jacket. This method also involved strengthening the non-plastic hinge region with a CFRP jacket. The second method was considered an emergency repair method that involved removal of damaged concrete, bonding and embedment of CFRP strips (pre-cured laminate) and CFRP jacket (prefabricated laminate), and repairing of the footing with externally bonded CFRP straps (fabric). Two columns (R-Calt-1 and R-Calt-2) damaged under uniaxial bending, shear, and torsion with varied T/M ratios of 0.2 and 0.6 were repaired with the first method with two different types of mechanical couplers. The third column (R-Calt-3) damaged under biaxial bending, shear, and torsion with T/M ratio of 0.2 was repaired with the second method. The repaired columns were tested under a similar loading protocol as

that applied to the corresponding original columns. Based on the construction work of the repair procedure and the test results, the following conclusions are made:

- (1) Both the proposed repair methods are practical and are achievable in field applications.

The facilities used in the first method included a commercial shoring system, concrete demolition equipment, coupler installation equipment, commercial formwork, and concrete a pump, all of which are available to contractors.

- (2) Two types of mechanical couplers were used in the first repair method, one of which was a sleeve with shear bolts, and the other was a swaged sleeve. The former was used in the repair for R-Calt-1 for the reason that the deformed portion of longitudinal bars was close to or penetrated into the footing, which resulted in short lengths of bars protruding from the footing after severing them. Thus, the space for coupler installation was limited, and the sleeve with shear bolts should be the better choice since the space is shorter than the required length for swaging machines. The latter type of coupler was used in R-Calt-2 for the reason that the deformed portion of longitudinal bars was far enough from the footing, which resulted in slightly longer lengths of bars protruding from the footing after severing them. Thus, the space for the swaging equipment was adequate, with the exception of two bars, where the couplers were only partially swaged with a portion about 1 in. (25 mm) unswaged. However, no failure was observed to the longitudinal bars within the coupler region during the testing of R-Calt-2, and tensile test results of partially swaged coupled bars showed that they performed as well as the fully swaged bars. Collectively, these couplers performed well in restoring the ductility capacity of the repaired columns.

- (3) The first repair method was able to restore the lateral strength (greater than 110% of that of the original columns) and ductility (possibly greater than 100% of that of the original columns). This was attributed to the effect of the CFRP jacket, which provided good confinement to the concrete and precluded the spalling and crushing of concrete. The first repair method resulted in a reduced equivalent lateral stiffness (less than 75% of that of the original columns), which was attributed to the unrepaired damage to the column and the intervention to the integrity of the interface between the column and footing or between the plastic hinge region and the non-plastic hinge region of the column during repair.
- (4) The second repair method was able to nearly restore the lateral strength (greater than 90% of that of the original column), ductility (greater than 90% of that of the original column), and equivalent elastic stiffness (greater than 90% of that of the original column). The restored strength showed that the well-anchored CFRP strips and the CFRP jacket were successful in transferring the bending moment from the column to the footing. The restored ductility may be due to the residual deformation capacity the existing longitudinal bars or the slip of the CFRP jacket and strips. The restored stiffness was also desirable and was attributed to the increased rotational stiffness of the plastic hinge region due to the enlarged cross-section and the CFRP jacket.
- (5) Both repair methods enhanced or restored the torsional strength (at least 90% of that of the corresponding original columns) but were unable to restore the torsional stiffness and ductility. The restored torsional strength showed that transverse CFRP was effective in torsional repair. However, the torsional stiffness may be reduced due to intervention during repair to the integrity of the interface between the column and the footing or

between the plastic hinge region and the non-plastic hinge region of the column. In practice, torsional behavior is usually designed as capacity protected, i.e., as elastic; thus, the reduced torsional ductility may not invalidate the success of the proposed repair methods, although this may need further investigation.

- (6) Both methods resulted in lower cumulative energy dissipation than that of the corresponding original columns. This reduces the equivalent damping ratio of the repaired columns and would result in a dynamic response that is different from the corresponding original columns; however, further research is needed to investigate the results of this aspect.
- (7) With the first repair method, the plastic hinge length of the repaired columns was similar to that of the original columns. Thus, the designated damage region would not shift locations, which is desirable in practice.
- (8) A repair method was proposed to repair the footing of R-Calt-3 with externally bonded CFRP. The method used was shown to be successful and effective. The required number of layers of CFRP was determined by assuming they would compensate for the loss of tensile force due to the severed bars in the footing (required for the column repair). A constant effective strain 0.004 was used in design of the number of layers of CFRP straps instead of the effective strain dependent on the number of layers as suggested by ACI440.2R-08. This may be valid since the CFRP was designed as U-shaped straps that were wrapped around the corner of footing, which increased the effectiveness of the bond.

## 8.2. RECOMMENDATIONS

Based on the repair design and procedure proposed in this study, guidelines to repair design of RC bridge columns are recommended and shown in Figure 8-1. As shown in this figure, prior to repair, it is recommended to determine whether permanent or emergency repair is to be conducted. If permanent repair is to be conducted, replacement bars with mechanical couplers are recommended to repair the fractured or buckled bars. If emergency repair is required, CFRP strips and jacket can be used to reduce the effort and time for the repair.

With the permanent repair as used for R-Calt-1 and R-Calt-2, the first step involves estimating the region in need of replacement, which is usually the designated plastic hinge region of the original column. The length of the plastic hinge region can be estimated using the method given by Caltrans (2006) as  $1.5D$ , where  $D$  is the dimension of the cross section in the bending direction, or with other methods. With the replacement (plastic hinge) length determined, all the concrete and spirals in this region are recommended to be removed to facilitate the installation of replacement bars and mechanical couplers. All the circumferential longitudinal bars within the replacement (plastic hinge) region are recommended to be severed and removed if they are noticeably deformed. The core bars are also to be severed and removed if they are also deformed. Concrete or grout with similar design strength to that of the original column is recommended to preclude possible shifting of the plastic hinge region. If possible, the same formwork as that used to construct the original column is suggested to be used to obtain the same cross section as that of the original column. If conventional concrete is used, a pump is necessary for the good consolidation of concrete for the reason that vibration in place is usually limited by the existing portion of the column and the footing. A CFRP jacket with fibers oriented in the transverse

(hoop) direction can be provided for restoration of the confinement, shear strength, and torsional moment strength. The number of layers for shear and torsion can be determined by equating the repair demand with the nominal strength of the original column computed with the design properties of the materials. Material reduction factors for the existing untreated bars and concrete (Vosooghi and Saiidi, 2012) are also used to consider the unrepaired damage. The number of layers for confinement can be determined by moment-curvature analysis or the retrofit method (Seible et. al., 2012), where the larger number is used with corresponding method. The total number of layers of the CFRP jacket is determined as the larger number as required for shear plus torsion or confinement plus torsion. An effective strain 0.004 for design of the transverse CFRP jacket is recommended with conservatism.

With the emergency repair as used for R-Calt-3, similar to the permanent method, the first step also involves estimating the repair (plastic hinge) length. The length of the plastic hinge region can be estimated by Caltrans (2006) as  $1.5D$ , where  $D$  is the dimension of the cross section in the bending direction, or with other methods. With the repair (plastic hinge) length determined, only loose concrete in this region are recommended to be removed with no treatment to the spirals and longitudinal reinforcement. The next step involves determining the required number of layers of the CFRP jacket in the transverse (hoop) direction by equating the repair demand with the nominal shear or torsion strength of the original section computed with the design properties of materials. Material reduction factors for the existing bars and concrete (Vosooghi and Saiidi, 2012) can be used to consider the unrepaired damage. For the composite used in this study, a minimum of two layers of transverse CFRP are suggested for confinement. An effective strain of 0.004 is suggested for the transverse CFRP with conservatism. The required number of CFRP

strips is determined by comparison of the equivalent tensile force provided by them and the loss of tensile force due to fracture bars, where the rupture strain of the CFRP strips can be used to compute the force. Moment-curvature analysis is suggested to verify the flexural repair including the CFRP strips and CFRP jacket, where the moment capacity of the repaired section should exceed that of the original column, while the curvature capacity is not considered. An embedment length within the footing greater than  $\frac{1}{2}$  of the weak axis of the cross section is suggested to fully develop the strength of longitudinal CFRP (either strips or jacket). U-shaped CFRP straps designed according to ACI 440.2R-08 with an effective strain 0.004 can be used to repair footing damage.

### 8.3. FUTURE WORK

This study was focused on developing repair methods for damaged bridge columns with fractured longitudinal bars to restore the seismic performance of them. Based on the experimental work and results, several fields related to this study are in need of further research.

As mentioned earlier in this report, the repaired columns showed a different hysteretic response from that of the corresponding original columns; thus, the influence of the repair methods on the response of the entire bridge structure should be investigated through dynamic analysis to validate the repair methods.

The repair method presented in Chapter 5 was successful in restoring the strength and ductility temporarily. However, the performance of this repair method depends on the bond provided by the epoxy that was filled in between the column and the CFRP jacket as well as the column-footing joint integrity provided by the gravel-filled epoxy within the trench. Therefore, long-term

durability and bond performance of the epoxy and epoxy-gravel should be investigated for the case of a permanent repair.

As shown in Chapter 6, the CFRP jacket was well anchored into the footing with the help of the epoxy-filled gravel. The bond strength as well as bond-slip behavior between pre-impregnated CFRP and the epoxy-filled gravel should be studied by testing small-scale specimens to investigate their influence on the overall behavior of the repaired column.

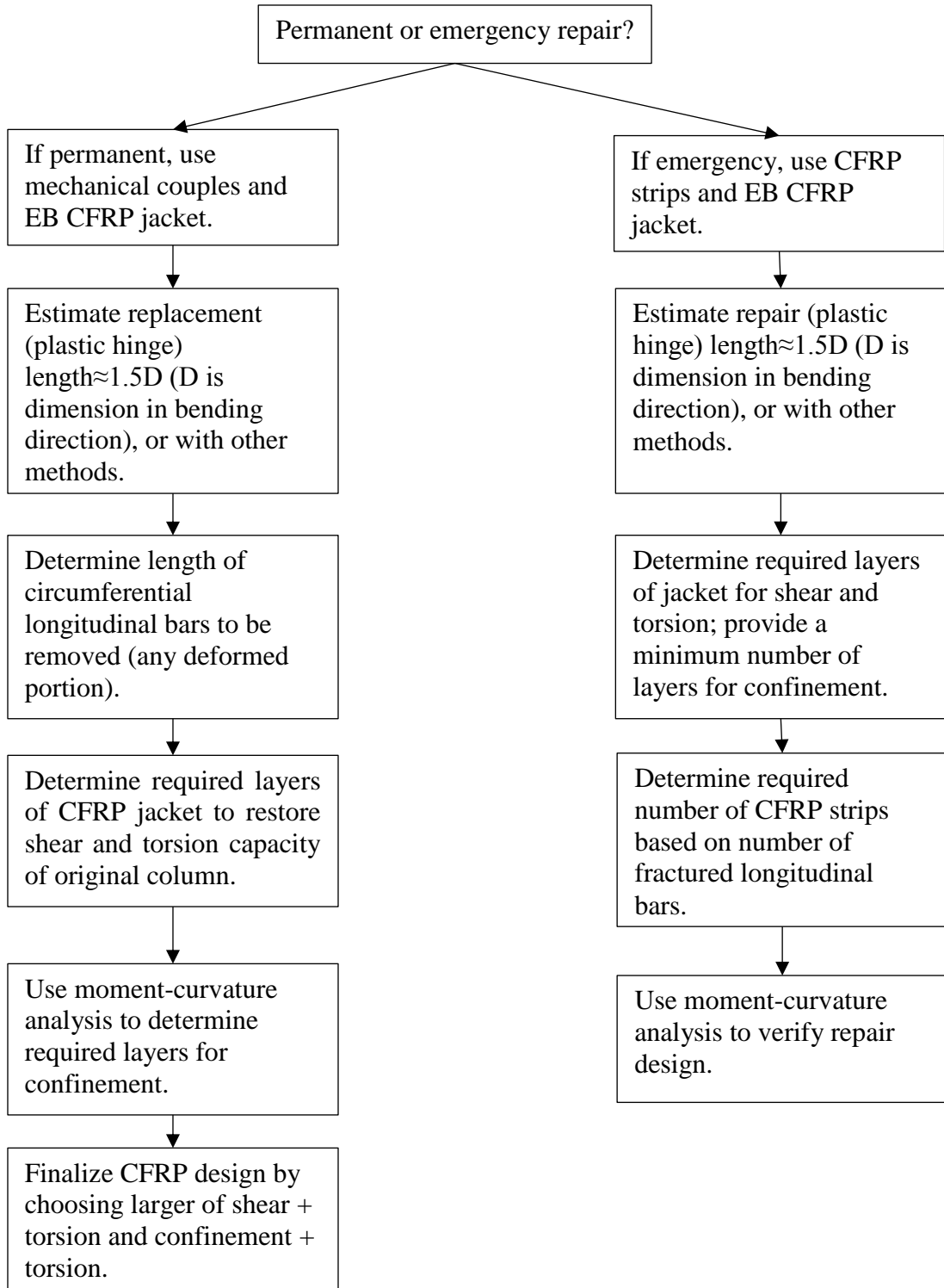


Figure 8-1 Repair Design Guide for RC Bridge Columns with Fractured Longitudinal Bars

## 9. REFERENCES

- AASHTO, "LRFD Bridge Design Specifications," American Association of State Highway and Transportation Officials, Washington, DC, 1998.
- ACI 440.2R-08, "Guide for the Design and Construction of Externally Bonded FRP Systems for Strengthening Concrete Structures," American Concrete Institute, Farmington Hills, MI, 2008.
- ASTM, A706/A706M-09b, "Standard Specification for Low-Alloy Steel Deformed and Plain Bars for Concrete Reinforcement," ASTM International, West Conshohocken, PA, 2009.
- ASTM, C39/C39M-12a, "Standard Test Method for Compressive Strength of Cylindrical Concrete Specimens," ASTM International, West Conshohocken, PA, 2012.
- ASTM, D3039/D3039M-08, "Standard Test Method for Tensile Properties of Polymer Matrix Composite Materials," ASTM International, West Conshohocken, PA, 2008.
- ASTM, C109/C109M, "Standard Test Method for Compressive Strength of Hydraulic Cement Mortars (Using 2-in. or [50-mm] Cube Specimens)," ASTM International, West Conshohocken, PA, 2013.
- ASTM, C496/C496M, "Standard Test Method for Splitting Tensile Strength of Cylindrical Concrete Specimens," ASTM International, West Conshohocken, PA, 2011.
- Bai, A., Ingham, J., and Hunt, R. "Assessing the Seismic Performance of Reinforcement Coupler Systems," In *2003 Pacific Conference on Earthquake Engineering*, Christchurch, New Zealand, 2003.
- Belarbi, A., Silva, P. F., and Bae, S.-W. "Retrofit Using CFRP Composites of RC Bridge Columns Under Combined Loads," In *Proc., 4th Int. Symp. on FRP Composites in Civil Engineering (CICE)*: EMPA Duebendorf, Switzerland, 2008.
- Billah, A., Muntasir, and Alam, M., Shahria "Seismic Performance of Concrete Columns Reinforced with Hybrid Shape Memory Alloy (SMA) and Fiber Reinforced Polymer (FRP) Bars," *Construction and Building Materials*, 28 (1), 2012, pp: 730-42.
- Caltrans, "Seismic Design Criteria," California Department of Transportation, Sacramento, CA, 2006.
- Caltrans, [www.dot.ca.gov/hq/esc/approved...list/.../steel\\_reinforcing\\_couplers.pdf](http://www.dot.ca.gov/hq/esc/approved...list/.../steel_reinforcing_couplers.pdf).
- Chang, S.-Y., Li, Y.-F., and Loh, C.-H., "Experimental study of seismic behaviors of as-built and carbon fiber reinforced plastics repaired reinforced concrete bridge columns," *Journal of Bridge Engineering*, 9 (4), 2004, pp: 391-402.
- Cheng, C.-T., Yang, J.-C., Yeh, Y.-K., and Chen, S.-E., "Seismic performance of repaired hollow-bridge piers," *Construction and Building Materials*, 17 (5), 2003, pp: 339-51.
- Correal, J. F., Saiidi, M. S., Sanders, D., and El-Azazy, S., "Shake table studies of bridge columns with double interlocking spirals," *ACI Structural Journal*, 104 (4), 2007.
- Fam, A., Cole, B., and Mandal, S., "Composite tubes as an alternative to steel spirals for concrete members in bending and shear," *Construction and Building Materials*, 21 (2), 2007, pp: 347-55.
- Federal Highway Administration, "Emergency Relief Manual," <https://www.fhwa.dot.gov/programadmin/erelief.cfm>, 2013.

- French, C. W., Hafner, M., and Jayashankar, V., "Connections Between Precast Elements-Failure Within Connection Region," *Journal of Structural Engineering*, 115 (12), 1989, pp: 3171-92.
- He, R., Grelle, S., Sneed, L. H., and Belarbi, A., "Rapid repair of a severely damaged RC column having fractured bars using externally bonded CFRP," *Composite Structures*, 2013.
- He, R., L.H. Sneed, and A. Belarbi. "Torsional Repair of Severely Damaged Column Using Carbon Fiber-Reinforced Polymer." *ACI Structural Journal*, American Concrete Institute, Farmington Hills, MI, 111 (3), 2014, pp. 705-716.
- Lee, D. H., Park, J., Lee, K., and Kim, B. H., "Nonlinear seismic assessment for the post-repair response of RC bridge piers," *Composites Part B: Engineering*, 42 (5), 2011, pp: 1318-29.
- Lehman, D. E., Gookin, S. E., Nacamuli, A. M., and Moehle, J. P., "Repair of earthquake-damaged bridge columns," *ACI Structural Journal*, 98 (3), 2001, pp: 233-38.
- Li, Q., and Belarbi, A., "Seismic Behavior of RC Columns with Interlocking Spirals under Combined Loadings Including Torsion," *Procedia Engineering*, 14, 2011, pp: 1281-91.
- Marsh, M. L., Wernli, M., Garrett, B. E., Stanton, J. F., Eberhard, M. O., and Weinert, M. D., "Application of Accelerated Bridge Construction Connections in Moderate-to-High Seismic Regions," *NCHRP Report. 698*, Transportation Research Board, Washington, DC, 2011.
- Mirmiran, A., Shahawy, M., and Samaan, M., "Strength and ductility of hybrid FRP-concrete beam-columns," *Journal of structural Engineering*, 125 (10), 1999, pp: 1085-93.
- Ozbakkaloglu, T., and Saatcioglu, M., "Seismic performance of square high-strength concrete columns in FRP stay-in-place formwork," *Journal of Structural Engineering*, 133 (1), 2007, pp: 44-56.
- Rowell, S. P., and Hager, K. P., "Investigation of the Dynamic Performance of Large Reinforcement Bar Mechanical Couplers," In *Structures Congress 2010*, 2010.
- Rutledge, S. T., Kowalsky, M. J., Seracino, R., and Nau, J. M., "Repair of Reinforced Concrete Bridge Columns Containing Buckled and Fractured Reinforcement by Plastic Hinge Relocation," *Journal of Bridge Engineering*, 2013.
- Saadatmanesh, H., Ehsani, M. R., and Jin, L., "Repair of earthquake-damaged RC columns with FRP wraps," *ACI Structural Journal*, 94, 1997, pp: 206-15.
- Sadeghian, P., and Fam, A., "Bond-Slip Analytical Formulation toward Optimal Embedment of Concrete-Filled Circular FRP Tubes into Concrete Footings," *Journal of Engineering Mechanics*, 136 (4), 2010, pp: 524-33.
- Sadeghian, P., and Fam, A., "Closed-Form Model and Parametric Study on Connection of Concrete-Filled FRP Tubes to Concrete Footings by Direct Embedment," *Journal of Engineering Mechanics*, 137 (5), 2011, pp: 346-54.
- Sadeghian, P., Lai, Y., and Fam, A., "Testing and Modeling of a New Moment Connection of Concrete-Filled FRP Tubes to Footings under Monotonic and Cyclic Loadings," *Journal of Composites for Construction*, 15 (4), 2011, pp: 653-62.
- Saiidi, M. S., and Cheng, Z., "Effectiveness of composites in earthquake damage repair of reinforced concrete flared columns," *Journal of Composites for Construction*, 8 (4), 2004, pp: 306-14.
- Saini, A., and Saiidi, M. S., "Post-Earthquake Damage Repair of Various Reinforced Concrete Bridge Components," *Draft Progress Report to Caltrans Post-Earthquake Bridge*

- Damage Mitigation*, Department of Civil and Environmental Engineering, University of Nevada, Reno, Reno, NV, 2013.
- Samaan, M., Mirmiran, A., and Shahawy, M., "Model of concrete confined by fiber composites," *Journal of Structural Engineering*, 124 (9), 1998, pp: 1025-31.
- Seible, F., Priestley, M. N., Hegemier, G. A., and Innamorato, D., "Seismic retrofit of RC columns with continuous carbon fiber jackets," *Journal of Composites for Construction*, 1 (2), 1997, pp: 52-62.
- Shao, Y., and Mirmiran, A., "Experimental investigation of cyclic behavior of concrete-filled fiber reinforced polymer tubes," *Journal of Composites for Construction*, 9 (3), 2005, pp: 263-73.
- Shin, M., and Andrawes, B., "Emergency repair of severely damaged reinforced concrete columns using active confinement with shape memory alloys," *Smart Materials and Structures*, 20 (6), 2011, pp: 065018.
- Tanaka, H., and Park, R., "Seismic design and behavior of reinforced concrete columns with interlocking spirals," *ACI Structural Journal*, 90 (2), 1993.
- Vecchio, F. J., and Collins, M. P., "Compression response of cracked reinforced concrete," *Journal of Structural Engineering*, 119 (12), 1993, pp: 3590-610.
- Vosooghi, A., and Saiidi, M. S., "Design Guidelines for Rapid Repair of Earthquake-Damaged Circular RC Bridge Columns Using CFRP," *Journal of Bridge Engineering*, 2012.
- Zakaib, S., and Fam, A., "Flexural Performance and Moment Connection of Concrete-Filled GFRP Tube-Encased Steel I-Sections," *Journal of Composites for Construction*, 16 (5), 2012, pp: 604-13.
- Zhu, Z., Ahmad, I., and Mirmiran, A., "Seismic performance of concrete-filled FRP tube columns for bridge substructure," *Journal of Bridge Engineering*, 11 (3), 2006, pp: 359-70.
- Zhu, Z., Mirmiran, A., and Saiidi, M., "Seismic Performance of Reinforced Concrete Bridge Substructure Encased in Fiber Composite Tubes," *Transportation Research Record: Journal of the Transportation Research Board*, 1976 (1), 2006, pp: 197-206.
- Zureick, A. H., Ellingwood, B. R., Nowak, A. S., Mertz, D. R., and Triantafillou, T. C., "Recommended guide specification for the design of externally bonded FRP systems for repair and strengthening of concrete bridge elements," *NCHRP Report 655*, Transportation Research Board, Washington, DC, 2010.